A Study of the Spontaneous Membrane Insertion of Chloride Intracellular Ion Channel Protein CLIC1 into Model Lipid Membranes

Khondker Rufaka Hossain

A thesis submitted in fulfilment of the requirements for the degree of Doctor of Philosophy

UNIVERSITY OF TECHNOLOGY SYDNEY

School of Life Sciences
Faculty of Science
2016

Certificate of Original Authorship

I, Khondker Rufaka Hossain, certify that the work in this thesis has not previously been submitted for a degree nor has it been submitted as part of requirements for a degree except as fully acknowledged within the text.

I also certify that the thesis has been written by me and to the best of my knowledge contains no materials previously published or written by another person. Any help that I have received in my research work and the preparation of the thesis itself has been acknowledged. In addition, I certify that all information sources and literature used are indicated in the thesis.

Signature of Student:

…….
Khondker Rufaka Hossain
2016

Acknowledgement

I would like to express my sincere thanks to my principle supervisor, Associate Professor Dr Stella Valenzuela from UTS for her constant guidance, help and support, for inspiring me, motivating me and for making it possible for me to work with dedicated research scientists at Australian Nuclear Science and Technology Organisation (ANSTO) and Australian Synchrotron. These experiences and research opportunities have been very rewarding, and would not have been possible without Dr Valenzuela and her dedication to my education and development.

I wish to gratefully acknowledge the support of my co-supervisor Dr Stephen A Holt from ANSTO for his high enthusiasm, dedication and continuous help and support throughout my PhD. He is an excellent educator and have dedicated hours of his time teaching me all the biophysical techniques used in this thesis. I would like to say to Dr Holt that "without your help I would have never been able to come this far in this research study".

I would like to extent my gratitude to all my friends, lab membranes, academics and colleagues from the faculty of science at UTS and from ANSTO for their assistance, friendship, supportive attitudes, helpful comments and feedbacks that have motivated and inspired me throughout my PhD degree. I would like to specifically thank Dr Heba Al Khamici for sharing her knowledge of protein purification with me; Dr Anton Le Brun for his constant guidance and assistance with all my reflectivity work and Dr Rekas Agata for teaching me how to use the CD spectrophotometer. I would also like to thank Dr Nicole Cordina and Dr Louise Brown from Macquarie University for allowing me to perform mutagenesis experiments in their lab.

I am extremely grateful to the Graduate Research School at UTS and the Australian Institute of Nuclear Science and Engineering (AINSE) for their financial support without which, this work would not have been possible. I would also like to thank AINSE and ANSTO for the three beam time awards (P3304, A2842 and A2839).

Lastly but most importantly a big thanks to my parents and my husband for their patience, endless support, believe and motivation that kept me going during this long and often challenging time. To you I dedicate this thesis.

Publications

Publications arising from this thesis

[1] Hossain, KR., Al Khamici, H., Holt, SA, and Valenzuela, SM. (2016) Cholesterol Promotes Interaction of the Protein CLIC1 with Phospholipid Monolayers at the Air-Water Interface., Membranes (Basel) 6 (1), E15.

Publications arising from collaborations during my PhD degree

[1] Charles C, Thomas B, Holt SA,; Hossain KR, Anton LB, Sonia C, Al Khamici H, Hans C, Valenzuela SM and Bruce C. (2016) Evidence for the Key Role of H_3O in Phospholipid Membrane Morphology, Langmuir, Manuscript ID: la-2016-01988p (Submitted for review).

[2] Al Khamici, H., Brown, L., Hossain, K., Hudson, A., Sinclair-Burton, A., Ng, J., Daniel, E., Hare, J., Cornell, B., Curmi, P., Davey, M., and Valenzuela, S. (2015) Members of the Chloride Intracellular Ion Channel Protein Family Demonstrate Glutaredoxin-Like Enzymatic Activity, PLoS One 10, e115699.

[3] Yepuri, N., Holt, S., Moraes, G., Holden, P., Hossain, K., Valenzuela, S., James, M., and Darwish, T. (2014) Stereoselective synthesis of perdeuterated phytanic acid, its phospholipid derivatives and their formation into lipid model membranes for neutron reflectivity studies., Chem Phys Lipids. 183, 22-33.

Conference Presentations

Oral presentations

- Hossain KR, Al Khamici H, Holt SA and Valenzuela SM. (2016) ELUCIDATING THE MECHANISM FOR STEROL REGULATION OF CHLORIDE INTRACELLULAR ION CHANNEL PROTEIN INTERACTIONS WITH LIPID MEMBRANES. 60th Annual Meeting, Biophysical Society, California, USA.

- Hossain KR, Al Khamici H, Holt SA and Valenzuela SM. (2015) Interaction of the Chloride Intracellular Ion Channel Protein CLIC1 with different sterols in Model Membranes. 2nd Asia-Oceania Conference on Neutron Scattering, Sydney, Australia.

- Hossain KR, Al Khamici H, Holt SA and Valenzuela SM. (2014) Effects of Cholesterol on the spontaneous membrane insertion of Chloride Intracellular Ion Channel Protein CLIC1. 12th AINSE-ANBUG Neutron Scattering Symposium (AANSS), Sydney, Australia.

- Hossain KR, Al Khamici H, Holt SA and Valenzuela SM. (2013) A Study of the Spontaneous Membrane Insertion of Chloride Intracellular Ion Channels (CLICs) into Model Lipid Membranes. 11th AINSE-ANBUG Neutron Scattering Symposium (AANSS), Sydney, Australia.

Poster presentations

- Hossain KR, Al Khamici H, Holt SA and Valenzuela SM. (2015) Investigating the mechanism for Sterol Regulation of CLIC1 with Lipid Membranes. New Horizons, Sydney, Australia.

- Hossain KR, Al Khamici H, Holt SA and Valenzuela SM. (2014) The Spontaneous Membrane insertion of Chloride Intracellular Ion Channel Protein CLIC1 into Model Membranes. 22nd Australian Society for Medical Research (ASMR), Sydney, Australia.

- Hossain KR, Al Khamici H, Holt SA and Valenzuela SM. (2014) Effects of Sterol Structure on the spontaneous membrane insertion of Chloride Intracellular Ion Channel Protein CLIC1. New Horizons, Sydney, Australia.

- Hossain KR, Al Khamici H, Holt SA and Valenzuela SM. (2013) A Study of the Spontaneous Membrane Insertion of CLIC1 into Model Lipid Membranes. Australian Society of Biophysics, Melbourne, Australia.

Table of Contents

Abbreviations

2D	Two-dimensional
A	Area per molecule
Å	Angström (10^{-10} m)
A9C	Anthracene-9-carboxylic acid
ACMW	Air Contrast Matched Water
AEBSF	4-(2-Aminoethyl) benzenesulfonyl fluoride hydrochloride
AKAP	A Kinase anchor protein
AMP	Adenosine monophosphate
Ano	Anoctamin
ANX	Annexin
APP	Amyloid precursor protein
AQP	Aquaporin
Arg	Arginine amino acid
Asn	Asparagine amino acid
ATP	Adenosine triphosphate
Bcl	B-cell lymphoma
BSA	Bovine serum albumin
C-domain	Carboxyl terminal domain
Ca^{2+}	Calcium ion
CaCC	Ca^{2+} - activated Cl- channel
$CaCl_2$	Calcium chloride
CD	Circular Dichroism
CDC	Cholesterol-dependent cytolysins
CFTR	Cystic fibrosis transmembrane conductance regulator
Ch-ane	Cholestane
Ch-one	5-cholesten-3-one
CHO-K1	Chinese hamster ovary cells
Chol	Cholesterol
CIC	Chloride ion channel
Cl^-	Chloride ion
CLIC	Chloride intracellular ion channel
CV	Column Volume
Cys	Cysteine amino acid

d_{31}-POPC	Deuterated 1-palmitoyl-(d31)-2-oleoyl-sn-glycero-3-phosphatidylcholine
*Dm*CLIC	*Drosophila melanogaster* CLIC protein
DPPC	1,2-dipalmitoyl-sn-glycero-3-phosphocholine
DSC	Differential Scanning Calorimetry
DTT	Dithiothreitol
E-64	Epoxide protease inhibitor
E.coli	*Escherichia coli*
EDTA	Ethylenediaminetetraacetic acid
EPR	Electron Paramagnetic Resonance
ErbB	Epidermal growth factor receptor
Erg	Ergosterol
ERK	Extracellular signal-regulated kinase
ERM	Ezrin, Radixin and Moesin proteins
EXC	Excretory canal abnormality
EXL	EXC-like
FRET	Fluorescence Resonance Energy Transfer
GABA	gamma-Aminobutyric acid
Gln	Glutamine amino acid
Glu	Glutamic acid amino acid
Gly	Glycine amino acide
GPHR	Golgi pH Regulator
Grx	Glutaredoxin
GSH	Reduced glutathione
GST	Glutathione S-transferase
H^+	Hydrogen ion
HEDES	2-hydroxyethyl disulphide
Hepes	4-(2-hydroxyethyl)-1-piperazineethanesulfonic acid
His	Histidine amino acid
Hyd	20-hydroxyecdysone
IAA-94	Indanyloxyacetic acid 94
IPTG	Isopropyl-thio-β-D-galactopyranoside
IQGAP	IQ motif containing GTPase activating protein
IR	Infra-Red
IRS	Interfacial Stress Rheometry
Kan	Kanamycin
KCl	Potassium chloride

kDa	kilo-Dalton
KH_2PO_4	Potassium dihydrogen phosphate
LC	Liquid condensed phase
LM	Langmuir monolayer
LSM	U6 snRNA-associated Sm-like protein
Lys	Lysine amino acid
M	Moles
MAP	Mitogen activated protein
MC	Monte-Carlo
mCLIC	mouse Chloride intracellular ion channel protein
$MgCl_2$	Magnesium chloride
$MgSO_4$	Magnesium sulphate
ml	milli-Litre
mM	milli-Molar
N-domain	Amino terminal domain
NaCl	Sodium chloride
NADPH	Nicotinamide adenine dinucleotide phosphate
NBD	Nucleotide binding domain
NCC27	Nuclear chloride channel protein 27kDa
NEM	N-Ethylmaleimide
Ni-NTA	nickel-nitrilotriacetic acid
NMR	Nuclear Magnetic Resonance
NR	Neutron Reflectivity
p64	Bovine chloride channel protein 64kDa
Panc	Pancreatic cancer cells
PC	Phosphatidylcholine
PCR	Polymerase chain reaction
PE	Phosphatidylethanolamine
PFT	Pore-forming toxin
Phe	Phenylalanine amino acid
PHR	Pam Highwire RPM-1 proteins
pI	Isoelectronic point
POPC	1-palmitoyl-2-oleoyl-sn-glycero-3-phosphatidylcholine
POPE	1-palmitoyl-2-oleoyl-*sn*-glycero-3-phosphatidylethanolamine
POPS	1-palmitoyl-2-oleoyl-*sn*-glycero-3-phosphatidylserine
PPI2	Serine/threonine phosphatase (PP1) isoform PP1 gamma 2
Pro	Proline amino acid

PS	Phosphatidylserine
PTMD	Putative Transmembrane Domain
Q	Momentum transfer
RyR	Ryanodine receptor
SANS	Small Angle Neutron Scattering
SAXS	Small Angle X-ray Scattering
SDS-PAGE	Sodium Dodecyl Sulfate-PolyAcrylamide
SEC	Size Exclusion Chromatography
Ser	Serine amino acid
Sito	ß-sitosterol
SLD	Scattering Length Density
SLS	Surface Light Scattering
t	Thickness
T84	Human colon cancer cell
tBLM	Tethered lipid bilayers
TCEP	tris-2-carboxyethyl-phosphine
TEMED	NNNN'-tetramethylethylenediamine
TMD	Transmembrane domain
TMR	Transmembrane region
TNF-α	Tumour necrosis factor- alpha
Trp	Tryptophan amino acid
Val	Valine amino acid
VGAT	Vesicular GABA transporter
VGLUT	Vesicular glutamate transporter
X	Any amino acid
XR	X-ray Reflectivity
XRD	X-ray Diffraction
Γ	Surface excess/ Surface coverage
ΔA	Percentage surface area expansion
λ	Wavelength
µl	micro-Litre
π	Surface pressure
σ	Roughness
Ω-GST	Omega class GST

List of Figures

Chapter 1

Chapter 2

Chapter 3

Chapter 4

Chapter 6

Chapter 7

List of Tables

Abstract

Sterols have been reported to modulate conformation and hence the function of several membrane proteins. One such group is the Chloride Intracellular Ion Channel (CLIC) family of proteins. These largely soluble proteins possess the intriguing property of spontaneous insertion into phospholipid bilayers to form integral membrane ion channels. To date, the structure of their membrane-bound form and factors influencing their auto-insertion remains largely unknown. In this thesis, we have performed Langmuir-film, X-ray, and neutron reflectivity experiments to study the interaction of wild-type or mutant versions of the protein CLIC1 with monolayers prepared using various mixtures of different phospholipids and sterol molecules, in order to investigate the regulatory role of the membrane lipid combination on the spontaneous membrane insertion of CLIC1 and to elucidate the structural features of the CLIC1 membrane-bound form within the lipid monolayers.

Our findings have demonstrated that the spontaneous membrane insertion of CLIC1 is dependent on the presence of cholesterol in lipid monolayers. In phospholipid monolayers only, CLIC1 was able to insert within the phospholipid head-group region with no penetration into the acyl chain region of the monolayers. However, in the presence of cholesterol, CLIC1 showed significant interaction with the phospholipid acyl chains thereby, suggesting that cholesterol is required for the penetration of CLIC1 into the hydrophobic tails of the lipid monolayer, which is considered necessary for the formation of functional ion channels. From reflectivity experiments, we were able to show that approximately 0.8 mg/m^2 of CLIC1 inserted into phospholipid monolayers containing cholesterol such that the protein occupied an area per molecule between 5 ~ 7 nm^2 with a total CLIC1 thickness ranging from ~ 51 Å to 59 Å throughout the entire monolayer. We have also demonstrated for the first time that the GXXXG motif in CLIC1 acts as the cholesterol-binding site used by the protein for its initial recognition and binding to membrane cholesterol. Furthermore, Langmuir and reflectivity experiments using different sterols have confirmed that the interaction between CLIC1 and sterols is dependent on an intact 3β-OH group in the sterol ring. Modification of the sterol structure by the introduction of additional hydroxyl

groups and methylation of the sterol alkyl chain was shown to facilitate greater spontaneous membrane insertion of the protein within the phospholipid monolayer. Taken together these findings provide clear evidence for the important role of sterols in the regulation of CLIC1 membrane interactions and a putative mechanism for its initial binding and membrane integration.

Chapter 1

Chloride Intracellular Ion Channel (CLIC) Proteins

(Literature Review)

Chapter 1

Chloride Intracellular Ion Channel (CLIC) Proteins

1. Introduction

The CLIC (Chloride Intracellular Ion Channel) proteins are a family of highly homologous proteins found in most human tissues and cells. These proteins are also highly conserved across species with CLIC-like proteins identified in numerous vertebrates, invertebrates as well as in plants [1-5]. To date, seven members of the human CLIC family have been identified: CLIC1-CLIC5A, CLIC5B and CLIC6. CLIC1 is an intracellular channel protein that exists either in a soluble state in the cytoplasm or bound to membranes [1-5]. The precise physiological mechanism controlling CLIC1's spontaneous insertion into membranes is currently unknown, although it is likely to involve processes such as oxidation [6-12], pH [3, 13-16] and lipid composition [6, 11, 17, 18]. Recent studies using impedance spectroscopy and tethered lipid membranes have revealed that cholesterol regulates the spontaneous insertion of CLIC1 into model membranes [18]. Interestingly, a number of pore-forming bacterial toxins (for example - listeriolysin, perfringolysin, streptolysin and pneumolysin) are known to demonstrate cholesterol dependent spontaneous insertion into lipid membranes [19]. Despite extensive experimental studies and review, much still remains unknown regarding the regulatory mechanisms controlling the spontaneous membrane insertion of CLIC1 and the structural conformation, membrane insertion, oligomerisation and arrangements of the CLIC proteins in cell membranes.

This research project hypothesises that CLIC1 forms a structural complex with cholesterol and that this regulates its spontaneous membrane insertion, followed by its oligomerisation to form functional ion channels in cell membranes. This chapter reviews key studies of the functional and structural characteristics of CLIC proteins (specifically CLIC1) confirming their ability to spontaneously insert into and form functional ion channels in the membranes of different cell lines and artificial lipid membrane models. The protein CLIC1, the pore forming toxins and other spontaneous membrane inserting proteins all share the remarkable ability of interacting with various membrane lipids, which is highly

regulated by the membrane phospholipid and sterol composition. This similarity provides clues to better understand the structural features of the membrane-bound CLIC1. A summary is provided of the structural data that indicates the likely ability of CLIC proteins to interact with cholesterol for their membrane insertion and some recent evidence that this occurs. In addition, this chapter reviews key factors that largely influence the spontaneous membrane insertion of CLIC proteins. Finally, this chapter highlights gaps in our present understanding of the autonomous insertion of the CLIC protein family into cell membranes and finishes with a summary of the main objectives of this project.

1.1 Chloride Ion Channels

Chloride (Cl^-) ion is the most predominant anion found in living organisms. In humans, the cellular cystolic Cl- concentration ranges from approximately 5 to 40 mM [20]. The physiological movement of Cl- ions across biological membranes is largely mediated by chloride ion channel proteins. Such transmembrane spanning ion channels have also been shown to exist on the membranes of intracellular organelles including the endoplasmic reticulum, mitochondria, Golgi, endosomes, lysosomes, nucleus and cell vesicles, where they act to facilitate the passage of Cl- ions across the intracellular membranes [20-22]. Electrophysiological studies have revealed a variety of different families of chloride channels that differ in structure, mechanism of action or anion selectivity and conductivity [20-23]. The topological structure and the mechanism of regulation of the chloride ion channels are illustrated in Figure 1.1 [23]. The largest known family of Cl- channels is formed by the ligand-gated GABA and glycine receptors (See [24] for review). GABA (γ-aminobutyric acid) and glycine-gated chloride channels are pentameric channels formed by α, β and γ subunits. Each subunit has four transmembrane segments, with a large extracellular N terminus. The second transmembrane segment of each subunit contributes to the formation of the central pore [23]. The N termini of the α and β subunits form the ligand binding site (Figure 1.1A).

The members of the CIC (chloride ion channel) family form the second largest family of Cl-transport proteins that are expressed in virtually all phyla, from bacteria to humans [20, 23, 25-27]. In mammals, the CIC gene family is comprised of

nine members [26, 27] that act as voltage-gated Cl-channels or mediate Cl- : H+ exchange activity in the plasma membrane or intracellular compartments respectively [21, 25-27]. The overall organization of voltage-gated chloride (ClC) channels is depicted in Figure 1.1B. Membrane structure of the CIC family is usually composed of 18 segments (labelled A to R) most of which span the plasma membrane partially and in a strongly tilted configuration [23]. CIC channels are arranged as dimers in the plasma membrane, with a slow gate controlling the activity of both channels simultaneously, while fast gating involves flipping of a pore-lining glutamate side chain into and out of the chloride pathway (Figure 1.1B) [23, 26, 28, 29].

The CFTR (cystic fibrosis transmembrane conductance regulator) is the third most established family of Cl channels [30, 31]. These families of Cl- channel proteins are involved in several physiological functions such as regulation of systemic electrolyte homeostasis, vesicular acidification, regulation of cell volume, cellular and organellar membrane potential and modulation of cellular excitability [22, 30, 31]. In addition, they also play vital roles in cell cycle regulation, apoptosis, blood pressure, neurotransmission, free radical release and bone resorption [21, 22]. They are composed of 12 membrane-spanning segments of CFTR plus two nucleotide binding domains (NBDs 1 and 2) and a regulatory R domain (Figure 1.1C) [23]. CFTR activation involves cyclic AMP-dependent phosphorylation and binding of ATP molecules at the NBDs [23]. Several genetic diseases such as myotonia, osteoporosis, epilepsy, cystic fibrosis and deafness are caused by mutation in the genes encoding these chloride ion channels or transporters [2, 21, 25].

In addition to these well-established and molecularly distinct gene families of chloride channels, Ca2+-activated Cl- channels (CaCC) have also been identified [2, 32]. Two members of the Anoctamin (Ano) gene family, Ano1 and Ano2 were shown to form Ca2+- activated Cl- channels [20, 25]. The predicted topology of CaCCs show eight transmembrane segments with cytosolic amino and carboxy termini (Figure 1.1D) [23]. The mechanism of calcium activation is still largely unknown. Compelling but controversial evidence exists that another gene family named Bestrophins can act as Ca2+- activated Cl- channels [2, 25]. Moreover, several prospective Cl- transporters have also been identified such as the AQP6 protein (aquaporin and glycerol channel family), GPHR (Golgi pH regulator), VGLUT1 (vesicular glutamate transporter) and VGAT (vesicular GABA

transporter) [20]. In conjunction with these groups of membrane chloride ion channels, is the more recently identified Cl^- channel family, the CLIC (chloride intracellular ion channel) protein family.

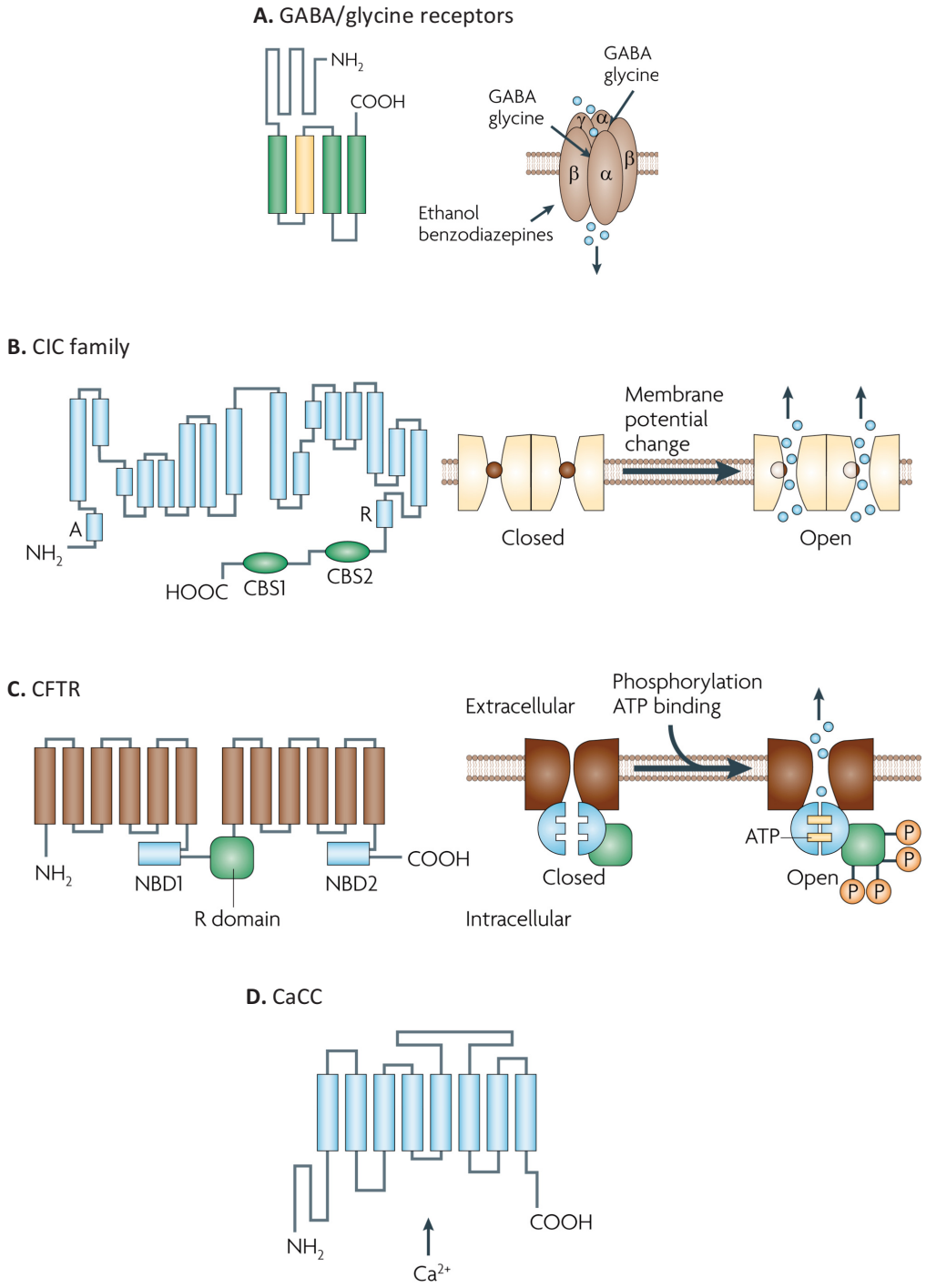

Figure 1.1 Schematic diagrams of the topological structures and mechanism of regulation of Chloride Ion Channels. The structures of the different Cl- channels shown are A) GABA/glycine receptors, B) CIC family, C) CFTR and D) CaCC [23].

1.2 The CLIC proteins

To date, seven members of the human CLIC family have been identified: CLIC1, CLIC2, CLIC3, CLIC4, CLIC5A, CLIC5B and CLIC6. CLIC1 to CLIC5A are almost identical in size consisting of a conserved C-terminal 240 residue module, with one major putative transmembrane domain [4, 5]. In contrast, CLIC5B and CLIC6 are two large variants and consists of an extended N-terminal domain in conjunction with the typical CLIC module [4, 5]. This C-terminal module has recently been shown to share weak sequence homology with the glutathione S-transferase (GST) superfamily [33], and structural studies have confirmed that the CLICs adopt the canonical GST fold [17, 34]. They are intracellular channel proteins that exist either in a soluble state in the cytoplasm or bound to membranes. The CLICs are unusual in that they lack a signal sequence and any obvious membrane spanning domains but still possess the intriguing property to spontaneously insert into lipid membranes to form integral membrane pores [12, 17]. However, the process that governs the CLICs' spontaneous insertion into membranes is still largely unknown.

The CLIC proteins are highly conserved across species with CLIC-like proteins identified in numerous vertebrates such as amphibians, birds, fish and mammals [4] as well as in invertebrates such as nematodes and insects [3, 35], furthermore, CLIC-like proteins have also been identified in plants [36]. Members of the vertebrate CLIC family show high sequence identity between 47% and 76% as shown in Figure 1.2 [4, 10]. However, there is a certain amount of variation between the vertebrate CLIC family members. For example, bony ray-finned fish have a second copy of CLIC5 (CLIC5L) while birds and lizards lack CLIC1 [4]. There are also several variants of CLIC proteins that are spliced, a process whereby introns in pre-mRNA are removed to produce a continuous protein coding sequence (for example in CLIC2, CLIC5 and CLIC6) [4].

Among the six conserved CLIC proteins in vertebrates, p64 was the founding member identified from bovine tracheal epithelium and kidney cortex cells due to its affinity for the chloride ion channel blocker indanyloxyacetic acid 94 (IAA-94) [37, 38]. The CLIC5B protein is the human homologue of p64, which is a 46kDa splice variant of CLIC5A [39]. CLIC5A was initially identified as a component of a cytoskeleton complex and was later found to function as a chloride ion channel [40].

Parchorin is another CLIC protein that was originally identified as a secretory epithelium phosphoprotein in gastric parietal and airway epithelia cells in rabbits [41]. The human homologue of parchorin is CLIC6 [42]. CLIC6 has a characteristic 6 residue N-terminal motif that is repeated 15 times. It has been implicated in playing a role in the regulation of secretion by modulating chloride ion channels [43]. CLIC2 is a 28.2 kDa protein that is widely distributed in human tissues including heart and skeletal muscle. It is structurally similar to the Omega class GST (18.6% sequence identity) and CLIC1 protein (58.8% sequence identity) [44]. It is a strong inhibitor of cardiac ryanodine receptor (RyR) channels and may play an important role in intracellular calcium homeostasis [44]. CLIC4 is another member of the CLIC family that is ubiquitously expressed in different cell and tissue types [45]. It is associated with several physiological functions and shows 67% of sequence identity to CLIC1. Of all the CLICs, the MAP kinase associated CLIC3 is the least studied CLIC protein and little is known about its exact function. It has been shown to share the lowest percentage of sequence identity to CLIC1 (49%) [46]. The human CLIC1 protein is perhaps the most extensively studied member of the CLIC family and was the first member to be discovered in humans. The CLIC1 protein has a broad tissue and subcellular distribution and is involved in several physiological functions within cells [12, 47, 48]. The molecular characteristics and functional properties of all the human CLIC family members are summarised in Table 1.

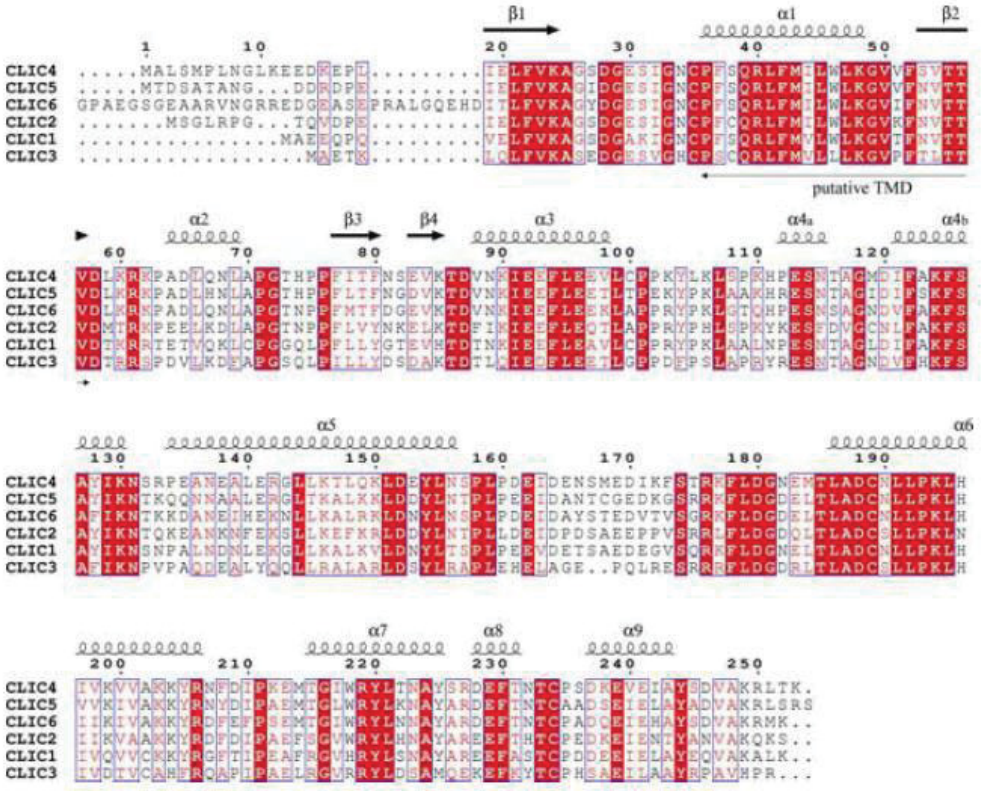

Figure 1.2 Multiple sequence alignment of the six human CLIC proteins. Sequence numbers and secondary structural elements correspond to CLIC4. The putative transmembrane domain (PTMD) is marked from residues 36-57. Source PDB1K0M.

Table 1.1: A summary of the molecular characteristics, tissue expression and localization and known functions of human CLIC proteins.

CLIC	Molecular Mass (kDa)	Number of residues	Genomic Location	Oligomerisation states known	Subcellular Localisation and Distribution	Molecular Function	Interaction Partners	Ref
1	26.9	241	6p21.3	Monomer Dimer	Plasma and Nuclear membrane Cytoplasm and nucleoplasm Intracellular Vesicles Expressed in most body tissue	Ion channel activity Cell cycle regulation Cell division and apoptosis Promotes cell motility and invasion Biomarker for colorectal cancer Potential therapeutic target in Alzheimer's disease and cancer therapy	AKAP350 PPI2 Sedlin LSM1	*2, 11, 12, 15, 16, 48-52*
2	28.2	243	Xq28	Monomer	Plasma membrane Cytoplasm Expressed in most body tissues, except brain Highly expressed in spleen and lungs	Ion channel activity Regulated cardiac ion channels	RyR	*44, 49, 53*
3	26.7	207	9q34.3	Monomer	Predominantly localizes to nucleus Highly expressed in placenta, heart and lungs Low expression in skeletal muscle, kidneys and pancreas.	Chloride channel activity Regulation of cell proliferation Cell growth control Protein binding	ERK7 MAP-Kinase	*46, 49, 54, 55*
4	28.6	253	1p36.11	Monomer Trimer	Plasma and intracellular membranes Cytoplasm ER and mitochondria Neurons Apical region of proximal tubule cells Highly expressed in brain, lungs, liver and skin	Chloride channel activity Angiogenesis and acidification of cells Cell differentiation Cytoskeleton organisation	AKAP350 PPI2 DIC Dynamin I Importin-α Actin Histamine (H3R)	*49, 56-59*
5A	32.0	251	6p12.3	Monomer	Microvillus Cytoskeleton Golgi apparatus Cortical actin cytoskeleton	Chloride channel activity Ion absorption and secretion Involved in formation of stereocilia Development of the organ of Corti	Actin Ezrin Gelsolin IQGAP1 PPI2 PHR	*49, 58, 60, 61*
5B	46.5	410			Golgi apparatus Plasma membrane Cytosol of HeLa cells Post-acrosomal region of sperm head Placenta			
6	73	704	21.q22.12	Monomer Dimer	Associated with C-terminus of Dopamine D2-liike Receptor Plasma membrane Cytoplasm Expressed in brain, liver, kidneys,	Chloride Channel Activity Dopamine Receptor binding Regulation of body fluid Involved in secretion of hormones from cells in pituitary gland.	D2/D3/D4 dopamine receptor PHR	*41, 42, 49*

Invertebrates also possess CLIC-like proteins. The nematode *Caenorhabditis elegans* is known to contain two CLIC homologues, EXC-4 and EXL-1 (EXC-4 like protein 1) while the arthropod *Drosophila melanogaster* contains a single CLIC1-like protein referred to as *Dm*CLIC [3]. Multiple sequence alignment of the vertebrate, invertebrate and plant CLIC-like proteins are shown in Figure 1.3. The sequences of the invertebrate CLIC-like proteins are rather different from the vertebrate CLIC proteins with lower sequence identities (Figure 1.3). Although in most instances the three characteristic cysteine residues (Cys^{24}, Cys^{178} and Cys^{223}) of the CLIC protein family are usually conserved. Human CLIC1 shares a sequence identity of 25% with *Dm*CLIC, 43% with EXC-4 and 42% with EXL-1 [1, 3, 53]. Mutating the genes encoding the invertebrate CLIC-like proteins have shown that mutation of EXC-4 protein resulted in the development of a cystic excretory canal in C. elegans [1, 53] and mutation of *Dm*CLIC protein caused the mutant fly to have a considerably (60-70%) shorter life span in comparison to the wild-type flies [3]. Furthermore, a single CLIC protein was found in the urochordate, *Ciona intestinalis* that is highly homologous (~ 45% sequence identity) to the vertebrate CLIC family members [4]. In addition, plant species also express CLIC-like proteins. Four CLIC-like proteins (DHAR1-4) with a sequence identity of about 26% to human CLIC1 were found in the plant *Arabidopsis thaliana* [36].

Figure 1.3 Multiple sequence alignment of the vertebrate, invertebrate and plant CLIC-like proteins. Sequence numbers and secondary structural elements correspond to CLIC1. The putative transmembrane domain (PTMD) is highlighted within the green box and conserved amino acid residues in red box.

1.3 The CLIC1 protein

1.3.1 Tissue and subcellular distribution

CLIC1 is the first cloned human member of the highly conserved CLIC family. The protein was cloned after screening activated monocytoid cells and characterised from a subtracted cDNA library enriched for macrophage activation-associated genes [62]. This novel protein contains 241 amino acid residues with a predicted molecular mass of 27 kDa and pI of 4.85. It is about 60% identical to the C-terminal region of the bovine p64 chloride channel [62]. Immunofluorescent and electrophysiological studies of CLIC1 transfected Chinese hamster ovary (CHO)-K1 cells showed that the protein localises primarily to the nuclear membrane and nucleoplasm. Hence, the protein was originally designated as Nuclear Chloride Channel-27 (NCC27), where 27 kDa refers to the apparent molecular weight of CLIC1 [62]. However, the soluble form of the protein is also found in the cytosol [62] and is now more commonly known as CLIC1. Other studies have also supported the identification of prominent CLIC1 nuclear localisation [47]. CLIC1 has also consistently been observed to localise to the apical membranes of several simple columnar epithelial cells of different tissues [47, 52].

CLIC1 is expressed in a wide variety of different tissues and cells, with the highest expression reported in muscle, liver and kidney. In the kidney, CLIC1 is highly expressed in the apical membrane of the proximal tubule, in glomeruli and in peri-arterial smooth muscle [47]. In sperm cells, CLIC1 localises to the acrosomal region of the sperm head [63]. A recent and comprehensive study of CLIC-like protein distribution in mice found mCLIC1, which shares 98% sequence identity to human CLIC1 protein, expressed in the apical domains of epithelial cells such as the stomach, small intestine, colon, bile ducts, pancreatic ducts, lungs and is present diffusely in skeletal muscle [52]. Distribution of CLIC1 in different human cell lines show that CLIC1 localises on the plasma membrane of Panc1 cells, human cell line derived from pancreatic cancer, and in an intracellular compartment below the apical plasma membrane in T84 cells, a human colon cancer cell line [52]. This high variability of CLIC1 localisation and distribution could suggest it has different cellular roles within different cell types or multiple roles within a particular cell type.

1.3.2 Physiological function of CLIC1

The biological function of CLIC1 is still unclear and its apparent capacity to fulfil various cellular roles makes it harder to definitively establish its function. Ion channel activity has been established for CLIC1 as well as for CLIC 2, 4, 5 and the invertebrate orthologues, EXC-4 from *Caenorhabditis elegans* [35] and *Dm*CLIC from *Drosophila melanogaster* [3]. These studies have been done both *in situ* [15, 48, 64] and by means of artificial lipid membrane systems [9-12, 16, 17, 65]. CLIC1 is a Cl- conducting ion channel and conducts both inward and outward current. A recent study using artificial lipid membrane system suggested that CLIC1 is a poorly selective multi-ion channel based on the proteins ability to conduct both anions and cations [11]. Furthermore, several studies have shown that the ion channel activity of CLIC1 is regulated by several factors such as pH, redox environment, lipid composition and cholesterol [4, 6, 7, 10, 11, 13, 14, 18].

Recent work has shown that CLIC1 channels may be concurrently regulated by cAMP and CFTRs, resulting in increased channel activity and membrane association [66]. CLIC1 (and CLIC5) channels also appear to be regulated by the presence of F-actin on the cytosolic (cis) side of the membrane in planar lipid bilayers [58]. The conductivity of CLIC1 ion channel varies at different stages of the cell cycle with CLIC1 being expressed only at the plasma membrane of cells in the G2/M phase [48]. It was demonstrated that blocking CLIC1 with Cl- ion channel blocker (IAA-94) resulted in the arrest of CHO-K1 cells in the G2/M stage of the cell cycle. Thus, it is evident that CLIC1 might also be involved in the regulation of cell cycle [48].

Our group has demonstrated for the first time that CLIC1, CLIC2 and CLIC4 possess "glutaredoxin-like" oxidoreductase activity using the 2-hydroxyethyl disulfide enzyme assay [67]. Structural studies have shown that in the soluble form, CLIC proteins adopt a glutathione S-transferase (GST) fold and have an active site with a conserved glutaredoxin monothiol motif, similar to that of the omega class GSTs (details discussed below) [67]. Al Khamici *et al* (2015) have demonstrated that CLIC proteins exhibit two independent functions; one as ion channels when in their membrane bound form and the other as oxidoreductase

soluble enzymes, which lead the CLIC proteins to be classified as "moonlighting proteins" [67].

CLIC1 has also been associated with roles as diverse as microglia-mediated β-amyloid-induced neurotoxicity [68] and sperm function [63]. CLIC1 was found to translocate from the cytoplasm to the plasma membrane in response to β-amyloid treatment in microglial cells [69]. By blocking these channels with the inhibitor IAA-94 or by suppressing CLIC1 expression using RNA interference, events involved in β-amyloid induced microglial activation (such as neuronal apoptosis or the release of TNF-α) were affected [68]. Further studies have additionally shown that blocking the β-amyloid induced CLIC1 channels affect the production of neurotoxic reactive oxygen species [69]. It has also been demonstrated that CLIC1 plays a role in angiogenesis via regulation of cell surface integrins [70]. The same study also showed that reduced CLIC1 expression decreases endothelial cell migration, cell growth, branching morphogenesis, capillary-like network formation and capillary-like spouting [70].

Recent publications indicate that CLIC1 function may involve protein-protein interactions. CLIC1 is highly expressed in macrophages where it has been found associated with ERM proteins, the Rho GTPases, Rac2 and RhoA, and NADPH oxidase components [51]. Comparison between macrophages from wildtype and CLIC1 knockout mice show that CLIC1 knockout macrophages displayed impaired phagosomal proteolytic capacity and reduced reactive oxygen species production [51]. Furthermore, CLIC1 knockout mice were protected from development of serum transfer-induced arthritis suggesting a role for CLIC1 in regulating macrophage function through its ion channel activity.

In humans, members of the CLIC family have been linked to several types of cancer. CLIC1 has been associated with nasopharyngeal carcinoma, gastric cancer, hepatocarcinoma, colorectal cancer, gallbladder carcinoma, ovarian and breast cancer [71-76]. CLIC1 protein expression was found to be up-regulated across a variety of tumour tissues regardless of tumour grade, pathological tumour-node-metastasis stage or localisation. Therefore, CLIC1 protein has the potential to be used as an effective biomarker or as a potent therapeutic target in cancer therapy

[71-76]. However, to understand the therapeutic potential of the protein, it is important to further deduce details regarding the functional and structural features of CLIC1.

1.4 Structure of CLIC1 protein

1.4.1 The N-terminal and C-terminal domain of CLIC1 protein

To date, the crystal structures of the soluble form of four monomeric vertebrate CLICs – CLIC1 [17], CLIC2 [53], CLIC3 [54] and CLIC4 [9], and two invertebrate CLIC-like proteins - *Drosophila melanogaster Dm*CLIC and *Caenorhabditis elegans* EXC4 [3] have been determined. The crystal structures of the CLICs confirm that they share structural similarity with the GST superfamily and like the GSTs they also contain two distinct domains (Figure 1.4) [17]. CLIC proteins are largely α-helical (47.7%) with only ~8% of its secondary structural content being β-strand in its reduced monomeric form. The crystal structure of the soluble CLIC1 protein has been resolved by X-ray crystallography to 1.4 Å resolution [17]. It was found that the soluble CLIC1 protein is monomeric and adopts a fold similar to the GST-family.

CLIC1 consists of two distinct domains referred to as the N- and C-terminal domains, which are joined by a short interdomain loop and has approximate dimensions of 50 Å x 50 Å x 20 Å. The crystal structure of CLIC1 protein is illustrated in Figure 1.5 [17]. The N-terminal domain has a thioredoxin-like fold that consists of four β-strands sandwiched between three α-helices [17] (Figure 1.5). The thioredoxin fold is a scaffold used by many proteins to carry out a wide variety of physiological functions. This versatile fold adopts a βαβαββα arrangement and can adapt to provide new functions while retaining its structure and stability [77]. Also, near the N-terminus of β-strand 3 is an invariant cis-proline (cis-Pro^{65} in CLIC1) that is conserved in all thioredoxin folds and therefore is likely to be structurally important.

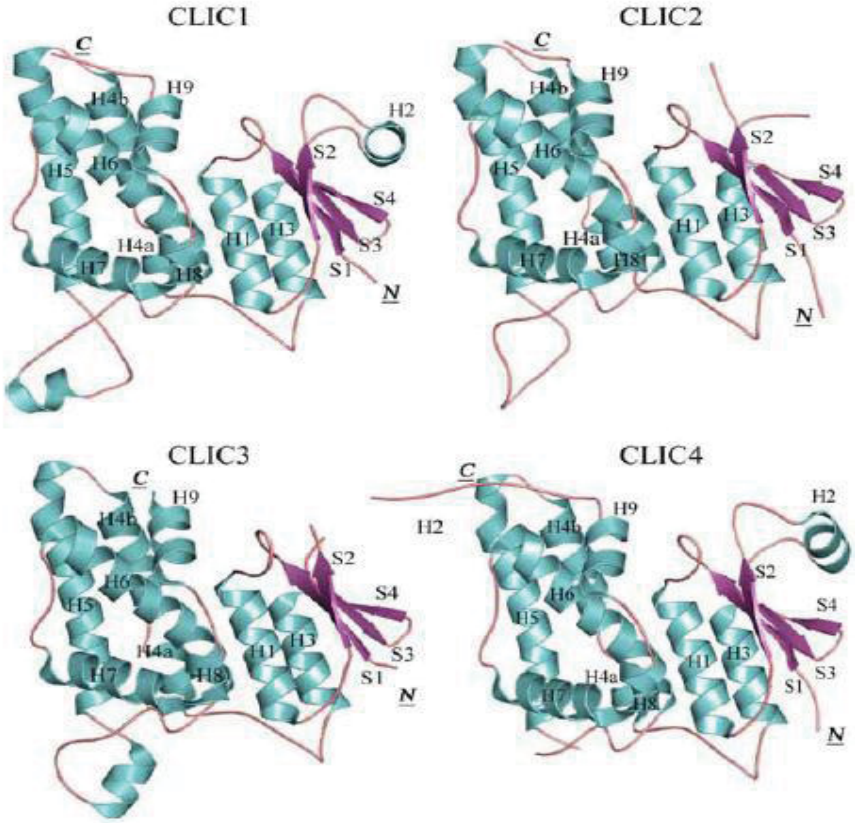

Figure 1.4 Crystal structures of human CLIC family members. Secondary structural elements are coloured and labelled according to type: α-helix (cyan; H1-H9); β-strand (purple, S1-S4) and random coil (pink). The N-and C-terminus are also labelled. Structures shown include CLIC1 (PDB:1K0M), CLIC2 (PDB: 2R4V), CLIC3 (PDB: 3FY7) and CLIC4 (PDB: 2AHE)

In contrast, the C-terminal domain of CLIC1 is entirely α-helical and contains a highly negatively charged loop known as the "foot" loop between helices 5 and 6 (Pro^{147}- Gln^{164}) (see Figure 1.5). This loop is spatially adjacent to a proline-rich loop (Cys^{89}-Asn^{100}) linking the two domains, and which may play a role in protein-protein interactions [17]. In CLIC1, this loop consists of seven acidic residues giving the protein a net charge of negative 7. The proline-rich loop links the N- and C-terminal domains of CLIC1 by joining α-helix 3 to α-helix 4a. There is evidence from the structure that the proline rich inter-domain loop exists as two different conformers as well as the N-terminal helices 1 and 3. In the proline-rich loop amino acid Pro^{90} and Pro^{94} form a sharp turn with Pro^{91} either in the trans or cis conformation [17].

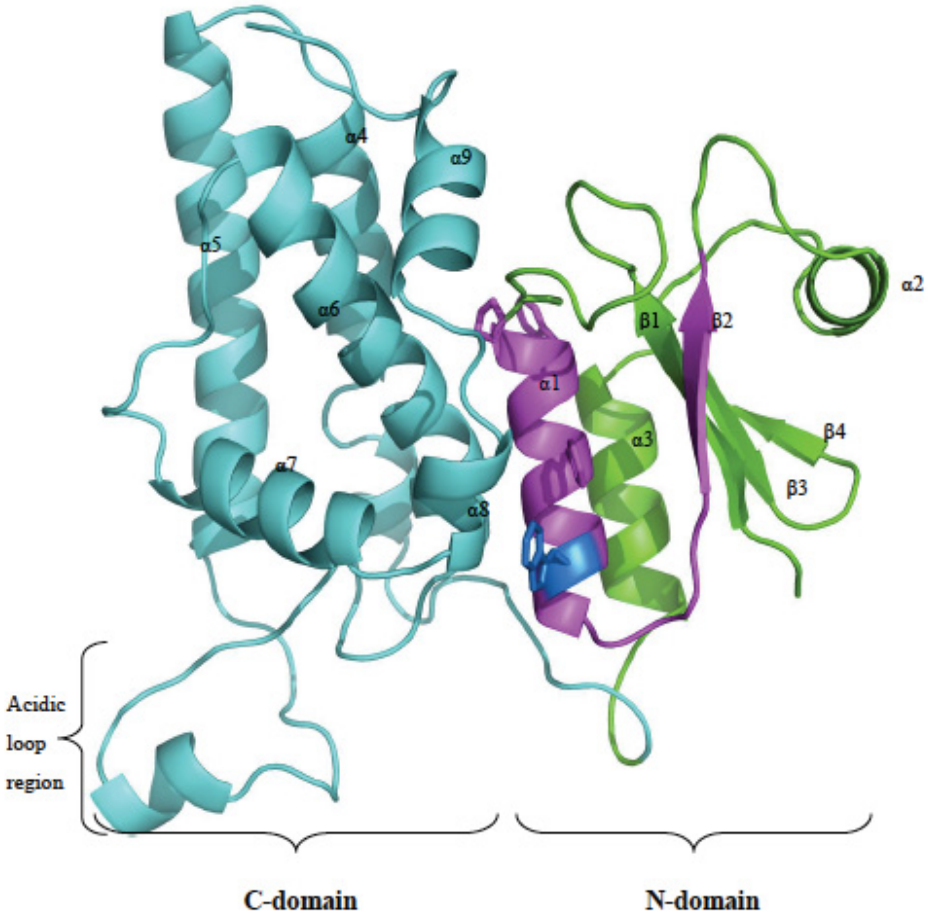

Figure 1.5 Schematic diagram of reduced CLIC1 in ribbon showing the putative transmembrane region of CLIC1. The N-and C-domains are shown in green and cyan, respectively. The putative transmembrane region (TMR) comprising the α1 helix and the β2 strand, located in the N-terminal domain is shown in pink. The single tryptophan (Trp35) is shown in blue. The acidic loop region exists in the C-domain of the protein. The PDB code was 1k0m.

1.4.2 The putative transmembrane regions of CLIC1 protein

Structural studies of the CLIC proteins show that they contain two hydrophobic regions. First is the putative trans-membrane domain (PTMD) which is conserved among all the CLIC proteins and the invertebrate CLIC-like proteins, *Drosophila melanogaster Dm*CLIC and *Caenorhabditis elegans* EXC4. Second is the proline rich inter-domain loop (Figure 1.5) [78]. In the N terminal domain, a highly hydrophobic region exists between the residues Cys^{24} to Val^{46} comprising of α-helix 1 and β-strand 2 (Figure 1.4 & 1.5). This region is common to all CLICs and it is likely to form a single transmembrane domain (PTMD) as shown in Figure 1.6 [78]. This putative transmembrane domain (PTMD) spans the N- and C-terminal domain interfaces and serves as a network of contacts between the α1, α3 and α5 helices. The amino acid residues Glu^{81}-Arg^{29} and Glu^{85}-Lys^{37} joins α-helix 1 and α-helix 3 at the N-domain with α-helix 5 at the C-domain [14, 78]. The unique tryptophan amino acid Trp^{35} (Figure 1.5) located in α-helix 1 is considered the major contact element of the PTMD making the most contact between the N- and C-terminal domains [14, 17]. The second hydrophobic region in CLIC1 is the proline rich inter-domain loop located within the C-terminal domain and comprised of α-helix 6 and some parts of the preceding loop [17, 78]. These hydrophobic regions are at the interface between the N-terminal and C-terminal domains [17] thus, the conformation of the proline-rich loop and the relative orientation of the two domains provide considerable plasticity that may facilitate the necessary structural rearrangement of the soluble monomeric structure into an integral membrane form.

Human	24	46
CLIC1	CPFSQRLFMVLWLKGVTFNVTTV	
CLIC2	CPFCQRLFMILWLKGVKFNVTTV	
CLIC3	CPSCQRLFMVLLLKGVPFTLTTV	
CLIC4	CPFSQRLFMILWLKGVVFSVTTV	
CLIC5	CPFSQRLFMILWLKGVVFNVTTV	
CLIC6	CPFSQRLFMILWLKGVIFNVTTV	

Figure 1.6 The hydrophobic region (PTMD) at the N-terminal domain conserved amongst all human CLIC proteins. In CLIC1 the PTMD starts from Cys24 to Val46 [17].

1.5 Structural similarity between GST superfamily and CLIC proteins

Based on the protein primary sequence and predicted structural models, it was proposed that CLIC1 could be a member of the glutathione S-transferase (GST) family [79]. The first crystal structure of the soluble form of CLIC1 confirmed the suggestion that there is a structural relationship between the GST superfamily and the CLICs. The 1.4 Å structural model of human CLIC1 was shown to adopt the canonical thioredoxin-like fold and the protein was classified as the newest member of the GST family [17].

The cytosolic glutathione S-transferase (GST) family of proteins are related to glutaredoxin by their thioredoxin domain that binds glutathione (GSH) in a topologically conserved location name the G-site [80]. Similarly, a 1.8 Å structure of CLIC1 showed a single glutathione (GSH) molecule covalently bound to CLIC1 protein [17]. In CLIC1, the N-terminal α-helix 1 contains a conserved glutaredoxin-like motif (CxxC) ^{24}CPFS^{27}. A comparison of the crystal structures of the Ω-GST and CLIC1 proteins are shown in Figure 1.7. This CxxC motif forms the covalent interaction with GSH through a disulphide bond between Cys^{24} and the GSH thiol group [17]. This GSH binding site (Cys24) in CLIC1 overlaps with the G-site in GST proteins and is partially conserved across mammalian CLIC proteins. There are four key residues conserved in all the GSTs and CLICs:

1) a Cis-proline residue which provides the active site for binding GSH in GSTs, 2) an aspartic acid residue that forms the N-terminal 3) two glycine residues that play structural roles and 4) a Cys-Pro-Phe motif that includes the cysteine active site of the Ω-GST class which was also found in the CLIC proteins [17, 45, 50, 73, 79, 80]. In the case of CLIC2 protein, the GSH molecules do not covalently bind to CLIC2, but rather interacts with the hydrophobic grooves on the protein surface [53]. The all α-helical C-terminus of CLIC1 closely resembles the canonical fold of the Omega class GSTs (Ω-GST) (16% identity) (Figure 1.7) [81].

Although CLIC proteins are considered members of the GST super-family there are major differences between the CLICs and GST proteins. CLICs are monomeric while GST proteins form dimers with the exception of glutaredoxin-2 (Grx2) [82]. Another distinguishing characteristic of CLIC1 that makes it different from GSTs is the presence of the highly negatively charged loop: the "foot" loop [17]. The C-terminal α-helix 9 of CLIC1 is also structurally unique and is another hotspot for negative charge [17]. Apart from structural differences, CLIC1 also differs from GSTs in that the CLIC1 active site cysteine residue (Cys^{24}) binds covalently with a low affinity to GSH, whereas the classical GSTs bind non-covalently and with a higher affinity with GSH [17]. CLIC1 is an amphitropic protein and exists in a soluble and membrane-bound state within the cell. The soluble structure of CLIC1 does not resemble the typical structure of other membrane proteins. Despite this CLIC1 can spontaneously insert into lipid membranes to form integral membrane pores [12, 17]. However, by comparison, the structurally similar members of the GST protein family do not normally possess the ability to auto-insert into the membrane [79].

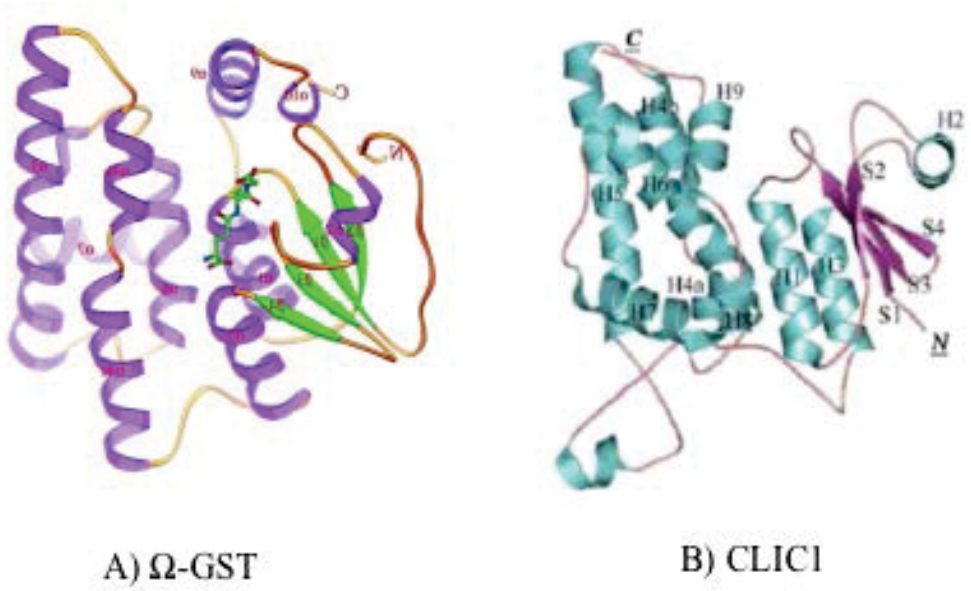

Figure 1.7 Comparison of A) Ω-GST and B) CLIC1 structure. Ω-GST and CLIC1 consist of a thioredoxin fold in the N terminal domain indicated in *green* in Ω-GST structure and in *purple* in CLIC1. The all α-helical C-terminal is indicated in purple in Ω-GST structure and in cyan in CLIC1. Source Ω-GST [81] and CLIC1 (PDB1k0m).

1.6 Conversion of soluble CLIC1 into membrane integral form

CLIC1 is known to exist both in soluble form and as an integral membrane protein. Although high-resolution structural data exists for the soluble form of the protein, not much is known about the structure of the integral membrane form or the exact mechanism of membrane insertion. CLIC1 being a relatively small protein (27kDa) has an unusual distribution within the cells [52] and it makes it very difficult to determine the structure of the integral membrane form. The structural homology between CLIC proteins and the GST proteins and the location of the PTMD (helix 1 and ß-strand 2) within the central part of the N-terminal domain, leads to the hypothesis that in order for CLIC proteins to traverse the membrane and form channels, major structural rearrangements of the N-terminal domain would have to occur.

The mechanism by which the putative transmembrane region of CLIC1 inserts into and spans the membrane was first proposed by Tulk *et. al.* (1998) [47] following their research on the resistance of CLIC1 to alkaline extraction. Resistance to alkali extraction of CLIC1 when it is in a membrane form suggests that the protein spans the membrane [47]. Subsequently, it was revealed that CLIC1 behaves as an integral membrane protein which interacts with the membrane by inserting into- and spanning the membrane [83]. Electrophysiological studies performed on transfected CHO-K1 cells using antibody to the FLAG epitope tag on recombinantly expressed CLIC1 have shown that CLIC1 inserts and spans the membrane an odd number of times and is associated with ion channel activity [83]. Later, a study using CLIC-like proteins showed that the first 55 residues at the N-terminal domain are necessary for membrane insertion with the tryptophan (Trp/W35) residue localised within the membrane (Figure 1.8) [35]. Moreover, functional studies have shown that the PTMD region in the N-domain is a key component in terms of localisation to the membrane and functioning in vivo by invertebrate CLIC proteins [84].

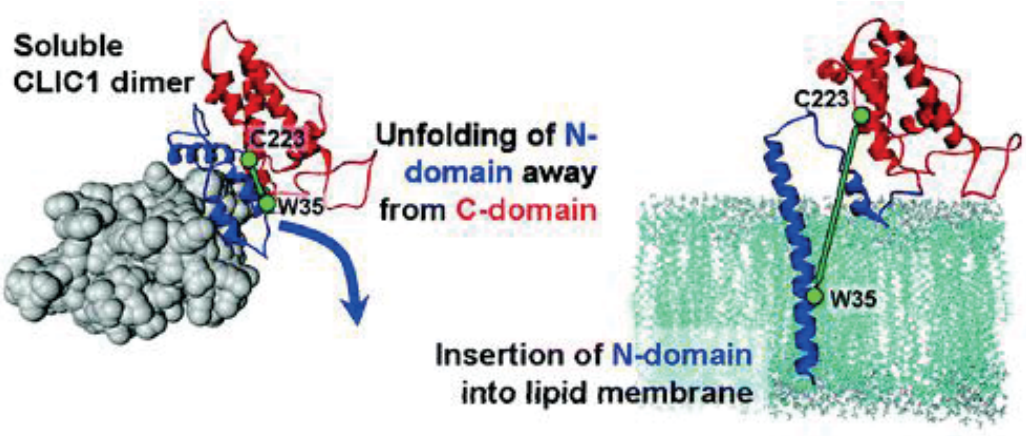

Figure 1.8 Membrane insertion model of CLIC1 protein. Conformational unfolding occurs between the N-and C-terminal domains of CLIC1 upon interaction with the membrane. The N-terminal domain of CLIC1 inserts into the lipid bilayer, while the C-terminal domain remains cytoplasmic [6].

In addition, hydrogen exchange studies have found the N-domain to be more flexible and less stable than the C-domain [78] probably in order to partially unfold prior to membrane insertion at low pH [14]. A recent study performed using fluorescence resonance energy transfer (FRET) spectroscopy and electron paramagnetic resonance (EPR) also supports the concept that upon CLIC1 interacting with membranes, the N- and C-domains are located on the opposite sides of the membrane with cysteine residue 24 localised at the trans face of the membrane [6-8]. Thus, it can be concluded that in order to form a channel by inserting into the membrane, the hydrophobic transmembrane region (ß1-a1-ß2) of CLIC1 must undergo a structural reorganisation involving a rapid unfolding and refolding of the N-terminal domain (Figure 1.8) [6].

The relatively small size of CLIC1 and the single TMD, suggests that the protein oligomerises to form fully functional ion channels. Whether this oligomerisation occurs before membrane insertion or after, remains unclear. It has been proposed that the CLIC1 ion channel is likely to consist of a tetrameric assembly of subunits (Figure 1.9) [16]. Studies have shown that CLIC1 when added to lipid bilayer membranes first produced small conductance channels with slow kinetics

(SCSK) and then underwent a transition to form high conductance channel with fast kinetics (4 times than that of SCSK) [16]. This then lead Singh *et. al.* (2006) to propose, according to their model, the conducting CLIC1 channels must contain a minimum of 4 subunits to correspond to the increase in conductance [11]. Furthermore, the oligomerisation of CLIC1 in the membrane was monitored using intermolecular FRET. The intermolecular FRET, performed between fluorescently labelled CLIC1 monomers in the membrane, showed CLIC1 forms oligomers upon oxidation in artificial membranes [6].

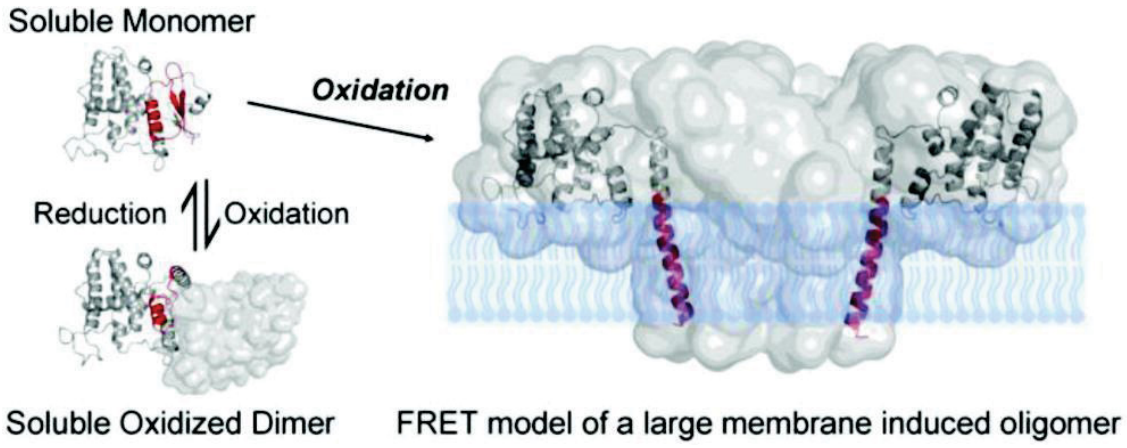

Figure 1.9 Oligomerisation model of CLIC1 protein upon membrane interaction. The intermolecular FRET shows that CLIC1 forms oligomers upon oxidation in the presence of membranes. The model of the CLIC1 transmembrane form indicates that the structure is large and is most likely to comprise of approximately six to eight CLIC1 subunits [6].

1.7 Factors regulating the membrane insertion of CLIC1

1.7.1 Redox regulated membrane insertion of CLIC1

As mentioned previously in Section 1.3.3, the GST family of proteins including CLICs contain a conserved thioredoxin fold in their N terminal domains [79]. This fold is utilised to regulate diverse redox reactions and plays a crucial role in several cellular functions such as cell growth, cell cycle, apoptosis and oxidative stress (See [85] for review). Moreover, recent studies demonstrate that redox controlled intrinsic flexibility of the thioredoxin fold promotes the formation of a membrane-bound conformation of CLIC proteins. In 2004, it was shown that upon oxidation, monomeric CLIC1 undergoes a reversible structural transition to a stable dimeric form due to formation of an intramolecular disulphide bond (Cys^{24}-Cys^{59}) [10]. Due to the ability of the soluble form to exist as two different stable conformations, CLIC1 protein is also classified as a metamorphic protein [8].

The crystal structure of the oxidised dimeric form of CLIC1 reveals a major structural rearrangement of the N terminal domain, exposing a large hydrophobic surface which is stabilised *in vitro* by dimerization [10], as shown in Figure 1.10. This hydrophobic surface may represent the membrane-docking interface *in vivo* where the monomer is believed to undergo similar alterations to its N-terminal domain before interacting with the membrane [10]. It is proposed that in the presence of a lipid bilayer the oxidised CLIC1 monomer will dock to the membrane, whereas in the absence of lipids it will form a dimer. The most apparent structural change between the soluble monomer and oxidised dimer subunits (Figure 1.10) is related to the α-helix 2 region. In the dimer, all the β-strands present in the monomeric form have become disordered and the N-terminal domain is entirely α-helical (Figure 1.10). The α-helix 2 region in the dimer is extended by two α-helical turns and residues between α-helix 2 and 3 form an extended loop and are loosely packed against the C-terminal domain [6, 8, 10, 11]. Interestingly, the structural arrangement of the subunits in the CLIC1 dimer bears no resemblance to that seen in dimers from other members of the GST superfamily. The oxidised CLIC dimer has been shown to form chloride selective ion channels in both artificial bilayers and vesicles, with mutational studies demonstrating that both Cys^{24} and Cys^{59} are required for channel activity [11].

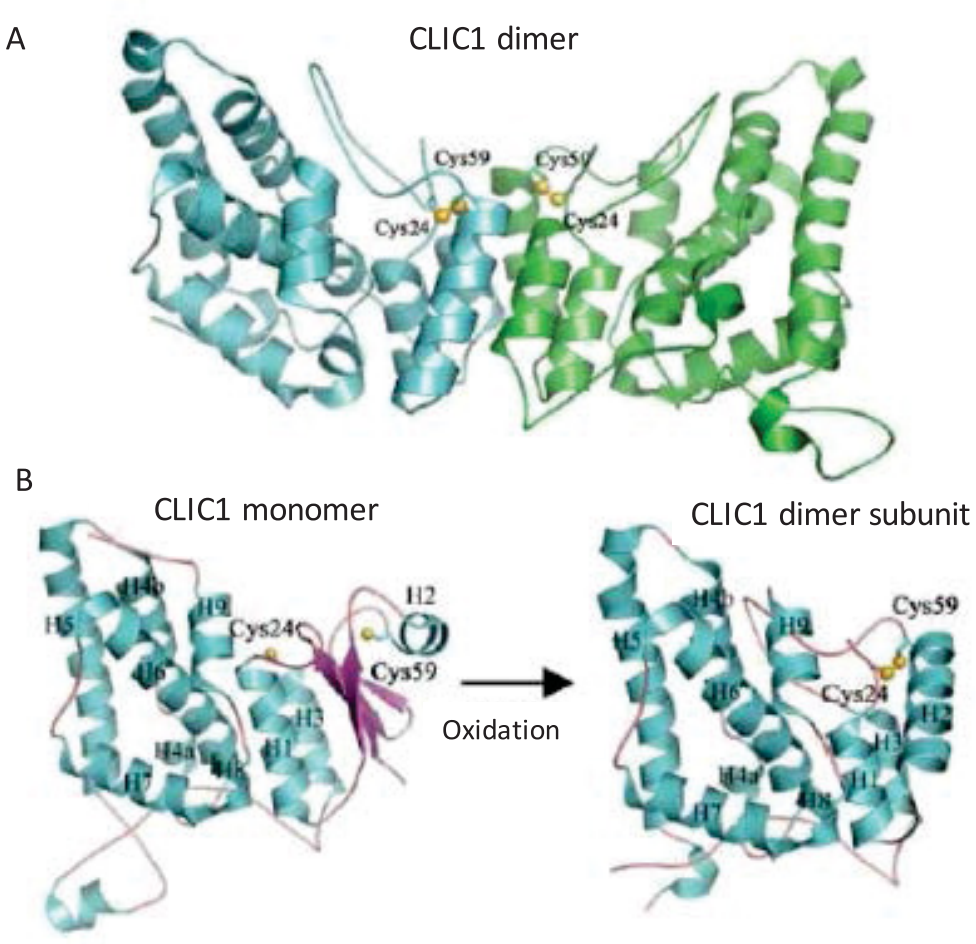

Figure 1.10 The oxidised CLIC1 dimer. (A) The all α-helical CLIC1 dimer showing the locations of critical cysteine residues (Cys24 and Cys59) that form intramolecular disulphide bonds (PDB:1RK4). The two subunits are shown in cyan and green. **(B)** The secondary structural elements of CLIC1 is shown coloured, with the location of Cys24 and Cys59 labelled. CLIC1 undergoes a redox controlled structural rearrangement which facilitates the formation of a disulphide bond between Cys24 and Cys59, which is shown in the CLIC1 dimer subunit [10].

Controversially, an increase in channel activity has been detected with an increase in the reducing agent dithiothreitol (DTT) [11]. On the other hand, an increase in the concentrations of the sulfhydryl modifying agents such as GSH and NEM, inhibit channel conductance from the trans side of the membrane (although not in the Cys^{24} mutant) [11, 12]. In addition, chloride channel blockers like IAA-94, A9C and potassium chloride, all dramatically reduced or totally inhibited channel activity [11, 58, 62]. Mutations of Cys^{24} to an alanine residue also resulted in diminished chloride conductance [10, 11]. Hence, it can be postulated that reduced sulfhydryls, particularly reduced Cys^{24}, may be favourable for channel conductance. Henceforth, it was concluded that oxidising conditions lead to a closure of the CLIC1 pore possibly via disulphide bond formation involving Cys^{24} that is located on the extracellular (or luminal) side of the CLIC1 subunits, and reducing conditions result in channel opening and conductance [10, 11]. Although this may be true for vertebrate CLICs, the active site cysteine residues are believed to be unnecessary for invertebrate CLIC function [84]. Studies with EXC-4 protein mutants where the active cysteine residue is replaced by an aspartic acid residue, showed the protein still forms functional ion channels in artificial lipid bilayers by a process that is not redox controlled [35, 84].

Similarly, Cys^{59}, found at the C-terminal end in CLIC1 is not conserved across the CLIC family and corresponds to a conserved alanine in most other members of the family. Thus, it is unlikely that a similar oligomerisation or membrane docking mechanism exists for the other CLIC proteins. The only other member of the CLIC family that is known to form a homodimer is CLIC6 [43]. This protein dimerises in solution at its GST-like C-terminus but nothing else is known about the structure or properties of the CLIC6 dimer. CLIC4 has also been shown to form a homo-trimer under non-reducing conditions [86]. This trimer is formed in the absence of disulphide bonds and suggests that hydrophobic contacts may be all that is required for a CLIC protein to multimerise [86]. Moreover, the fact that the cytoplasm contains up to 10 mM GSH and presents a particularly reducing environment [87], it seems unlikely that soluble CLIC1 would exist as the oxidised dimer state in the cell cytosol. Hence, it is speculated that additional mechanisms apart from redox control are involved in regulating the spontaneous membrane insertion of the CLIC proteins.

1.7.2 Role of pH on spontaneous membrane insertion of CLICs

The structure, stability, solubility and functions of several proteins are also influenced by the net charge and ionisation states of individual amino acid residues and hence are pH-dependent. Recently, urea-induced equilibrium unfolding studies on reduced soluble CLIC1, in the absence of membranes, revealed that the protein molecule became destabilised at low pH (5.5) [14]. However, at pH 7 CLIC1 unfolds via a two-state transition in a cooperative manner much like the dimeric GST proteins [88-90] and monomeric glutaredoxin 2 [91]. Therefore, the conformational stability of CLIC1 has been shown to be pH-dependent [16]. When CLIC1 moves from the cytosol (pH 7) to the membrane surface (pH 5.5) prior to membrane insertion, changes in the pH changes the ionisation states of acidic residues within the PTMD region thus altering the conformational stability of the soluble CLIC1 thereby enabling it to be "primed" for membrane insertion (Figure 1.11) [3, 14-16, 53]. The pH-dependent spontaneous membrane insertion has also been observed for vertebrate CLIC2 and CLIC4 and invertebrate CLICs (EXC-4 and *Dm*CLIC) in which the channel activity was highest at low pH (5.5) and found to decrease with increase in pH [3, 9, 53].

Low pH has also been shown to be a requirement for membrane insertion in other metamorphic proteins such as the bacterial pore-forming toxins (PFTs), apoptotic proteins and annexin protein family. These proteins are largely α-helical in structure and are present in either a water-soluble form in the cytosol or a membrane-bound form (See review [92]). The low pH (pH 5-5.5) on the membrane surface is found to play a fundamental role in the conformational changes of PFTs that take place during their conversion from soluble to a membrane-bound form. Several α pore-forming toxins, for instance, colcin A [93], exotonin A [94], diphtheria toxins [95, 96], ANX12 [97], α-toxin [98], Cyt1 A δ-endotoxin [99] and equinatoxin [100] have been shown to exhibit pH sensitivity and partially unfold forming a molten globule state at low pH. A molten globule comprises a conserved secondary structure along with a loss of tertiary structural properties in which hydrophobic surfaces are more exposed than in the native conformation [101].

In contrast, the destabilised form of soluble CLIC1 at low pH results in the formation of an intermediate with a solvent-exposed hydrophobic surface [14]. The intermediate is not a molten globule as it was shown to have a defined tertiary

structure and unfolded in a cooperative manner at high urea concentrations [14]. Fanucchi *et al.* (2008) concluded that the acid-induced destabilisation and partial unfolding of CLIC1 involve α-helix 1. This is interesting because as mentioned previously, helix 1 forms part of the PTMD and may provide the plasticity the molecule requires to partially unfold [14]. Fanucchi *et al*. (2008) also suggested that the acidic environment found at the membrane surface may prime the CLIC1 TMR at the N-terminal domain by protonating certain amino acids thereby lowering the energy barrier for the conversion of soluble CLIC1 to its membrane-bound form [14]. However, pH alone does not seem to trigger structural changes in CLIC proteins. This can be verified by looking at the crystal structures of CLIC proteins and mutations thereof solved under various pH conditions ranging from pH 4.5 to pH 8.5 [4, 10, 17, 102]. Also, experimental work done on CLIC1 using amide hydrogen-deuterium exchange mass spectrometry (HXMS) confirms that the structure of CLIC1 is unchanged at pH 5.5 when compared to pH 7 [14, 78]. Thus, additional factors may be involved in facilitating the conformational changes required for spontaneous membrane insertion of the soluble CLIC1.

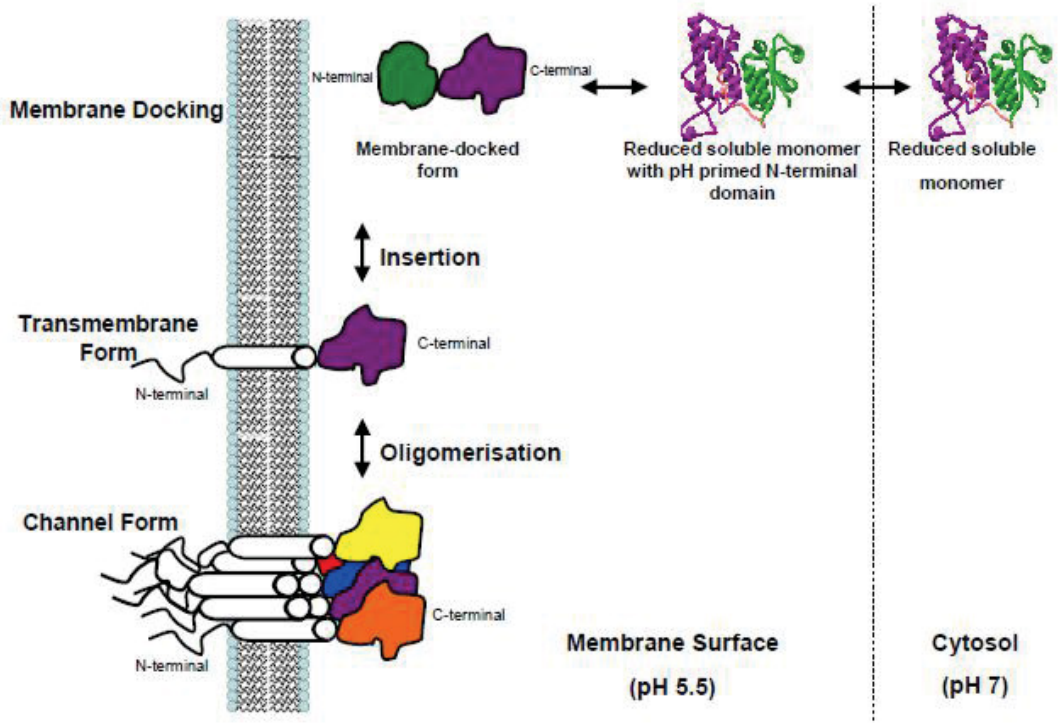

Figure 1.11: The proposed model for the CLIC1 transition from its soluble to membrane-bound form [4].

1.7.3 Role of Lipid composition on spontaneous membrane insertion of CLIC1

The phospholipid composition and membrane cholesterol are also known contributors that influence the autonomous membrane insertion of several spontaneous membrane inserting proteins. There are in fact a number of soluble human proteins which are known to spontaneously insert and self-assemble into lipid membranes in the absence of cellular machinery. One such group is the annexin family of proteins [103]. They are involved in ion channel formation, cell adhesion and other membrane related mechanisms [104, 105]. Studies have shown that the membrane-related functions of these proteins are either Ca2+-dependent or Ca2+-independent. Ca2+-independent membrane interaction is regulated by phospholipid composition [97] and/or by transient changes in pH [105]. Similarly, the Bcl-2 family of proteins are also found to incorporate into the membrane (*in vitro* and *in vivo*) particularly in the presence of acidic lipid bilayers with low dielectric constant and at low pH [106]. They act somehow as selective ion and/or protein channels that release apoptotic factors from the mitochondria to the cytoplasm [107]. The membrane cholesterol content was found essential for the spontaneous membrane insertion by the cholesterol-dependant cytolysins (CDCs) *19*. The CDCs are pore-forming toxins (examples: listeriolysin, perfringolysin, streptolysin and pneumolysin) secreted by several species of Gram-positive bacteria. The CDCs belong to a large family of pore-forming proteins that also include the human proteins- perforins and the complement membrane attack complex [19]. These pore-forming proteins require the presence of cholesterol in the membrane in order to bind and insert into the membrane. These proteins share the common feature of interacting with membranes via a two-step process, of which the first involves binding to cholesterol within the membrane followed by insertion [19, 108].

Despite differences in sequence and function, there is a striking structural similarity between the human annexin and Bcl-2 proteins and many pore-forming toxins. Both these family of proteins have two hydrophobic helices that form a helical hairpin in the centre of a bundle, surrounded by six to seven amphipathic α-helices which shield the helical hairpin [107, 109]. Therefore, in the presence of lipid membranes, these proteins undergo a structural reorganisation in order to expose the hydrophobic helices for penetration into the membrane [106, 110, 111].

Correspondingly, the C terminal region of CLIC1 protein consists of alpha helical bundles with long hydrophobic helix (h6) and two negatively charged regions at the base of CLIC1 and acidic α-helix 9 which makes CLIC1 proteins somewhat structurally similar to the PFTs [17]. Hence, it can be speculated that the phospholipid composition of the membrane dramatically influences the spontaneous membrane interaction of CLIC1.

Interestingly, the interaction of the protein CLIC1 with membranes has also been found to be lipid dependent, with studies showing increased ion channel activity of the CLIC proteins in the presence of cholesterol in membranes (a process that could be similar to CDCs) [18]. Recently in our laboratory, CLIC1 spontaneous membrane insertion was monitored using impedance spectroscopy on tethered lipid bilayers and by Langmuir studies [18]. These studies have revealed that CLIC1 neither inserts nor form functional ion channels in the absence of cholesterol in the membrane [18]. Thus suggesting that cholesterol is required as the binding molecule used by CLIC1 for its initial docking onto the membrane, and it may also be required or assists in the formation of the final quaternary CLIC1 channel structure within the membrane [18]. However, the precise mechanism of the interaction of CLIC1 protein with cholesterol remains unsolved and warrants further investigation.

1.8 Aims and Objective

The metamorphic response of the Chloride intracellular ion channel protein, CLIC1 upon its membrane interaction is still largely unknown. Members of the CLIC protein family possess the intriguing property that they can spontaneously insert from a stable soluble state into lipid membranes to form integral membrane channels. Factors such as redox environment, pH and lipid composition have been found to regulate the membrane interactions of the soluble CLIC1 protein to insert into the membrane. However, the precise mechanism of how CLIC1 autonomously inserts into membranes and what physiological mechanisms and actions this insertion causes is still largely unresolved. Recent studies using impedance spectroscopy on tethered bilayer membranes have revealed that cholesterol in membranes regulates the spontaneous insertion of CLIC1 into model membranes. However, the question still remains unanswered regarding how the physiological lipid composition regulates the structural conformation, membrane insertion, oligomerisation and arrangements of the CLIC proteins in cell membranes. Hence, this research project aims to:

1. Further, elucidate the specific factors such as the oxidative state of the proteins, pH and the lipid composition of the membrane and their role in regulating the CLIC1 structural configurations and oligomerisation state both in solution and in its membrane-associated forms. Artificial monolayer membrane systems will be utilised to study the interaction between the proteins and the lipid environment. This interaction will be assessed by Langmuir trough film surface pressure measurements and quartz crystal microbalance.

2. Elucidate structural features and oligomerisation state of CLIC1 protein in solution and in its membrane-associated forms using X-ray and Neutron reflectivity assays.

3. Determine the structure of the CLIC1-Cholesterol complex. This will be accomplished by applying a contrast series of Small Angle Neutron Scattering (SANS) and Small Angle X-ray Scattering (SAXS)

techniques to deduce features of the solution structure of the CLIC1-cholesterol complex.

Interestingly, analysis of amino acid sequences have revealed a GXXXG motif that is highly conserved amongst the CLIC proteins, pore forming proteins (examples: listeriolysin, perfringolysin-O) as well as several human membrane proteins (examples: glycophorin-A, ErbB receptor, G-protein couples receptors etc.) [112, 113]. Studies have shown that GXXXG motif facilitates the homo or hetero-oligomerisation of membrane proteins [112, 113] and acts as a cholesterol binding site in amyloid precursor proteins [114, 115]. Hence this project also aims to:

4. Determine the importance of the GXXXG motif for the interaction of CLIC1 with cholesterol. The aim is to engineer point mutations in the GXXXG motif to produce CLIC1 mutants and analyse how the mutations affect CLIC1 interactions with cholesterol using similar artificial monolayer membrane systems and compare the data to wild-type or recombinant CLIC1 protein.

5. A number of individual amino acid residues within CLIC1 have been identified as important in its function. Dependent upon time, a number of point mutations will be made and then studied in the systems outlined above.

6. This project also aims to use different natural sterols such as ergosterol, β-sitosterol etc., and cholesterol derivatives in the artificial membrane systems in order to define the structural features of cholesterol that interacts with CLIC1.

Furthermore, we anticipate being able to define mechanisms that are likely to influence protein localisation and function. In future, these structural findings can help give insights into the use of these proteins as therapeutic targets or biomarkers and may help in the design of "particles" with unique membrane insertion properties for the purposes of drug delivery or cell regulatory system.

1.9 References

[1] Cromer, B., Morton, C., Board, P., and Parker, M. (2002) From glutathione transferase to pore in a CLIC., *Eur Biophys J. 31*, 356-364.

[2] Edwards, J., and Kahl, C. (2010) Chloride channels of intracellular membranes., *FEBS Letters 584*, 2102-2111.

[3] Littler, D., Harrop, S., Brown, L., Pankhurst, G., Mynott, A., Luciani, P., Mandyam, R., Mazzanti, M., Tanda, S., Berryman, M., Breit, S., and Curmi, P. (2008) Comparison of vertebrate and invertebrate CLIC proteins: the crystal structures of *Caenorhabditis elegans* EXC-4 and *Drosophila melanogaster* DmCLIC., *Proteins 71*, 364-378.

[4] Littler, D., Harrop, S., Goodchild, S., Phang, J., Mynott, A., Jiang, L., Valenzuela, S., Mazzanti, M., Brown, L., Breit, S., and Curmi, P. (2010) The enigma of the CLIC proteins: Ion channels, redox proteins, enzymes, scaffolding proteins?, *FEBS Letters 584*, 2093-2101.

[5] Singh, H. (2010) Two decades with dimorphic Chloride Intracellular Channels (CLICs). *FEBS Letters 584*, 2112-2121.

[6] Goodchild, S., Angstmann, C., Breit, S., Curmi, P., and Brown, L. (2011) Transmembrane extension and oligomerization of the CLIC1 chloride intracellular channel protein upon membrane interaction., *Biochemistry 50*, 10887-10897.

[7] Goodchild, S., Howell, M., Cordina, N., Littler, D., Breit, S., Curmi, P., and Brown, L. (2009) Oxidation promotes insertion of the CLIC1 chloride intracellular channel into the membrane., *Eur Biophys J. 39*, 129-138.

[8] Goodchild, S., Howell, M., Littler, D., Mandyam, R., Sale, K., Mazzanti, M., Breit, S., Curmi, P., and Brown, L. (2010) Metamorphic response of the CLIC1 chloride intracellular ion channel protein upon membrane interaction., *Biochemistry 49*, 5278-5289.

[9] Littler, D., Assaad, N., Harrop, S., Brown, L., Pankhurst, G., Luciani, P., Aguilar, M., Mazzanti, M., Berryman, M., Breit, S., and Curmi, P. (2005) Crystal structure of the soluble form of the redox-regulated chloride ion channel protein CLIC4., *FEBS J. 272*, 4996-5007.

[10] Littler, D., Harrop, S., Fairlie, W., Brown, L., Pankhurst, G., Pankhurst, S., DeMaere, M., Campbell, T., Bauskin, A., Tonini, R., Mazzanti, M., Breit, S., and Curmi, P. (2004) The intracellular chloride ion channel protein CLIC1 undergoes a redox-controlled structural transition., *J Biol Chem. 279*, 9298-9305.

[11] Singh, H., and Ashley, R. (2006) Redox regulation of CLIC1 by cysteine residues associated with the putative channel pore., *Biophys J. 90*, 1628-1638.

[12] Tulk, B., Kapadia, S., and Edwards, J. (2002) CLIC1 inserts from the aqueous phase into phospholipid membranes, where it functions as an anion channel., *Am J Physiol Cell Physiol. 282*, 1103-1112.

[13] Achilonu, I., Fanucchi, S., Cross, M., Fernandes, M., and Dirr, H. (2012) Role of individual histidines in the pH-dependent global stability of human chloride intracellular channel 1., *Biochemistry 51*, 995-1004.

[14] Fanucchi, S., Adamson, R., and Dirr, H. (2008) Formation of an unfolding intermediate state of soluble chloride intracellular channel protein CLIC1 at acidic pH., *Biochemistry 47*, 11674-11681.

[15] Tulk, B., Schlesinger, P., Kapadia, S., and Edwards, J. (2000) CLIC-1 functions as a chloride channel when expressed and purified from bacteria., *J Biol Chem. 275*, 26986-26993.

[16] Warton, K., Tonini, R., Fairlie, W., Matthews, J., Valenzuela, S., Qiu, M., Wu, W., Pankhurst, S., Bauskin, A., Harrop, S., Campbell, T., Curmi, P., Breit, S., and Mazzanti, M. (2002) Recombinant CLIC1 (NCC27) assembles in lipid bilayers via a pH-dependent two-state process to form chloride ion channels with identical characteristics to those observed in Chinese hamster ovary cells expressing CLIC1., *J Biol Chem. 277*, 26003-26011.

[17] Harrop, S., DeMaere, M., Fairlie, W., Reztsova, T., Valenzuela, S., Mazzanti, M., Tonini, R., Qiu, M., Jankova, L., Warton, K., Bauskin, A., Wu, W., Pankhurst, S., Campbell, T., Breit, S., and Curmi, P. (2001) Crystal structure of a soluble form of the intracellular chloride ion channel CLIC1 (NCC27) at 1.4-A resolution., *J Biol Chem. 276*, 44993-45000.

[18] Valenzuela, S., Alkhamici, H., Brown, L., Almond, O., Goodchild, S., Carne, S., Curmi, P., Holt, S., and Cornell, B. (2013) Regulation of the Membrane Insertion and Conductance Activity of the Metamorphic Chloride Intracellular Channel Protein CLIC1 by Cholesterol., *PLoS ONE 8*, 56948.

[19] Gilbert, R. (2010) Cholesterol-dependent cytolysins., *Adv Exp Med Biol 677*, 56-66.

[20] Stauber, T., and Jentsch, T. (2012) Chloride in Vesicular Trafficking and Function, *Annu.Rev.Physiol 75*, 453-477.

[21] Jentsch, T., Stein, V., Weinreich, F., and Zdebik, A. (2002) Molecular Structure and Physiological Function of Chloride Channels, *Physiol Rev 82*, 503-568.

[22] Tomaskova, Z., and Ondrias, K. (2010) Mitochondrial chloride channels-What are they for?, *FEBS Letters 584*, 2085-2092.

[23] Verkman, A., and Galietta, L. (2009) Chloride channels as drug targets., *Nat Rev Drug Discov. 8*, 153-171.

[24] Betz, H. (1990) Ligand-gated ion channels in the brain: the amino acid receptor superfamily., *Neuron 5*, 383-392.

[25] Darun, C., Thompson, C., Xiao, Q., and Haetzell, H. (2010) Chloride Channels: Often enigmatric, rarely predictable., *Annu.Rev.Physiol 72*, 95-121.

[26] Jentsch, T. (2008) CLC chloride channels and transporters: From genes to protein structure, pathology, and physiology., *Crit. Rev. Biochem. Molec. Biol 43*, 3-36.

[27] Stauber, T., Weinert, S., and Jentsch, T. (2012) Cell biology and physiology of CLC chloride channels and transporters., *Comprehensive Physiol 2*, 1701-1744.

[28] Dutzler, R., Campbell, E., Cadene, M., Chait, B., and MacKinnon, R. (2002) X-ray structure of a ClC chloride channel at 3.0 A reveals the molecular basis of anion selectivity., *Nature 415*, 287-294.

[29] Dutzler, R., Campbell, E., and MacKinnon, R. (2003) Gating the selectivity filter in ClC chloride channels., *Science 300*, 108-112.

[30] Kerem, B., Rommens, J., Buchanan, J., Markiewicz, D., Cox, T., Chakravarti, A., Buchwald, M., and Tsui, L. (1989) Identification of the cystic fibrosis gene: genetic analysis., *Science 245*, 1073-1080.

[31] Riordan, J., Rommens, J., Kerem, B., Alon, N., Rozmahel, R., Grzelczak, Z., Zielenski, J., Lok, S., Plavsic, N., and Chou, J., et al. (1989) Identification of the cystic fibrosis gene: cloning and characterization of complementary DNA., *Science 245*, 1066-1073.

[32] Al-Awqati, Q. (1995) Chloride channels of intracellular organelles., *Curr Opin Cell Biol. 7*, 504-508.

[33] Dulhunty, A., Gage, P., Curtis, S., Chelvanayagam, G., and Board, P. (2001) The glutathione transferase structural family includes a nuclear chloride channel and a ryanodine receptor calcium release channel modulator., *J Biol Chem. 276*, 3319-3323.

[34] Littler, D., Assaad, N., Harrop, S., Brown, L., Pankhurst, G., Luciani, P., Aguilar, M., Mazzanti, M., Berryman, M., Breit, S., and Curmi, P. (2005.) Crystal structure of the soluble form of the redox-regulated chloride ion channel protein CLIC4. , *FEBS J. 272*, 4996-5007.

[35] Berry, K., Bülow, H., Hall, D., and Hobert, O. (2003) A C. elegans CLIC like protein required for intracellular tube formation and maintenance., *Science 302*, 2134-2137.

[36] Elter, A., Hartel, A., Sieben, C., Hertel, B., Fischer-Schliebs, E., Lüttge, U., Moroni, A., and Thiel, G. (2007) A plant homolog of animal chloride intracellular channels (CLICs) generates an ion conductance in heterologous systems., *J Biol Chem. 282*, 8786-8792.

[37] Landry, D., Sullivan, S., Nicolaides, M., Redhead, C., Edelman, A., Field, M., al-Awqati, Q., and Edwards, J. (1993) Molecular cloning and characterization of p64, a chloride channel protein from kidney microsomes., *J Biol Chem. 268*, 14948-14955.

[38] Redhead, C., Edelman, A., Brown, D., Landry, D., and al-Awqati, Q. (1992) A ubiquitous 64-kDa protein is a component of a chloride channel of plasma and intracellular membranes., *Proc Natl Acad Sci U S A. 89*, 3716–3720.

[39] Shanks, R., Larocca, M., Berryman, M., Edwards, J., Urushidani, T., Navarre, J., and Goldenring, J. (2002) AKAP350 at the Golgi apparatus. II. Association of AKAP350 with a novel chloride intracellular channel (CLIC) family member., *J Biol Chem 277*, 40973-40980.

[40] Berryman, M., and Bretscher, A. (2000) Identification of a novel member of the chloride intracellular channel gene family (CLIC5) that associates with the actin cytoskeleton of placental microvilli., *Mol Biol Cell. 11*, 1509-1521.

[41] Nishizawa, T., Nagao, T., Iwatsubo, T., Forte, J., and Urushidani, T. (2000) Molecular cloning and characterization of a novel chloride intracellular channel-related protein, parchorin, expressed in water-secreting cells., *J Biol Chem. 275*, 11164-11173.

[42] Friedli, M., Guipponi, M., Bertrand, S., Bertrand, D., Neerman-Arbez, M., Scott, H., Antonarakis, S., and Reymond, A. (2003) Identification of a novel member of the CLIC family, CLIC6, mapping to 21q22.12., *Gene 320*, 31-40.

[43] Griffon, N., Jeanneteau, F., Prieur, F., Diaz, J., and Sokoloff, P. (2003) CLIC6, a member of the intracellular chloride channel family, interacts with dopamine D(2)-like receptors., *Brain Res Mol Brain Res. 117*, 47-57.

[44] Board, P., Coggan, M., Watson, S., Gage, P., and Dulhunty, A. (2004) CLIC-2 modulates cardiac ryanodine receptor Ca2+ release channels., *Int J Biochem Cell Biol. 36*, 1599-1612.

[45] Howell, S., Duncan, R., and Ashley, R. (1996) Identification and characterisation of a homologue of p64 in rat tissues., *FEBS Letters 390*, 207-210.

[46] Qian, Z., Okuhara, D., Abe, M., and Rosner, M. (1999) Molecular cloning and characterization of a mitogen-activated protein kinase-associated intracellular chloride channel., *J Biol Chem. 274*, 1621-1627.

[47] Tulk, B., and Edwards, J. (1998) NCC27, a homolog of intracellular Clchannel p64, is expressed in brush border of renal proximal tubule., *Am J Physiol. 274*, 1140-1149.

[48] Valenzuela, S., Mazzanti, M., Tonini, R., Qiu, M., Warton, K., Musgrove, E., Campbell, T., and Breit, S. (2000) The nuclear chloride ion channel NCC27 is involved in regulation of the cell cycle., *J Physiol. 529*, 541-552.

[49] Ashley, R. (2003) Challenging accepted ion channel biology: p64 and the CLIC family of putative intracellular anion channel proteins (Review). *Mol Membr Biol. 20*, 1-11.

[50] Edwards, J., Tulk, B., and Schlesinger, P. (1998) Functional expression of p64, an intracellular chloride channel protein., *J Membr Biol. 163*, 119-127.

[51] Jiang, L., Salao, K., Li, H., Rybicka, J., Yates, R., Luo, X., Shi, X., Kuffner, T., Tsai, V., Husaini, Y., Wu, L., Brown, D., Grewal, T., Brown, L., Curmi, P., and Breit, S. (2012) Intracellular chloride channel protein CLIC1 regulates macrophage function through modulation of phagosomal acidification., *J Cell Sci. 125*, 5479-5488.

[52] Ulmasov, B., Bruno, J., Woost, P., and Edwards, J. (2007) Tissue and subcellular distribution of CLIC1., *BMC Cell Biol. 8*, 8.

[53] Cromer, B., Gorman, M., Hansen, G., Adams, J., Coggan, M., Littler, D., Brown, L., Mazzanti, M., Breit, S., Curmi, P., Dulhunty, A., Board, P., and Parker, M. (2007) Structure of the Janus protein human CLIC2., *J Mol Biol. 374*, 719-731.

[54] Littler, D., Brown, L., Breit, S., Perrakis, A., and Curmi, P. (2010) Structure of human CLIC3 at 2 A resolution., *Proteins 78*, 1594-1600.

[55] Money, T., King, R., Wong, M., Stevenson, J., Kalionis, B., Erwich, J., Huisman, M., Timmer, A., Hiden, U., Desoye, G., and Gude, N. (2007) Expression and cellular localisation of chloride intracellular channel 3 in human placenta and fetal membranes., *Placenta 28*, 429-436.

[56] Fernández-Salas, E., Suh, K., Speransky, V., Bowers, W., Levy, J., Adams, T., Pathak, K., Edwards, L., Hayes, D., Cheng, C., Steven, A., Weinberg, W., and Yuspa, S. (2002) mtCLIC/CLIC4, an organellular chloride channel protein, is increased by DNA damage and participates in the apoptotic response to p53., *Mol Cell Biol. 22*, 3610-3620.

[57] Rønnov-Jessen, L., Villadsen, R., Edwards, J., and Petersen, O. (2002) Differential expression of a chloride intracellular channel gene, CLIC4, in transforming growth factor-beta1-mediated conversion of fibroblasts to myofibroblasts., *Am J Pathol. 161*, 471-480.

[58] Singh, H., Cousin, M., and Ashley, R. (2007) Functional reconstitution of mammalian 'chloride intracellular channels' CLIC1, CLIC4 and CLIC5 reveals differential regulation by cytoskeletal actin., *FEBS J. 274*, 6306-6316.

[59] Suh, K., Crutchley, J., Koochek, A., Ryscavage, A., Bhat, K., Tanaka, T., Oshima, A., Fitzgerald, P., and Yuspa, S. (2007) Reciprocal modifications of CLIC4 in tumor epithelium and stroma mark malignant progression of multiple human cancers., *Clin Cancer Res. 13*, 121-131.

[60] Edwards, J. (2010) What's a CLIC doing in the podocyte?, *Kidney Int. 78*, 831-833.

[61] Li, F., Yin, J., Yue, T., Liu, L., and Zhang, H. (2010) The CLIC5 (chloride intracellular channel 5) involved in C2C12 myoblasts proliferation and differentiation., *Cell Biol Int. 34*, 379-384.

[62] Valenzuela, S., Martin, D., Por, S., Robbins, J., Warton, K., Bootcov, M., Schofield, P., Campbell, T., and Breit, S. (1997) Molecular cloning and expression of a chloride ion channel of cell nuclei., *J Biol Chem. 272*, 12575-12582.

[63] Myers, K., Somanath, P., Berryman, M., and Vijayaraghavan, S. (2004) Identification of chloride intracellular channel proteins in spermatozoa., *FEBS Letters 566*, 136-140.

[64] Valenzuela, S., Martin, D., Por, S., Robbins, J., Bootcov, M., Schofield, P., Campbell, T., and Breit, S. (1996) NCC27- A novel nuclear chloride ion channel associated with macrophage activation., *Journal of leukocyte biology*, 106.

[65] Singh, H., and Ashley, R. (2007) CLIC4 (p64H1) and its putative transmembrane domain form poorly selective, redox-regulated ion channels., *Mol Membr Biol. 24*, 41-52.

[66] Edwards, J. (2006) The CLIC1 chloride channel is regulated by the cystic fibrosis transmembrane conductance regulator when expressed in Xenopus oocytes., *J Membr Biol. 213*, 39-46.

[67] Al Khamici, H., Brown, L., Hossain, K., Hudson, A., Sinclair-Burton, A., Ng, J., Daniel, E., Hare, J., Cornell, B., Curmi, P., Davey, M., and Valenzuela, S. (2015) Members of the Chloride Intracellular Ion Channel Protein Family Demonstrate Glutaredoxin-Like Enzymatic Activity., *PLoS One 10*, e115699.

[68] Novarino, G., Fabrizi, C., Tonini, R., Denti, M., Malchiodi-Albedi, F., Lauro, G., Sacchetti, B., Paradisi, S., Ferroni, A., Curmi, P., Breit, S., and Mazzanti, M. (2004) Involvement of the intracellular ion channel CLIC1 in microglia-mediated beta-amyloid-induced neurotoxicity., *J Neurosci. 24*, 5322-5330.

[69] Milton, R., Abeti, R., Averaimo, S., DeBiasi, S., Vitellaro, L., Jiang, L., Curmi, P., Breit, S., Duchen, M., and Mazzanti, M. (2008) CLIC1 function is required for beta-amyloid-induced generation of reactive oxygen species by microglia., *J Neurosci. 28*, 11488-11499.

[70] Tung, J., and Kitajewski, J. (2010) Chloride intracellular channel 1 functions in endothelial cell growth and migration., *J Angiogenes Res. 2*, 23.

[71] Chen, C., Wang, C., Huang, Y., Chien, K., Liang, Y., Chen, W., and Lin, K. (2007) Overexpression of CLIC1 in human gastric carcinoma and its clinicopathological significance., *Proteomics 7*, 155-167.

[72] Huang, J., Chao, C., Su, T., Yeh, S., Chen, D., Chen, C., Chen, P., and Jou, Y. (2004) Diverse cellular transformation capability of overexpressed genes in human hepatocellular carcinoma., *Biochem Biophys Res Commun. 315*, 950-958.

[73] Kim, W., Oe Lim, S., Kim, J., Ryu, Y., Byeon, J., Kim, H., Kim, Y., Heo, J., Park, Y., and Jung, G. (2003) Comparison of proteome between hepatitis B virus- and hepatitis C virus-associated hepatocellular carcinoma., *Clin Cancer Res. 9*, 5493-5500.

[74] Petrova, D., Asif, A., Armstrong, V., Dimova, I., Toshev, S., Yaramov, N., Oellerich, M., and Toncheva, D. (2008) Expression of chloride intracellular channel protein 1 (CLIC1) and tumor protein D52 (TPD52) as potential biomarkers for colorectal cancer., *Clin Biochem. 41*, 1224-1236.

[75] Wang, J., Peng, S., Li, J., Wang, Y., Zhang, Z., Cheng, Y., Cheng, D., Weng, W., Wu, X., Fei, X., Quan, Z., Li, J., Li, S., and Liu, Y. (2009) Identification of metastasis-associated proteins involved in gallbladder carcinoma metastasis by proteomic analysis and functional exploration of chloride intracellular channel 1., *Cancer Lett. 281*, 71-81.

[76] Wang, J., Xu, X., Wang, W., Shao, W., Li, L., Yin, W., Xiu, L., Mo, M., Zhao, J., He, Q., and He, J. (2011) The expression and clinical significance of CLIC1 and HSP27 in lung adenocarcinoma., *Tumour Biol. 32*, 1199-1208.

[77] Martin, J. (1995) Thioredoxin--a fold for all reasons., *Structure 3*, 245-250.

[78] Stoychev, S., Nathaniel, C., Fanucchi, S., Brock, M., Li, S., Asmus, K., Woods, V. J., and Dirr, H. (2009) Structural dynamics of soluble chloride intracellular channel protein CLIC1 examined by amide

hydrogendeuterium exchange mass spectrometry., *Biochemistry 48*, 8413-8421.

[79] Dulhunty, A., Gage, P., Curtis, S., Chelvanayagam, G., and Board, P. (2001) The glutathione transferase structural family includes a nuclear chloride channel and a ryanodine receptor calcium release channel modulator., *J Biol Chem 276*, 3319-3323.

[80] Sheehan, D., Meade, G., Foley, V., and Dowd, C. (2001) Structure, function and evolution of glutathione transferases: implications for classification of non-mammalian members of an ancient enzyme superfamily., *Biochem J. 360*, 1-16.

[81] Board, P., Coggan, M., Chelvanayagam, G., Easteal, S., Jermiin, L., Schulte, G., Danley, D., Hoth, L., Griffor, M., Kamath, A., Rosner, M., Chrunyk, B., Perregaux, D., Gabel, C., Geoghegan, K., and Pandit, J. (2000) Identification, characterization, and crystal structure of the Omega class glutathione transferases., *J Biol Chem. 275*, 24798-24806.

[82] Xia, B., Vlamis-Gardikas, A., Holmgren, A., Wright, P., and Dyson, H. (2001) Solution structure of Escherichia coli glutaredoxin-2 shows similarity to mammalian glutathione-S-transferases., *J Mol Biol. 10*, 907-918.

[83] Tonini, R., Ferroni, A., Valenzuela, S., Warton, K., Campbell, T., Breit, S., and Mazzanti, M. (2000) Functional characterization of the NCC27 nuclear protein in stable transfected CHO-K1 cells., *FASEB J. 14*, 1171-1178.

[84] Berry, K., and Hobert, O. (2006) Mapping functional domains of chloride intracellular channel (CLIC) proteins *in vivo*., *J Mol Biol. 359*, 1316-1333.

[85] Powis, G., and Montfort, W. (2001) Properties and biological activities of thioredoxins., *Annu Rev Biophys Biomol Struct. 30*, 421-455.

[86] Li, Y., Li, D., Zeng, Z., and Wang, D. (2006) Trimeric structure of the wild soluble chloride intracellular ion channel CLIC4 observed in crystals., *Biochem Biophys Res Commun. 343*, 1272-1278.

[87] Hwang, C., Sinskey, A., and Lodish, H. (1992) Oxidized redox state of glutathione in the endoplasmic reticulum., *Science 257*, 1496-1502.

[88] Hornby, J., Luo, J., Stevens, J., Wallace, L., Kaplan, W., Armstrong, R., and Dirr, H. (2000) Equilibrium folding of dimeric class mu glutathione transferases involves a stable monomeric intermediate., *Biochemistry 39*, 12336-12344.

[89] Wallace, L., Burke, J., and Dirr, H. (2000) Domain-domain interface packing at conserved Trp-20 in class alpha glutathione transferase impacts on protein stability., *Biochem Biophys Acta. 1478*, 325-332.

[90] Wallace, L., Sluis-Cremer, N., and Dirr, H. (1998) Equilibrium and kinetic unfolding properties of dimeric human glutathione transferase A1-1., *Biochemistry 37*, 5320-5328.

[91] Gildenhuys, S., Wallace, L., and Dirr, H. (2008) Stability and unfolding of reduced Escherichia coli glutaredoxin 2: a monomeric structural homologue of the glutathione transferase family., *Biochemistry 47*, 10801-10808.

[92] Gonzalez, M., Bischofberger, M., Pernot, L., van der Goot, F., and Frêche, B. (2008) Bacterial pore-forming toxins: the (w)hole story?, *Cell Mol Life Sci. 65*, 493-507.

[93] van der Goot, F., González-Mañas, J., Lakey, J., and Pattus, F. (1991) A 'molten-globule' membrane-insertion intermediate of the pore-forming domain of colicin A., *Nature 354*, 408-410.

[94] Jiang, J., and London, E. (1990) Involvement of denaturation-like changes in Pseudomonas exotoxin a hydrophobicity and membrane penetration determined by characterization of pH and thermal transitions. Roles of two distinct conformationally altered states., *J Biol Chem. 265*, 8636-8641.

[95] Jiang, J., Abrams, F., and London, E. (1991) Folding changes in membraneinserted diphtheria toxin that may play important roles in its translocation., *Biochemistry 30*, 3857-3864.

[96] London, E. (1992) How bacterial protein toxins enter cells; the role of partial unfolding in membrane translocation., *Mol Microbiol. 6*, 3277-3282.

[97] Isas, J., Patel, D., Jao, C., Jayasinghe, S., Cartailler, J., Haigler, H., and Langen, R. (2003) Global structural changes in annexin 12. The roles of phospholipid, Ca2+, and pH., *J Biol Chem. 278*, 30227-30234.

[98] Bortoleto, R., and Ward, R. (1999) A stability transition at mildly acidic pH in the alpha-hemolysin (alpha-toxin) from Staphylococcus aureus. , *FEBS Letters 459*, 438-442.

[99] Manceva, S., Pusztai-Carey, M., and Butko, P. (2004) Effect of pH and ionic strength on the cytolytic toxin Cyt1A: a fluorescence spectroscopy study., *Biochem Biophys Acta. 1699*, 123-130.

[100] Ulrih, N., Anderluh, G., Macek, P., and Chalikian, T. (2004) Salt-induced oligomerisation of partially folded intermediates of equinatoxin II., *Biochemistry 43*, 9536-9545.

[101] Parker, M., and Feil, S. (2005) Pore-forming protein toxins: from structure to function. , *Prog Biophys Mol Biol. 88*, 91-142.

[102] Mi, W., Liang, Y., Li, L., and Su, X. (2008) The crystal structure of human chloride intracellular channel protein 2: a disulfide bond with functional implications. , *Proteins 71*, 509-513.

[103] Rescher, U., and Gerke, V. (2004) Annexins--unique membrane binding proteins with diverse functions., *J Cell Sci. 117*, 2631-2639.

[104] Cartailler, J., Haigler, H., and Luecke, H. (2000) Annexin XII E105K crystal structure: identification of a pH-dependent switch for mutant hexamerization., *Biochemistry 39*, 2475-2483.

[105] Gerke, V., and Moss, S. (2002) Annexins: from structure to function., *Physiol Rev. 82*, 331-371.

[106] Shimizu, S., Narita, M., and Tsujimoto, Y. (1999) Bcl-2 family proteins regulate the release of apoptogenic cytochrome c by the mitochondrial channel VDAC., *Nature 399*, 483-487.

[107] García-Sáez, A., Mingarro, I., Pérez-Payá, E., and Salgado, J. (2004) Membrane-insertion fragments of Bcl-xL, Bax, and Bid., *Biochemistry 43*, 10930-10943.

[108] Gilbert, R., Jiménez, J., Chen, S., Tickle, I., Rossjohn, J., Parker, M., Andrew, P., and Saibil, H. (1999) Two structural transitions in membrane pore formation by pneumolysin, the pore-forming toxin of *Streptococcus pneumoniae*. , *Cell Biol Int. 97*, 647-655.

[109] Chou, P., and Fasman, G. (1978) Empirical predictions of protein conformation. , *Annu Rev Biochem 47*, 251-276.

[110] Minn, A., Vélez, P., Schendel, S., Liang, H., Muchmore, S., Fesik, S., Fill, M., and Thompson, C. (1997) Bcl-x(L) forms an ion channel in synthetic lipid membranes., *Nature 385*, 353-357.

[111] Vander Heiden, M., Li, X., Gottleib, E., Hill, R., Thompson, C., and Colombini, M. (2001) Bcl-xL promotes the open configuration of the voltage-dependent anion channel and metabolite passage through the outer mitochondrial membrane., *J Biol Chem. 276*, 19414-19419.

[112] Prakash, A., Janosi, L., and Doxastakis, M. (2011) GxxxG motifs, phenylalanine, and cholesterol guide the self-association of transmembrane domains of ErbB2 receptors., *Biophys J. 101*, 1949-1958.

[113] Senes, A., Engel, D., and DeGrado, W. (2004) Folding of helical membrane proteins: the role of polar, GxxxG-like and proline motifs., *Curr Opin Struct Biol. 14*, 465-479.

[114] Barrett, P., Song, Y., Van Horn, W., Hustedt, E., Schafer, J., Hadziselimovic, A., Beel, A., and Sanders, C. (2012) The amyloid precursor protein has a flexible transmembrane domain and binds cholesterol., *Science 336*, 1168-1171.

[115] Yu, X., and Zheng, J. (2012) Cholesterol promotes the interaction of Alzheimer β-amyloid monomer with lipid bilayer., *J Mol Biol. 421*, 561-571.

Chapter 2

Theory and Applications of the Langmuir Monolayer and Reflectivity Techniques used in this Study

Chapter 2

Theory and Applications of the Langmuir Monolayer and Reflectivity Techniques used in this Study

2.1 Introduction

Integral membrane proteins account for more than 50% of the total cell membrane [1-4] where they interact with both the lipid bilayer and the aqueous environment [5-7]. These proteins are implicated in vital cellular processes ranging from cell signalling to structural support and molecular transport [5-7]. Despite their clear biological significance, only a handful of membrane proteins have been structurally and functionally characterised. Out of the 100,000 existing protein structures, there is an extremely low number of membrane protein structures available in the Protein Data Bank (http://www.rcsb.org) with only a dozen of those being human membrane proteins [8]. As a result, the final membrane-bound structures of many proteins remain relatively unknown and also very little is specifically known about the mechanism of insertion of spontaneous membrane inserting proteins.

X-ray crystallography and nuclear magnetic resonance (NMR) techniques have been successfully applied to solve the crystal structures of numerous membrane proteins, providing insightful details that led to several breakthroughs in our understanding of membrane-protein interactions [9-14]. However, these studies rely mainly on detergent-solubilized protein and are unable to provide the precise structure of the protein in its native form inside a lipid environment. Furthermore, many integral membrane proteins oligomerise to form multimeric complexes within the biological membrane. Hence, in addition to the crystalline structure, obtaining information about the protein's membrane structure inside the lipid bilayer is thus fundamental for the understanding of the protein's functionality at the molecular and cellular levels [15]. A number of model membrane systems have been developed that allow proteins to be studied inside their native or native-like-environment [2, 3], of which Langmuir monolayer model is one [16].

The Langmuir monolayer is a well-established model that allows the investigation of lipid monolayers at the air-water interface and their interaction with substances,

like proteins, dissolved in the water subphase [16]. A Langmuir monolayer represents a simple model of the cell membrane and when coupled with X-ray and neutron scattering techniques [17], in particular, specular reflectivity, is capable of providing kinetic and structural information that complements crystallographic studies [18]. Because of the hypothesised link between membrane lipids and the membrane insertion of the Chloride Intracellular Ion Channel 1 protein (CLIC1) (details in Chapter 1), this study aimed to investigate the spontaneous membrane insertion of CLIC1 protein into lipid monolayers at the air-water interface. In addition, this study also aimed to elucidate the CLIC1 membrane-bound structure using X-ray and neutron scattering techniques. This chapter will outline the basic principles and applications of a Langmuir monolayer model. It will also discuss the basic theory and principle behind X-ray and neutron scattering techniques. However, details of specific instrumentation and data analysis for the associated Langmuir and scattering methods will be left to subsequent chapters.

2.2 Langmuir Monolayer Model

A one-molecule thick insoluble layer of an organic material at the air-water interface is called a Langmuir monolayer (LM) or Langmuir film, named after its inventor Irving Langmuir, who first developed the theoretical and experimental concepts of the monolayer at the molecular level [16]. His studies revealed the fact that amphiphilic molecules show a preferential orientation and form an isolated essentially two-dimensional (2D) system at the air-water interface. Thus, the Langmuir monolayer model provides a unique methodology to study matter in two dimensions [16] and allows for the use of physiochemical techniques whose interpretation would be much more difficult when applied to natural biological membranes [19].

2.2.1 Advantages of the Langmuir Monolayer as a model membrane system

There are several advantages of the Langmuir monolayer as a model for lipid membrane systems [19]. The Langmuir monolayer is an excellent model for studying ordering in two dimensions [16, 19]. LM at the air-water interface can provide information about the intra-monolayer and monolayer-subphase interactions at a molecular level. By changing head and/or tail groups of the lipid molecules or their surrounding environment (such as pH values or ionic strengths

of the aqueous subphase), it is possible to precisely control the interactions [20, 21]. Another important reason to study LMs is their close relationship to membrane biophysics. Membranes of all living cells and organelles within cells consist of lipid bilayers (two weakly coupled monolayers) interpenetrated with specific proteins, cholesterol, and other organic compounds [2, 4]. LMs can therefore be used as a model system to simulate the chemical and biological reactions of membranes in living cells.

In addition, there are certain advantages of lipid monolayer films over bilayer systems. It is relatively easy to control the phase state and the structure of the monolayer by changing the molecular area through compression. Also, the composition of the subphase can be changed very easily so that various monolayer conditions can be produced [16, 19, 22]. Another feature of the Langmuir monolayer model is the fact that the in-plane lipid-lipid and lipid-protein interactions can be isolated from the influence of changing trans-bilayer compositional distributions that may occur in bilayer systems [20, 21, 23, 24]. As a result, several different combinations of phospholipids, sterols or sphingolipids can be used to form a monolayer to mimic one-half of naturally existing membranes. Thus, it provides various advantages in its use as a model system to study aspects of lipid-lipid and lipid-protein interactions. However, it also has certain drawbacks or limitations, most important being the requirement for planar substrates, the sensitivity to environmental contaminants and the large number of mechanical handlings required to produce stable monolayers [25]. It should also be taken into account that LMs lack typical cell membrane characteristics and as a result the biophysical interactions of the protein with model membranes may not exactly replicate all the aspects of the cellular process [25].

2.2.2 Lipid as amphiphilic molecules for Langmuir Monolayer

The biological membrane surrounding a eukaryotic cell is primarily composed of three major classes of lipids: phospholipids, glycolipids and sterols, with phospholipids representing the largest lipid class. Phospholipids are amphiphilic molecules that consist of two main regions: the hydrophilic ‘head’ group and the hydrophobic hydrocarbon ‘tail’ (Figure 2.1) [26]. In most phospholipids, the tail is composed of two fatty acyl chains (saturated or

unsaturated) connected via a glycerol backbone to a phosphate group carrying the hydrophilic head-group. In eukaryotes, the phosphate group is esterified either to a choline (phosphatidylcholine), ethanolamine (phosphatidylethanolamine), serine (phosphatidylserine), glycerol (phosphatidylglycerol), inositol (phosphatidylinositol) or cardiolipin (di-phosphatidylglycerol) head-group [26]. Figure 2.1 shows the structure of the three phospholipids and cholesterol used predominantly throughout the various experiments reported in this thesis.

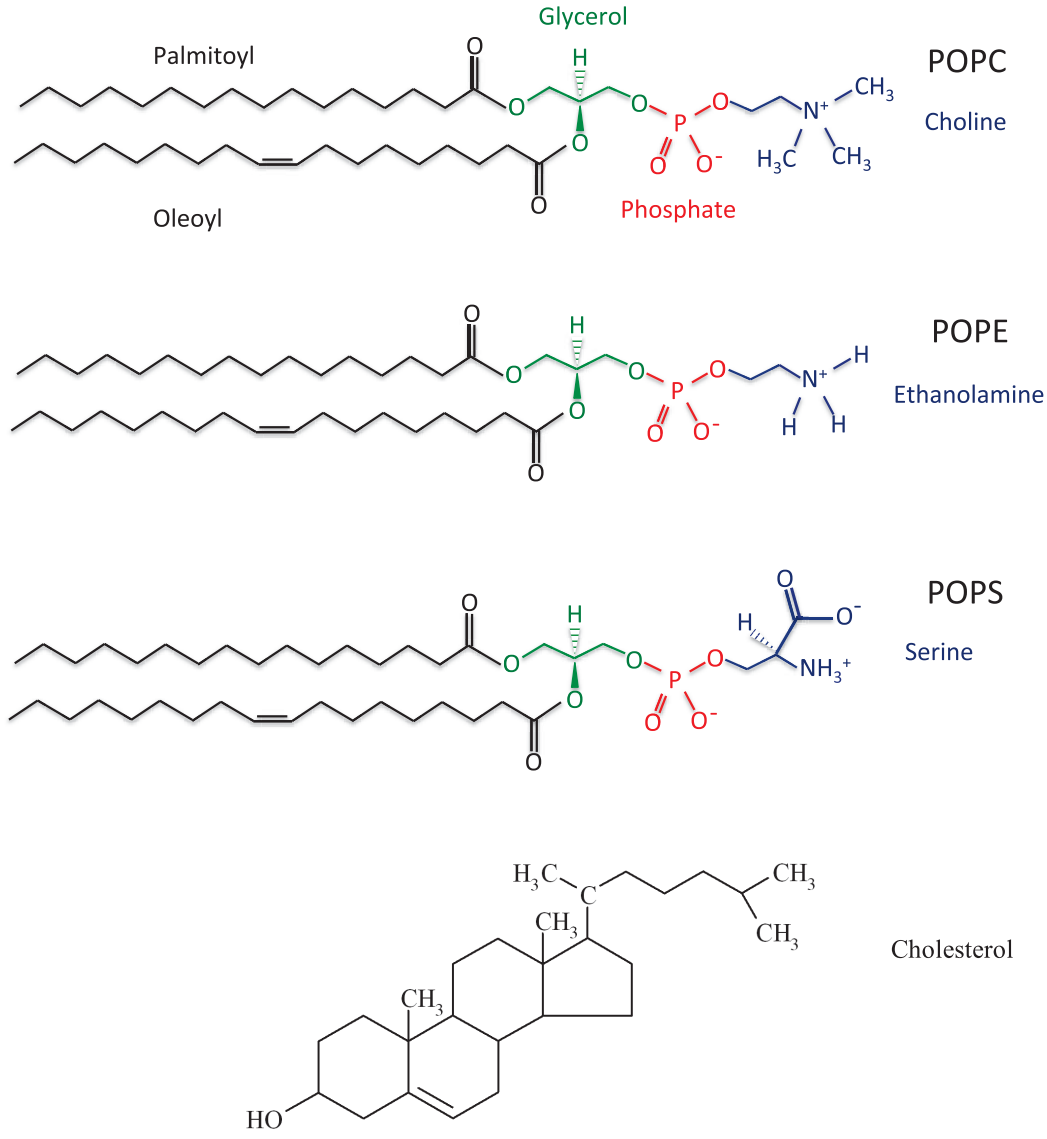

Figure 2.1 Chemical structures of the phospholipids and cholesterol used in this study. The structures presented are: 1-palmitoyl-2-oleoyl-sn-glycero-3-phosphatidylcholine (POPC), 1-palmitoyl-2-oleoyl-*sn*-glycero-3-phosphatidylethanolamine (POPE) and 1-palmitoyl-2-oleoyl-*sn*-glycero-3-phosphatidylserine (POPS). The two hydrocarbon tails are shown in *black*, the glycerol backbone in *green*, the phosphate group in *red* and the polar head-groups in *blue*.

The hydrophobic tail of all the three phospholipids is composed of a saturated palmitoleic chain (16:0 i.e., composed of 16 carbon atoms) in sn-1 position and an unsaturated oleic fatty acid chains (18:1, 18 carbon atoms with a single double bond at carbon-9 position) in sn-2 position that usually mimics mammalian phospholipid composition. The acyl chain being composed of palmitoleic and oleic acid chains is abbreviated as PO. The hydrophobic tail is connected either to a phosphatidylcholine (PC), phosphatidylethanolamine (PE) or a phosphatidylserine (PS) head-group. Thus, abbreviated as POPC, POPE and POPS lipids. Cholesterol and glycolipids are two other major components of the eukaryotic membrane. Cholesterol is an unusually important lipid for mammalian membranes and plays a crucial role in membrane organisation, dynamics, function and sorting [27-29]. It is an amphiphilic molecule with a polar hydroxyl group bonded to four planar fused carbon rings and a short hydrocarbon tail (Figure 2.1). Cholesterol has a finite but very low solubility in aqueous media and is hence found incorporated in biological membranes, or bound to proteins, both soluble or membrane proteins [28].

It is the geometric properties of the phospholipid and cholesterol molecules such as the volume of the hydrocarbon chain, chain length and the optimal area of the polar region that determines which structure the molecules can assemble into [26, 30]. The amphiphilic nature of the phospholipids give them the ability to spontaneously self-assemble into planar bilayers with the hydrocarbon tails facing each other and the hydrophilic head-groups interacting with the aqueous environment [2, 3, 26, 30]. It is also the amphiphilic nature of the monolayer materials that dictates the orientation of the molecules at the air-water interface. At a polar/apolar interface, for example the air-water interface or the oil/water interface, lipids form a monolayer, where the hydrophilic region of the molecules points into the polar phase (water) and their hydrophobic region points into the apolar phase (air or oil) [19-21, 24, 31]. One example of a real bio-monolayer is at the lungs' alveolar surface, which is in direct contact with air [32]. The phospholipid DPPC (1,2-dipalmitoyl-sn-glycero-3-phosphocholine) acts as a surfactant regulating surface tension, which in turn aids in the normal expansion and contraction of the alveoli during breathing. It also aids in reducing fluid accumulation keeping the airways dry [32].

2.2.3 Lipid Monolayer at the Air-Water interface

In a typical Langmuir experiment, lipid molecules dissolved in a volatile solvent, specifically chloroform, are spread dropwise onto the water subphase. Due to the volatile nature of chloroform, the droplets spread spontaneously over the water subphase to cover the available trough area and as the solvent evaporates, a monolayer is formed as dictated by the amphiphilic nature of the lipid [19, 33]. For example, in the case of POPC lipid, the head-group (phosphatidylcholine) is immersed into water while the hydrocarbon tails remain suspended in air. A schematic diagram of a lipid monolayer is illustrated in Figure 2.2.

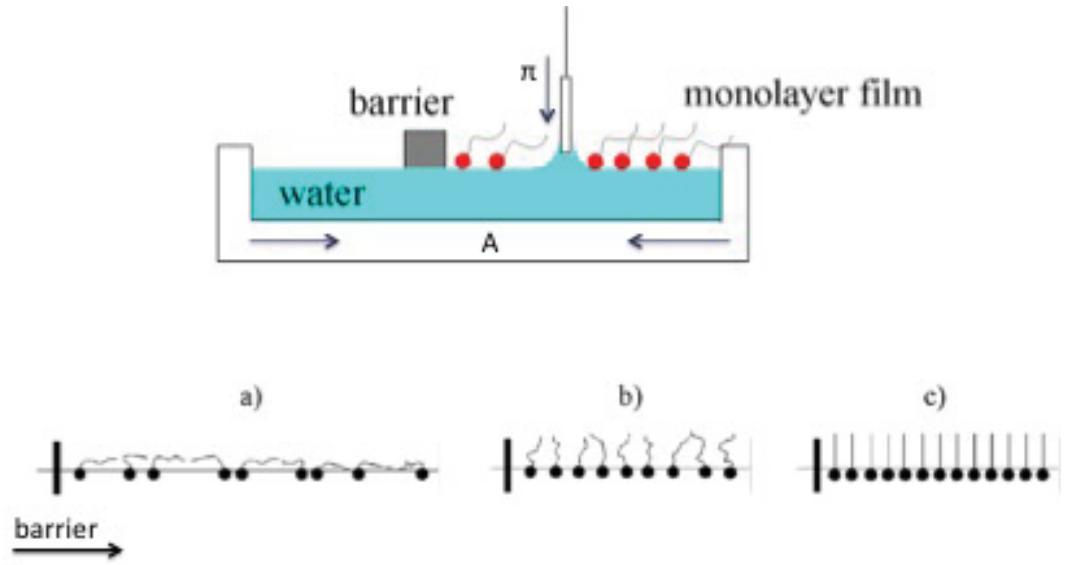

Figure 2.2 A Langmuir trough showing the principle assembly of a Lipid monolayer on a water surface: a) expanded, b) partly compressed, and c) close-packed.

Initially, the distance between the lipid molecules is large, as a result their intermolecular interactions are small and the monolayer has relatively little effect on the surface tension (γ) of the water (Figure 2.2a) [34, 35]. However, as the movable barriers compress the monolayer, the available area per lipid molecule on the water subphase reduces (Figure 2.2b & c) causing a decrease in γ. Therefore, the surface pressure (π) is defined by the equation:

$$\pi = \gamma_0 - \gamma \qquad \text{Eq. 2.1}$$

where, γ_0 is the surface tension of the clean water subphase and γ is the surface tension in the presence of lipid molecules [34, 35]. The surface pressure (π) can be measured as a function of monolayer area using a Wilhelmy balance technique which consists of a thin plate, usually glass, quartz, mica, platinum or filter paper, suspended in such a way as to cross the air-water interface [19, 35, 36]. The physics and the mathematical approach to measure surface tension and surface pressure at the air-water interface have been treated in detail elsewhere [19, 20, 22, 23]. Since the measurements are usually carried out at a constant temperature, the resulting plot is known as a Surface pressure-Area isotherm.

2.2.4 Surface pressure – Area isotherm

The Surface pressure – Area (π-A) isotherm is recorded by compressing the lipid molecules at the air-water interface until a closely packed one-molecule thick monolayer has been formed [34-38]. The π-A isotherm acts as the two-dimensional fingerprint of the lipid molecule, as the shape of the isotherm is characteristic of the molecule forming the Langmuir monolayer. As a result, the isotherm can provide valuable information on the stability of the monolayer at the air-water interface, the reorientation of molecules in the two-dimensional system, phase transitions, and conformational transformations [34-38]. In the absence of lipid molecules, π-A isotherm of pure water or buffer subphase is relatively stable (zero) over time as there are no molecules on the subphase to reduce the surface tension.

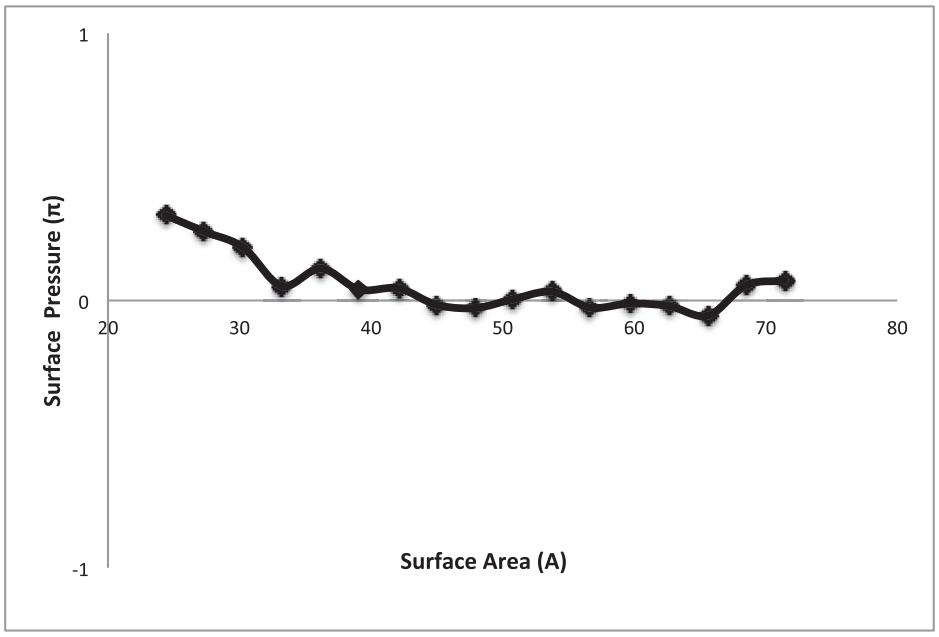

Figure 2.3 The π-A isotherm of the KCl/Hepes buffer pH 6.5.

The π-A isotherm of the KCl/Hepes buffer pH 6.5 (0.1M KCl, 0.1mM Hepes and 0.01mM $CaCl_2$), used as the liquid subphase for all Langmuir experiments mentioned in this thesis, is illustrated in Figure 2.3. As seen in the figure, the isotherm shows little to no change in π with area reduction and further confirms the absence of contaminants such as amphiphilic substances or dust on the buffer subphase. However, in the presence of lipids or amphiphiles on the water subphase, π changes significantly with the compression of the monolayer area and as a result the π-A isotherm shows distinct phase transitions as shown in Figure 2.4 [36].

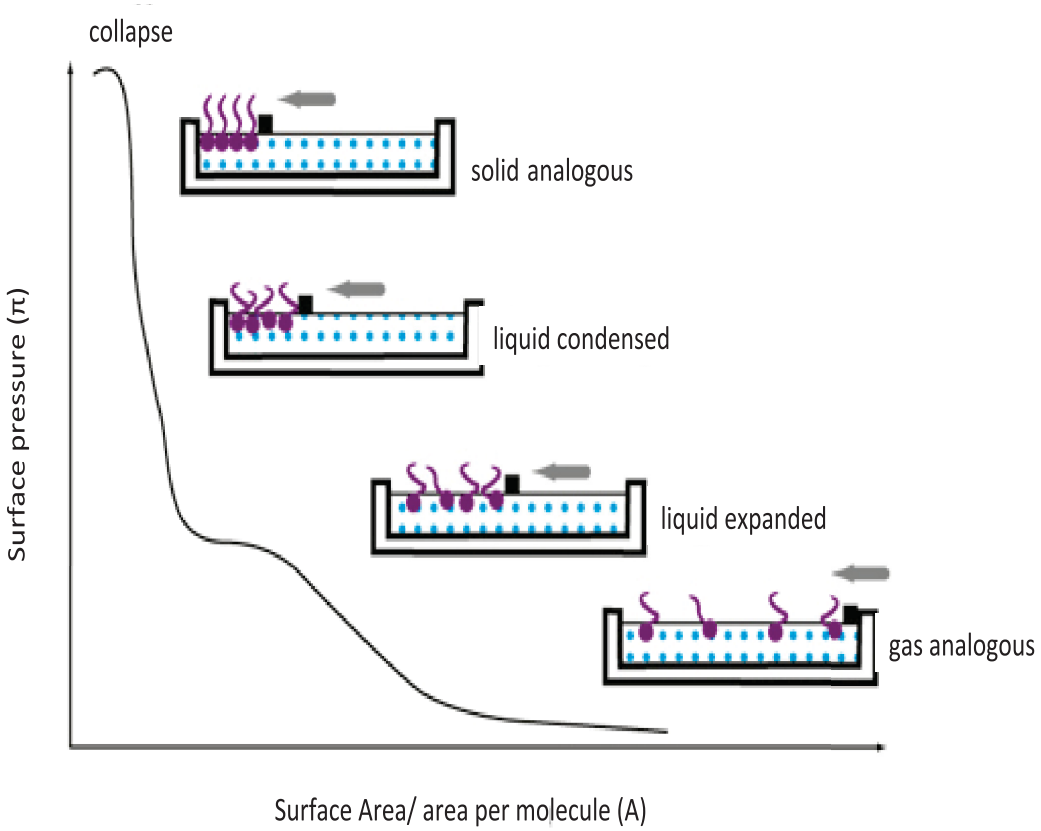

Figure 2.4 Schematic illustration of a π-A isotherm of a lipid monolayer at the air-water interface and descriptors of various phases [36].

In the gas analogous phase, the lipid molecules behave as a two-dimensional gas with negligible interactions between the amphiphiles [35]. As the surface area of the monolayer is reduced from its initial value, the amphiphiles undergo a phase transition to the liquid expanded phase where short-range-order between the molecules becomes noticeable with the increase in π. As the monolayer area is progressively reduced, the intermolecular distance between the molecules decreases, leading to an increase in surface pressure, and the liquid expanded phase transforms into the liquid condensed phase (LC) at constant surface pressure [34, 35]. In this region, the hydrocarbon chains of the lipid molecules begin to crystallise two-dimensionally *i.e.* there are solid analogous domains in a liquid analogous matrix. As this LC lipid packing density is reported to be comparable to a lipid bilayer under physiological conditions, lipid monolayers in the LC state are frequently used as membrane models [37]. A further compression of the

monolayer leads to a continuous transition to a solid analogous phase till the monolayer collapses to form disordered multilayers [34, 35].

2.2.5 Surface pressure- Area isotherms of POPC, POPE and POPS monolayers

The phospholipid monolayers were prepared by spreading dropwise 10 µl of a 1 mg/ml solution of either POPC, POPE or POPS lipid dissolved in chloroform onto the surface of a KCl/Hepes buffer subphase pH 6.5 in a Nima Technologies Langmuir trough (Nima Technologies, UK). For all Langmuir experiments, the volume of the buffer subphase in the trough was kept constant at 25 ml. Once spread, the lipid monolayers were allowed to equilibrate for 10 minutes (to allow complete evaporation of chloroform) before the barrier was compressed at 20 cm^2/min to run isotherm cycles. The π-A isotherms of the three different phospholipids were measured at room temperature (~ 25 °C) in triplicate using a freshly prepared monolayer each time, with the surface pressure being recorded by the Wilhelmy method using a filter paper plate. The phospholipid monolayers were compressed to a pressure of about 40 mN/m followed by expansion to reduce the pressure back to 0 mN/m. The resulted compression and expansion π-A isotherm cycles of POPC, POPE and POPS are shown in Figure 2.5. The room temperature was well above the transition temperature of POPC and POPS which are – 20 °C and 14 °C respectively [37]. However, the transition temperature of POPE (25 °C) [37] is close to the working temperature but considering the fact that a cold buffer subphase was used and no phase transitions were observed in the π-A isotherm cycles of POPE (Figure 2.5), one could rule out the effects of the transition temperature on POPE monolayer.

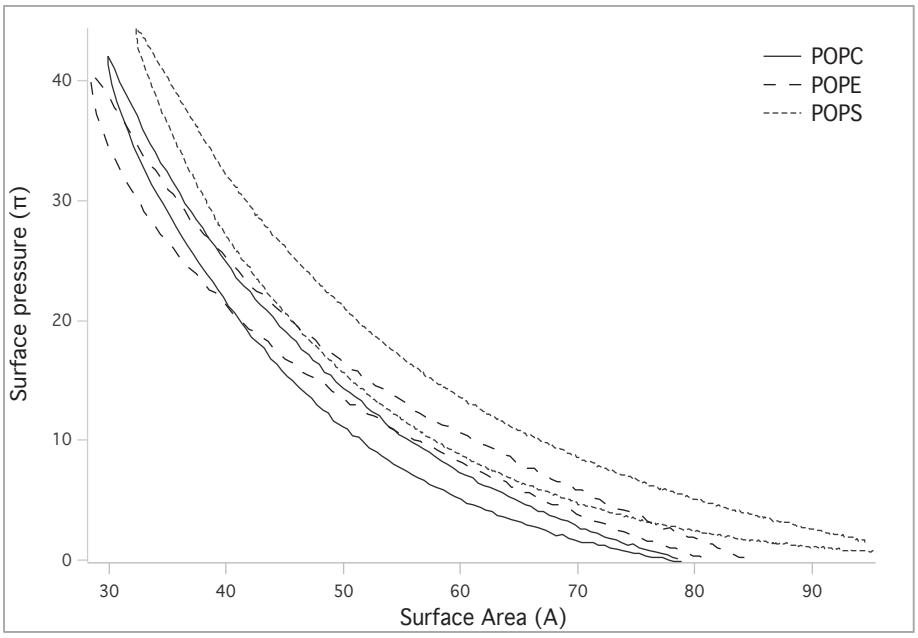

Figure 2.5 Surface pressure-area (π-A) isotherms of POPC, POPE and POPS phospholipid monolayers. The isotherms indicate that the monolayers are primarily in the liquid-expanded phase and do not exhibit any clear phase transitions.

The isotherms recorded for all the three phospholipids: POPC, POPE and POPS indicate that the monolayers are primarily in the liquid-expanded phase. Initially, POPC was in the gaseous analogous phase and the surface pressure was nearly constant around zero (Figure 2.5). As the barrier started to compress the POPC monolayer from an initial surface area of 90 cm^2, the area per lipid molecule decreased causing the phospholipid to transform into the liquid-expanded phase. Progressive compression of the POPC monolayer reduced the surface area available per lipid molecule resulting in an increase in surface pressure but showed no further phase transitions at room temperature as indicated by the smooth compression and expansion π-A isotherm. The phase transitions behaviour of POPE and POPS was similar to that observed for POPC (Figure 2.5). Since all the three phospholipids formed closely packed ordered monolayers at 20 mN/m, subsequent Langmuir experiments were carried out following CLIC1 injection underneath lipid monolayers held at a constant pressure of 20 mN/m.

2.3 Lipid-protein interaction at the Air-Water interface

Lipid monolayers have been used extensively for studying lipid-protein interactions [23, 39-45]. The binding and insertion of various peptides and proteins into lipid monolayers can be studied by recording pressure or area changes as a function of time and concentration, after injecting the protein or peptide into the subphase underneath the preformed lipid monolayer.

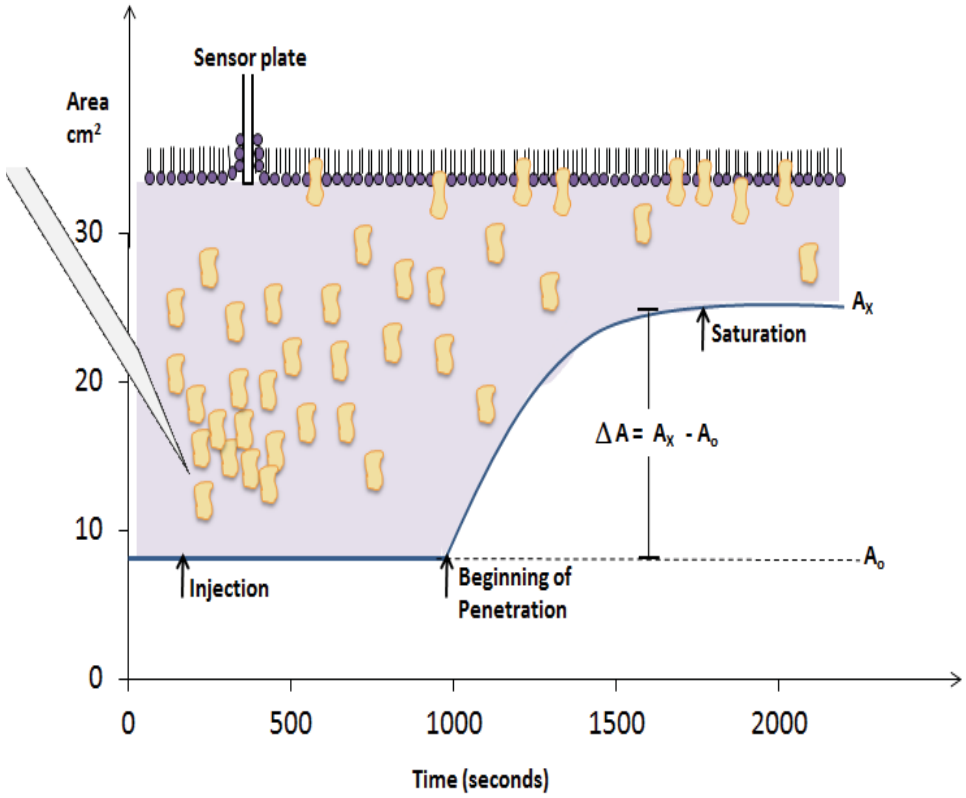

Figure 2.6 A schematic diagram of protein insertion into a lipid monolayer at the air-water interface and its subsequent surface area vs. time plots.

Figure 2.6 shows a representative diagram of protein insertion into a lipid monolayer at the air-water interface and its subsequent surface area vs. time plots. The initial area of a lipid monolayer held at a constant pressure should remain stable over time unless there is a perturbation (Figure 2.6). However, if the protein inserts into the lipid monolayer, in order to maintain a constant pressure, the initial area increases until it reaches a saturation point where no further protein insertion is observed (Figure 2.6). As a result, one can plot the recorded area changes as a function of the initial surface area where the so-called maximum

insertion area can be determined, which is a measure of the surface activity of the peptides or proteins on one hand and the strength of the interaction with the lipids on the other.

Hence, the Langmuir monolayer technique was considered as the ideal model system to study the spontaneous membrane insertion of CLIC1 protein into different lipid monolayers held at a constant pressure of 20 mN/m in real time. Another advantage of using such a model was that it allowed us to investigate the structural parameters of the lipid-protein monolayer using X-ray and neutron reflectivity [17], in order to elucidate the structural features of the CLIC1 membrane-bound form. A description of these two techniques and their application to Langmuir monolayers is given in the subsequent sections. There are many other methods that have been used to characterise monolayers, i.e. x-ray diffraction techniques (XRD) [46], infra-red (IR) and Raman spectroscopy [47], surface light scattering (SLS) [48], interfacial stress rheometry (IRS) [49], and non-linear optical techniques. Applications of these techniques have been reported but will not be discussed here.

2.4 X-ray and Neutron Reflectivity studies give structural information about CLIC1 and Lipid Monolayer upon their interaction at the Air-Water interface

X-ray and neutron reflection techniques have been increasingly applied to the study of Langmuir monolayers recently [17, 50-52]. X-ray and neutron reflectivity (XR and NR) provide a non-destructive technique for measuring density in thin films. These techniques utilise the wave characteristics of either X-rays or neutrons near conditions of perfect reflection, in order to provide information about the molecular scale composition and ordering of molecules at interfaces [17, 18, 50, 53-55]. After being incident upon the atoms in the monolayer film, X-rays are scattered from the electrons of the atoms while neutrons are scattered from the nuclei. These reflected X-rays or neutrons are then incident upon a detector. The resulting signals from the detector give valuable and detailed information about the molecular composition and ordering of the films. Since X-ray reflection probes the variation of electron density (SLD_e) normal to the interfacial plane, XR provides valuable and detailed information about the electron density composition of the film [18, 52]. On the other hand, neutron reflection detects the variation in scattering length density (SLD_n) across the interface providing detailed information about the chemical composition of the film [53, 56]. The optics of X-ray and neutron reflectivity (XR and NR) at the air-water interface have been treated in detail elsewhere [18, 50, 52-54, 56] and only a brief description of the theoretical background of reflectivity is given below.

2.4.1 Fundamental principles for X-ray and Neutron Reflectivity

The same fundamental principles apply to both X-ray and neutron reflectivity [18, 54, 55]. The principle of the specular reflectivity is sketched out in Figure 2.7. As seen in the figure, a collimated X-ray or neutron beam with wave-vector k_{in}, incident at an angle θ_i is specularly reflected with a wave-vector k_{out}. In specular reflection the angle of incident θ_i is equal to the angle of reflection θ_r, (i.e., reflected angle $\theta_r = \theta_i \equiv \theta$). The reflection is usually described in terms of a momentum transfer vector, Q that describes the change in momentum of an X-ray or neutron after reflecting from the thin film. In this case the momentum transfer vector, $Q \equiv |k_{out} - k_{in}|$ is strictly parallel to the surface normal (n) which is chosen to be the z coordinate. By monitoring the incident and the reflected wave

intensities at a given wavelength λ, the reflectivity is reported as a function of momentum transfer *(Q)* defined by:

$$Q = \frac{4\pi \sin\theta}{\lambda} \qquad \text{Eq. 2.2}$$

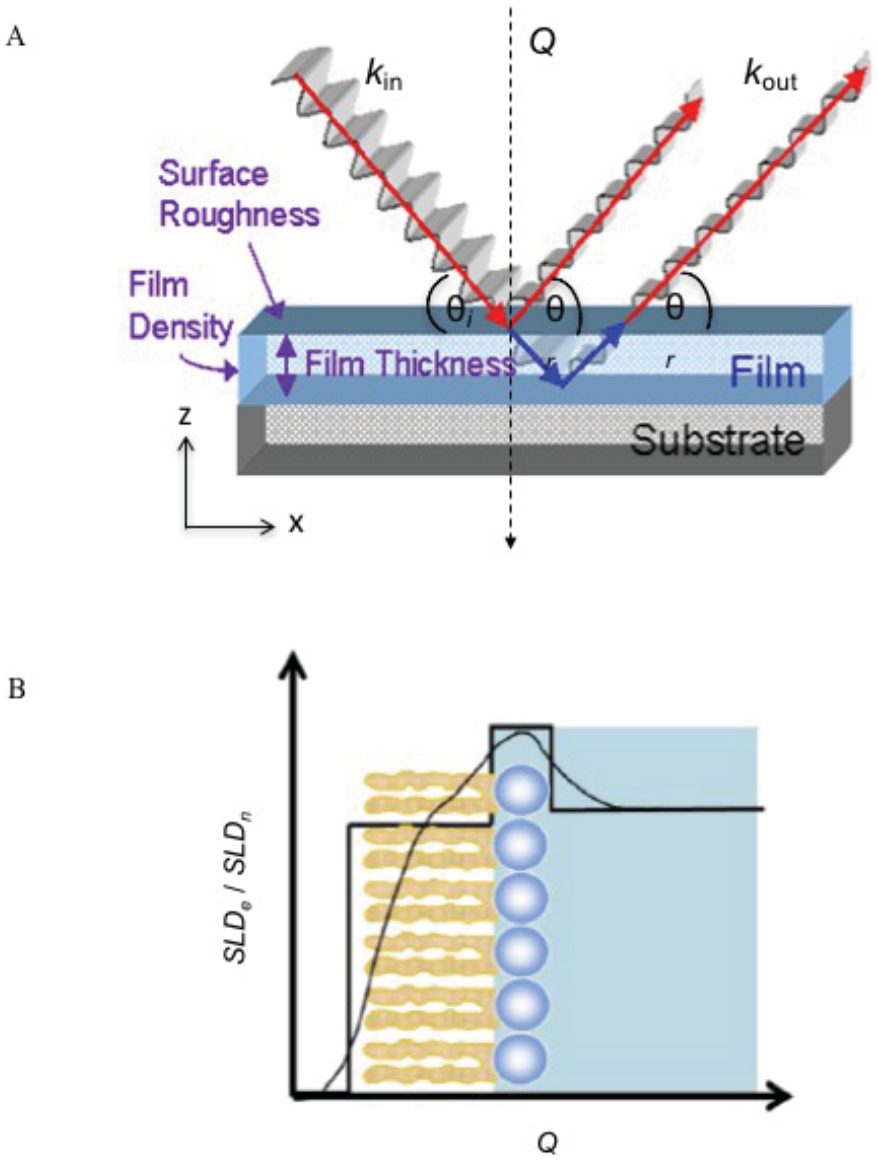

Figure 2.7 The geometry of specular reflectivity. A) A monochromatic wave with wave-vector k_{in} impinging on to an interface at an incidence angle θ_i. The momentum transfer, Q is aligned with the interface normal along the z-direction. **B)** *SLD* versus Q plot of the lipid monolayer provides information about the thickness, density and surface roughness of the monolayer along the surface normal.

Like all other scattering techniques, the reflection of the X-ray or neutron beam depends on the complex refractive index of the lipid monolayer [54, 55]. For X-rays, the refractive index of a thin film is usually a little less than 1 and is defined as:

$$n = 1 - \delta + i\beta \qquad \text{Eq. 2.3}$$

where $\delta = \frac{r_e}{2\pi} \lambda^2 \rho_e$ and $\beta = \frac{\lambda}{4\pi} \mu$. Here λ is the wavelength of the incident wave, r_e is the classical electron radius and ρ_e is the electron density of the monolayer film. The μ is the linear absorption coefficient. The ρ_e of the monolayer film is the electron density of the molecule that constitutes the film. For X-rays, the electron density of a molecule with different atoms *i* can be transformed to a scattering length density *(SLD_e)*, approximated by:

$$SLD_e = \frac{\sum_{i=1}^{n} Z_i r_e}{V_m} \qquad \text{Eq. 2.4}$$

where *Z* is the atomic number and V_m is the volume of the molecule. X-rays react with in-homogeneities of the electron density while neutrons react to changes in the scattering length density. For neutrons, δ and β are given by $\delta = \frac{Nb}{2\pi} \lambda^2$ and $\beta = \frac{\lambda \alpha_a N}{4\pi}$. Here, N is the atomic number density, b is the bound coherent scattering length, α_a is the adsorbtion cross-section and λ is the wavelength of the neutron beam. The scattering length density of a lipid monolayer interacting with neutrons is given by

$$SLD_n = \frac{\sum_{i=1}^{n} b_i}{V_m} \qquad \text{Eq. 2.5}$$

where b_i is the tabulated coherent scattering length of the i^{th} atom in the molecule that constituent the monolayer film. In practice, if we assume the monolayer is homogeneous and has a different electron density (in the case of XR) or scattering length density (in the case of NR) compared with that of the liquid subphase, then a sinusoidal modulation of the density profile of the monolayer-covered surface can be made in order to fit the experimental data [56]. Once the electron or scattering density profile is known, the reflectivity of the monolayer-covered

surface can be calculated and best fit parameters that are used to describe the properties of the monolayer such as film thickness, surface roughness and density, can be determined (Figure 2.7B). For example, in the case of a lipid monolayer only, XR and NR provide information about the thickness of the headgroup and acyl chain group layers, electron density (scattering length density in the case of NR) of the headgroup and acyl chain group layers and the roughness between each of the layers along the *z*-direction. Insertion of proteins into the lipid monolayer can cause the intensities of the reflected beam to change in comparison to that of the lipid monolayer, resulting in a different electron or scattering length density profiles that provide valuable and detailed information about the protein structure within the monolayer film. Comparison of the fitted *SLD* for each layer to the theoretically calculated *SLD* values of each component within the layer enables the volume fraction of each of the component of the monolayer to be calculated [17, 51-53, 55, 56]. As a result, the XR and NR techniques enable us to study the structural features of CLIC1 when inserted into different lipid monolayers.

2.4.2 Advantages of NR over XR

Although X-ray reflectivity data can be used alone to determine certain structural details of CLIC1 interaction with lipid monolayers at the air-water interface, it was complimented with neutron reflectivity data in this thesis, as neutron measurements are advantageous over X-rays in a number of significant ways [18, 52, 54, 56]. The fact that NR technique probes nuclear contrast rather than electron density provides more complex and specific information regarding the structure of the monolayer. In addition, neutrons being typically non-perturbing and highly penetrating allows for great flexibility in sample environments and allows for the use of delicate sample materials (e.g., biological specimens) [51]. Finally, neutrons being able to interact with nuclei have isotopic sensitivity. For example, Hydrogen atom, ^{1}H has a coherent scattering length of -3.74 x 10^{5} Å whereas its isotope ^{2}H commonly known as Deuterium has a value of positive 6.67 x 10^{5} Å [56, 57]. Thus, by replacing hydrogen in biological samples with deuterium, the contrast of the monolayer film can be greatly and selectively enhanced. This technique of contrast variation can be used to highlight a region in a molecule under investigation, and is one of the key advantages of neutron scattering over X-rays and light scattering for soft matter.

2.4.3 Contrast variation of protein and lipids in the monolayer film

Multiple experiments of the same monolayer film that differ only in contrast variation can be used to resolve the chemical composition and structure of different components within the LMs [58]. In contrast variation methods, the natural contrast between different biological compounds such as proteins and lipids can be highlighted either through the manipulation of the H_2O/D_2O ratio of the liquid subphase or by selective deuteration of the compounds under study. Contrast variation of the subphase can cause the scattering length density of a specific component within the monolayer film to match that of the solvent background, thus rendering the compound "neutron invisible". As a result, the reflectivity data generated will only yield structural information of the highlighted components within the multiunit system [58]. For example, in a lipid-protein monolayer system, if the scattering length density of the lipid is matched to that of the buffer subphase, then the reflectivity profile obtained will only represent the chemical and structural composition of the protein within the lipid monolayer film.

Selective deuteration, on the other hand, relies on partial, selective or full chemical or biological deuteration to change the scattering length density of the complex in question [51, 58, 59]. For a lipid-protein monolayer system, which consists of both a membrane mimic and a protein, the selective deuteration method offers a means of altering the scattering length density of the different components within the LMs. This gives the opportunity to visualise the components separately, which can greatly simplify data analysis in order to underline the position, structure and dynamics of individual compounds within the system [59]. One can argue that isotopic substitution of biological compounds should render them chemically different, however, studies have shown that substitution of hydrogen in biological samples with deuterium results in only limited to no impact on the sample's structure and function [59-61]. Therefore, in this thesis, both hydrogenated and deuterated CLIC1 protein and POPC lipid was used in two different H_2O/D_2O contrast buffer subphase: D_2O and ACMW (a mixture of composition 92% H_2O and 8% D_2O by volume) to yield reflectivity profiles in order to elucidate the structure of the CLIC1 membrane-bound form.

2.5 Conclusion

Members of the CLIC protein family possess the intriguing property that they can spontaneously insert from a stable soluble state into lipid membranes to form integral membrane ion channels. Factors such as redox environment, pH and lipid composition (mentioned in detail in Chapter 1) have been found to trigger the structural conformation of the soluble CLIC1 protein to insert into the membrane. However, the precise mechanism of how CLIC1 autonomously inserts into membranes and what regulates this insertion is still largely unresolved. In a broader sense, this thesis aims to determine the role of phospholipids and cholesterol in the spontaneous membrane insertion of CLIC1 protein using the Langmuir monolayer (LM) technique (to be reviewed in Chapter 3).

The LM technique is an insightful method to study the interactions between proteins, peptides and the lipid membrane. The surface pressure-area isotherms are useful to extract information regarding the nature of the interactions between the molecules especially the lipids and the CLIC1 proteins at the air-water interface. An increase in the initial surface area of the lipid monolayer (held at a π of 20mN/m) upon protein insertion is indicative of attractive forces between the molecules and can provide information regarding the surface activity of the proteins, insertion capacity of CLIC1 protein into different lipid films and CLIC1's lipid specificity requirements. Scattering methods like X-ray reflectivity (XR) and neutron reflectivity (NR) at the air-water interface provide insight into the structural characterization and orientation of the molecules in the LM. Chapter 4 will discuss the methodology and results of the X-ray and neutron reflectivity (XR and NR) techniques used to resolve the structure of the CLIC1 membrane-bound form. NR, in particular, has an advantage because of the availability of isotopic contrast variation and has been particularly used in this thesis to investigate the CLIC1 configuration within the lipid monolayers. In addition, Chapters 5 and 6 aim to investigate the structural requirements of CLIC1 protein and lipid molecules deemed necessary for the lipid-protein interactions. In summary, the LM, XR and NR techniques provide a complete picture to investigate the membrane-associated studies, which would be helpful in detecting the origin and mechanism of the spontaneous membrane insertion of the protein, CLIC1.

2.6 References

[1] Engelman, D. (2005) Membranes are more mosaic than fluid., *Nature 438*, 578-580.

[2] Goñi, F. (2014) The basic structure and dynamics of cell membranes: an update of the Singer-Nicolson model., *Biochim Biophys Acta. 838*, 1467-1476.

[3] Nicolson, G. (2014) The Fluid-Mosaic Model of Membrane Structure: still relevant to understanding the structure, function and dynamics of biological membranes after more than 40 years., *Biochim Biophys Acta. 838*, 1451-1466.

[4] Singer, S., and Nicolson, G. (1972) The fluid mosaic model of the structure of cell membranes., *Science 175*, 720-731.

[5] Alan, F. (1999) *Structure and Mechanism in Protein Science:A Guide to Enzyme Catalysis and Protein Folding*, 1st edition ed., W. H. Freeman and Company, United States of America.

[6] Brown, M. (2012) Curvature forces in membrane lipid-protein interactions., *Biochemistry 51*, 9782-9795.

[7] David, W. (2005) *Proteins: Structure and Function*, 1 ed., Wiley.

[8] Baker, M. (2010) Structural biology: The gatekeepers revealed., *Nature 465*, 823-826.

[9] Blakeley, M., Hasnain, S., and Antonyuk, S. (2015) Sub-atomic resolution X-ray crystallography and neutron crystallography: promise, challenges and potential., *IUCrJ. 2*, 464-474.

[10] Céolin, R., and Rietveld, I. (2016) X-ray crystallography, an essential tool for the determination of thermodynamic relationships between crystalline polymorphs., *Ann Pharm Fr 74*, 12-20.

[11] Oxenoid, K., and Chou, J. (2016) A Functional NMR for Membrane Proteins: Dynamics, Ligand Binding, and Allosteric Modulation., *Protein Sci.*

[12] Shi, Y. (2014) A glimpse of structural biology through X-ray crystallography., *Cell 159*, 995-1014.

[13] Wu, B., Barile, E., De, S., Wei, J., Purves, A., and Pellecchia, M. (2015) High-Throughput Screening by Nuclear Magnetic Resonance (HTS by NMR) for the Identification of PPIs Antagonists., *Curr Top Med Chem. 15*, 2032-2042.

[14] Zheng, H., Handing, K., Zimmerman, M., Shabalin, I., Almo, S., and Minor, W. (2015) X-ray crystallography over the past decade for novel drug discovery - where are we heading next?, *Expert Opin Drug Discov 10*, 975-989.

[15] Brown, M. (1994) Modulation of rhodopsin function by properties of the membrane bilayer., *Chem Phys Lipids. 73*, 159-180.

[16] Langmuir, I. (1917) THE CONSTITUTION AND FUNDAMENTAL PROPERTIES OF SOLIDS AND LIQUIDS. II. LIQUIDS., *J. Am. Chem. Soc. 39*, 1848–1906.

[17] Majewski, J., Kuhl, T., Wong, J., and Smith, G. (2000) X-ray and neutron surface scattering for studying lipid/polymer assemblies at the air-liquid and solid-liquid interfaces., *J Biotechnol. 74*, 207-231.

[18] Eisenberger, P., and Feldman, L. (1981) New approaches to surface structure determinations., *Science 214*, 300-305.

[19] Gaines, G. L. (1966) *Insoluble monolayers at liquid-gas interfaces*, New,York Interscience Publishers

[20] Feng, S. (1999) Interpretation of Mechanochemical Properties of Lipid Bilayer Vesicles from the Equation of State or Pressure−Area Measurement of the Monolayer at the Air−Water or Oil−Water Interface, *Langmuir 15*, 998–1010.

[21] Feng, S., and MacDonald, R. (1995) Effects of chain unsaturation on the equation of state for lipid monolayers at the air-water interface., *Biophys J. 69*, 460-469.

[22] Cantor, R., and Dill, K. (1986) Theory for the equation of state of phospholipid monolayers, *Langmuir 2*, 331–337.

[23] Möhwald, H. (1990) Phospholipid and phospholipid-protein monolayers at the air/water interface., *Annu Rev Phys Chem. 41*, 441-476.

[24] Nagle, J. (1976) Theory of lipid monolayer and bilayer phase transitions: effect of headgroup interactions., *J Membr Biol. 27*, 233-250.

[25] Thakur, G., Micic, M., and Leblanc, R. (2009) Surface chemistry of Alzheimer's disease: a Langmuir monolayer approach., *Colloids Surf B Biointerfaces. 74*, 436-456.

[26] Lipowsky, R., and Sackmann, E. (1995) *Structure and dynamics of membranes*, Oxford: Elsevier., Amsterdam.

[27] Liscum, L., and Underwood, K. (1995) Intracellular cholesterol transport and compartmentation., *J Biol Chem. 270*, 15443-15446.

[28] Mouritsen, O., and Zuckermann, M. (2004) What's so special about cholesterol?, *Lipids 39*, 1101-1113.

[29] Simons, K., and Ikonen, E. (2000) How cells handle cholesterol., *Science 290*, 1721-1726.

[30] van Meer, G., Voelker, D., and Feigenson, G. (2008) Membrane lipids: where they are and how they behave., *Nat Rev Mol Cell Biol. 9*, 112-124.

[31] Williams, A., Day, B., Kite, B., McPherson, M., Slebodnick, C., Morris, J., and Gandour, R. (2005) Homologous, long-chain alkyl dendrons form homologous thin films on silver oxide surfaces., *Chem Commun (Camb). 40*, 5053-5055.

[32] Piknova, B., Schram, V., and Hall, S. (2002) Pulmonary surfactant: phase behavior and function., *Curr Opin Struct Biol. 12*, 487-494.

[33] Collinsa, S., Maheshb, G., Radhakrishnanb, G., and Dhathathreyan, A. (1995) Effects of spreading solvents on the monolayers of poly(methyl methacrylate), *Colloids Surf. A: Physicochem. Eng. Aspects 95*, 293-297.

[34] Kaganer, V., and Loginov, E. (1993) Crystallization phase transitions and phase diagram of Langmuir monolayers., *Phys Rev Lett. 71*, 2599-2602.

[35] Kaganer, V., Möhwald, H., and Dutta, P. (1999) Structure and phase transitions in Langmuir monolayers, *Rev. Mod. Phys. 71*, 779-819.

[36] Petty, M. C. (1996) *Langmuir-Blodgett films an introduction*, Cambridge ; New York : Cambridge University Press.

[37] Blume, A. (1979) A comparative study of the phase transitions of phospholipid bilayers and monolayers., *Biochim Biophys Acta. 557*, 32-44.

[38] Feigenson, G. (2006) Phase behavior of lipid mixtures., *Nat Chem Biol. 2*, 560-563.

[39] Bonmatin, J., Laprévote, O., and Peypoux, F. (2003) Diversity among microbial cyclic lipopeptides: iturins and surfactins. Activity-structure relationships to design new bioactive agents., *Comb Chem High Throughput Screen. 6*, 541-556.

[40] Brezesinski, G., and Möhwald, H. (2003) Langmuir monolayers to study interactions at model membrane surfaces, *Advances in Colloid and Interface Science, 100-102*, 563-584.

[41] Gzyl-Malcher, B., and Paluch, M. (2008) Studies of lipid interactions in mixed Langmuir monolayers, *Thin Solid Films, 516*, 8865-8872.

[42] Mouritsen, O., and Bloom, M. (1984) Mattress model of lipid-protein interactions in membranes., *Biophys J. 46*, 141-153.

[43] Nobre, T., Pavinatto, F., Caseli, L., Barros-Timmons, A., Dynarowicz-Łątka, P., and Oliveira Jr, O. (2015) Interactions of bioactive molecules & nanomaterials with Langmuir monolayers as cell membrane models, *Thin Solid Films 593*, 158-188.

[44] Stefaniu, C., Brezesinski, G., and Möhwald, H. Langmuir monolayers as models to study processes at membrane surfaces, *Advances in Colloid and Interface Science 208*, 197-213.

[45] Taneva, S., and Keough, K. (1995) Calcium ions and interactions of pulmonary surfactant proteins SP-B and SP-C with phospholipids in spread monolayers at the air/water interface., *Biochim Biophys Acta. 236*, 185-195.

[46] Dutta, P., Peng, J., Lin, B., Ketterson, J., Prakash, M., Georgopoulos, P., and Ehrlich, S. (1987) X-ray diffraction studies of organic monolayers on the surface of water., *Phys Rev Lett. 58*, 2228-2231.

[47] Dluhy, R., Stephens, S., Widayati, S., and Williams, A. (1995) Vibrational spectroscopy of biophysical monolayers. Applications of IR and Raman spectroscopy to biomembrane model systems at interfaces, *Spectrochimica Acta Part A: Molecular and Biomolecular Spectroscopy 51*, 1413-1447.

[48] Langevin, D. (1981) Light-scattering study of monolayer viscoelasticity, *Journal of Colloid and Interface Science 80*, 412-425.

[49] Brooks, C., Fuller, G., Frank, C., and Robertson, C. (1999) An Interfacial Stress Rheometer To Study Rheological Transitions in Monolayers at the Air−Water Interface, *Langmuir 15*, 2450–2459.

[50] Als-Nielsen, J., Jacquemain, D., Kjaer, K., Leveiller, F., Lahav, M., and Leiserowitz, L. (1994) Principles and applications of grazing incidence X-ray and neutron scattering from ordered molecular monolayers at the air-water interface, *Physics Reports 246*, 251-313.

[51] Penfold, J., and Thomas, R. (2014) Neutron reflectivity and small angle neutron scattering: An introduction and perspective on recent progress, *Current Opinion in Colloid & Interface Science 19*, 198-206.

[52] Stefaniu, C., and Brezesinski, G. (2014) X-ray investigation of monolayers formed at the soft air/water interface, *Current Opinion in Colloid & Interface Science 19*, 216-227.

[53] James, M., Nelson, A., Holt, S., Saerbeck, T., Hamilton, W., and Klose, F. (2011) The multipurpose time-of-flight neutron reflectometer “Platypus” at Australia's OPAL reactor, *Nuclear Instruments and Methods in Physics Research Section A: Accelerators, Spectrometers, Detectors and Associated Equipment 632*, 112-123.

[54] Russell, T. (1990) X-ray and neutron reflectivity for the investigation of polymers, *Materials Science Reports, 5*, 171-271.

[55] Russell, T. (1996) On the reflectivity of polymers: Neutrons and X-rays, *Physica B: Condensed Matter 221*, 267-283.

[56] Pedersen, J., and Hamley, I. (1994) Analysis of neutron and X-ray reflectivity data by constrained least-squares methods, *Physica B 198*, 16-23.

[57] Schlossman, M. (2002) Liquid–liquid interfaces: studied by X-ray and neutron scattering, *Current Opinion in Colloid & Interface Science, 7*, 235-243.

[58] Jacrot, B. (1976) The study of biological structures by neutron scattering from solution., *Reports on Progress in Physics 39*.

[59] Clifton, L., Neylon, C., and Lakey, J. (2013) Examining protein-lipid complexes using neutron scattering., *Methods Mol Biol. 974*.

[60] Bragina, N., and Chupin, V. (1997) Methods of synthesis of deuterium-labelled lipids, *Russian Chemical Reviews 66*, 975-986.

[61] Leiting, B., Marsilio, F., and O'Connell, J. (1998) Predictable deuteration of recombinant proteins expressed in Escherichia coli., *Anal Biochem. 265*, 351-355.

Chapter 3

Cholesterol Promotes the Interaction of the protein CLIC1 with Phospholipid Monolayers at the Air-Water Interface

Chapter 3

Cholesterol Promotes the Interaction of the protein CLIC1 with Phospholipid Monolayers at the Air-Water Interface

(This chapter has been published in *Membranes* and appears as Khondker R. Hossain, Heba Al Khamici, Stephen A. Holt and Stella M. Valenzuela. 2016. Cholesterol Promotes Interaction of the Protein CLIC1 with Phospholipid Monolayers at the Air-Water Interface, *Membranes*, 6(1), doi: 10.3390/membranes6010015).

3.1 Introduction

Protein structure and function are modulated via interactions with their environment. For integral membrane proteins, the environment represents both the bulk water and lipid membranes that have an active role in shaping the structural topology of the protein [1]. Compared to a decade ago, there is now an abundance of structural data, in particular from X-ray crystallography, on specific lipid-protein interactions. There are multiple examples of Phosphatidylcholine (PC) binding to membrane proteins. The X-ray crystal structure of numerous proteins like the mitochondrial ADP/ATP carrier protein [2], the Na+ K+ ATPase [3], the voltage-gated sodium channel NavRh [4], enzymes such as zinc metalloprotease (ZMPSTE24) [5], bovine heart cytochrome c oxidase [6] etc. have been shown bound to one or more PC molecules. Other proteins like the mitochondrial respiratory membrane protein complex II [7, 8], calcium pump from rabbit sarcoplasmic reticulum [9], membrane water channel protein like aquaporin [10] have been shown to crystallise with different amounts of Phosphatidylethanolamine (PE) molecules in their structure. Cholesterol has also been found facilitating structural rearrangements of proteins upon association with the lipid bilayer, resulting in the spontaneous conversion of the protein from water-soluble to membrane-bound form.

Cholesterol-dependent membrane insertion is a widely observed phenomenon and occurs in many bacterial pore-forming toxins (PFTs), specifically by the cholesterol-dependent cytolysins (CDCs), as well as the human protein perforin, members of the complement membrane attack complex [11] and the amyloid

precursor protein [12, 13] (for details see Chapter 1, Section 1.7.3). Recently, studies have shown that different combinations of phospholipids and cholesterol regulate the functional activity of CLIC1 in artificial lipid membranes [14, 15]. One of these studies, conducted by our group, demonstrated that CLIC1 shows significantly greater ion channel activity in membranes containing cholesterol [15]. Similarly, studies with different CDCs have highlighted different regulatory roles of cholesterol in the toxins' cytolytic mechanisms. For example, studies with streptolysin O have shown that the toxin requires cholesterol for the initial event of membrane binding and this binding can be inhibited by exogenous cholesterol or oxidation [16]. On the other hand, preincubation of listeriolysin O with cholesterol interfered with oligomerisation thus inhibiting its cytolytic activity but did not impair its membrane binding ability [17]. Previously, our group has shown that pre-incubating CLIC1 protein with cholesterol resulted in complete inhibition of ion channel conductivity in artificial phospholipid membranes by mechanisms still largely unknown [15].

In this thesis, we hypothesise that the lipid and sterol components of the biological membrane plays a crucial role in facilitating the spontaneous membrane insertion of CLIC1 protein followed by its oligomerisation to form functional ion channels in cell membranes. We also propose that the cholesterol dependent ion channel activity is due to the regulatory effect of cholesterol on the spontaneous membrane insertion of CLIC1 into artificial lipid membranes. A strong interaction between CLIC1 and cholesterol may induce conformational changes in CLIC1 that facilitates its membrane insertion, followed by its subsequent assembly into functional ion channels within model membranes. The focus of the current investigation is characterisation of the recombinant human CLIC1 protein interactions with pure or mixed phospholipids in the presence or absence of cholesterol. This chapter reports on the spontaneous membrane insertion of CLIC1 into different lipid monolayers at the air-water interface. We found that although highly charged and soluble, CLIC1 is surface active, strongly interacting with pure or mixed phospholipid monolayers containing cholesterol, and may form a relatively stable pre-complex when pre-incubated with cholesterol.

3.2 Materials and Method

The Escherichia coli BL21 cells transformed with pET-28a plasmid containing the genetic sequence of the recombinant His-CLIC1 fusion protein was a gift from Dr S. N. Breit, Centre of Immunology, St. Vincent's hospital, University of New South Wales, Sydney Australia. HiPrep 16/60 Sephacryl S-100 HR GE Healthcare column (pre-packed gel filtration column) was purchased from VWR International (Queensland, Australia). Phospholipids: 1-palmitoyl-2-oleoyl-*sn*-glycero-3-phosphocholine (POPC), 1-palmitoyl-2-oleoyl-*sn*-glycero-3-phosphoserine (POPS) and 1-palmitoyl-2-oleoyl-*sn*-glycero-3-phosphoethanolamine (POPE) were purchased from Avanti Polar Lipids (Alabaster, USA) and used as received. Cholesterol (Chol) was purchased from Sigma Aldrich (Australia). Lipid stock solutions were prepared in spectroscopic grade chloroform (Sigma) at a concentration of 1 mg/ml and stored at -20°C. The following reagents used in HEDS enzyme assay were all purchased from Sigma Aldrich: glutathione reductase (GR) from yeast, reduced glutathione (GSH), reduced nicotinamide adenine dinucleotide phosphate (NADPH) and 2-hydroxyethyl disulphide (HEDS).

All other chemicals used were of standard analytical grade. All buffers and solutions were prepared using demineralised, ultrapure water that was prepared with the Arium® Pro (Sartorius) water system. Ultrapure, demineralised water for aseptic preparation of solutions was sterilised before use by a steam autoclave (Systec DX-150). In addition, all media and solutions were sterilised by filtration using 0.22 μm Millex®GP filter sets (Millipore).

3.2.1 CLIC1 heterologous over-expression

Homologous over-expression of recombinant CLIC1-wild type (CLIC1-wt) protein was enabled by the inducible expression vector system, pET-28a, into which the CLIC1 cDNA was cloned. The pET vector system uses a strong transcriptional promoter, pT7 to induce expression of the CLIC1 coding gene placed downstream from it. The pT7 transcriptional promoter and IPTG inducible promoter controls the expression of bacteriophage T7 RNA polymerase; this is highly selective and active that, when fully induced almost all of the cell's resources are directed towards the expression of the target gene and production of the encoded protein. Hence, the expression of the CLIC1 gene is induced by the addition of the lactose analogue Isopropyl-thio-β-D-galactopyranoside (IPTG); use of this operon allows the expression of T7 RNA polymerase, which in turn transcribes the CLIC1 gene. CLIC1 is expressed as a fusion protein with a 6x Histidine-tag (His) to facilitate protein purification on a nickel-nitrilotriacetic acid (Ni-NTA) matrix affinity column with a fairly high degree of purity and yield. The pET-28a plasmid is engineered to contain a thrombin cleavage site between the His and the target protein, allowing on- or off-column cleavage of the target, CLIC1, from the His with plasma bovine thrombin. Because of the fact that the pET expression vector also contains a kanamycin (Kan) resistant marker, kanamycin was added to all bacterial growth media to maintain selection pressure for the vector containing cells.

CLIC1-wt over-expression and purification were based upon the methods used by Valenzuela et al. (1997) [18]. Glycerol stocks of *Escherichia coli* BL21 (DE3) (Stratagene, USA), transformed with the CLIC1-pET-28a plasmid were spread onto sterile Lennox Broth (LB)-Kanamycin agar plates (1 g tryptone, 0.5 g yeast extract, 0.5 g NaCl, 1.5 g agar per 1 litre distilled H_2O containing 30 μg/ml kanamycin) and incubated overnight at 37 °C. A single colony was collected from the transformants and added to 100 ml of sterile 2xYT media (1.6 g tryptone, 1 g yeast extract, 0.5 g NaCl per 1 litre distilled H_2O) containing kanamycin (30 μg/ml) and incubated overnight (~16 hours) at 37 °C with shaking at 200 rpm. This overnight culture was then added into fresh 2xYT media (2 litres containing 30 μg/ml kanamycin) and incubated for approximately 3 hours to reach an OD_{600nm} of 0.6 - 0.8. IPTG (1 mM) was subsequently added to induce the over-

expression of the fusion protein and cells were left overnight for further growth at 20 °C with shaking at 200 rpm to achieve optimum protein over-expression.

The cells were then harvested by centrifugation in a CR22GIII High Speed Refrigerated Centrifuge (Hitachi) using an R13A rotor at 6200 rpm for 30 minutes at 6°C. The pellet was either stored at - 80 ^{o} C for later use or resuspended in approximately 8 ml Lysis buffer, pH 8.0 (300 mM KCl, 50mM KH_2PO_4, 5mM Imidazole). 1 mM protease inhibitor cocktail (2 mM AEBSF, 0.3 μM Aprotinin, 130 μM Bestatin, 1 mM EDTA, 14 μM E-64, 1 μM Leupeptin) was added fresh per litre of original culture and incubated at 4°C to initiate cell lysis. Cells were lysed by sonication on ice for 3-4 cycles of 30 seconds pulsed (intensity 3, pulse 0.5 sec) on a Vibra^{M} Cell sonicator (Sonics and Materials Inc.) followed by the addition of 50 μl of 20% (v/v) Triton X-100 solution. The remaining cell debris was removed by centrifugation using a R18A rotor at 12,000 rpm for 45 minutes at 6°C. The supernatant containing soluble proteins was collected and filtered through a 0.45 μm filter to remove any remaining cell debris and subjected to further purification.

3.2.2 His-CLIC1 fusion protein purification and cleavage

3.2.2.1 Nickel Affinity Chromatography

His-tagged fusion proteins can be purified a number of ways, including cation exchange and affinity chromatography. The high specificity of affinity chromatography, however, makes it an attractive purification option despite its cost. A specific ligand is covalently immobilised on a suitable matrix (agarose). Only molecules in the mobile phase that have an affinity for the immobilised ligand will be bound to the column. This principle was used to bind soluble His-CLIC1 fusion protein (located in the supernatant of *Escherichia coli* BL21 (DE3) lysate) to Ni^{2+} ions covalently bonded to the immobilised nitrilotriacetic acid matrix (NTA), where Ni-NTA and His-CLIC1 are the immobilised ligand and the target molecule, respectively (Figure 3.1). After binding to the immobilised ligand, the protein can be eluted by introducing a competing agent such as imidazole or an additional metal chelating agent (EDTA). Purification and all experimental procedures were performed under reducing conditions, using 1 mM

Dithiothreitol (DTT) or 0.5 mM *tris*-2-carboxyethyl-phosphine (TCEP) to prevent oxidative dimerization of the protein [19].

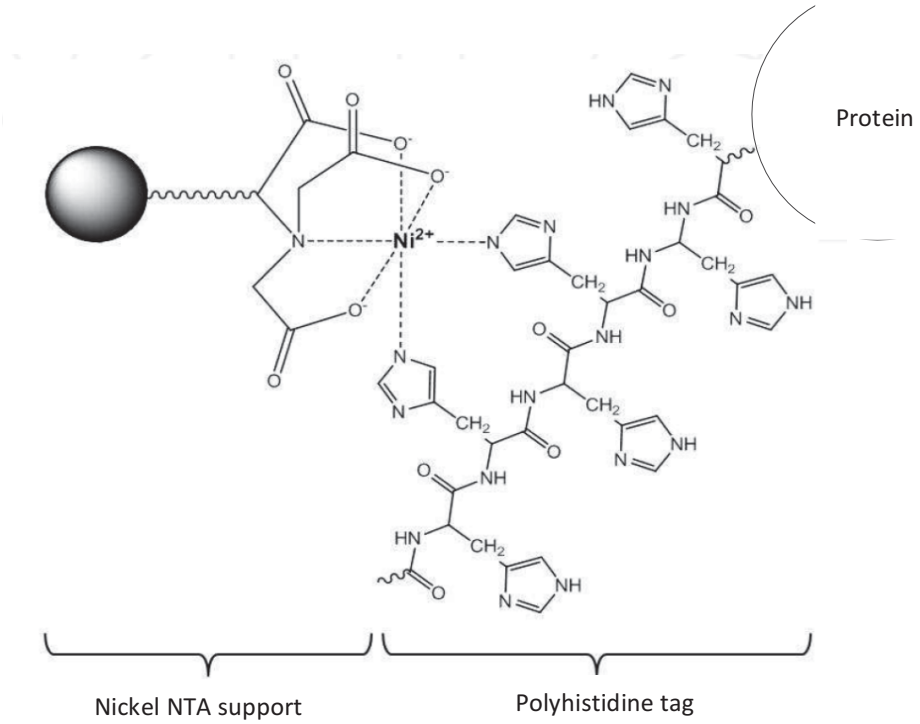

Figure 3.1 Schematic diagram showing the complex formed between the poly-Histidine tagged protein and a Ni-NTA matrix.

A 10 ml Bio-Rad column was packed with 2 ml Ni-NTA suspension (Bio-Rad) and equilibrated at 20°C with 10-column volumns (CV) of Binding buffer, pH 8.0 (300 mM KCL, 50 mM KH_2PO_4, 10 mM Imidazole). The supernatant was loaded onto the column and incubated at 4°C for one hour with mild agitation to allow optimum binding between His-CLIC1 fusion protein and the Ni-NTA matrix, whilst other proteins that have no affinity for Ni^{2+} elute through the column. The column was subsequently washed twice with 10 CV of Binding buffer followed by Wash Buffer, pH 8.0 (300 mM KCL, 50 mM KH_2PO_4, 20 mM Imidazole) to remove any non-specifically bound proteins and any unbound His-CLIC1. The fusion protein was eluted using Elution Buffer, pH 8.0 (300 mM KCL, 50 mM KH_2PO_4, 250 mM Imidazole) in fractions of 1 ml and pooled together in

preparation for off-column thrombin digestion. The column was regenerated with 0.5 M NaOH solution according to the manufacturer's instructions.

Thereafter, a volume of 50 μl (1 U/ml) of bovine plasma thrombin per litre of cell culture, was added to the His-CLIC1 fusion protein and incubated at 4°C for at least 16 hours with mild agitation. Thrombin is a site-specific protease that cleaves proteins guided by a recognition sequence (Leu-Val-Pro-Arg-Gly-Ser) [20, 21]. The thrombin cleaves between the arginine and glycine residues, releasing the CLIC1 from the His tag with glycine and serine appended to the N-terminal of the CLIC1 protein. This cleavage results in a solution of CLIC1-wt, His and thrombin, which were further purified using Size Exclusion Chromatography. During purification, samples of whole cell, supernatant, pellet, supernatant flow-through, washes, His-CLIC1 elution and thrombin-CLIC1 solutions were collected for analysis by SDS-PAGE and quantified by absorbance spectrometry at A_{280nm} using a ND-1000 spectrophotometer (Nanodrop).

3.2.2.2 Size Exclusion Chromatography

Size Exclusion Chromatography (SEC), using a Hiprep 16/60 Sephacryl S-100 column (VWR International), was used to further purify recombinant CLIC1-wt protein following its cleavage from the His-tag by the enzyme, bovine plasma thrombin. SEC by gel filtration is based on the fractionation of proteins by their size and/or their molecular weight. Different molecules in a solution are separated as the sample flows through the porous inert matrices, characterised by an exclusion limit. The exclusion limit on the Sephacryl S-100 column is 1 kDa to 100 kDa, meaning molecules in this range are able to enter the pores in the beads. The smallest molecules are able to enter more pores and are retained in the beads longer resulting in them being eluted last, while molecules of a greater size remain in the mobile phase and are eluted first. Therefore, a massive advantage of using SEC is its ability to separate different oligomeric forms of the protein resulting in the collection of either monomeric (27 kDa) or dimeric (46 kDa) forms of CLIC1-wt protein.

Size exclusion chromatography was performed using the ÄKTA prime plus system. Prior to start of the protein purification, the system was washed and pre-equilibrated with degassed filtered milliQ H_2O followed by Column Sizing Buffer pH 7.5 (100 mM KCL, 20 mM Hepes, 1 mM sodium azide, 1 mM DTT or 0.5 mM TCEP). Hiprep 16/60 Sephacryl S-100 column was attached to the ÄKTA prime plus system through the inlet and outlet tubing and manually washed with 1 CV of Column Sizing Buffer. A maximum column pressure of 0.15 MPa and flow rate of 0.3 ml/min was fixed for all purification methods. After pre-equilibrating the system and column with Column Sizing Buffer, the CLIC1 thrombin solution was applied to a 15 ml sample loop and a pre-programmed method that transferred the sample to the column at a flow rate of 0.25 ml/min was commenced. Eluted fractions were collected in volumes of 2 ml. The purity of the eluted CLIC1-wt protein was then determined by Western Blot analysis and HEDS enzyme assay was performed to check for functionality. At the end of the purification run, the column was rinsed with at least 2 CV of Column Sizing Buffer at a flow rate of 0.3 ml/min to remove any impurities and was then disconnected from the ÄKTA prime plus system. Finally, the system was rinsed 2-3 times with degassed filtered milliQ H_2O and then stored in 20% ethanol to prevent microbial contamination.

3.2.3 Protein Concentration Determination

A colorimetric protein assay was used for the measurement of protein concentration. The Bradford protein quantification assay was performed in accordance with the manufacturer's instructions (Bio-Rad). This assay is based on a shift in the absorbance maximum when Coomassie® Brilliant Blue G-250 dye associates with proteins and the protein concentration quantified using the Lambert-Beer's Law. The Bradford reagent was mixed with the protein sample in a volumetric ratio of 1:1, incubated for 5 min at room temperature (RT) and absorbance was determined at 595 nm. Measurement readings were carried out in triplicates. A calibration curve was established each time a protein assay was performed with bovine serum albumin (BSA) dilutions of known concentrations of 0 – 2 mg/ml. Using the standard curve, the protein concentration of each sample was determined according to its absorbance by interpolation [22].

3.2.4 SDS-PAGE

Sodium Dodecyl Sulfate-PolyAcrylamide (SDS-PAGE) Gel Electrophoresis was carried out using a Bio-Rad Mini Transfer-Blot®Cell to analyse the protein samples. 12.5% SDS-polyacrylamide gels were prepared using 10 ml of Next Gel®12.5% Acrylamide solution (Amresco) and polymerisation was initiated using 60 µl of ammonium persulphate solution (100 mg/ml in H_2O) and 6 µl of NNNN'-tetramethylethylenediamine (TEMED) prior to pouring the gels. The gels were allowed to set at RT for approximately 1-2 hours and then submerged in running buffer in the Cell. The running buffer was prepared by diluting 50 mL of 20x Next Gel®Running buffer (Amresco) in 950 mL of milli-Q H_2O.

For SDS-PAGE electrophoresis, cell lysates and protein samples were prepared by a 1:1 dilution with 4x Laemmli buffer pH 6.8 (20% glycerol (v/v), 2% SDS, 0.02% bromophenolblue, 2mM DDT and 90 mM Tris-HCl). The samples were boiled at 95°C for 10 minutes prior to being loaded onto the gels. Separation was achieved at a voltage of 200 V for variable times. The Precision Plus Protein™ Unstained Standard (Bio-Rad) was used to estimate the apparent MW on the gel. After completion of electrophoresis, gels were stained for approximately 1 hour with Coomassie Staining (0.2% Coomassie G-250, 10% acetic acid and 40% methanol) and destained overnight using Destaining buffer (10% acetic acid and 50% methanol).

3.2.5 Western Blotting

To further analyse the purity of CLIC1-wt proteins after SEC, protein fractions were analysed using NuPAGE®Novex Bis-tris Mini Gels according to the manufacturer's instruction (Invitrogen). The samples were prepared as mentioned above and were loaded onto a 12 well NuPAGE® Novex® 10% Bis-Tris gel (Invitrogen). The voltage was set to a constant 200 V and the gel was run for approximately 30 minutes in 1x NuPAGE®MES SDS Running Buffer pH 7.3 (50 mM MES, 50 mM Tris Base, 0.1% SDS, 1 mM EDTA). After electrophoresis, samples were transferred onto a polyvinylidene fluoride membrane (PVDF) (iBlot®2 Transfer Stacks, PVDF, regular size kit) for 7 minutes at 20 V using an iBlot2 (Life Technologies) according to the manufacturer's instruction.

Following the electrotransfer of proteins, the membrane was blocked with 2% (w/v) BSA in PBST pH 7.4 (137 mM NaCl, 2.7 mM KCl, 10 mM Na_2HPO_4, 2 mM KH_2PO_4, and 0.1% Tween 20) and gently shaken overnight at 4°C. After washing 3x for 10 minutes with PBST, the membrane was then incubated for 1 hour with either anti-CLIC1 primary antibody (Sapphire Bioscience) or mouse anti-His antibody (Invitrogen) which was diluted in 1:5,000 with 2% BSA in PBST. After incubation at RT for 1 hour, the membrane was washed 3x for 10 minutes with PBST, and then incubated with 1:10,000 dilutions of anti-mouse IgG-Alkaline phosphatase secondary antibody (Santa Cruz Technologies) for an additional 1 hour. Excess secondary antibody was removed by washing the membrane 3x for 10 minutes with PBST. Detection was performed using the protocol for the SIGMA*FAST*™ BCIP®/NBT detection kit provided by Sigma Aldrich (Australia).

3.2.6 HEDS Enzyme Assay

HEDS enzyme assay was performed according to the method described in Al Khamici *et al.* (2015) to evaluate the functional activity of the purified CLIC1-wt protein [23]. Each enzymatic assay was performed in triplicate in a 96-well plate containing 5 mM potassium phosphate buffer, pH 7. Final concentrations of 1 mM EDTA, 250 µM NADPH, 50 nM GR and 1 mM HEDS was added to the buffer solution followed by the addition of 5 µM CLIC1 protein and the mixture was incubated at 37°C for 5 minutes. Enzymatic reaction was initiated by the addition of 1 mM GSH to make up a final volume of 200 µl. Consumption of NADPH was monitored at A_{340nm} using a BioTek microplate spectrophotometer. All kinetic data analysis was performed using Microsoft Excel 2010. HcTrx-5 (IS5) protein from *Haemonchus contortus* was also purified as previously described [24] and equivalent amount of IS5 was used as a positive control in the HEDS enzyme assay.

3.3 Langmuir Film Experiments

All Langmuir experiments were carried out in triplicate at room temperature (~25°C) on a 25 ml KCl/Hepes buffer, pH 6.5 (0.1 M KCL, 0.1 mM HEPES and 0.01 mM $CaCl_2$) subphase using a computer controlled Langmuir trough (Nima Technologies, Coventry, UK). The rectangular trough had a surface

area of 90 cm^2 and the surface pressure (π) was measured by the Wilhelmy method using a filter paper plate. Prior to each experiment, the Langmuir trough was thoroughly cleaned with chloroform and rinsed with milli-Q water and then filled with 25 ml KCl/Hepes buffer solution and checked for contaminants by running isotherm cycles. The pressure was set to zero using the NIMA program and surface pressure-area isotherm was carried out at a barrier speed of 20 cm^2/min. The pressure was allowed to vary ± 0.5 from the set point. If the pressure increased above the set point, the surface of the buffer was aspirated to remove any impurities and isotherm cycles were repeated until no change in pressure was detected (Figure 2.3, Chapter 2). Once the buffer maintained a constant surface pressure, CLIC1 surface activity and its interaction with different lipid monolayers were analysed. For all Langmuir experiments, 50 µg of CLIC1 in 0.2 ml KCL/Hepes buffer (pH 6.5) was injected into the subphase using a glass microsyringe in order to achieve a final CLIC1 concentration of 2 µg/ml. All lipid and lipid:cholesterol (5:1 mole ratio) monolayers were prepared by spreading dropwise 10 µl of 1 mg/ml stock solution onto the surface of the KCl/Hepes buffer (pH 6.5) in the Langmuir trough.

3.3.1 Surface activity of CLIC1 protein at the Air-Water interface

To evaluate the "surface activity" of CLIC1-wt protein, the change in surface pressure (π) due to the movement of the protein from the KCl/Hepes buffer subphase (pH 6.5) to the air-water interface was measured. Before injecting CLIC1 into the buffer subphase, barriers were partially closed to give a total surface area of 50 cm^2, roughly the same as the surface area of the lipid monolayers compressed to 20 mN/m for the subsequent insertion experiments. 50 µg of CLIC1 was then injected into the subphase using a glass microsyringe.

3.3.2 Interaction of CLIC1 with Phospholipid or Cholesterol Monolayers

To evaluate the interactions between CLIC1 and lipid membranes, insertion of CLIC1 into lipid monolayers held at a constant surface pressure (π) was measured. The phospholipids or cholesterol (details mentioned in Chapter 2, Section 2.2.2) monolayers were prepared by spreading dropwise 10 µl of 1 mg/ml lipid or cholesterol stock solution onto the surface of the KCl/Hepes buffer in the Langmuir trough (Nima Technologies, Coventry, UK). Once spread, the lipid

monolayer was allowed to equilibrate for 5 min (to ensure complete evaporation of the chloroform) prior to commencing isotherm cycles in order to form a uniform monolayer (Figure 2.5, Chapter 2). The barrier then symmetrically compressed the monolayer at 20 cm^2/min to a target π of 20 mN/m. The speed at which the barrier moves to maintain this target pressure was controlled by a feedback loop and depends upon how fast the barrier needs to expand or contract in response to a perturbation. Recombinant CLIC1-wt protein (50 μg) was then injected into the subphase underneath the lipid monolayer and changes in surface area were measured. The data is represented as percentage surface area expansion ΔA= [(A-Ai)/Ai]*100, where A is the surface area at time t and Ai is the initial surface area of the monolayer when it reached 20 mN/m. Since the monolayer was kept at a constant π, the barrier expanded as a result of protein insertion and the percentage area expansion was taken as a measure of favourable CLIC1-lipid interactions.

3.3.3 Interaction of CLIC1 with Mixed Lipid Monolayers

To determine the regulatory role of cholesterol in the spontaneous membrane insertion of CLIC1, phospholipid monolayers of POPC, POPS and POPE containing cholesterol in a mole ratio of 5:1 were formed as mentioned above. In addition, to evaluate the interaction of CLIC1 in different lipid environments, a variety of mixed lipid monolayers were formed using a combination of two of the three following lipids: POPC, POPE or POPS in a mole ratio of 5:1 alone or with cholesterol in a mole ratio of 4:1:1. The mixed lipid monolayers were held at a constant pressure of 20 mN/m and the percentage surface area expansion, ΔA, after 3 hours following CLIC1 injection into the subphase was recorded.

3.3.4 Pre-incubation of CLIC1 with Cholesterol

50 μl of the cholesterol stock solution (1 mg/ml in chloroform) was added gently to 200 μl of KCl/Hepes buffer in a glass test tube. The chloroform was removed using N_2 gas for duration of 1 hour. Recombinant CLIC1-wt protein (50 μg) was then added to the buffer solution containing the cholesterol and incubated for an hour on ice prior to addition of this pre-incubated protein sample to the corresponding POPC:Chol monolayer held at a constant π of 20 mN/m in the

Langmuir trough. To ensure that there was no precipitation or aggregation of CLIC1 protein upon incubation with cholesterol, CLIC1 samples pre-incubated with cholesterol (at mole ratio 1:1) in 200 μl of KCL/Hepes Buffer solution (pH 6.5) were centrifuged and the various fractions collected for SDS-PAGE analysis. Samples were collected at different time points: at the start of pre-incubation (time 0) and after 1 hour pre-incubation (post-incubation). The soluble fraction and pellet samples post-incubation and after centrifugation at 14,000 rpm for 15 mins were also collected for analysis. As a control, CLIC1 was pre-incubated in buffer only without cholesterol and samples were collected and treated in the same way as outlined above. Samples were run on SDS-PAGE gel as described in Section 3.2.4.

3.4 Results

3.4.1 Protein Overexpression and Purification

Recombinant CLIC1-wt protein was readily purified from *E.coli* cell lysates following induced expression and two chromatography steps. The over-expression conditions for CLIC1-wt had been previously determined [25] and the recombinant protein was over-expressed and purified as described in Section 3.2. The initial purification step was performed manually by nickel-affinity chromatograph, yielding a protein recovery of 10-12 mg per litre bacterial culture.

3.4.1.1 SDS-PAGE analysis of samples collected from Affinity Chromatography

The purity of His-CLIC1 fusion protein was assessed by SDS-PAGE (Figure 3.2). Lane 2 in Figure 3.2 represents the flow through off the Ni-NTA column and indicates that considerable amount of CLIC1 fusion protein is bound to the column while a fraction did not bind. The column was washed several times to remove any impurities, with relatively small amount of unbound His-CLIC1 protein lost during wash 1 (Lane 3). The eluted protein bands in Lanes 6 and 7, Figure 3.2 showed more than one protein band as a result of dimerisation of CLIC1 under oxidative environment. Since CLIC1 protein has the ability to reversibly convert between two distinct conformational structures under redox environment [14], 1 mM DTT or 0.5 mM TCEP solution was added to the eluted samples to maintain CLIC1 in its monomeric state under reducing condition. The eluted samples were pooled together and thrombin was then added to cleave the 6x Histidine tag from the CLIC1 protein. The protein band in Lane 8 of Figure 3.2 shows the CLIC1 thrombin mixture and the band correlates to the theoretical molecular mass of approximately 27 kDa for CLIC1. A protein band for thrombin was not visible in Lane 8 as the concentration of the enzyme was comparatively low for visualisation. The control band in Figure 3.2, Lane 9 indicates that His-CLIC1 protein was successfully purified.

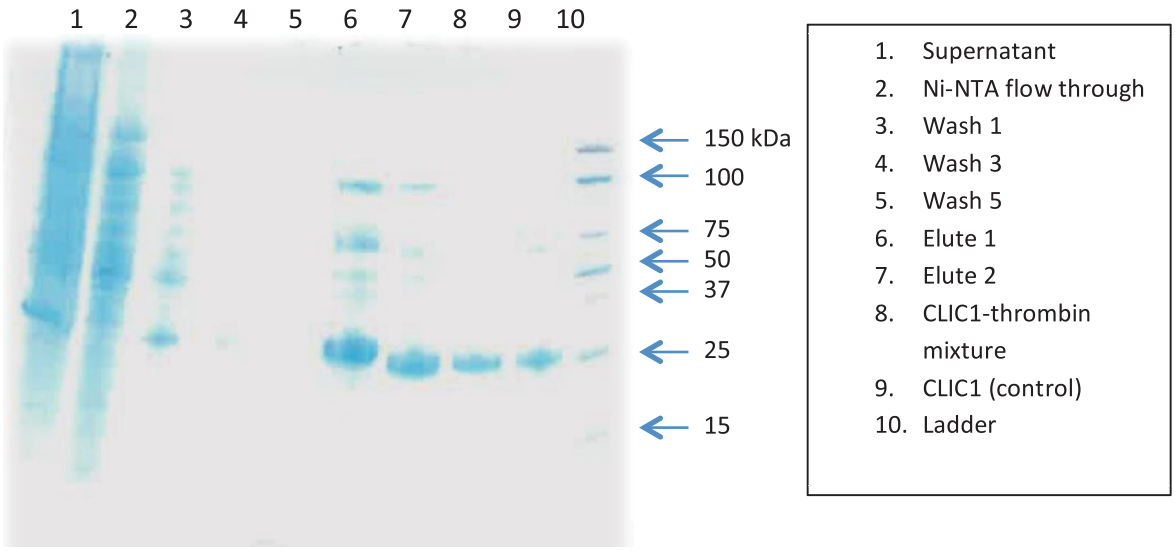

Figure 3.2 SDS-PAGE gel showing a representative CLIC1 purification. The supernatant of the lysate of CLIC1 and the flow through off the Ni-NTA column are shown in Lane 1 and 2 respectively. Samples collected after several washes of the column are shown in Lanes 3-5. Lane 6 and 7 indicates the eluted protein samples and the CLIC1-thrombine mixture is shown in Lane 8. The recombinant CLIC1 protein used as a control in Lane 9 indicates that His-tagged CLIC1 protein purification was successful. The ladder in Lane 10 also confirms the presence of CLIC1 protein as the protein bands in Lanes 6-9 correlate to the molecular weight of approximately 27 kDa for CLIC1.

3.4.1.2 Size Exclusion Chromatography Results

The CLIC1-thrombine solution was then subjected to the second purification step performed by Size Exclusion Chromatography, SEC (Figure 3.3). The chromatogram revealed two peaks, one between elution fractions F13-F17 and the other from F21-F27 (Figure 3.3). Such a result was not surprising as CLIC1 is known to exist as a monomer under reducing conditions or oxidises to form a dimer in the presence of an oxidizing agent like H_2O_2 [19].

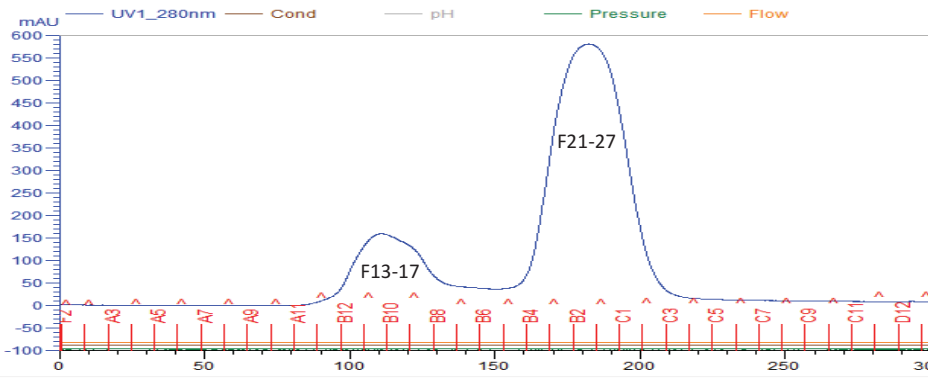

Figure 3.3 Eluted fractions of CLIC1-wt protein from Size Exclusion Chromatography Column. The second peak area of the fractions (F21-27) represents 15 ml of eluted CLIC1-wt protein that was aliquoted and stored at -80°C.

To verify the identity of the eluted CLIC1 protein in the SEC fractions, SDS-PAGE followed by Western blot analysis were conducted as described in Sections 3.2.4 and 3.2.5. CLIC1-wt protein concentration was then determined using the Bradford protein quantification assay kit. As seen in Figure 3.4A, a faint band in Lane 3 confirmed that the first peak area of fractions (F13-17) belongs to dimeric CLIC1 protein as the band correlates to the molecular weight of 46 kDa for CLIC1 dimer. The size of the band also suggested that only a very little amount of the pooled CLIC1 protein had oxidised to form a dimer with the majority of the CLIC1 protein purified in its monomeric form. The clear protein bands in Lanes 4 and 5 of the SDS-PAGE gel established the SEC fractions (F21-27) being monomeric CLIC1. As seen in Figure 3.4B, Western blot analysis using anti-CLIC1 antibody, resulted in a single protein band of molecular mass of approximately 27 kDa, thus confirming the presence of CLIC1-wt. In addition, the absence of a band when stained with anti-His antibody (Figure 3.4C) confirmed the successful cleavage of 6x Histidine-tag off CLIC1 protein, thus

resulting in a purity of approximately 90-95%. Notably, no degradation products were detected as seen by the absence of other protein bands in the SDS-PAGE gel (Figure 3.4A). Protein concentration was then determined by Bradford assay (Figure 3.4D) for each of the fractions collected, yielding approximately 20-22 mg of purified CLIC1-wt protein. The purified protein fractions were aliquoted and stored at -80°C and were subjected to functional analysis as described below.

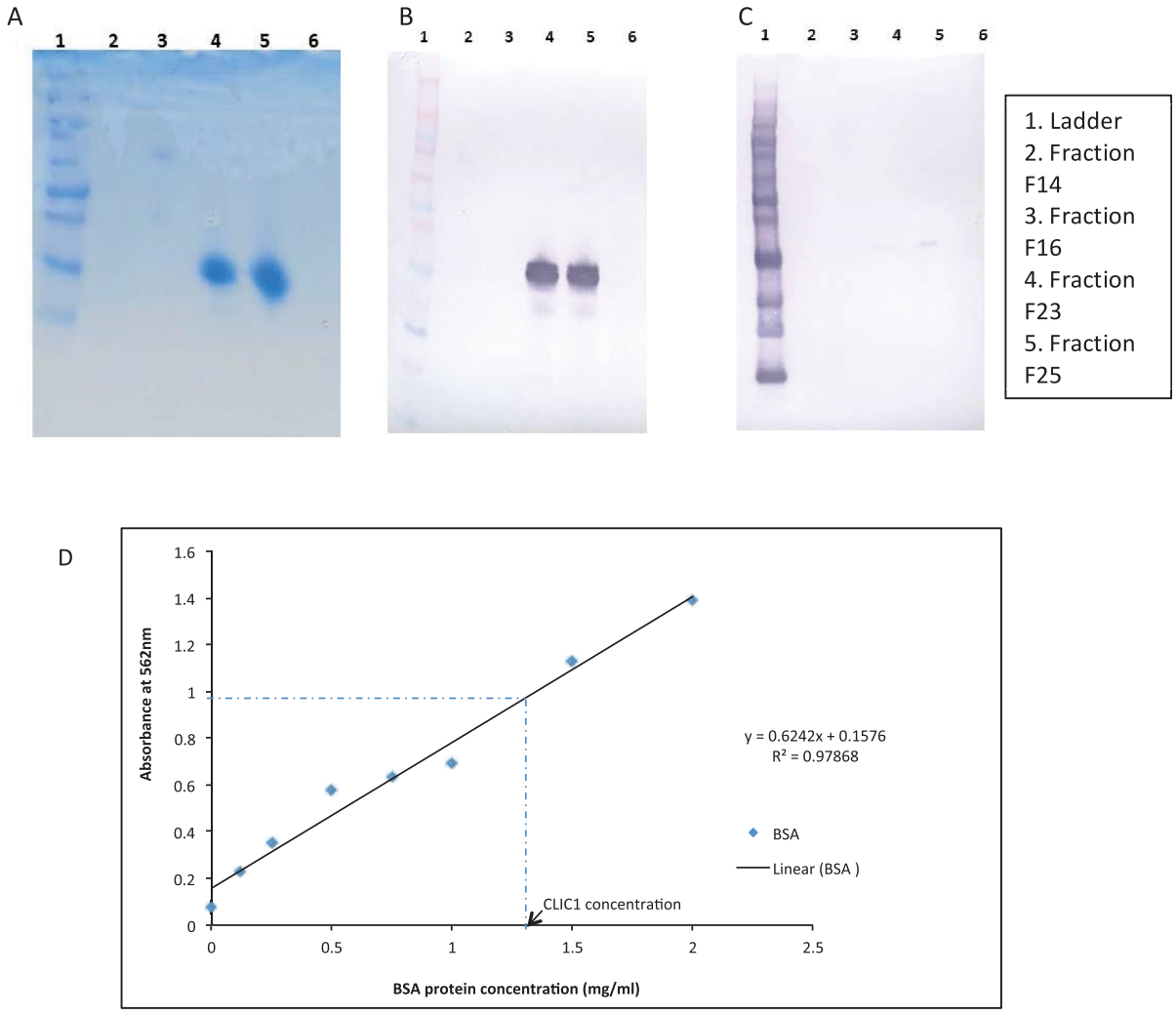

Figure 3.4 SDS-PAGE, Western blot and Bradford Protein Quantification assay results of the SEC CLIC1-wt fractions. A) SDS-PAGE analysis of the SEC CLIC1 fractions: 14, 16, 23 and 25. **B)** Western blot analysis of the SEC CLIC1 fractions with anti-CLIC1 antibody **C)** Anti-His antibody labeling of the SEC CLIC1 fractions. **D)** Standard calibration curve of BSA dilutions of known concentrations of 0 – 2 mg/ml. The protein concentration of each SEC CLIC1 fraction was determined according to its absorbance by interpolation (as shown by the dash line).

3.4.2 HEDS Enzyme Assay

The functional activity of a protein is often related to the correct structural fold of that protein. Hence, to determine the functional activity of the purified CLIC1-wt protein, HEDS enzyme assay was performed as described previously [23]. Al Khamici *et. al.* (2015) have demonstrated that the soluble form of CLIC proteins have an enzymatic activity that is distinct from the channel activity of their integral membrane forms [23]. Structural studies have shown that in the soluble form, CLIC proteins adopt a glutathione S-transferase (GST) fold and have an active site with a conserved glutaredoxin monothiol motif, similar to that of the omega class GSTs (details mentioned in Chapter 1). In this assay, 2-hydroxyethyl disulphide (HEDS), a low molecular weight compound found to act as a specific and sensitive substrate suitable for studying glutaredoxin enzymatic activity, was therefore used to study the enzymatic activity of CLIC1 proteins [23]. The assay is based on the concept of protein de/glutathionylation and the enzymatic activity is depicted by the ability of the CLIC1 protein to reduce the HEDS substrate when coupled with glutathione (GSH) and glutathione reductase (GR) resulting in the consumption of NADPH that is monitored at A_{340} nm [23]. As seen in Figure 3.5, the buffer control sample containing all the reagents, expect for CLIC1 and IS5 (positive control) proteins, shows no enzymatic activity over time. However, as seen in Figure 3.5, addition of the positive control IS5 or CLIC1 protein to the buffer results in a decrease in the absorbance at 340 nm, that in turn correlates to the consumption of NADPH indicating significant enzymatic activity.

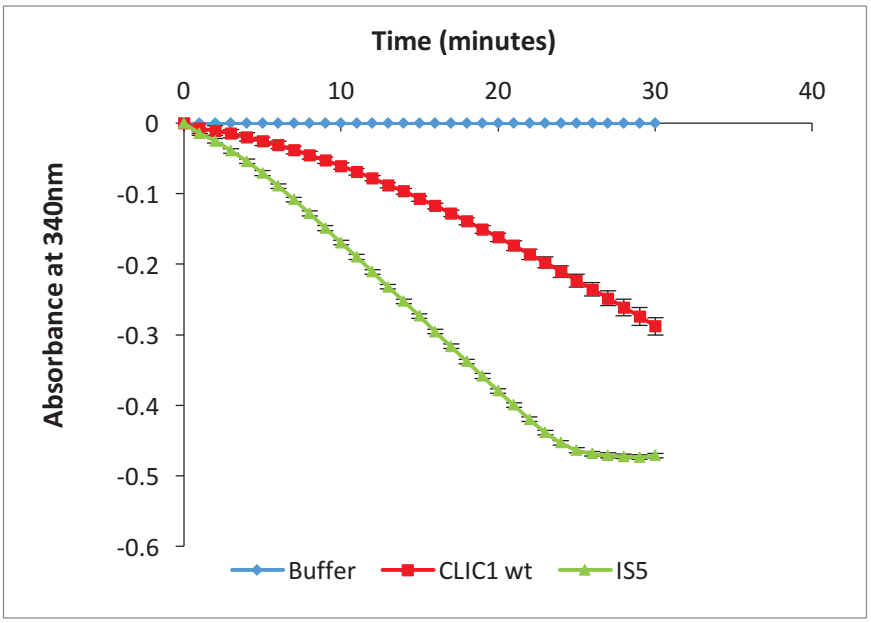

Figure 3.5 Oxidoreductase activity of the purified CLIC1 protein. 5 µM reduced CLIC1 or IS5 (positive control) protein was added to 5 mM potassium phosphate buffer, pH 7 containing 1 mM EDTA, 250 µM NADPH, 50 nM GR and 1 mM HEDS. The reaction was initiated by the addition of 1 mM GSH and the absorbance of NADPH was monitored at $A_{340\ nm}$. CLIC1-wt protein showed significant enzymatic activity.

3.4.3 Surface activity of CLIC1 protein

With the aim of understanding CLIC1-wt protein interactions with lipid monolayers formed on a buffer subphase, we first assessed CLIC1's inherent propensity to localise to the air-water interface. This is done by measuring changes in π while maintaining a constant surface area following the injection of 50 µg of CLIC1-wt protein into the buffer subphase. The surface activity of CLIC1 protein was measured in triplicate using a Langmuir trough as described in Section 3.3.1. The adsorption isotherm of CLIC1-wt protein shown in Figure 3.6 represents the averaged of the three individual experiments. Remarkably, the adsorption isotherm of CLIC1-wt protein showed a two-stage behaviour where after a lag time of 10 minutes, the surface-pressure (π) increased sharply to about 2.5 mN/m and then plateaued followed by a subsequent slow increase to achieve a final π of 14 mN/m. This unusual two-phase adsorption behaviour of CLIC1-wt protein was reproducible and may reflect a protein specific effect following injection of the protein into the buffer subphase.

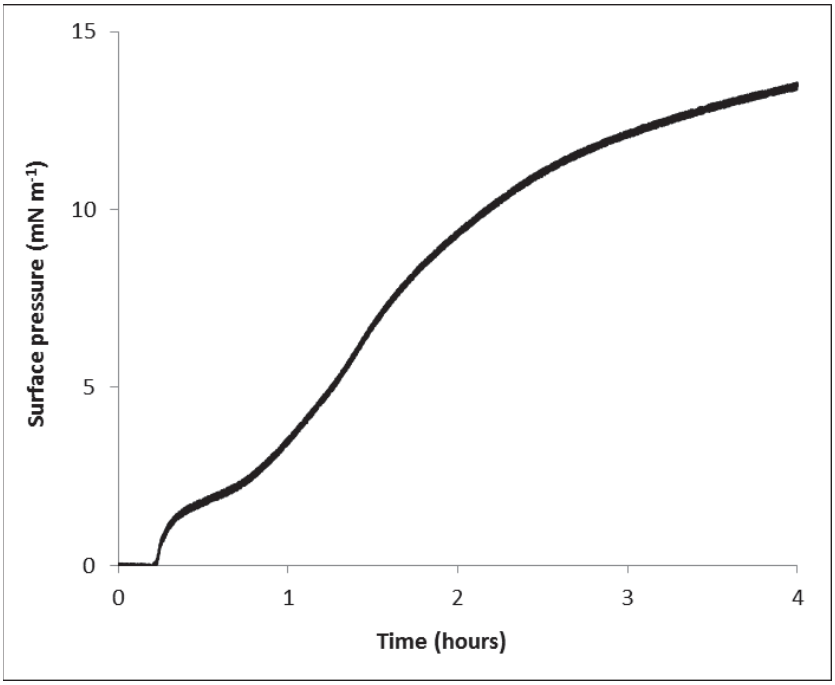

Figure 3.6 Adsorption isotherm of CLIC1 to an air-water interface at 25°C at a final concentration of 2 µg/ml. The CLIC1 adsorption isotherm showed a two-stage behaviour with a maximum π increase of 14 mN/m. (number of experiments, N=3)

3.4.4 Interaction of CLIC1 with Lipid Monolayers

Due to the complexity of interacting molecules in cells, a model membrane system was used to investigate the interaction of CLIC1 protein with lipid films. Previously published studies of CLIC1 ion channel activity within tethered lipid bilayers (tBLMs) monitored using impedance spectroscopy have revealed that CLIC1 does not form functional ion channels in the absence of cholesterol in the membrane [15]. The tBLMs system provided a direct functional measurement of the conductive properties of the protein once embedded within the membrane, it however revealed very little information about the interaction or insertion of CLIC1 within the artificial phospholipid membrane. Hence, the Langmuir monolayer system was used to provide a measure of the protein's association and / or insertion into the phospholipid film allowing independent comparison of these two distinct processes. On the one hand the protein's functional membrane activity, and on the other, it's association with, and / or insertion into, the phospholipid monolayer.

Lipid monolayers were formed using POPC, POPE, POPS phospholipids or cholesterol (Chol) on a KCL/Hepes buffer subphase (pH 6.5). The percentage change in the initial lipid monolayer area (ΔA) over a period of 3 hours following CLIC1 addition underneath preformed monolayers held at a constant pressure of 20 mN/m are shown in Figure 3.7A and 3.7B respectively. As seen in Figure 3.7A, the insertion of CLIC1 protein in the different phospholipid or cholesterol monolayers also shows a two-stage interaction behaviour, an initial sharp increase in ΔA after a lag phase followed by a plateau and subsequent slow increase in ΔA over a period of 3 hours, as previously seen in Figure 3.6. This further suggests that during the lag phase CLIC1 may undergo a structural reorganisation likely to involve a rapid rearrangement of the N-terminal domain for insertion into the monolayer, followed by oligomerisation to form fully functional ion channels.

In the absence of CLIC1 protein, the lipid monolayers held at a constant surface pressure of 20 mN/m (Figure 3.7B, white bars) were relatively stable over a number of hours followed by an insignificant amount of relaxation or decrease in film area. These minor changes are likely caused by the loss of water from the subphase due to evaporation over time. The percentage change in area of the lipid or cholesterol monolayers after 3 hours following addition of CLIC1 into the subphase were plotted in Figure 3.7B (solid black bars). CLIC1 protein favourably interacted with zwitterionic lipid monolayers showing the greatest percentage of surface area expansion (ΔA) of 11.3 ± 0.3% for POPE monolayer followed by a ΔA of 3.7 ± 0.6 % for POPC monolayer. CLIC1 protein showed little to no obvious interaction with the anionic POPS monolayer. CLIC1 protein also showed significant interaction with the cholesterol monolayer resulting in a ΔA value of 11.2 ± 0.5%.

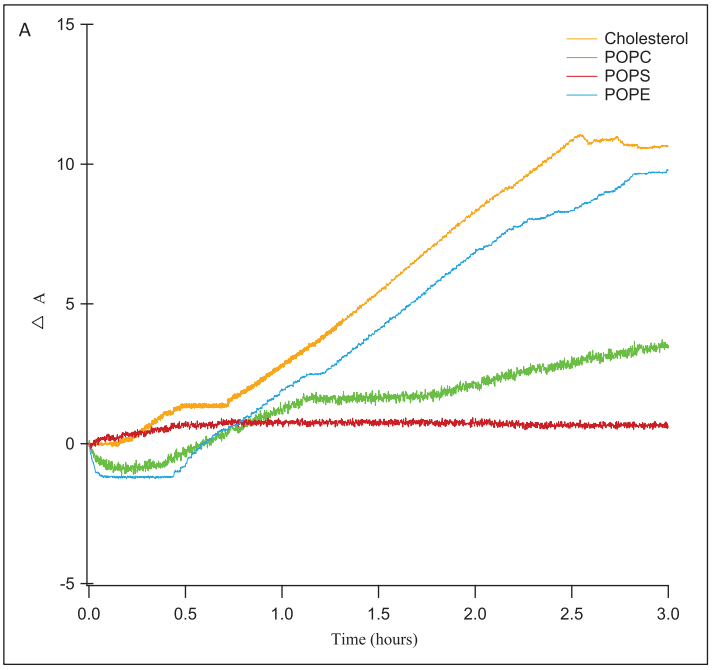

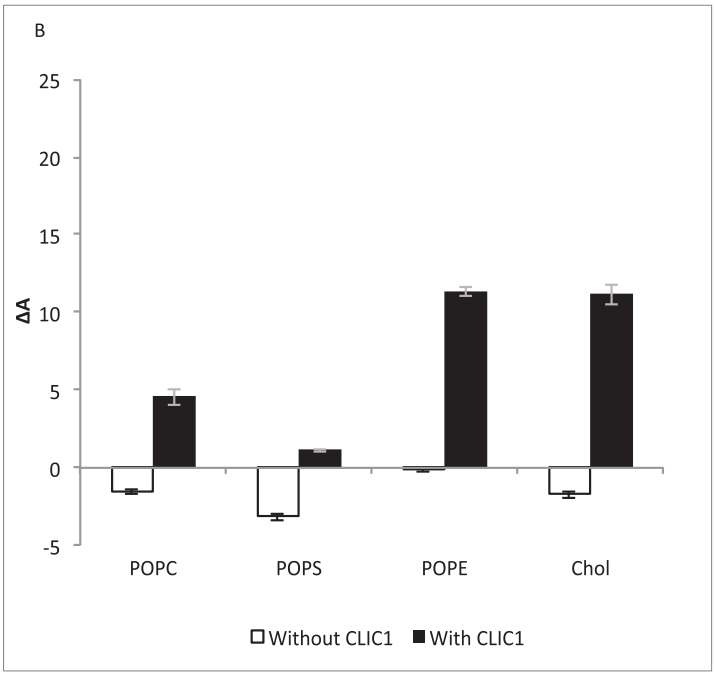

Figure 3.7 CLIC1 protein interactions with different phospholipid or cholesterol monolayers.

A) Percentage area expansion profiles for CLIC1 insertion into cholesterol (orange line), POPC (green line), POPS (red line) and POPE (blue line) monolayers on buffer subphase. (N=1)

B) Corresponding percent area expansion profiles of different lipids or cholesterol monolayers without (white) and with (black) recombinant CLIC1 wild-type protein after 3 hours following protein injection into the subphase. The insertion of CLIC1 in the different lipid or sterol monolayers shows two-stages of interaction, an initial sharp increase in ΔA after a lag phase followed by a plateau and subsequent slow increase in ΔA over a period of 3 hours. (N=3)

3.4.5 Interaction of CLIC1 with Phospholipid Monolayers containing Cholesterol

The spontaneous membrane insertion or interaction of CLIC1 with POPC, POPS and POPE monolayers containing cholesterol (in a mole ratio of 5:1) was found to be entirely different in comparison to that observed for the phospholipid monolayers in the absence of cholesterol. Comparison of the percentage trough area expansion (ΔA) of POPC, POPS and POPE monolayers without cholesterol (Figure 3.8, white bars) and with cholesterol (Figure 3.8, black bars), 3 hours after CLIC1 addition to the buffer subphase are shown in Figure 3.8. The addition of cholesterol to POPC and POPS lead to a significant increase in ΔA of approximately 18.01 ± 0.73 % for POPC:Chol monolayer and 18.62 ± 0.45% for POPS:Chol monolayer thus indicating a preferential interaction and / or insertion of CLIC1 into phospholipid monolayers containing cholesterol. Contrariwise, the interaction of CLIC1 with POPE monolayer decreased from a ΔA value of 11.3 ± 0.3% (Figure 3.7B) to a ΔA value of 5.8 ± 0.24 % (Figure 3.8) in the presence of cholesterol.

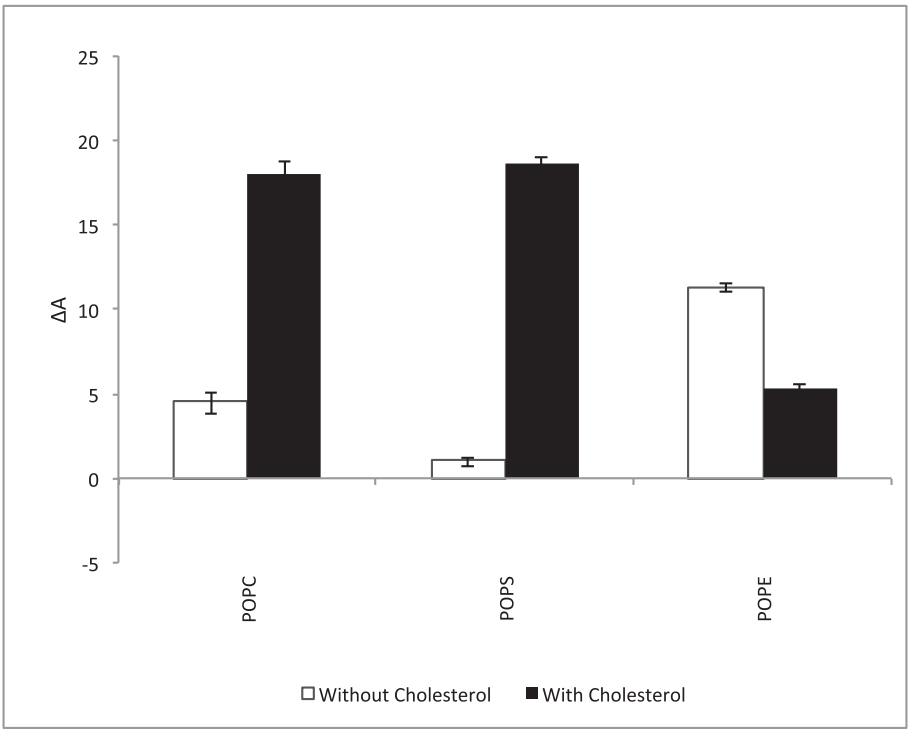

Figure 3.8 CLIC1 protein interactions with phospholipid monolayers containing cholesterol. The figure shows percentage area expansion profiles of different lipid monolayers without (white bars) and with (black bars) cholesterol after 3 hours following recombinant CLIC1 protein injection into the subphase (N=3).

3.4.6 Interaction of CLIC1 with Mixed Lipid Monolayers

To evaluate the interaction of CLIC1 protein in different lipid environments, a variety of mixed monolayers were formed using either of the two lipids: POPC, POPE or POPS in a mole ratio of 5:1 alone or with cholesterol in a mole ratio of 4:1:1. The mixed monolayers were held at a constant pressure of 20 mN/m and the percentage surface area expansion ΔA after 3 hours of CLIC1 injection into the subphase was recorded (Figure 3.9). Among the several lipid combinations tested, only the combinations that showed significant CLIC1 membrane insertion are shown in Figure 3.9. CLIC1 protein did not insert into POPE:POPS monolayer but when this lipid monolayer combination was supplemented with cholesterol, the highest percentage change in area of approximately ~22.04± 0.51% was observed. CLIC1 also showed membrane interaction only after supplementing POPC:POPE and POPS:POPE monolayers with cholesterol. As seen in Figure 3.8, CLIC1 showed greater insertion in POPE monolayer containing no cholesterol. Similarly, CLIC1 injection into a POPE:POPC (5:1 mole ratio) monolayer resulted in a percentage change in area of ΔA ~9.04 ± 0.71%, whereas inclusion of cholesterol in a POPE:POPC monolayer resulted in a reduced ΔA value of 4.8 ± 0.46% (Figure 3.9). It is also not surprising that CLIC1 shows greater levels of insertion to a POPC:POPE:Chol monolayer (ΔA ~ 9.3± 0.3) in comparison to POPE:POPC:Chol monolayer (ΔA ~4.8 ± 0.46%) (See figure 3.8, black bars) for such an interaction was evident from the results shown in Figure 3.7B and 3.8.

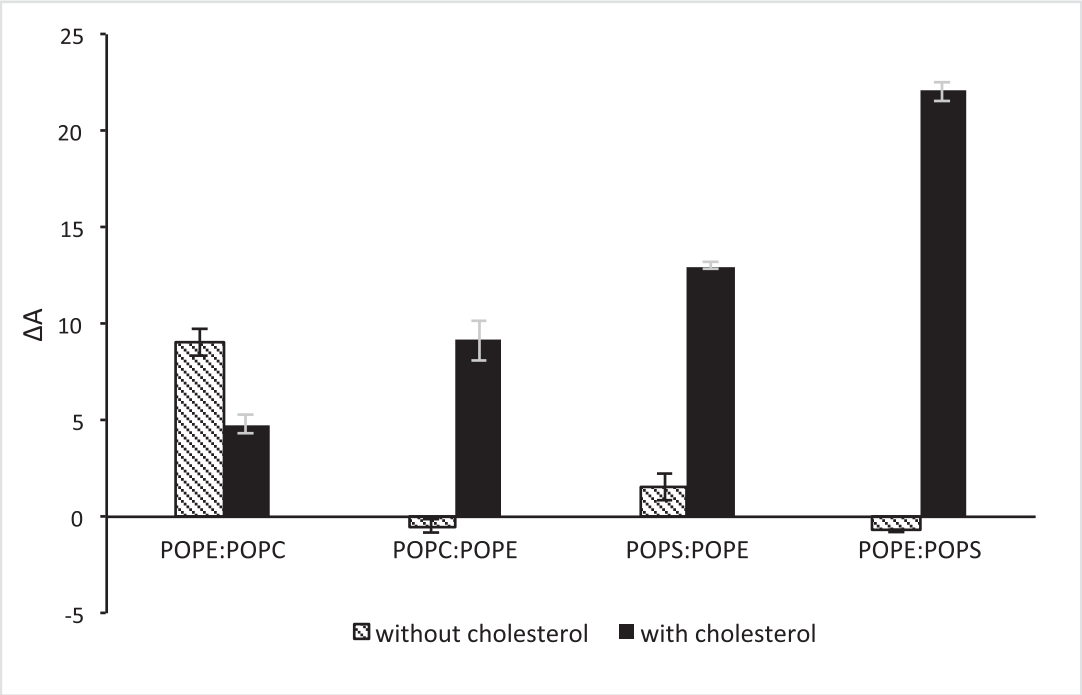

Figure 3.9 CLIC1 protein interactions with mixed lipid monolayers. The figure shows percentage area expansion profiles of monolayers made of different lipid combinations with/without cholesterol (black/white bars) after 3 hours of CLIC1 protein injection into the subphase. CLIC1 protein showed the greatest amount of insertion and/or membrane interactions in POPE:POPS monolayer containing cholesterol. (N=3)

3.4.7 Surface pressure-Area isotherms of Mixed Phospholipid Monolayers

CLIC1 shows varying degrees of interactions with different mixtures of phospholipid monolayers either in the absence or presence of cholesterol. It should be taken into account that although all the phospholipids have similar acyl chain lengths, their head-groups vary drastically. As such, it is expected that the packing behaviour of the different mixed lipid monolayers would be distinct between one another. This difference in packing behaviour is quite evident from Figure 3.10, which displays the surface pressure-area isotherms of the various different lipid mixtures in the absence (Figure 3.10A) and presence of cholesterol (Figure 3.10B). As seen in Figure 3.10A, lipid combinations containing a greater mole percentage of POPE proceed to a more condensed phase upon compression, with the mean area of ~67 $Å^2$ and ~58 $Å^2$ per molecule for POPE:POPC and POPE:POPS (5:1 mole ratio) monolayers respectively. In contrast, monolayers of POPC:POPE and POPS:POPE (where the mole ratios have been reversed) show a mean area of ~96 $Å^2$ and ~90 $Å^2$ per molecule respectively. However, in the presence of cholesterol, the ordering of the mixed lipid monolayers due to the cholesterol is obvious from the condensing effect observed from the surface pressure-area isotherms in Figure 3.10B. Although cholesterol condenses the POPE:POPC and POPE:POPS monolayers to a similar mean area of ~60 $Å^2$ per molecule, the insertion of CLIC1 within these monolayers was significantly different and may account for the presence of a completely different protein-lipid interaction that warrants further investigation.

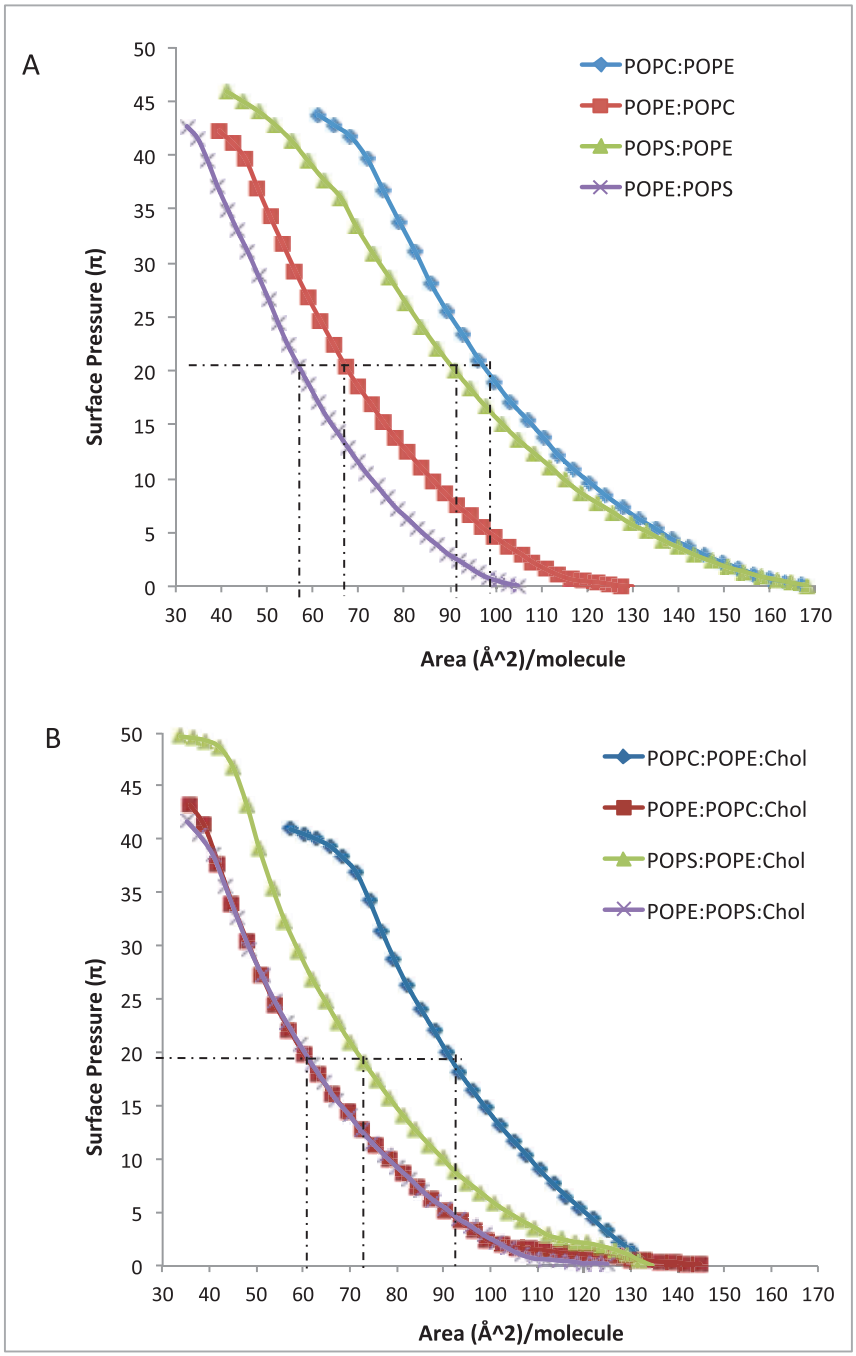

Figure 3.10 Surface pressure-Area isotherms of mixed lipid monolayers. The calculated area per molecule in these graphs is based on the total number of molecules present in the different lipid monolayers. **A)** Surface pressure-Area isotherms of different phospholipid mixtures of 5:1 mole ratio in the absence of cholesterol **(B)** Surface pressure-Area isotherms of the same phospholipid mixtures containing cholesterol in a 4:1:1 mole ratio measured with a Langmuir film balance (N=3).

3.4.7 CLIC1-Cholesterol interaction

Recent studies with impedance spectroscopy on tBLMs have shown that cholesterol in membranes regulates the ion channel activity of CLIC1 into model membranes [15]. Comparable results were also obtained with Langmuir experiments where CLIC1 showed strong preference for associating with or intercalating into pure phospholipid or mixed phospholipid monolayers containing cholesterol. Impedance spectroscopic studies revealed that pre-incubation of CLIC1 protein with cholesterol completely diminished ion channel conductivity [15]. Whether pre-incubation of CLIC1 with cholesterol hampered the proteins' ability to insert into the membrane and / or interfered with the oligomerisation process of the protein within the model membrane to form function ion channels, is a question that still remains unresolved. In order to elucidate whether the interaction between CLIC1 and cholesterol was occurring pre- or post- CLIC1 insertion into the membrane, experiments were carried out which involved pre-incubation of CLIC1 with cholesterol prior to its addition to the POPC:Chol (5:1 mole ratio) monolayer.

To ensure that pre-incubation of CLIC1 with cholesterol did not result in any precipitation or aggregation of the protein, samples were analysed by SDS-PAGE before and after one hour of CLIC1 incubation with cholesterol followed by centrifugation at 14,000 rpm for 15 min. As a control, recombinant CLIC1-wt protein was pre-incubated in buffer only without cholesterol and samples were collected and analysed as described above. The result of the SDS-PAGE analysis of protein samples collected pre- and post- CLIC1 incubation with cholesterol (followed by high speed centrifugation) is shown in Figure 3.11. In Figure 3.11, Lanes 6 and 7 represent protein bands of CLIC1-cholestrol pre-incubated samples collected pre- and post-centrifugation respectively. The protein bands confirmed that the bulk of the protein remains soluble in the buffer solution even after centrifugation and thus, is available for interaction with the POPC:Chol monolayer. The absence of a protein band in Lane 8 further confirmed that pre-incubation of CLIC1 with cholesterol showed no traces of protein precipitation or aggregation.

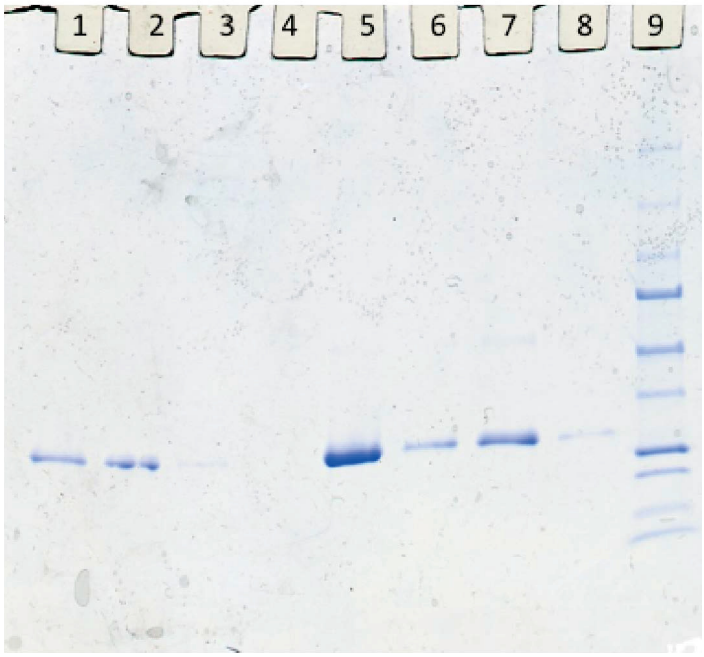

Wells 1-4: CLIC1-wt (control)

1. Incubated in buffer only (no cholesterol) - time 0
2. Post incubation and post centrifugation – soluble fraction
3. Post incubation and post centrifugation- pellet
4. Empty

Wells 5-8: CLIC1 pre-incubated with Cholesterol

5. Incubation time 0
6. Post incubation- time 1 hour
7. Post incubation and post centrifugation – soluble fraction
8. Post incubation and post centrifugation – pellet
9. Protein standards

Figure 3.11 SDS-PAGE gel showing CLIC1- cholesterol pre-incubation. Samples of CLIC1 pre-incubated with cholesterol (at mole ratio 1:1) in 200ul of KCL/Hepes Buffer solution (pH 6.5) were collected for SDS-PAGE analysis. Samples were collected at different time points: at the start of pre-incubation (time 0) (**Lane 5**) and after 1 hour pre-incubation (post-incubation) (**Lane 6**). The soluble fraction (**Lane 7**) and pellet (**Lane 8**) samples after post-incubation and centrifugation at 14,000 rpm for 15 mins were also collected for analysis. As a control, CLIC1 was pre-incubated in buffer only without cholesterol and samples were collected and analysed (**Lanes 1-3**). Pre-incubation of CLIC1 protein with cholesterol did not result in any protein precipitation or aggregation, rather bulk of the protein remained soluble for interaction with lipid monolayers.

The percentage area expansion of POPC:Chol monolayer held at a constant surface pressure of 20 mN/m after 3 hours without CLIC1 and following injection of recombinant CLIC1-wt/pre-incubated CLIC1 into the subphase is shown in Figure 3.12. As seen in Figure 3.12, pre-incubation of CLIC1 protein with cholesterol prior to its addition to the monolayer, significantly ($p > 0.005$) reduced the spontaneous membrane insertion of CLIC1 into POPC:Chol monolayer by 96 ± 0.5% in comparison to the insertion of non-pre-incubated CLIC1 protein into the monolayer. These findings thereby suggest that pre-incubation of CLIC1 with cholesterol results in the formation of a relatively stable interaction (pre-complex) between the protein and cholesterol in the aqueous subphase which in turn prevents CLIC1 from inserting into the membrane.

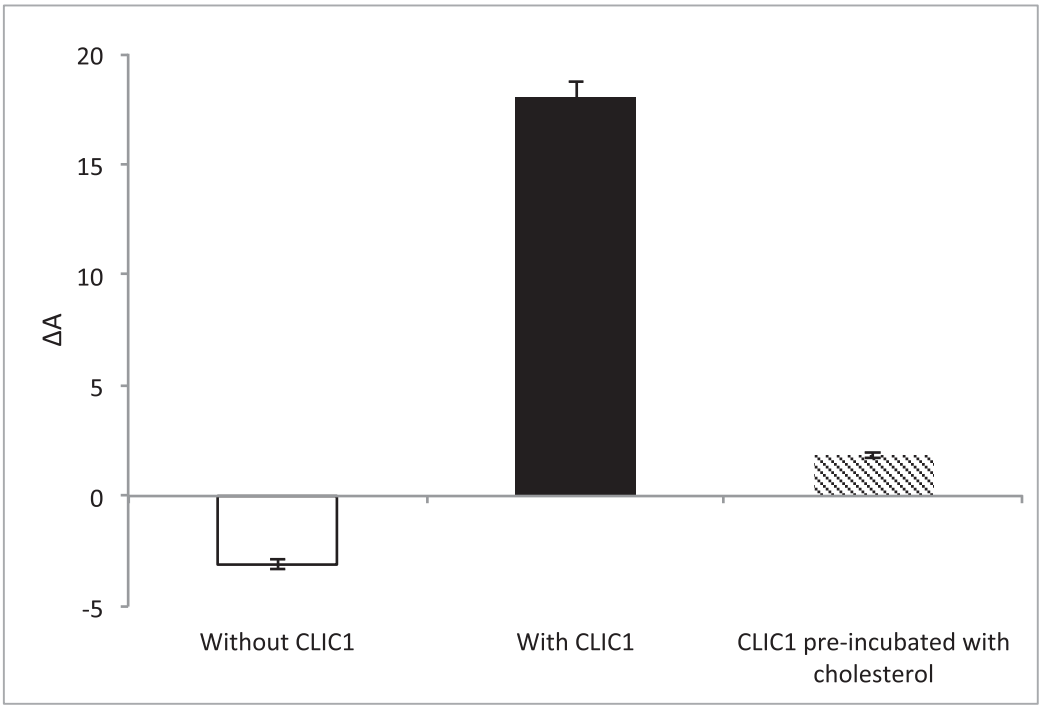

Figure 3.12 Percentage area expansion profiles of POPC:Chol monolayer after 3 hours without CLIC1 protein or after injection of recombinant CLIC1-wt and pre-incubated CLIC1 protein. CLIC1 was pre-incubated with cholesterol for an hour on ice prior to addition of the pre-incubated protein sample to the monolayer held at a constant surface pressure of 20 mN/m. Pre-incubation of CLIC1 protein with cholesterol resulted in complete abrogation of CLIC1 insertion into the monolayer.

3.5 Discussion

Expression and purification of recombinant CLIC1-wt protein by the method described by Valenzuela *et al*. (1997) [18] resulted in the effective purification of approximately 20-22 mg of reduced monomeric CLIC1 protein (Figure 3.4). The results from the HEDS enzyme assay as seen in Figure 3.5 confirmed that the purified CLIC1 protein is functionally active and can be assumed to have the correct structural configuration. The N-terminal domain of soluble CLIC1 has sufficient hydrophobicity to render the molecule amphiphilic [19, 26] as such CLIC1 demonstrates strong surface activity as seen in Figure 3.6. It appears that CLIC1-wt protein has a reasonable affinity for the air-water interface, resulting in a two-stage adsorption behaviour that produces a maximum pressure increase of 14 mN/m. Strikingly, the adsorption isotherm of CLIC1 is comparable to that observed for the Aβ peptide [27] that achieved an equilibrium surface pressure of 15 mN/m in PBS buffer also as a result of its amphiphilic nature. This result is suggestive of a mechanism by which to explain previously published tip-dip electrophysiology data where CLIC1 was found to have two different ionic conductance stages in pure PC lipid bilayers [28]. CLIC1, after a variable lag period of null events, first produced small conductance channels with slow kinetics (SCSK) and then underwent a transition to form high conductance channel with fast kinetics (4 times than that of SCSK) [28]. Similarly, the ion channel activity of CLIC1 in tBLMs measured using impedance spectroscopy also suggests the existence of two types of protein-membrane interactions [15]. The ability of CLIC1 to conduct in the absence of cholesterol in tBLMs suggests distinct cholesterol-dependent and independent events [15]. Likewise, the two-stage adsorption behaviour of CLIC1 at the air-water interface in the absence of lipids (Figure 3.6), suggests the protein undergoes phase transitions, which in the presence of a lipid bilayer would likely involve protein structural rearrangements to form functional ion channels. However, such interpretations must be tempered by the artificial nature of the monolayer system employed in this study.

The membrane insertion ability of CLIC1 was studied using a Langmuir monolayer system. To minimise the possibility that the protein may adsorb into its own monolayer at the interface but not interact with the phospholipid, the surface pressure of the lipid monolayer was pre-set at 20 mN/m, higher than the CLIC1

adsorption pressure of 14 mN/m (Figure 3.6). Therefore, an increase in π following CLIC1 addition underneath lipid monolayers indicated that the protein was interacting with the lipid components of the monolayer. Thus, from the results in Figure 3.7B, it was apparent that CLIC1 showed greater insertion into the zwitterionic lipids POPE followed by POPC but showed little to no interaction with the anionic POPS phospholipid. The apparent preference for CLIC1 insertion into the zwitterionic POPE monolayer may be related to the following differences between the three phospholipids; (i) POPE has the ability to form hydrogen bonds with water and other molecules while POPC cannot [29, 30] and (ii) that the ethanolamine group is smaller than both the choline or serine head-groups and upon compression the lipid molecules may be arranged in a more favourable orientation in the monolayer to facilitate greater protein interaction [30, 31 32].

A strong and preferential interaction also exists between the protein and cholesterol molecule and this was evident from the significant amount of CLIC1 insertion (ΔA ~ 11.2%) (Figure 3.7B) into the cholesterol monolayer. Similar *in vivo* and *in vitro* studies using several different CDCs including listeriolysin O, streptolysin, and pneumolysin have shown that these toxins bind to phospholipid membranes only when they contain cholesterol [11, 33]. Previous studies have also suggested that CLIC1 may require specific lipids or lipid combinations to refold or form oligomers following its membrane insertion [14, 15]. Studies with impedance spectroscopy on tBLMs showed that CLIC1 exhibited cholesterol-dependent ion channel activity in model membranes [15]. Singh H *et al.* (2006) studied the ion channel activity of CLIC1 protein in planar lipid bilayers, finding that CLIC1 protein failed to form functional ion channels in a variety of lipid mixtures but showed highly reproducible ion channel activity in a POPE, POPS and cholesterol combination of 4:1:1 mole ratio respectively [14]. Complementary results were obtained from Figure 3.8 and 3.9 that show supplementing cholesterol into pure phospholipid or mixed phospholipid monolayers significantly increased CLIC1 membrane insertion. The optimal membrane composition for CLIC1 insertion is a combination of POPE, POPS and cholesterol in a mole ratio of 4:1:1 (Figure 3.9) which is consistent with the observations recorded by Singh H *et al.* (2006) [14]. The results shown in Figure 3.8 and 3.9 suggest that the previously reported increase in CLIC1 ion channel conductivity with increasing cholesterol

concentration in model membranes (as measured by impedance spectroscopy [15]) arises due to an increase in membrane insertion of CLIC1 protein facilitated by membrane cholesterol. In addition, CLIC1 interactions with pure or mixed phospholipid monolayers in the absence or presence of cholesterol resulted in varying kinetics based on the lipid profile.

Several conventional studies of binary mixtures of two or more phospholipids have indicated that cholesterol may preferentially associate with different lipid classes in the same mixture [34]. Recent studies have shown clear evidence for the formation of cholesterol-poor or cholesterol-rich microdomains or clusters, which are also enriched or depleted of certain phospholipid classes, which occur in both model and biological membranes [34-36]. It was concluded that limiting amounts of cholesterol show comparable or higher affinities for anionic phospholipids than for zwitterionic phospholipids and the order of preference of cholesterol thus established was Sphingomyelin (SM) > Phosphatidylserine (PS) > Phosphatidylglycerol (PG) > Phosphatidylcholine (PC) > Phosphatidylethanolamine (PE) [34-36]. Hence, CLIC1 proteins show greater interaction in mixed monolayers containing anionic POPS and cholesterol (Figure 3.8 & 3.9). The fact that CLIC1 interacts to a significantly greater extent with POPE than POPS in the absence of cholesterol (see Figure 3.7B), and that cholesterol preferentially forms microdomains with POPS over POPE, suggests that CLIC1's greater interaction with a POPE:POPS:Chol monolayer (mole ratio 4:1:1) is due to the presence of a greater mole percentage of POPE, in comparison to a POPS:POPE:Chol monolayer.

In stark contrast, a decrease in ΔA value was observed following addition of CLIC1 under POPE monolayers containing cholesterol (Figure 3.8). This observation is highly surprising and may possibly be a result of the difference in the packing nature of the lipid/cholesterol monolayer in comparison to that of the pure lipid or pure cholesterol as seen in Figure 3.10. However, further analysis is required in order to understand the exact nature of CLIC1 protein interactions with POPE monolayers. To shed some light regarding CLIC1 interactions with different lipid monolayers, X-ray and neutron reflectivity experiments were performed to acquire structural insights into CLIC1's insertion into different phospholipid monolayers, including POPE, in the absence and presence of

cholesterol. The X-ray and neutron reflectivity data will be presented in the subsequent chapters, which provide further insights into the nature of CLIC1's interaction with different lipid monolayers. However, it is evident from the Langmuir results shown in this chapter that the autonomous membrane insertion of CLIC1 is highly regulated by cholesterol as well as the membrane phospholipid composition typically found in eukaryotic membranes.

Moreover, previous studies using tBLMs, had shown that pre-incubation of CLIC1 protein with cholesterol diminishes ion channel activity of the protein [15]. Similar results were seen in Figure 3.12, where pre-incubation of CLIC1 protein with cholesterol prior to its addition to the Langmuir film, showed reduced membrane insertion even in monolayers containing cholesterol, suggesting the formation of a CLIC1-cholesterol pre-complex. Hence, it can be concluded that the previously reported inhibition of CLIC1 ion channel activity by cholesterol resulted from a reduction in CLIC1 membrane insertion. It appears likely that in its soluble form CLIC1 may interact with cytosolic cholesterol and this may in turn regulate the proteins' insertion into the membrane. Whether cholesterol is also needed for the proteins' oligomerisation remains unclear but it seems clear that it is required and facilitates CLIC1 insertion/ binding to the membrane. The formation of a pre-complex with cholesterol also suggests that CLIC1 contains a cholesterol-binding domain and when this is occupied by cholesterol the protein in solution can no longer bind to membrane cholesterol. Interestingly, analysis of amino acid sequences done previously by our group [15] have revealed a GXXXG motif at the N-terminal domain that is highly conserved amongst all the human CLIC proteins, several members of the CDCs (examples: listeriolysin, perfringolysin-O) [15] as well as several human membrane proteins (examples: glycophorin-A, ErbB receptor, G-protein coupled receptors etc.) [37]. Studies have shown that the GXXXG motif facilitates the homo or hetero-oligomerisation of membrane proteins [38] and acts as a cholesterol binding site in amyloid precursor proteins [12]. This GXXXG motif may well be the cholesterol-binding site in the CLIC proteins and subsequent chapters in this thesis investigate the role of this motif in CLIC1's interaction with cholesterol.

3.6 Conclusion

Our results provide insights into the regulatory role that phospholipids and cholesterol play in the spontaneous membrane insertion of the protein CLIC1. Although, there are variations in CLIC1 interactions with different phospholipid monolayers, it is however clear that CLIC1 has a strong preference for associating with or intercalating into pure lipid or mixed lipid monolayers containing cholesterol. The Langmuir monolayer film experiments reported here show that the optimal membrane composition for CLIC1 insertion is a combination of POPE, POPS and cholesterol in a mole ratio of 4:1:1. Since cholesterol has been shown to induce insertion of several other membrane proteins, it seems that cholesterol also regulates the largely soluble and stable cytosolic CLIC1 in its optimal membrane insertion. Furthermore, CLIC1's apparent ability to form a relatively stable pre-complex with cholesterol suggests the presence of a cholesterol-binding domain in CLIC1. The Langmuir results shown in this study complement the previously published study done by our laboratory using tBLMs [15]. This study supports the model that CLIC1 binds to cholesterol in the membrane via a putative cholesterol-binding domain for its initial docking onto the membrane. It then inserts into phospholipid monolayers with varying kinetics dependent upon the lipid profile. Subsequent oligomerisation of CLIC1 protein monomers in the membrane then likely occurs, in order for functional ion channels to be formed.

3.7 References

[1] Phillips, R., Ursell, T., Wiggins, P., and Sens, P. (2009) Emerging roles for lipids in shaping membrane-protein function., *Nature 459*, 379-385.

[2] Pebay-Peyroula, E., Dahout-Gonzalez, C., Kahn, R., Trézéguet, V., Lauquin, G., and Brandolin, G. (2003) Structure of mitochondrial ADP/ATP carrier in complex with carboxyatractyloside., *Nature 426*, 39-44.

[3] Morth, J., Pedersen, B., Toustrup-Jensen, M., Sørensen, T., Petersen, J., Andersen, J., Vilsen, B., and Nissen, P. (2007) Crystal structure of the sodium-potassium pump., *Nature 450*, 1043-1049.

[4] Payandeh, J., Gamal El-Din, T., Scheuer, T., Zheng, N., and Catterall, W. (2012) Crystal structure of a voltage-gated sodium channel in two potentially inactivated states., *Nature 486*, 135-139.

[5] Quigley, A., Dong, Y., Pike, A., Dong, L., Shrestha, L., Berridge, G., Stansfeld, P., Sansom, M., Edwards, A., Bountra, C., von Delft, F., Bullock, A., Burgess-Brown, N., and Carpenter, E. (2013) The structural basis of ZMPSTE24-dependent laminopathies., *Science 339*, 1604-1607.

[6] Shinzawa-Itoh, K., Aoyama, H., Muramoto, K., Terada, H., Kurauchi, T., Tadehara, Y., Yamasaki, A., Sugimura, T., Kurono, S., Tsujimoto, K., Mizushima, T., Yamashita, E., Tsukihara, T., and Yoshikawa, S. (2007) Structures and physiological roles of 13 integral lipids of bovine heart cytochrome c oxidase., *EMBO J 26*, 1713-1725.

[7] Sun, F., Huo, X., Zhai, Y., Wang, A., Xu, J., Su, D., Bartlam, M., and Rao, Z. (2005) Crystal structure of mitochondrial respiratory membrane protein complex II., *Cell 121*, 1043-1057.

[8] Huang, L., Sun, G., Cobessi, D., Wang, A., Shen, J., Tung, E., Anderson, V., and Berry, E. (2006) 3-nitropropionic acid is a suicide inhibitor of mitochondrial respiration that, upon oxidation by complex II, forms a covalent adduct with a catalytic base arginine in the active site of the enzyme., *J Biol Chem 281*, 5965-5972.

[9] Toyoshima, C., Iwasawa, S., Ogawa, H., Hirata, A., Tsueda, J., and Inesi, G. (2013) Crystal structures of the calcium pump and sarcolipin in the Mg2+-bound E1 state., *Nature 495*, 260-264.

[10] Tani, K., Mitsuma, T., Hiroaki, Y., Kamegawa, A., Nishikawa, K., Tanimura, Y., and Fujiyoshi, Y. (2009) Mechanism of aquaporin-4's fast and highly selective water conduction and proton exclusion., *J Mol Biol 389*, 694-706.

[11] Gilbert, R. (2010) Cholesterol-dependent cytolysins., *Adv Exp Med Biol 677*, 56-66.

[12] Barrett, P., Song, Y., Van Horn, W., Hustedt, E., Schafer, J., Hadziselimovic, A., Beel, A., and Sanders, C. (2012) The amyloid precursor protein has a flexible transmembrane domain and binds cholesterol., *Science 336*, 1168-1171.

[13] Yu, X., and Zheng, J. (2012) Cholesterol promotes the interaction of Alzheimer β-amyloid monomer with lipid bilayer., *J Mol Biol. 421*, 561-571.

[14] Singh, H., and Ashley, R. (2006) Redox regulation of CLIC1 by cysteine residues associated with the putative channel pore., *Biophys J. 90*, 1628-1638.

[15] Valenzuela, S., Alkhamici, H., Brown, L., Almond, O., Goodchild, S., Carne, S., Curmi, P., Holt, S., and Cornell, B. (2013) Regulation of the Membrane Insertion and Conductance Activity of the Metamorphic Chloride Intracellular Channel Protein CLIC1 by Cholesterol, *PLoS ONE 8*, 56948.

[16] Alouf, J., Geoffroy, C., Pattus, F., and Verger, R. (1984) Surface properties of bacterial sulfhydryl-activated cytolytic toxins. Interaction with monomolecular films of phosphatidylcholine and various sterols., *Eur J Biochem. 141*, 205-210.

[17] Jacobs, T., Darji, A., Frahm, N., Rohde, M., Wehland, J., Chakraborty, T., and Weiss, S. (1998) Listeriolysin O: cholesterol inhibits cytolysis but not binding to cellular membranes., *Mol Microbiol. 28*, 1081-1089.

[18] Valenzuela, S., Martin, D., Por, S., Robbins, J., Warton, K., Bootcov, M., Schofield, P., Campbell, T., and Breit, S. (1997) Molecular cloning and expression of a chloride ion channel of cell nuclei., *J Biol Chem. 272*, 12575-12582.

[19] Littler, D., Harrop, S., Fairlie, W., Brown, L., Pankhurst, G., Pankhurst, S., DeMaere, M., Campbell, T., Bauskin, A., Tonini, R., Mazzanti, M., Breit, S., and Curmi, P. (2004) The intracellular chloride ion channel protein CLIC1 undergoes a redox-controlled structural transition., *J Biol Chem. 279*, 9298-9305.

[20] Lottenberg, R., Christensen, U., Jackson, C., and Coleman, P. (1981) Assay of coagulation proteases using peptide chromogenic and fluorogenic substrates., *Methods Enzymol. 80*, 341-361.

[21] Chang, J. (1985) Thrombin specificity. Requirement for apolar amino acids adjacent to the thrombin cleavage site of polypeptide substrate., *Eur J Biochem. 151*, 217-224.

[22] Bradford, M. (1976) A rapid and sensitive method for the quantitation of microgram quantities of protein utilizing the principle of protein-dye binding., *Anal Biochem. 72*, 248-254.

[23] Al Khamici, H., Brown, L., Hossain, K., Hudson, A., Sinclair-Burton, A., Ng, J., Daniel, E., Hare, J., Cornell, B., Curmi, P., Davey, M., and Valenzuela, S. (2015) Members of the Chloride Intracellular Ion Channel Protein Family Demonstrate Glutaredoxin-Like Enzymatic Activity, *PLoS One 10*, e115699.

[24] Sotirchos, I., Hudson, A., Ellis, J., and Davey, M. (2009) A unique thioredoxin of the parasitic nematode *Haemonchus contortus* with glutaredoxin activity., *Free Radic Biol Med. 46*, 579-585.

[25] Tulk, B., Schlesinger, P., Kapadia, S., and Edwards, J. (2000) CLIC-1 functions as a chloride channel when expressed and purified from bacteria., *J Biol Chem. 275*, 26986-26993.

[26] Harrop, S., DeMaere, M., Fairlie, W., Reztsova, T., Valenzuela, S., Mazzanti, M., Tonini, R., Qiu, M., Jankova, L., Warton, K., Bauskin, A., Wu, W., Pankhurst, S., Campbell, T., Breit, S., and Curmi, P. (2001) Crystal structure of a soluble form of the intracellular chloride ion channel CLIC1 (NCC27) at 1.4-A resolution., *J Biol Chem. 276*, 44993-45000.

[27] Ege, C., and Lee, K. (2004) Insertion of Alzheimer's A beta 40 peptide into lipid monolayers, *Biophys J. 87*, 1732-1740.

[28] Warton, K., Tonini, R., Fairlie, W., Matthews, J., Valenzuela, S., Qiu, M., Wu, W., Pankhurst, S., Bauskin, A., Harrop, S., Campbell, T., Curmi, P., Breit, S., and Mazzanti, M. (2002) Recombinant CLIC1 (NCC27) assembles in lipid bilayers via a pH-dependent two-state process to form chloride ion channels with identical characteristics to those observed in Chinese hamster ovary cells expressing CLIC1., *J Biol Chem. 277*, 26003-26011.

[29] Hauser, H., Pascher, I., Pearson, R., and Sundell, S. (1981) Preferred conformation and molecular packing of phosphatidylethanolamine and phosphatidylcholine., *Biochim Biophys Acta. 650*, 21-51.

[30] Dill, K., and Stigter, D. (1988) Lateral interactions among phosphatidylcholine and phosphatidylethanolamine head groups in phospholipid monolayers and bilayers., *Biochemistry 27*, 3446-3453.

[31] Langner, M., and Kubica, K. (1999) The electrostatics of lipid surfaces., *Chem Phys Lipids 101*, 3-35.

[32] Domènech, O., Torrent-Burgués, J., Merino, S., Sanz, F., Montero, M., and Hernández-Borrell, J. (2005) Surface thermodynamics study of monolayers formed with heteroacid phospholipids of biological interest., *Colloids Surf B Biointerfaces 41*, 233-238.

[33] García-Sáez, A., Mingarro, I., Pérez-Payá, E., and Salgado, J. (2004) Membrane-insertion fragments of Bcl-xL, Bax, and Bid., *Biochemistry 43*, 10930-10943.

[34] Demel, R., Jansen, J., van Dijck, P., and van Deenen, L. (1977) The preferential interaction of cholesterol with different classes of phospholipids, *Biochim Biophys Acta. 465*, 1-10.

[35] McMullen, T., Lewis, R., and McElhaney, R. (2000) Differential scanning calorimetric and Fourier transform infrared spectroscopic studies of the effects of cholesterol on the thermotropic phase behavior and organization of a homologous series of linear saturated phosphatidylserine bilayer membranes, *Biophys J. 79*, 2056-2065.

[36] Van Dijck, P., De Kruijff, B., Van Deenen, L., De Gier, J., and Demel, R. (1976) The preference of cholesterol for phosphatidylcholine in mixed phosphatidylcholine-phosphatidylethanolamine bilayers., *Biochim Biophys Acta. 455*, 576-587.

[37] Prakash, A., Janosi, L., and Doxastakis, M. (2011) GxxxG motifs, phenylalanine, and cholesterol guide the self-association of transmembrane domains of ErbB2 receptors., *Biophys J. 101*, 1949-1958.

[38] Senes, A., Engel, D., and DeGrado, W. (2004) Folding of helical membrane proteins: the role of polar, GxxxG-like and proline motifs., *Curr Opin Struct Biol. 14*, 465-479.

Chapter 4

Elucidating the structure of CLIC1 at the Air-Water Interface: An X-ray and Neutron Reflectivity Study

Chapter 4

Elucidating the structure of CLIC1 at the Air-Water Interface: An X-ray and Neutron Reflectivity Study

4.1 Introduction

The transmembrane domain(s) of several integral membrane proteins often possess a hydrophobic surface for interaction with the lipid bilayer. Lipids may influence conformational changes in a protein in order to assist the hydrophobic protein domains to bury within the limited thickness of the hydrophobic interior of the biological membrane. Studies have shown that a protein may also alter conformation such as tilt [1-3] or bend [4, 5], especially in the transmembrane portion, to better accommodate itself within the bilayer, or the bilayer may distort to cover the hydrophobic surface of the membrane protein [6, 7]. To date, the crystal structures of the soluble form of four monomeric vertebrate CLICs – CLIC1 [8], CLIC2 [9], CLIC3 [10] and CLIC4 [11]; and two invertebrate CLIC-like proteins - *Drosophila melanogaster Dm*CLIC and *Caenorhabditis elegans* EXC4 [12] have been determined. It has now been well established that the CLICs possess a single N-terminal transmembrane domain (residues Cys^{24} to Val^{46} for CLIC1) [8, 13, 14] and evidence exists to support the model that CLIC1 undergoes redox sensitive oligomerisation [13, 15, 16] and the ion channel is likely to consist of a tetrameric to hexameric assembly of subunits within a phospholipid bilayer [16, 17]. Despite considerable progress in understanding CLIC1-membrane interactions, the structural details of the CLIC1-membrane assembly during the pore formation process are not well understood.

Evidence from numerous studies have shown that the N-terminal domain of CLIC1 upon interaction with membranes, changes conformation such that the N- and C-domains are located on the opposite sides of the membrane with the cysteine residue (Cys^{24}) localised at the trans face of the membrane while the tryptophan (Trp^{35}) residue localised within the phospholipid bilayer [15, 17] (details mentioned in Chapter 1). Our group has demonstrated that CLIC1 interactions within a phospholipid monolayer bear strong similarities to those observed within a bilayer [18, 19]. As a result, it was speculated that the structural features of CLIC1 within the monolayer would resemble somewhat (if not fully) the model structure

[16, 17] previously proposed for CLIC1 within a bilayer. Based on previous studies, we postulated a structural model as shown in Figure 4.1, to schematically represent a number of interactions that may arise between CLIC1 and the phospholipid monolayer. Based on previous studies we can assume that the C-domain of CLIC1 remains in the buffer subphase, while the N-terminal domain is available for interaction with the lipid monolayers. A recent study performed using FRET spectroscopy and EPR demonstrated that the hydrophobic transmembrane region (ß1-a1-ß2) of CLIC1 undergoes a structural reorganisation resulting in the N-terminal domain being composed of α-helices 1 and 2, which then inserts into the artificial phospholipid bilayer [17]. Since, in this study a lipid monolayer is used instead of a bilayer, it is likely that the α-helices, comprising of the N-domain, are folded rather than extending out completely, or one of the α-helix may be lying on top of the hydrophobic tails as shown in Figure 4.1.

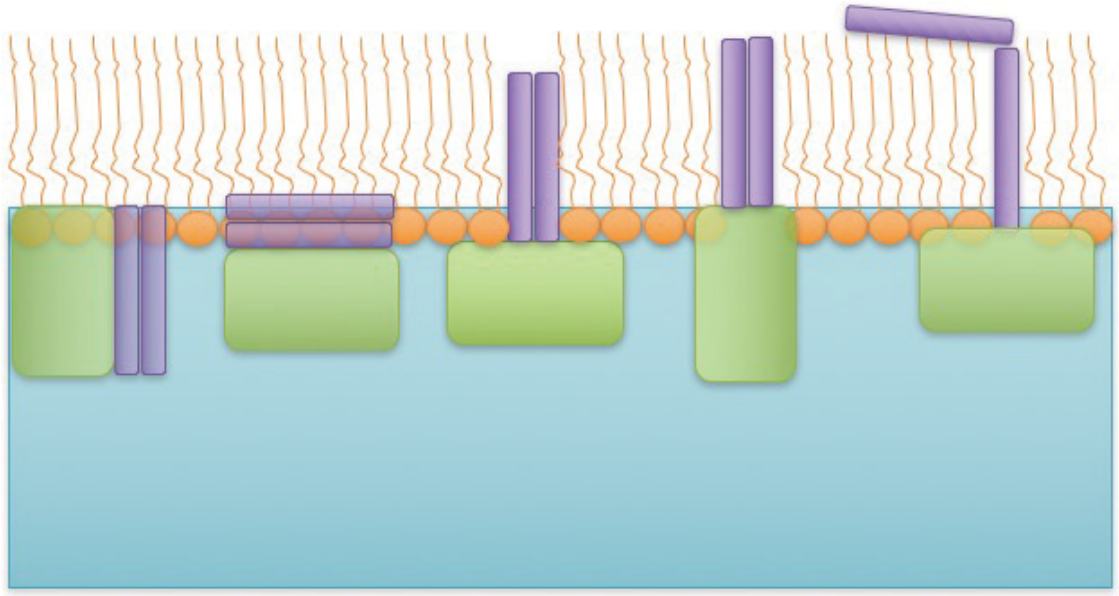

Figure 4.1 Schematic representation of putative structural models of CLIC1 interacting with a lipid monolayer. The lipid monolayer is shown in orange and the N-terminal and C-terminal domains of CLIC1 are shown in purple and green respectively.

In order to determine the structural model that best describes the membrane-bound form of CLIC1 and to determine how the nature of membrane cholesterol influences the auto-insertion of the protein, this chapter reports specular X-ray (XR) and neutron reflectivity (NR) studies, performed on different phospholipids and phospholipid-cholesterol monolayers, before and after addition of CLIC1 protein. Specular reflection allows the depth (thickness, t) of proteins to be determined in artificial monolayer membranes at the nanometer scale and also helps determine protein structural changes once in contact with the monolayer model membrane. XR and NR data shows that supplementing the phospholipid monolayer with cholesterol results in a deeper penetration of CLIC1 into the hydrophobic core of the lipid film. We also show that the greater CLIC1-wt insertion into pure POPE monolayers in comparison to POPC or POPS as determined by the Langmuir experiments, may be due to a difference of orientation of the protein within the POPE monolayer.

4.2 Materials and Method

Phospholipids: 1-palmitoyl-2-oleoyl-*sn*-glycero-3-phosphatidylcholine (POPC), 1-palmitoyl-2-oleoyl-*sn*-glycero-3-phosphatidylserine (POPS), 1-palmitoyl-2-oleoyl-*sn*-glycero-3-phosphatidylethanolamine (POPE) and chain deuterated 1-palmitoyl-(d_{31})-2-oleoyl-sn-glycero-3-phosphatidylcholine (d_{31}-POPC) were purchased from Avanti Polar Lipids (Alabaster, USA) and used as received. Cholesterol (Chol) was purchased from Sigma Aldrich (Australia). Lipid stock solutions were prepared in spectroscopic grade chloroform (Sigma) at a concentration of 1 mg/ml and stored at -20°C. Deuterated water (D_2O) (>99%) was provided by the National Deuteration Facility ANSTO, Australia.

4.2.1 Deuterated-CLIC1 protein expression, purification and activity

Wild-type Deuterated CLIC1 (d-CLIC1) was expressed in *E. coli* BL21 cells transformed with the pET-28a plasmid containing the genetic sequence of the recombinant His-CLIC1 fusion protein. *E. coli* grown in a 100% D_2O medium combined with a fully deuterated carbon source allows the expression of approximately fully (100%) per-deuterated recombinant proteins in a reproducible and predicted manner [20]. Optimization of the soluble expression level and large scale production of recombinant d-CLIC1 was carried out in the National Deuteration Facility at the Australian Nuclear Science and Technology Organization (ANSTO), Lucas Heights, Australia, using the same protocol as mentioned in Chapter 3 for recombinant CLIC1-wt protein. Deuterated proteins were harvested and purified as described previously in Chapter 3 and stored in aliquots at -80°C. In order to determine the effects of deuteration on CLIC1, the functional activity of the deuterated and non-deuterated CLIC1-wt proteins was measured by the consumption of NADPH in HEDS enzymatic assay, by methods previously described in Chapter 3, Section 3.2.6.

4.2.2 Sample preparation for X-ray and Neutron Reflectivity experiments

X-ray Reflectivity (XR) and Neutron Reflectivity (NR) Measurements were performed at the Australian Nuclear Science and Technology Organization (ANSTO), Lucas Heights, Australia. The XR and NR profiles were recorded for phospholipid and phospholipid-cholesterol (5:1 mole ratio) monolayers prepared using a Nima Technologies 601 Langmuir trough (Nima Technologies, Coventry,

UK) by methods previously mentioned in Chapter 3, Section 3.3. Briefly, the phospholipid (± cholesterol) monolayer was compressed to a surface pressure of 20 mN/m at a rate of 20 cm^2/min and then held at that constant pressure to ensure the formation of a stable monolayer. The surface area of the monolayer was monitored to ensure it remained constant for periods of up to 40 min, the maximum time required to perform a specular x-ray and neutron reflectivity experiment. Once XR and NR data of the phospholipid (± cholesterol) monolayer was collected, recombinant CLIC1-wt (in XR experiments) and deuterated or hydrogenated (d/h)-CLIC1-wt (in NR experiments) (50 μg) was injected underneath the preformed monolayer into the KCL/Hepes buffer subphase (pH 6.5). For NR experiments, two different contrast KCL/Hepes buffer (pH 6.5) subphase: D_2O and air contrast matched water, (ACMW) which is a mixture of composition 92% H_2O and 8% D_2O by volume, were used to generate sufficient contrast variation. The XR and NR reflectivity profiles of CLIC1 interaction with the monolayer was recorded with the exception of holding the monolayer at a constant area (instead of constant pressure) in order to prevent structural changes in the monolayer while collecting the data. For NR experiments, the reflectivity data was recorded after a 20% increase in area was observed following d/h-CLIC1 insertion into the monolayer. Details about the XR and NR instrumentation are given below.

4.2.3 X-ray Reflectometry measurements at the Air-Water interface

The Panalytical X'Pert Pro reflectometer (Cu-Ka X-rays, k = 1.5 Å) at ANSTO (Lucas Heights, Australia) was used to perform XR measurements. Calibration of the reflectometer was performed on a KCl/Hepes buffer subphase (pH 6.5) in a Langmuir trough. The background scattering from the subphase was measured at every data point with the detector offset by $2\theta = \pm 0.7°$. For each experiment, the lipid monolayer was aligned to the incident X-ray beam and measurements were performed by scanning from an angle of incidence of 0.04° degrees to 4.00° degrees in 0.01° degree steps for a total time period of 40 min. Previously from Langmuir experiments it was known that CLIC1 interacts with varying kinetics with different phospholipids in the absence and presence of cholesterol. Therefore, in order to obtain kinetic information from X-ray reflectivity, 3 cycles of scans were performed for each phospholipid (±

cholesterol) monolayer after CLIC1 addition, thus obtaining three XR profiles of lipid-CLIC1 interactions over a total period of three hours. For XR experiments, the absolute reflectivity, *R* was derived by subtracting the background scattering followed by normalisation of the data to the incident beam flux. The error bars on the data represent the counting statistics at each data point. Details on the principle and theory of XR have been reviewed elsewhere [21-25]. The XR profile of the Langmuir film contains information on the sample-normal profile (along the z direction) of in-plane average of the electron density. CLIC1 and phospholipid acyl chains and head-groups have different electron densities resulting in chemically distinct molecular layers each having its own electron density profile (ρ_e). Analysis of this ρ_e profile, therefore, provides information on the location and thickness of the protein layer associated within the lipid monolayer.

4.2.4 Specular Neutron Reflectometry measurements at the Air-Water interface

The Platypus, time-of-flight reflectometer at the 20MW OPAL Research Reactor at ANSTO (Lucas Heights, Australia) was used to probe interfacial thickness and density of the lipid-CLIC1 monolayer in the direction normal to the substrate surface [26]. In the Platypus, neutrons of wavelengths ranging between 2.8 and 18 Å and measurements taken at two incident angles, namely 1.1° and 4.8°, were used to give a Q-range from ~0.013 to ~0.32 $Å^{-1}$. Calibration of the Platypus was performed using a D_2O KCL/Hepes buffer subphase (pH 6.5). Additional data were also collected on the CRISP reflectometer at the ISIS pulsed neutron source, Rutherford Appleton Laboratory, UK. The neutron wavelength range used for the CRISP reflectometer was between 0.5-6.5 Å and data was collected at incident angles of 0.3°, 0.7° and 1.5° producing an overall similar *Q* range for both instruments. Data reduction followed the same procedure for both the NR instruments. The data was reduced by stitching together each angle at the appropriate overlap regions, rebinning to a resolution of 5% and correcting for background and detector efficiency.

The biggest advantage of NR experiments over XR is the use of contrast variation. Although H_2O and D_2O are chemically similar, D_2O has an SLD of 6.35 X 10^{-6} $Å^{-2}$ meanwhile; H_2O has an SLD of -0.56 X 10^{-6} $Å^{-2}$. This difference in the SLDs of the protonated and deuterated samples are exploited in NR experiments

(details mentioned in Chapter 2, Section 2.4.3). In this study, NR data was obtained using two different contrast KCL/Hepes buffer (pH 6.5) subphase: D_2O and ACMW, which has an SLD similar to air (SLD = 0 X 10^{-6} $Å^{-2}$). Figure 4.2 shows the different scattering contrast used for POPC:Chol monolayers interacting with CLIC1. Both hydrogenated and deuterated POPC and CLIC1, abbreviated as h/d_{31}-POPC and h/d-CLIC1 respectively, were used in ACMW buffer subphase to create contrast variation such that particular components of the monolayer can be highlighted or made invisible to the neutrons. The colouring in Figure 4.2 illustrates the sensitivity of each contrast to different features of the structure. For example, the contrast of h-POPC:Chol + d-CLIC1 in ACMW (Figure 4.2), the aqueous subphase was contrast matched to the lipid making the two species indistinguishable by the neutrons while highlighting only the protein providing maximum sensitivity to the structure of the inserted CLIC1 layer. However due to the unavailability of deuterated POPE and POPS phospholipids, the NR data of these phospholipids were obtained using two different H/D contrasts: namely h-lipid monolayer on D_2O and h-lipid monolayer on ACMW with d-CLIC1, to yield two reflectivity profiles for each structure examined.

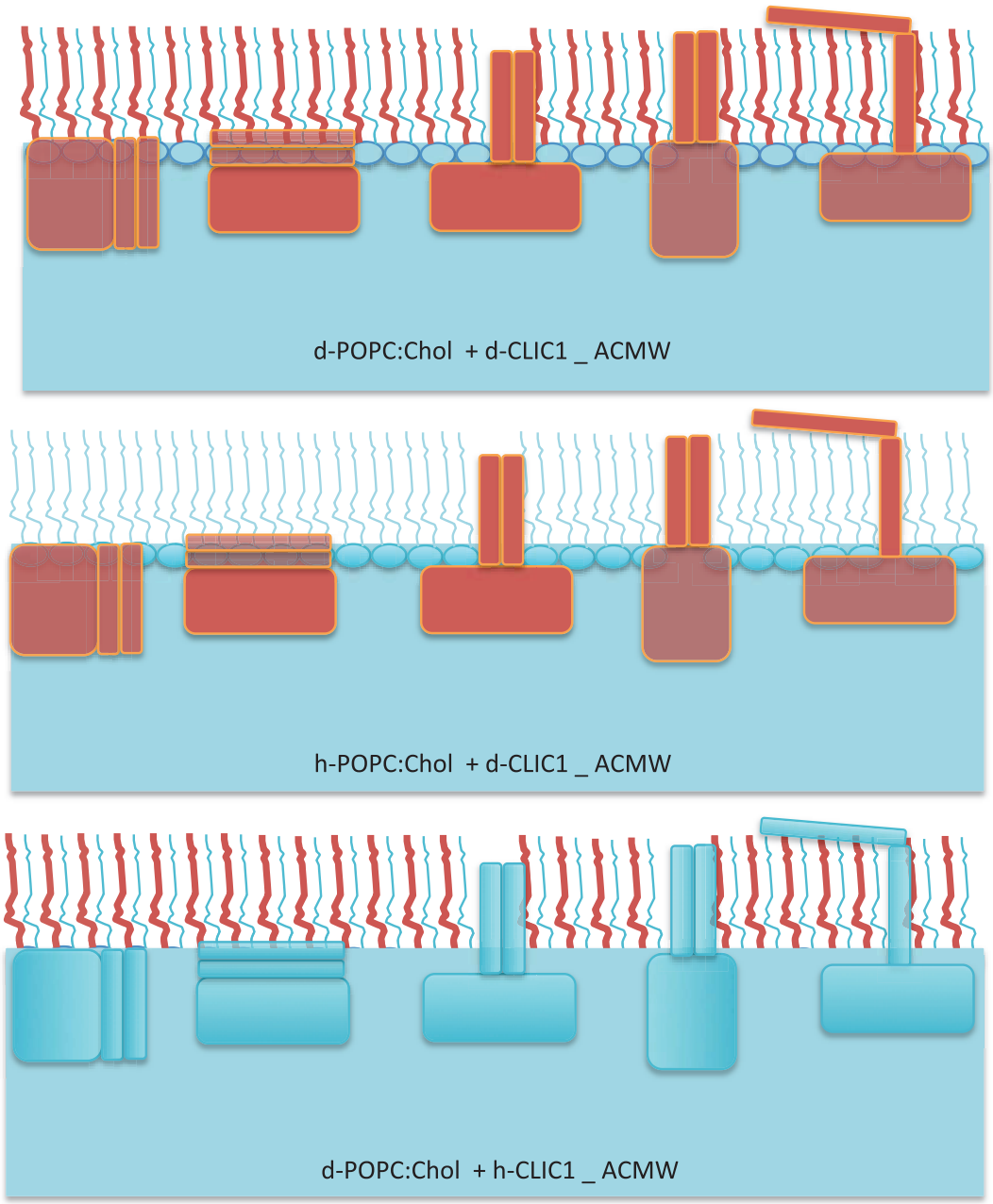

Figure 4.2 Schematic representation of the structural model and contrasts used to fit data from POPC:Chol monolayer after interaction with CLIC1. Red represents deuterium labelling and blue hydrogenated material.

4.2.5 XR and NR data analysis

XR and NR measurements were made as a function of incident angle (θ), measuring the specularly reflected beam as a function of the momentum transfer, Q perpendicular to the surface as defined by the equation:

$$Q = (4\pi \sin \theta)/\lambda \quad \text{Eq. 4.1}$$

where, λ is the wavelength of the x-ray or neutron incident beam. The principles and theory of X-ray and neutron reflectivity has been presented in detail in Chapter 2 of this thesis. The procedure to obtain and fit lipid-protein profiles was as described [27-29] and is briefly outlined here. X-ray reflectivity data and NR data from both Platypus and CRISP were modelled using the Motofit analysis program [30] in the Igor Pro environment (Wavemetrics). Motofit uses the optical matrix method [31] to calculate the reflectivity of the XR and NR data. This approach assumes that the interface can be described as a series of slabs (layers), with each layer characterised by a certain thickness (***t****, Å*), a Gaussian interfacial roughness (**σ**, Å) and a x-ray electron density ($\boldsymbol{\rho_e}$, Å^{-2}) / neutron scattering length density ($\boldsymbol{\rho_n}$, Å^{-2}) profile normal to the surface. A least chi squares, χ^2 fitting routine which selects the best fit by minimizing χ^2 values by varying thickness, $\rho_e/\ \rho_n$, solvent penetration and roughness of each layer was utilised [28].

For NR experiments, multiple reflectivity profiles were collected for each phospholipid and CLIC1 interactions using different contrast variation. Since isotopic variation has no apparent impact on the structure, as a result, data from multiple H/D contrasts for each sample were simultaneously constrained to fit to the same layer where the thickness and roughness was kept constant and only the ρ_n was allowed to vary between datasets as required. Comparison of the fitted $\rho_e/\ \rho_n$ for each layer to the theoretical SLD_e /SLD_n values of each component within the layer enables the volume fraction to be calculated. The theoretical electron density (SLD_e) or the scattering length densities (SLD_n) of the phospholipids and CLIC1 were calculated using equations 2.4 and 2.5 respectively as mentioned in details in Chapter 2. The molecular volumes (V_m) of the lipid components were obtained from molecular dynamic simulations [32] and X-ray diffraction [33]

techniques and for CLIC1 it was calculated from the sequences and amino acid volumes [8]. Since CLIC1 and phospholipid head-groups have exchangeable protons in their structure, the theoretical SLD_n of the hydrogenated and deuterated lipids and proteins were calculated for two different contrasts: D_2O and ACMW. The percentage deuteration of CLIC1 was also taken into consideration when calculating the scattering length density of the protein in the different solvent contrasts. Table 4.1 represents the molecular volumes and the theoretically calculated SLD_e and SLD_n values of the lipids and CLIC1 used in this study.

In monolayers containing lipids (L), proteins (P) and water (W), the electron density/ scattering length density ρ of each layer (ρ_{layer}) is the sum of the theoritical SLD_i weighted by the volume fractions φ_i of each component and water as given by the equation:

$$\rho_{layer} = (SLD_{Lipid} \text{ x } \varphi_{Lipid}) + (SLD_{Protein} \text{ x } \varphi_{Protein}) + (SLD_{Water} \text{ x } \varphi_{Water}) \quad \text{Eq. 4.2}$$

Therefore, due to significant differences in the molecular electron densities and scattering length densities of the lipid, protein and water (see Table 1), their individual volume fractions were computed from the fitted ρ_e / ρ_n profile of the layer and subsequently used to determine the average area per molecule (***A***, $Å^2$) of a component (*i*) using the equation:

$$A = \frac{V_m}{t} \quad \text{Eq. 4.3}$$

Once the average area per molecule is known, the surface excess of a component (**Γ**, mol/m^2) can be calculated by the given equation:

$$\Gamma = \left(\frac{1}{A \text{ x } 10^{-20}} \text{ x } \frac{1}{N_A} \right) \varphi_i \quad \text{Eq. 4.4}$$

where, N_A is the Avogadro's number (6.023 x 10^{23}) and φ_i is the calculated volume fraction of the component (*i*) in the monolayer.

Table 4.1 Summary of the Molecular Volumes (V_m), theoretical electron densities (SLD_e) and neutron scattering length densities (SLD_n) of CLIC1 and the different lipids used in this study.

	Component	V_m Å^3	SLD_e 10^{-6} Å^{-2}	SLD_n 10^{-6} Å^{-2} (ACMW)	SLD_n 10^{-6} Å^{-2} (D_2O)
CLIC1	Whole molecule *(h/d)*	34211	12.10	1.85/3.23	2.86/7.48
Cholesterol	Whole molecule *(h)*	655	9.31	0.215	0.361
POPC	Whole molecule *(h/d_{31})*	1263	9.39	0.26/2.82	0.26/2.82
	Head-group *(h/d_{31})*	319	14.51	1.88	1.88
	Acyl chains (*h/d_{31})*	944	7.66	-0.283/3.14	-0.28/3.14
POPS	Whole molecule *(h)*	1188	9.91	0.49	0.58
	Head-group *(h)*	244	18.63	3.5	3.89
	Acyl chains (*h)*	944	7.66	-0.28	-0.28
POPE	Whole molecule *(h)*	1196	9.35	0.3	0.30
	Head-group *(h)*	252	15.68	2.48	2.48
	Acyl chains (*h)*	944	7.66	-0.28	-0.28

In all cases, the simplest possible model with the least number of parameters that adequately described the data was selected. For XR experiments, the errors given are the standard deviations reported by MOTOFIT. For NR experiments, in order to have a precise measure of parameter uncertainties, a Monte-Carlo (MC) resampling technique was applied by methods described by Holt *et.al* (2009) [34]. This technique quantifies confidence limits on the fitted parameters and provides correlations between the fit parameters. The MC resampling synthesises 'new' datasets by applying random perturbations (linked to the counting statistics) to individual data points. This new dataset is then fitted with the same model parameters. At least N = 5000 synthetic datasets were produced and analysed in this manner N variations of each parameter [34]. The fits to the synthetic data were analysed producing a frequency plot of fitted values. These parameter distributions were statistically analysed with the parameter value reported as the midpoint of the 95% confidence interval. The error is reported as twice the standard deviation of the distributions. A histogram is produced for the frequency distribution obtained from MC analysis [34].

4.3 Results

4.3.1 Functional activity of deuterated CLIC1 (d-CLIC1) protein

E. coli strain BL21(DE3) transformed with pET-28a plasmid, used for the expression of CLIC1, was already adapted to grow in D_2O media over a long period of time (at Deuteration Facility, ANSTO) to facilitate the expression of deuterated CLIC1 (d-CLIC1) according to the already established method for predictable deuteration of proteins [20]. The purity of d-CLIC1 was verified by SDS-PAGE and the deuteration level of the protein was shown to be approximately 80% by mass spectroscopy by Deuteration Facility, ANSTO. Expression of recombinant proteins under deuterated conditions can have subtle effects on the physicochemical properties of proteins. To determine the effect of deuteration on CLIC1, the functional activity of the protein was analysed using HEDS enzyme assay and the results are illustrated in Figure 4.3. The enzymatic activity shown by both d-CLIC1 and CLIC1-wt protein resulted in an insignificant difference (p value > 0.1) between the functional activity of the deuterated and hydrogenous forms of the protein, therefore, suggesting that deuteration had little to no impact on the physiochemical properties of CLIC1.

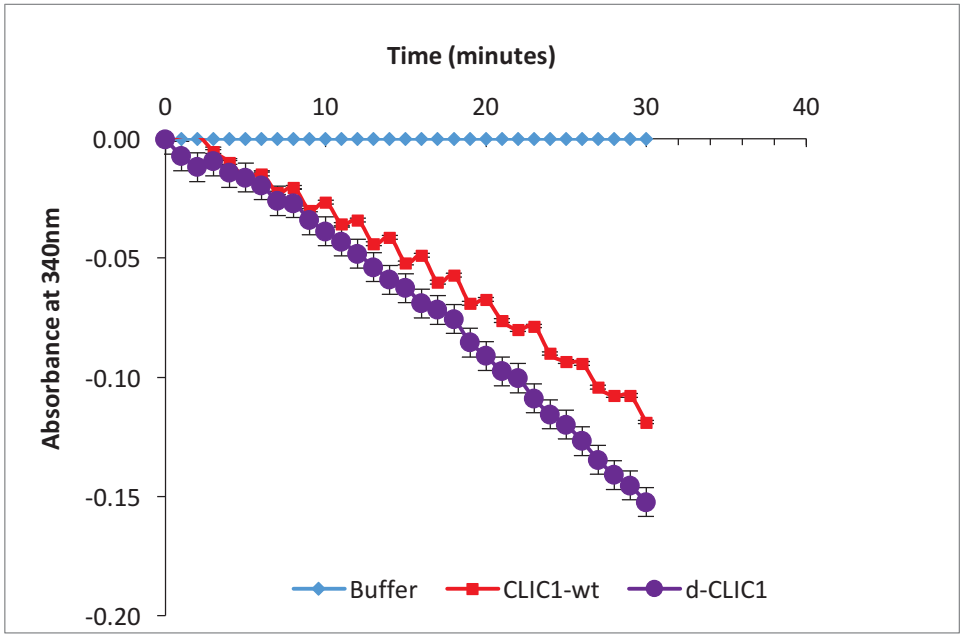

Figure 4.3 Oxidoreductase activity of the purified d-CLIC1 protein. 5 µM reduced CLIC1-wt or d-CLIC1 protein was added to 5 mM potassium phosphate buffer, pH 7 containing 1 mM EDTA, 250 µM NADPH, 50 nM GR and 1 mM HEDS. The reaction was initiated by the addition of 1 mM GSH and the absorbance of NADPH was monitored at A_{340nm}. d-CLIC1 showed similar enzymatic activity as the hydrogenous CLIC1-wt protein.

4.3.2 CLIC1 interaction with POPC monolayer in the absence and presence of Cholesterol

XR and NR measurements were obtained for different compositions of phospholipid and phospholipid-cholesterol monolayers deposited at the air-water interface on a KCL/Hepes buffer subphase (pH 6.5) by methods described above. The purpose of these measurements was to examine the structural changes in the phospholipid monolayer following addition of CLIC1 into the buffer subphase by comparing the density profile of the monolayer with and without CLIC1 present and in the absence and presence of cholesterol. The XR and NR results will be presented successively for each phospholipid (± cholesterol) monolayer with and without CLIC1 and then discussed together. The XR results for the third scan (C3) for each phospholipid (± cholesterol) monolayer, which is collected after 3 hours of CLIC1 addition, are only presented in this thesis in order to complement the Langmuir results previously discussed in Chapter 3.

4.3.2.1 Characterisation of CLIC1 insertion into POPC (± cholesterol) monolayer by X-ray Reflectivity

Figure 4.4 shows the XR profile, model fit and the electron density profile obtained for POPC monolayer held at a constant pressure of 20 mN/m on a KCL/Hepes buffer subphase (pH 6.5) in a Langmuir trough. The density profile was determined by fitting the monolayer to a simple two-layer model, starting from air to buffer subphase with one layer corresponding to the phospholipid acyl chains and the second to the phospholipid head-group regions (see Figure 4.4B). The structural parameters obtained from the fit are shown in Table 4.2. A volume fraction of ($\varphi_{POPC\ acyl}$) of ~ 95% was calculated for the POPC acyl chain region having a thickness of 12.1 Å. The head-group region was less densely packed, more likely that the projected area of the tails, particularly at 20 mN/m is larger than that of the headgroups. This leaves 'voids' between the headgroups which are filled with water, giving a volume fraction of $\varphi_{POPC\ head}$ of ~75% with a thickness of 7.11 Å. The area per molecule calculated for the POPC monolayer was found to be 65.08 Å^2, which is in good agreement with previously published data [32, 33, 35].

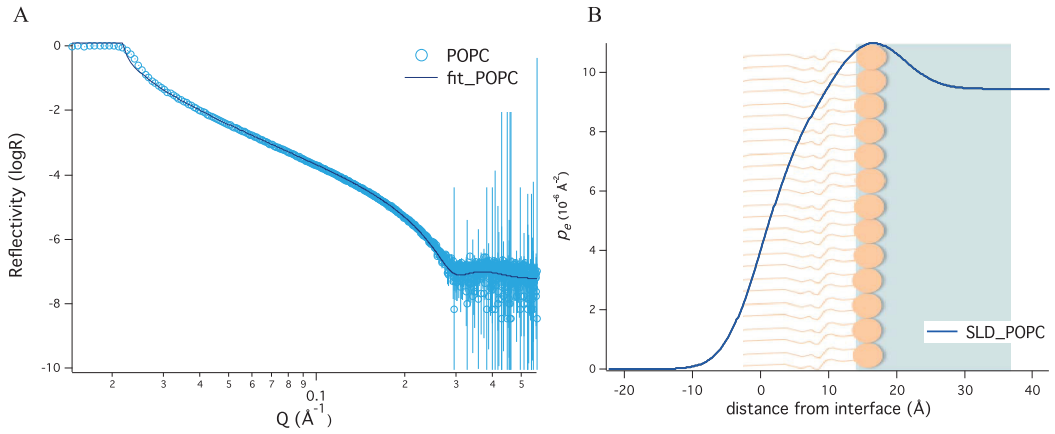

Figure 4.4 (A) X-ray reflectivity profile and model data fit and (B) the electron density profile the fit describes for air-water interface containing POPC monolayer held at a constant pressure of 20 mN/m. The air-water interface was set to be between the acyl chains and head-group region of the POPC monolayer.

Previously, Langmuir experiments have confirmed that CLIC1 shows very little insertion in POPC monolayer. The XR profile of CLIC1 association with POPC monolayer exhibited differences compared to that of the lipid data alone (Figure 4.5B). Analysis of the XR data using Motofit yielded reflectivity profile perpendicular to the lipid-protein film as illustrated in Figure 4.5B. With the insertion of CLIC1, three slabs (layers) were required to provide a good model fit to the POPC-CLIC1 XR profile. The layer at the air interface corresponds to POPC acyl chains and this layer increased in thickness with a slight increase in electron density. This increase in acyl chain ρ_e may be due to partial incorporation of the lipid head-groups and CLIC1 into the acyl chains. The layer corresponding to the head-group region of POPC decreased in thickness and in ρ_e with CLIC1 insertion. Additionally, a layer, adjacent to the POPC head-groups on the subphase side, with a slightly higher ρ of 9.74 x 10^{-6} Å^2 compared to ρ_{H2O} (9.45 x 10^{-6} Å^2) was required to fit the POPC-CLIC1 XR data. These physical changes of the POPC monolayer following CLIC1 insertion indicate the presence of a diffuse layer of protein underneath the head-groups and in the head-group region. The XR model fitting parameters are summarised in Table 4.2.

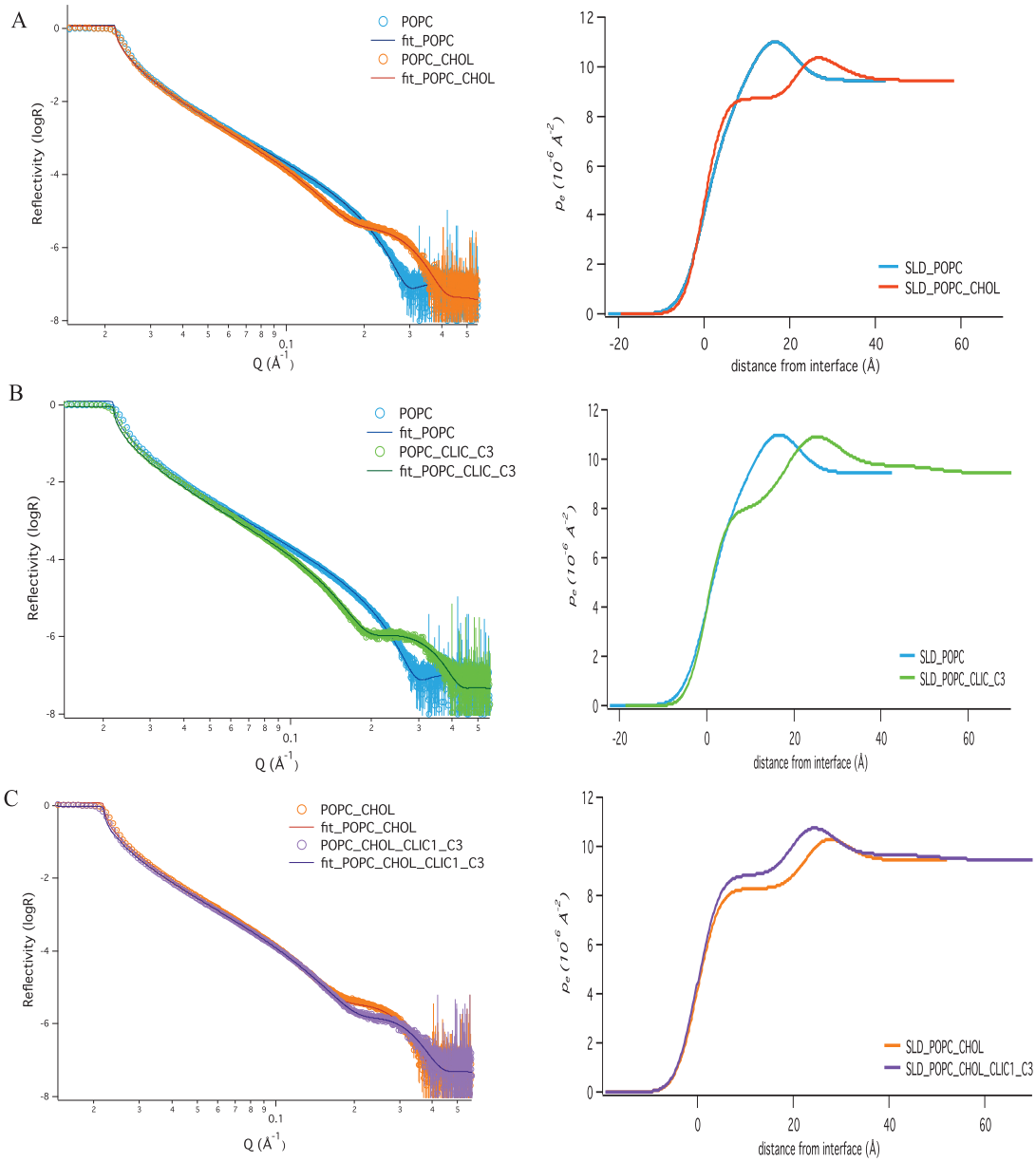

Figure 4.5 Comparisons of X-ray reflectivity profiles and model data fits and the electron density profile the fits describe for CLIC1-lipid monolayer at the air-water interface in the presence and absence of cholesterol. **(A)** POPC (blue line) and POPC:Chol (5:1 mole ratio) monolayer (orange line) held at a constant pressure of 20mN/m; **(B)** POPC monolayer with (green line) and without (blue line) CLIC1 and **(C)** POPC:Chol (5:1 mole ratio) monolayer with (purple line) and without (orange line) CLIC1.

The POPC monolayer when supplemented with cholesterol in a mole ratio of 5:1 resulted in completely different XR profiles and structural parameters in comparison to the POPC only monolayer both in the presence and complete absence of CLIC1 (see Figure 4.5A and C). The condensing effect of cholesterol was evident from the reduction in the area per lipid molecule from 65.08 $Å^2$ to 43.2 $Å^2$ in the presence of cholesterol. The fitted structural parameters for POPC:Chol monolayer with and without CLIC1 are illustrated in Table 4.2. CLIC1 showed relatively uniform insertion across the POPC:Chol acyl chain (1st layer) and head group (2nd layer) regions of the monolayer to give protein volume fractions (φ_{CLIC1}) of ~ 8% in these layers, respectively (see Table 4.2). There was also a layer of protein only found below the lipid monolayer, with a φ_{CLIC1} of ~ 8% found as a result of protein insertion, with the thickness of this layer found to be 22.9 Å. The addition of cholesterol to the POPC monolayer resulted in deeper penetration of CLIC1 into the acyl chain region of the monolayer. This finding was also evident from the lipid acyl chain volume fraction (φ_{lipid}), which was found to be ~ 84% prior to the introduction of CLIC1 and ~ 60% after CLIC1 insertion, thus suggesting that the lipid content is diluted by the insertion of CLIC1 and associated water.

Table 4.2 Parameters obtained from fits of XR data from POPC monolayer and POPC:Chol monolayer with and without CLIC1.

Lipids	Layers	t Å	ρ_e 10^{-6} $Å^2$	σ Å	$lipid$	$H2O$	$CLIC1$	A $Å^2$	A nm^2	Γ mg/m^2
POPC	Acyl chains	12.09	7.75	4.31	0.95	0.05		65.80	0.65	1.82
	Head-group	7.11	13.23	5.62	0.75	0.25				
POPC + CLIC1	Acyl chains	19.87	7.92	3.44	0.85	0.15	0.00	N/A		
	Head-group	6.86	13.03	5.34	0.65	0.24	0.11			
	CLIC1/ H_2O	25.90	9.74	5.81		0.89	0.11	1044	10.4	0.47
POPC: Chol	Acyl chains	23.27	8.28	3.52	0.84	0.16		43.20	0.43	2.25
	Head-group	6.07	11.30	3.76	0.44	0.56				
POPC: Chol + CLIC1	Acyl chains	20.10	8.83	3.56	0.60	0.32	0.08	N/A		
	Head-group	7.18	11.48	3.50	0.43	0.57	0.08			
	CLIC1/ H_2O	22.95	9.67	4.27		0.92	0.08	681	6.81	0.53

4.3.2.2 Characterisation of CLIC1 insertion into POPC (± cholesterol) monolayer by Neutron Reflectivity

We used neutron reflectrometry to investigate the molecular structure of CLIC1 during its interaction with POPC and POPC:Chol (5:1mole ratio) monolayers. Reflectivity profiles of the lipid monolayers were measured before and after a consecutive 20% increase in the monolayer area following CLIC1 insertion into the lipid film. Since, the underlying protein and membrane structure are invariant under isotopic substitution, hence to characterise the thickness and the composition of the lipid (± cholesterol) monolayers before and after CLIC1 insertion and to reduce the parameter uncertainties, neutron reflectivity profiles of the same sample were fitted simultaneously using the MOTOFIT analysis package. The analysis was based on modeling the thickness (***t, Å***), neutron scattering length density ($\boldsymbol{\rho_n}$, $Å^{-2}$), and roughness ($\boldsymbol{\sigma}$, Å) of different layers to achieve the best fitted data with the least χ^2 value.

The simultaneous fits to the NR data for the h/d_{31}- POPC (± cholesterol) monolayers at π = 20 mN/m (See Appendix Figure A1) was divided into two discrete layers: a hydrophobic acyl chain region of 13.01 Å, and a lipid head-group region of 7.01 Å with a hydration comprised between 8% and 23% respectively (Table 4.3). The POPC interfacial area was determined as 63.1 $Å^2$ and these results are in good agreement with previously published data [36, 37]. The total thickness of the monolayer is determined as 20 Å and this is comparable to the molecular length of the POPC molecule in the fluid state (~ 23 Å) [32, 35]. The model describing the NR fits for POPC:Chol monolayer shows that addition of cholesterol to the phospholipid (in a 5:1 mole ratio combination) condenses the POPC monolayer to a molecular interfacial area of 47.06 $Å^2$ which is nevertheless close to the figure reported by Smaby *et.al* (1997) [38]. The ordering effect of cholesterol on the acyl chains is also evident from the total POPC:Chol monolayer thickness of 24.6 Å. The acyl chain and head-group layer thicknesses of the POPC:Chol monolayer (Table 4.2) are of the same order as those reported by Foglia *et.al* (2014), 17.3 Å vs 17.0 Å and 7.4 Å vs 8.0 Å [39].

Langmuir experiments have confirmed that CLIC1 only results in a 3.7% increase in POPC monolayer area after 3 hours of CLIC1 addition to the subphase. The time required to achieve a 20% increase in POPC monolayer area following CLIC1 addition will result in structural deformation in the lipid film to collect NR profiles of the lipid-protein monolayer. Hence, in the present work, neutron reflectivity profiles were only collected for CLIC1 interaction with POPC:Chol monolayer on ACMW buffer subphase. The simultaneously fitted reflectivity profiles and the scattering length density measured from different POPC:Chol and CLIC1 contrasts in ACMW buffer subphase are shown in Figure 4.6 with the fitted parameters shown in Table 4.3.

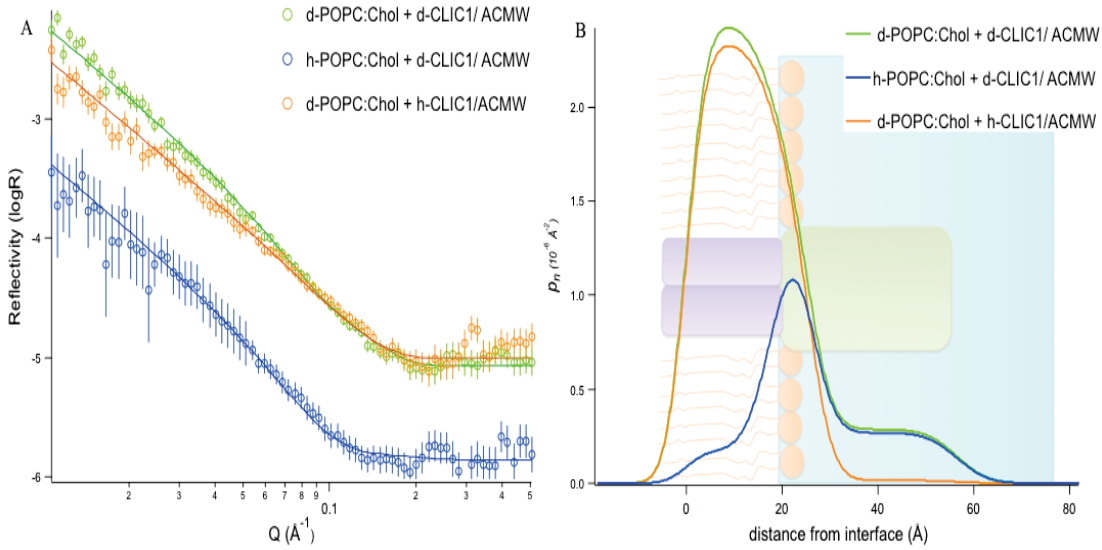

Figure 4.6 Neutron reflectivity profiles and model data fits (A) and the scattering length density profiles these fits describe (B) for CLIC1 interaction with POPC:Chol monolayer in ACMW KCl/Hepes buffer subphase (pH 6.5). The three simultaneously fitted isotopic contrasts shown are d-CLIC1 in d_{31}-POPC:Chol (green line); d-CLIC1 in h-POPC:Chol (blue line) and h-CLIC1 in d_{31}-POPC:Chol (orange line).

To provide contrasting scattering length density, NR profiles were generated using deuterated lipid and protein in the following contrasts: d-CLIC1 in d_{31}-POPC:Chol monolayer; d-CLIC1 in h-POPC:Chol monolayer and h-CLIC1 in d_{31}-POPC:Chol monolayer, which allowed moderately accurate modelling of the

lipid-protein system. The fitted $\boldsymbol{\rho_n}$ profile, (Figure 4.6B) demonstrates that CLIC1 protein interacts with POPC:Chol monolayer with this expected structure (see Table 4.3). In the NR experiments, the datasets were simultaneously fitted with the thickness and roughness of corresponding layers constrained and only the ρ_n was allowed to vary as required. Figure 4.7A shows the results of the Monte-Carlo (MC) resampling applied to the constrained fit from the three different samples, resulting in a CLIC1 best-fit thickness of 30.6 ± 6 Å underneath the lipid head-group layer in the buffer subphase. The MC resampling results of the protein ρ_n (Figure 4.7B) obtained from the contrast h-POPC:Chol + d-CLIC1 in ACMW, was used to calculate the area per CLIC1 molecule which was found to be 607 $Å^2$ (6.07 nm^2) with a surface coverage of 0.81 mg/m^2. This NR contrast was used because it provides the most detailed structure for CLIC1 association with the POPC:Chol monolayer (Figure 4.2). The lipid acyl chains ρ_n (0.012 x 10^{-6} $Å^{-2}$ for acyl chains of POPC:Chol monolayer) increases to 0.21 x 10^{-6} $Å^{-2}$ upon interaction with CLIC1, which corresponds to 11% of the lipid acyl chain volume being occupied by the protein. On the other hand, the ρ_n of the head-group region decreased from 2.97 x 10^{-6} $Å^{-2}$ to 1.53 x 10^{-6} $Å^{-2}$ upon interaction with CLIC1 protein. Lipid tails, which have significantly lower scattering length density, most likely caused the decrease in the electron density of this middle layer as more of the tail region became incorporated into this layer. This suggests that the middle layer is comprised of a portion of lipid tails, lipid head-groups, and protein, all of which contribute to the overall ρ_n fitted for this layer. These physical changes to the POPC:Chol monolayer in the presence of the protein suggests deeper penetration of CLIC1 into the acyl chain region giving a total CLIC1 thickness of 56.3 ± 6 Å.

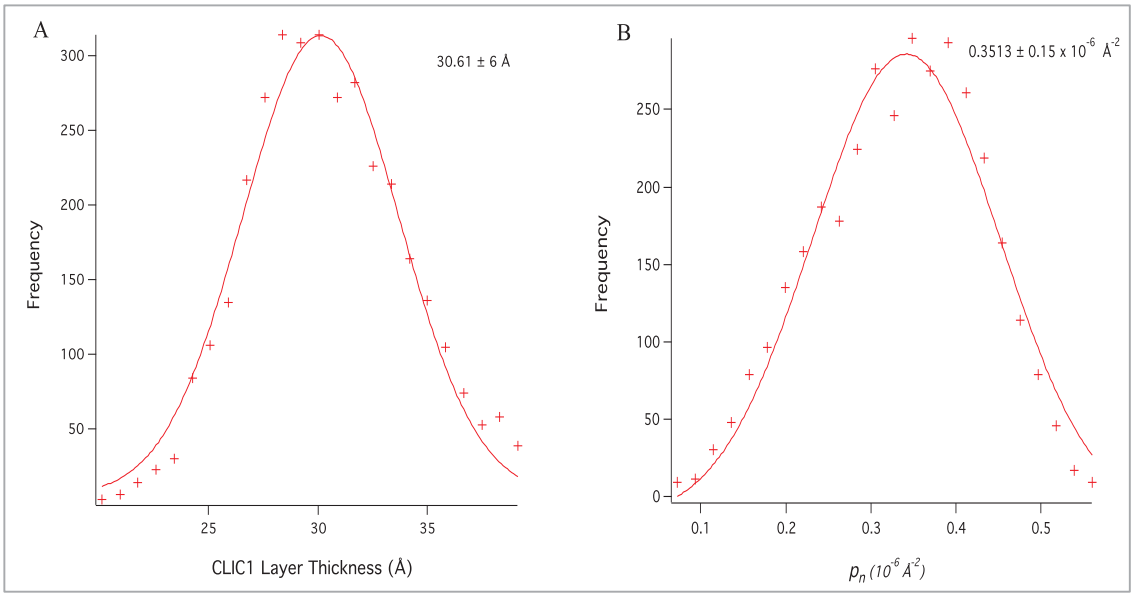

Figure 4.7 Results from the Monte-Carlo resampling of neutron contrast for CLIC1 layers where the line is a Gaussian fit intended to provide a guide to the eye. The frequency axis represents the number of times a particular result was obtained in the 1000 trail fits. (A) CLIC1 layer thickness and (B) $\boldsymbol{\rho_n}$ of the CLIC1 layer (see Figure 4.6).

Table 4.3 Parameters obtained from simultaneous fits of NR data from POPC monolayer without CLIC1 and POPC:Chol monolayer with and without CLIC1.

	t Å	ρ_n 10^{-6} Å^2	σ Å	*lipid*	*POPC*	*Chol*	*H2O*	*CLIC1*	A Å^2	nm^2	mg /m^2
POPC											
Acyl chains	13.01	3.41	3	0.92			0.08		63.09	0.63	1.84
Head-group	7.01	2.92	5.32	0.77			0.23				
POPC:Chol											
Acyl chains	17.29	0.012	4.6	0.97	0.82	0.15	0.03		47.06	0.47	1.99
Head-group	7.35	2.974	2.8	0.71	0.58	0.13	0.29				
POPC:Chol + CLIC1											
Acyl chains	18.4 ± 0.6	0.21 ± 0.25	2.99 ± 1.2	0.73	0.61	0.12	0.16	0.11			
Head-group	7.3 ± 0.5	1.53 ± 0.2	4.56 ± 1.9	0.70	N/A	N/A	0.19	0.11			
CLIC1/H_2O	30.6 ± 6	0.35 ± 0.15	3.22 ± 1.6					0.11	607	6.07	0.81

4.3.3 CLIC1 interaction with POPE monolayer in the absence and presence of Cholesterol

Langmuir film experiments of CLIC1 interaction with POPE presents an interesting case in that the spontaneous membrane insertion of CLIC1 was greater in POPE monolayer and was shown to decrease in the presence of cholesterol (see Figure 3.8, Chapter 3). Such an interaction of CLIC1 was exclusive to POPE lipid in comparison to the other phospholipids used in this study and may result from a different structural orientation of the protein within the lipid monolayer. To investigate the structural features of CLIC1-POPE interaction, both XR and NR measurements were collected for POPE monolayer before and after addition of CLIC1 protein. Unfortunately, CLIC1 interaction with POPE monolayer in the presence of cholesterol (in a 5:1 mole ratio) was analysed using XR data only as it was not feasible to collect NR data due to time constraint. For NR experiments, due to the unavailability of deuterated POPE, reflectivity data were collected after a 20% increase in area following d-CLIC1 insertion into POPE monolayer on D_2O and ACMW buffer subphase, to yield only two reflectivity profiles for the structure examined. The lack of sufficient contrast variation in NR experiments resulted in the possibility that multiple different models producing similar reflectivity curves representing a non-physical model could fit the NR data. This issue was mitigated to some extent by fitting the X-ray and neutron reflectivity profiles simultaneously using the MOTOFIT analysis package to create a more accurate model as previously described by Clifton *et al.* (2012) [40].

4.3.3.1 Characterisation of CLIC1 insertion into POPE monolayer

Two reflectivity profiles were used to determine the structure of the POPE monolayer held at a constant pressure of 20 mN/m: POPE on an H_2O buffer subphase examined using X-ray reflectometry and POPE on an D_2O buffer subphase examined using neutron reflectometry. XR and NR reflectivity and corresponding ρ profiles for POPE monolayer are shown in Figure 4.8A and the structural parameters are shown in Table 4.4. The system was described using two slabs: a POPE acyl chain layer of 13.6 Å and a head-group layer of 6.8 Å thick with volume fractions of ~ 86% and ~73% respectively. The area per molecule calculated for the POPE monolayer was 57.90 $Å^2$ with a surface coverage of 1.83 mg/m^2.

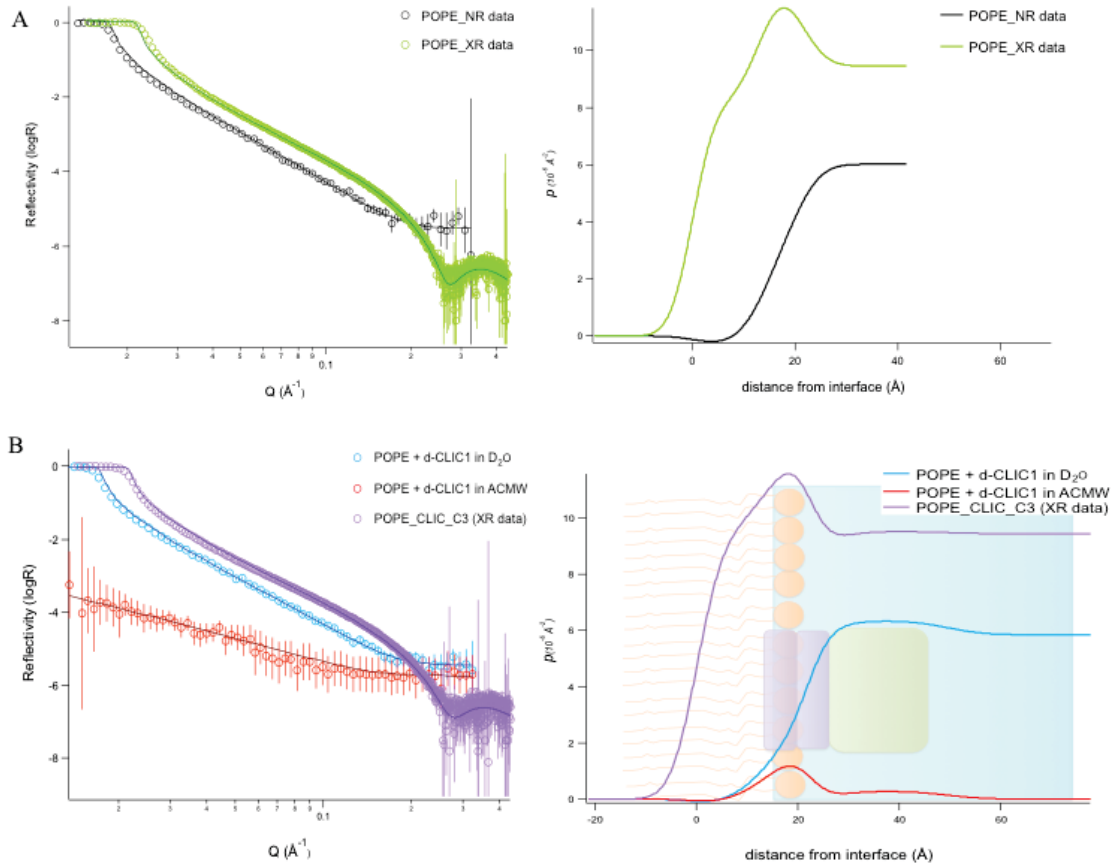

Figure 4.8 XR and NR profiles and model data fits and the scattering length density profiles these fits describe for (A) POPE monolayer and for (B) CLIC1 interaction with POPE monolayer. (A) XR data and NR data for POPE monolayer are shown in green and black line respectively. (B) The three simultaneously fitted data shown are d-CLIC1 in POPE in D_2O (blue line); d-CLIC1 in POPE in ACMW (red line) and CLIC1 in POPE (XR data) (purple line).

.

The reflectivity-derived model for the POPE monolayer reveals a very different structure with CLIC1 inserted across the core of the lipid head-group region (Figure 4.8B). This resolution was possible because deuterated CLIC1 provided a contrast with the hydrogenous POPE lipid. The structural parameters are illustrated in Table 4.4. CLIC1 protein extends 24 Å into the buffer subphase and comprises of a volume fraction of approximately ~13%. The Layer 2 corresponding to the head-group region of POPE slightly decreased in thickness but increased in ρ with CLIC1 insertion. On the other hand, the scattering length density profile of Layer 1 (comprising of POPE acyl chain) was almost unchanged following CLIC1 insertion suggesting the absence of the protein within that layer (see Table 4.4). However, the increase in thickness of the acyl

chains from 13.6 Å to 15.7 Å in the presence of CLIC1 may be due to incorporation of a part of the head-group region within Layer 1. Due to the lack of sufficient contrast between the acyl chain and head-group layer of POPE monolayer, it was not possible to precisely distinguish between the first two layers and as a result their volume fractions could not be determined.

Table 4.4 Parameters obtained from simultaneous fits of XR and NR data from POPE monolayer with and without CLIC1.

	t Å	ρ_n 10^{-6} Å^2	σ Å	*POPE*	*H2O*	*CLIC1*	A Å^2	nm^2	Γ mg/m^2
POPE									
Acyl chain Layer									
POPE in D2O (NR data)	13.6	-0.24	3.51	0.86 ± 0.17	0.14				
POPE (XR data)		8.16							
							57.6	0.58	1.83
Head-group Layer									
POPE in D2O (NR data)	6.8	2.97	4.1	0.73 ± 0.15	0.27				
POPE (XR data)		13.2							
POPE + CLIC1									
Layer 1									
POPE +d-CLIC1 in D2O	15.7	-0.22	3.59	N/A		0.0	-		
POPE +d-CLIC1 in ACMW		-0.18							
POPE + CLIC1 (XR data)		8.06							
Layer 2									
POPE +d-CLIC1 in D2O	6.14	3.08	7.42	N/A		0.13	-		
POPE +d-CLIC1 in ACMW		2.11							
POPE + CLIC1 (XR data)		14.7							
Layer 3									
POPE +d-CLIC1 in D2O	24.2	6.3	3.46			0.13 ± 0.08	1127	11.3	0.52
POPE +d-CLIC1 in ACMW		0.26							
POPE + CLIC1 (XR data)		9.71							

4.3.3.2 Characterisation of CLIC1 insertion into POPE:Chol monolayer

The model fitted XR reflectivity profiles and their corresponding ρ_e profiles of POPE:Chol monolayer (5:1 mole ratio) held at 20 mN/m, in the absence and presence of CLIC1 protein are illustrated in Figure 4.9. In the presence of cholesterol, the POPE monolayer was condensed to a smaller area per lipid molecule of 36 $Å^2$ with a surface coverage of 2.20 mg/m^2 and a total thickness of 28.3 Å. CLIC1-wt interacts very weakly with POPE:Chol monolayer (5:1 mole ratio), as shown in Figure 4.9, in which the normalized X-ray reflectivity profiles of the monolayers before and after CLIC1 injection show only modest changes. The structural parameters fitted to POPE:Chol monolayer before and after CLIC1 interaction are summarised in Table 4.5.

From the changes in the ρ_e model shown in Figure 4.9 we can infer that CLIC1 penetrates into the POPE:Chol acyl chain and head-group regions, which have a thickness of 22.8 Å and 5.07 Å respectively, and extends 21.8 Å into the buffer subphase. The lipid acyl chains ρ_e (8.37×10^{-6} $Å^{-2}$ for acyl chains of POPE:Chol monolayer) increases to 8.86×10^{-6} $Å^{-2}$ upon interaction with CLIC1, which corresponds to 5% of the lipid acyl chain volume being occupied by the protein. On the other hand, the ρ_e of the head-group region decreased from 12.72×10^{-6} $Å^{-2}$ to 12.13×10^{-6} $Å^{-2}$ upon interaction with CLIC1 protein due to increase level of hydration. The physical changes to the fitted parameters of POPE:Chol monolayer in the presence of CLIC1 is found to be similar to that observed for POPC:Chol monolayer. It can be concluded that addition of cholesterol to phospholipid monolayers facilitates CLIC1 insertion into both the head-group and tail regions of the lipid monolayer with a diffuse layer of protein underneath the head-groups.

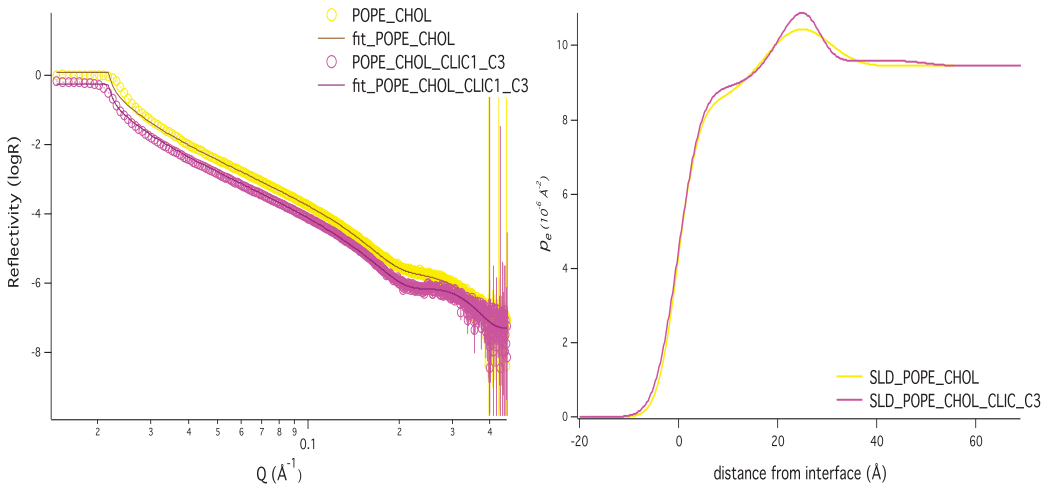

Figure 4.9 Comparisons of X-ray reflectivity profiles and model data fits and the electron density profile the fits describe for CLIC1-POPE:Chol monolayer at the air-water interface. POPE:Chol (5:1 mole ratio) monolayer held at a constant pressure of 20mN/m without (yellow line) and with CLIC1 (pink line).

Table 4.5 Parameters obtained from fits of XR data from POPE:Chol monolayer with and without CLIC1.

Lipids	Layers	t Å	ρ_e 10^{-6} Å^2	σ Å	*lipid*	*H2O*	*CLIC1*	A Å^2	A nm^2	Γ mg/m^2
POPE: Chol	Acyl chains	21.2	8.37	3.27	0.77	0.23		35.9	0.36	2.20
	Head-group	7.09	12.72	7.90	0.64	0.36				
POPE: Chol + CLIC1	Acyl chains	22.8	8.86	3.72	0.52	0.48	0.05	N/A		-
	Head-group	5.07	12.13	5.48	0.49	0.51	0.05			
	CLIC1/ H_2O	21.8	9.59	2.86			0.05	689	6.89	0.32

4.3.4 CLIC1 interaction with POPS monolayer in the absence and presence of Cholesterol

The interaction of CLIC1 with POPS monolayer in the absence and presence of cholesterol was investigated using XR experiments. The structural parameters are summarised in Table 4.6, with the electron density profiles and corresponding reflectivity data and model fits shown in Figure 4.10. The model fits to the POPS monolayer after 3 hours of CLIC1 addition to the subphase (Figure 4.10B) confirmed that there is no CLIC1 protein within the monolayer, which is consistent with our findings in Langmuir experiments. However, significant CLIC1 insertion was observed when POPS monolayer was supplemented with cholesterol in a mole ratio of 5:1 (Figure 4.10C). A four slab model was required to fit the lipid-protein XR profile (Table 4.6). Comparison of the electron density profiles of POPS:Chol monolayer with and without CLIC1 suggests that approximately ~11% of CLIC1 is present underneath the head-group regions and throughout the POPS:Chol monolayer in Layer 2 and Layer 3 respectively. The presence of cholesterol also causes CLIC1 to penetrate across the hydrophobic lipid core resulting in an additional Layer 1, with a thickness of 3.44 Å. However, it was not possible to precisely distinguish the composition of the different layers from just the ρ_e profiles.

Table 4.6 Parameters obtained from fits of XR data from POPS monolayer and POPS:Chol monolayer with and without CLIC1.

Lipids	Layers	t Å	ρ_e 0^{-6} Å^2	σ Å	*lipid*	*H2O*	*CLIC1*	A Å^2	A nm^2	Γ ng/m^2
POPS	Acyl chains	13.22	7.93	3.21	0.85	0.15		58.10	0.58	1.85
	Head-group	7.23	16.01	4.61	0.71	0.29				
POPS + CLIC1	Acyl chains	13.02	7.84	4.42	0.90	0.10		59.3	0.59	1.92
	Head-group	7.01	15.96	5.83	0.71	0.29				
	CLIC1/ H_2O									
POPS: Chol	Acyl chains	20.17	8.49	3.24	0.68	0.32		36.8	0.37	1.99
	Head-group	7.57	12.02	3.94	0.34	0.66				
POPS: Chol + CLIC1	Layer 1	3.44	9.38	3.15						
	Layer 2	14.05	10.57	6.72	N/A			N/A		
	Layer 3	8.49	13.47	2.85						
	CLIC1/ H_2O	15.63	9.74	3.63		0.91	0.11	822	8.22	0.6

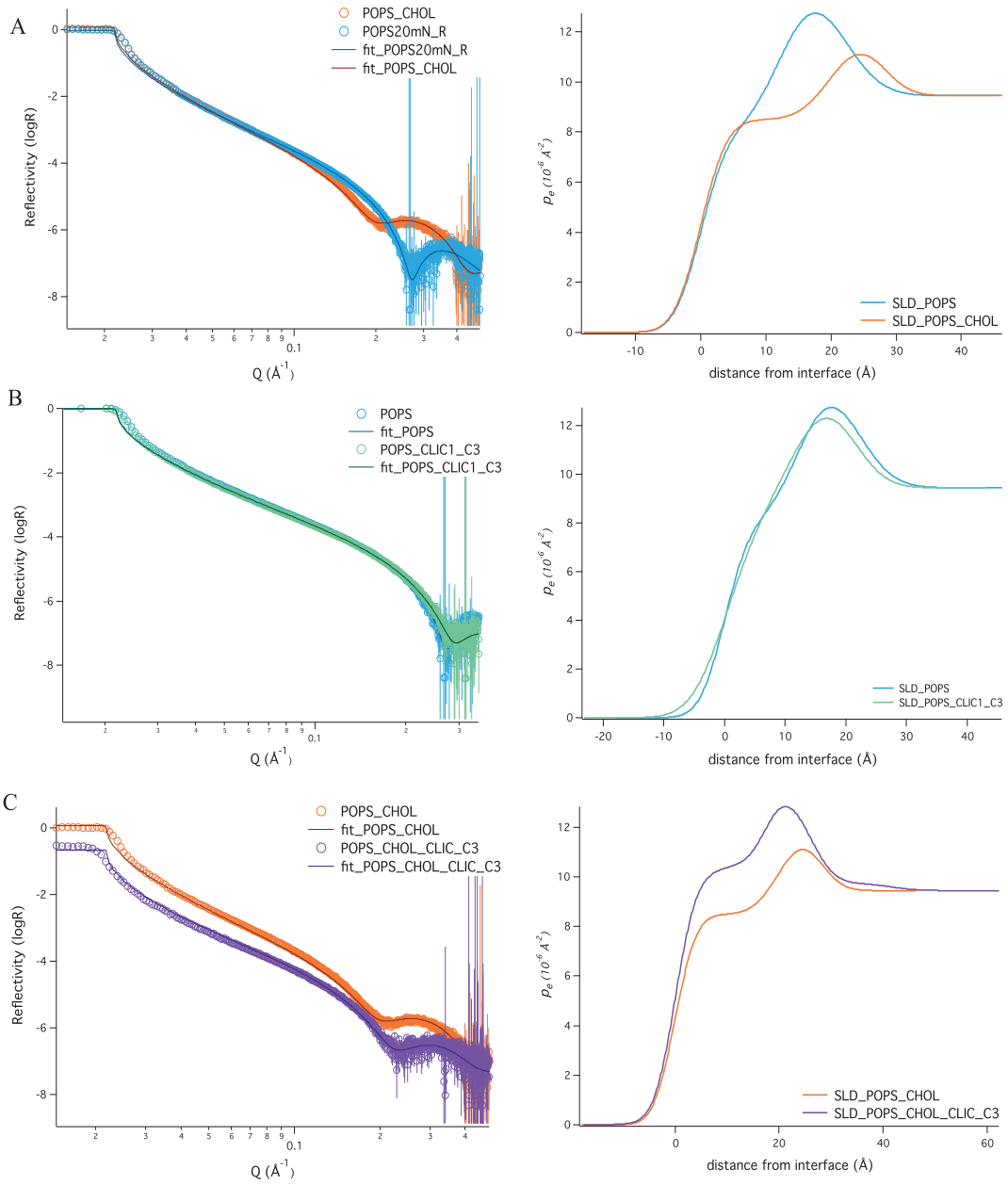

Figure 4.10 Comparisons of X-ray reflectivity profiles and model data fits and the electron density profile the fits describe for CLIC1-lipid monolayer at the air-water interface. **(A)** POPS (blue line) and POPS:Chol (5:1 mole ratio) monolayer (orange line) held at a constant pressure of 20mN/m; **(B)** POPS monolayer with (green line) and without (blue line) CLIC1 and **(C)** POPS:Chol (5:1 mole ratio) monolayer with (purple line) and without (orange line) CLIC1.

4.4 Discussion

The sensitivity of X-ray and neutron reflectivity methods to the relative location, dimensions and quantification of protein at the membrane interface, as well as the ability to observe structural changes taking place in the lipid matrix upon protein interaction, enabled us to reveal several new details about the spontaneous membrane insertion process of CLIC1 into artificial lipid membrane. Our results allow us to speculate a model of the conformational changes of CLIC1 from its soluble state to its membrane-bound state in differing phospholipid membrane environments. Furthermore, we describe the structural, dynamic and hydration changes of different lipid monolayers induced by the interaction with CLIC1 protein. From XR and NR data, we propose a schematic model that summarises our findings as shown in Figure 4.11.

Previous studies using impedance spectroscopy on tBLMs [19] and our current Langmuir monolayer results confirm that CLIC1 has a lower insertion and ion channel activity in phospholipid only membranes compared to corresponding membranes formed with cholesterol. In this study, we have used three different phospholipids POPC, POPS and POPE at the air-water interface to observe the initial stages of CLIC1 binding and penetration into these lipid monolayers in the absence and presence of cholesterol. The structural parameters of POPC and POPE monolayers were measured using both XR and NR reflectivity profiles. Deuterated POPC (d_{31}-POPC) on a D_2O and ACMW buffer subphase was used to generate NR profiles, while h-POPC on H_2O buffer subphase was used to generate XR profile (Figure 4.4). Unfortunately, due to the unavailability of deuterated POPE, NR data was collected from h-POPE on D_2O buffer subphase and simultaneously fitted with XR data collected from h-POPE on H_2O subphase (Figure 4.8). The monolayer structure of hydrogenous POPS phospholipid monolayer was determined using its respective XR profile only (Figure 4.10).

Volume fractions of the acyl chains and head-group regions of the monolayers were calculated to be 92% and 77% respectively for POPC, 85% and 71% for POPS and 86% and 73% for POPE suggesting the formation of compact stable monolayers for all three phospholipids, deemed suitable for the study of protein interactions. The POPC monolayer was 20 Å thick with an area per molecule of

63 $Å^2$ while POPS and POPE monolayers had the same thickness, but a smaller area per molecule of 58.1 $Å^2$ and 57.6 $Å^2$ respectively. These values were consistent with previously published data obtained by X-ray diffraction, molecular dynamic studies and and other scattering techniques [32, 33, 41].

The NR and XR profiles of CLIC1 interaction with different phospholipid monolayers (see Figures 4.5B, 4.8B and 4.10B) show that CLIC1 interacts with the phospholipid head-groups of POPC and POPE (Tables 4.2 and 4.4), and partially inserts into the tail region of POPC. However, XR data of CLIC1 interaction with POPS monolayer did not show any change in the anionic POPS monolayer (Table 4.6). Such a result was consistent with our Langmuir data and further confirmed that CLIC1 does not insert into POPS monolayer. A possible explanation for this may well be the presence of possible repulsive forces between the protein and the negatively charged lipid molecules. The crystal structure of CLIC1 protein resolved at 1.4 Å by X-ray crystallography showed a highly negatively charged loop between helices h5 and h6 in CLIC1 giving the molecule a net charge of -7 [8]. It can be speculated that it is the presence of the negative charge that prevents CLIC1 insertion into POPS while, conversely contributing favourable interaction with the neutral POPC and POPE phospholipids.

For CLIC1 interaction with POPC or POPE, it was not possible to satisfactorily fit the reflectivity data using the same two-layer models as used for the corresponding POPC/POPE monolayers in the absence of CLIC1. Instead, the best fits to the data were obtained assuming the existence of an additional hydrated CLIC1-containing layer underneath the lipid head-groups towards the buffer subphase. The fitted XR profile of POPC (Figure 4.2) and the simultaneously fitted XR and NR profiles of POPE (Figure 4.4) showed similar structural parameters for CLIC1-lipid interaction. A schematic model of CLIC1 interaction with phospholipid monolayers in the absence and presence of cholesterol is shown in Figure 4.11. The fitted parameters resulted in a CLIC1 layer of 25.9 Å thick under POPC head-groups and 24.2 Å thick under POPE head-groups which is consistent with the thickness of the short axis of the CLIC1 protein of 23 Å from X-ray crystallography data [8]. This suggests that the protein lies flat with an interfacial area of 1080 ± 0.6 $Å^2$ (10.8 nm^2) and a surface

coverage of approximately 0.49 ± 0.3 mg/m^2 in phospholipid monolayers. The literature also supports the theory that CLIC1 accumulates below the lipid layer before inserting the hydrophobic core of the membrane [14, 15, 17].

In our studies we have seen evidence of CLIC1 accumulation and interaction with the phospholipid head-groups, however no significant penetration of CLIC1 into the acyl chain region was observed in all three phospholipid monolayers which is considered necessary to form functional ion channels. These results therefore suggest that other factors are more likely involved to facilitate the spontaneous membrane insertion of CLIC1 into artificial lipid membranes in order to form functional ion channels. Previously, our group has published impedance spectroscopy studies that confirm that CLIC1 does form functional ion channels in tethered phospholipid bilayers in the absence of cholesterol [19]. We have also shown through Langmuir monolayer experiments that CLIC1 has a strong preference for associating with or intercalating into pure phospholipid or mixed phospholipid monolayers that contain cholesterol (see Chapter 3) [18]. Hence to elucidate the structural features of CLIC1 interaction with phospholipid monolayers supplemented with cholesterol, in a mole ratio of 5:1, both XR and NR data were collected for CLIC1 interaction with phospholipid-cholesterol monolayers and analysed using the Motofit analysis package as described above.

The mechanism by which the putative transmembrane region of CLIC1 inserts into and spans the membrane was first proposed by Tulk and Edwards (1998) [42] following their research on the resistance of CLIC1 to alkaline extraction. Resistance to alkali extraction of CLIC1 when it is in a membrane form suggests that the protein spans the membrane [42]. Subsequently, electrophysiological studies performed on transfected CHO-K1 cells using antibody to the FLAG epitope tag on recombinantly expressed CLIC1 have shown that CLIC1 inserts and spans the membrane an odd number of times, with the amino terminus spanning the membrane to protrude out to the extracellular face of the plasma membrane, while the carboxyl terminal domain of the protein remains in the cytosol [14]. A recent study performed using fluorescence resonance energy transfer (FRET) spectroscopy and electron paramagnetic resonance (EPR) also supports the concept that upon CLIC1 interacting with membranes, the N- and C-domains are

located on the opposite sides of the membrane with cysteine residue 24 localised at the trans face of the membrane [15, 17].

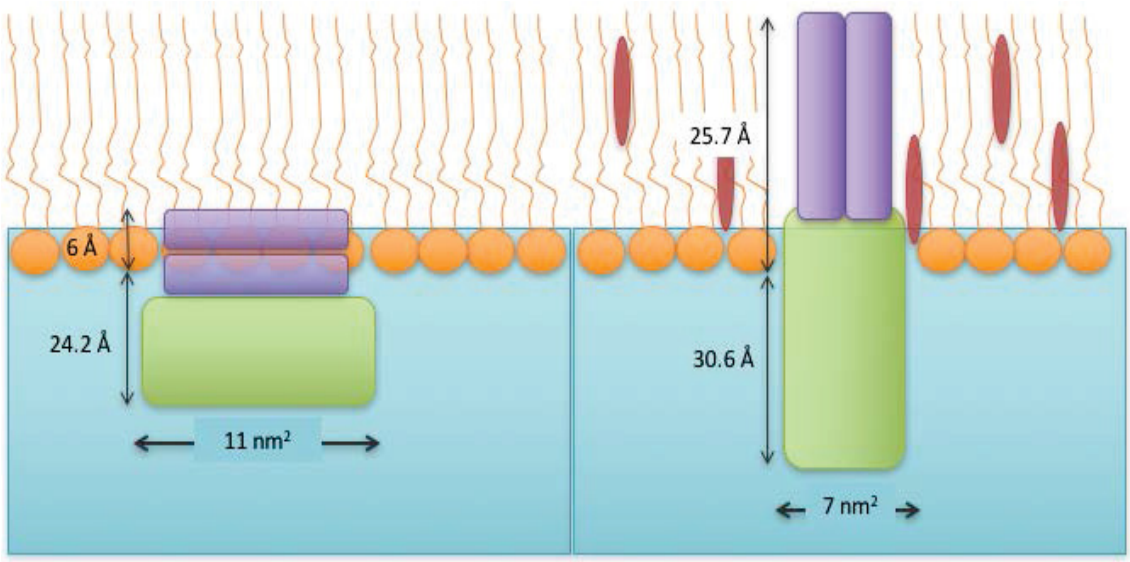

Figure 4.11 A schematic model summary of the interaction of CLIC1 with phospholipid monolayers in the absence and presence of cholesterol. The phospholipid monolayer is shown in orange in the absence (left) and the presence of cholesterol molecule shown in red (right). A schematic model of the N- and C-terminal domains of CLIC1 molecule is shown in purple and green respectively. The presence of cholesterol causes deeper penetration of CLIC1 protein into the hydrophobic acyl chains of the lipid monolayer.

Similar results were obtained from the simultaneous fits of the NR data of CLIC1 interaction with POPC monolayer in the presence of cholesterol (see Figure 4.6 and Table 4.3). The presence of cholesterol was shown to cause structural changes in the protein that resulted in deeper penetration of CLIC1 into the acyl chain regions of the lipid (Figure 4.11). Such penetration is required if the protein is to form functional membrane spanning channels. CLIC1 penetration into the hydrophobic tails of the monolayer was evident from the increase in lipid acyl chains ρ_n (0.012 x 10^{-6} Å^{-2} for acyl chains of POPC:Chol monolayer) value to 0.21 x 10^{-6} Å^{-2} upon interaction with CLIC1, which corresponds to 11% of the lipid acyl chain volume being occupied by the protein. This finding was also confirmed from the lipid acyl chain volume fraction (φ_{lipid}), which was found to be ~ 82% prior to the introduction of CLIC1 and ~ 61% after CLIC1 insertion, thus suggesting the displacement of lipid from the interface during the insertion

process and an increase in the hydration level. From previous studies it was proposed that in order to form a channel by inserting into the membrane, the hydrophobic transmembrane domain of CLIC1 must undergo a structural reorganisation involving a rapid unfolding and refolding of the N-terminal domain [8, 14, 15, 42]. Studies using CLIC-like proteins also showed that the first 55 residues at the N-terminal domain are necessary for membrane insertion with the tryptophan (Trp^{35}) residue localised within the membrane [43]. From our results, it can be speculated that cholesterol promotes conformational changes in the N-terminal domain of CLIC1 in order to expose the hydrophobic transmembrane domain for greater interaction and insertion of CLIC1 within the hydrophobic tails of the lipid film.

The thickness of the CLIC1 layer underneath the lipid monolayer increased from 24 Å to 30.6 ± 6 Å with a smaller area per molecule of 607 $Å^2$ (6.1 nm^2 compared to the 11 nm^2 area per molecule in phospholipid monolayers only) suggesting different structural conformations of the protein within the POPC monolayer in the absence and presence of cholesterol. The conformational changes of CLIC1 in POPC:Chol monolayer resulted in a total CLIC1 thickness of 56.3 ± 6 Å, which is in excellent agreement with the X-ray crystallography results that suggested CLIC1 to be a flat molecule with dimensions of 55 x 52 x 23 Å. Similar results where CLIC1 showed deeper membrane penetration into the hydrophobic region of the lipid film were also obtained when POPE (Table 4.5) and POPS (Table 4.6) monolayers were supplemented with cholesterol. Therefore, further confirming the regulatory role of cholesterol in the spontaneous membrane insertion of CLIC1 proteins in biological membrane mimics. Previous studies with spontaneous membrane inserting PFTs, especially the CDCs have shown that these toxins also bind to cholesterol for deeper penetration into the membrane [44-47].

NR and XR data also confirmed that CLIC1 binding to POPE:Chol monolayer was small (see Table 4.5) which is consistent with our Langmuir results (see Figure 3.8, Chapter 3). CLIC1 interaction with POPE:Chol monolayer gave a surface excess of 0.32 mg/m^2 compared to 0.81 mg/m^2 and 0.6 mg/m^2 for CLIC1 binding to POPC:Chol and POPS:Chol respectively. Moreover, the volume

fraction of CLIC1 decreased from 13% to only 5% upon CLIC1 interaction with POPE:Chol monolayer in comparison to POPE monolayer only. Likewise, Langmuir experiments have shown that CLIC1 inserts into POPE:POPC at a ratio of 5:1 but when the ratio is reversed to 1:5 insertion does not occur. However, CLIC1 inserts into POPC:POPE monolayer following addition of cholesterol (4:1:1 mole ratio of POPC:POPE:Cholesterol) (see Figure 3.9, Chapter 3). Such an interaction of CLIC1 is unique to POPE phospholipid only and warrants further investigation, however it is beyond the scope of this study.

4.5 Conclusion

By using X-ray and neutron reflectivity, we have elucidated the structures of different phospholipid monolayers interacting with the chloride intracellular ion channel protein, CLIC1. We have shown that CLIC1 inserts into the monolayer in several distinct orientations depending on membrane lipid composition, which has not been observed previously. We have also confirmed that cholesterol is required for the penetration of the N-terminal domain of CLIC1 into the hydrophobic acyl chains of the lipid monolayer, which is considered necessary for the formation of functional ion channels. A relatively stable orientation of CLIC1 was observed upon interaction with the three different phospholipid monolayers containing cholesterol, resulting in an average total CLIC1 thickness of approximately 49.3 ± 7 Å. The average area per molecule of CLIC1 within the different phospholipid-cholesterol monolayers was calculated to be approximately 706 ± 1 $Å^2$ (7 nm^2) with a surface coverage of 0.8 mg/m^2. In humans, members of the CLIC family have been linked to nasopharyngeal carcinoma, gastric cancer, hepatocarcinoma, colorectal cancer, gallbladder carcinoma, ovarian and breast cancer. CLIC1 protein has the potential to be used as an effective biomarker or as a potent therapeutic target in cancer therapy. Structurally understanding the mechanism by which CLIC proteins interact with the membrane is therefore crucial if these applications are to be realised. In addition, although this study was specific to the protein CLIC1, these findings provide wider implications in our understanding of protein-membrane interactions for several spontaneous membrane inserting proteins.

4.6 References

[1] Park, S., and Opella, S. (2005) Tilt angle of a trans-membrane helix is determined by hydrophobic mismatch., *J Mol Biol. 350*, 310-318.

[2] Kandasamy, S., and Larson, R. (2006) Molecular dynamics simulations of model trans-membrane peptides in lipid bilayers: a systematic investigation of hydrophobic mismatch., *Biophys J. 90*, 2326-2343.

[3] Strandberg, E., Esteban-Martín, S., Ulrich, A., and Salgado, J. (2012) Hydrophobic mismatch of mobile transmembrane helices: Merging theory and experiments., *Biochim Biophys Acta. 1818*, 1242-1249.

[4] Yeagle, P., Bennett, M., Lemaître, V., and Watts, A. (2007) Transmembrane helices of membrane proteins may flex to satisfy hydrophobic mismatch., *Biochim Biophys Acta. 1768*, 530-537.

[5] Daily, A., Greathouse, D., van der Wel, P., and Koeppe, R. I. (2008) Helical distortion in tryptophan- and lysine-anchored membrane-spanning alpha-helices as a function of hydrophobic mismatch: a solid-state deuterium NMR investigation using the geometric analysis of labeled alanines method., *Biophys J. 94*, 480-491.

[6] de Planque, M., Greathouse, D., Koeppe, R. I., Schäfer, H., Marsh, D., and Killian, J. (1998) Influence of lipid/peptide hydrophobic mismatch on the thickness of diacylphosphatidylcholine bilayers. A 2H NMR and ESR study using designed transmembrane alpha-helical peptides and gramicidin A., *Biochemistry 37*, 9333-9345.

[7] Lee, A. (2003) Lipid-protein interactions in biological membranes: a structural perspective., *Biochim Biophys Acta. 1612*, 1-40.

[8] Harrop, S., DeMaere, M., Fairlie, W., Reztsova, T., Valenzuela, S., Mazzanti, M., Tonini, R., Qiu, M., Jankova, L., Warton, K., Bauskin, A., Wu, W., Pankhurst, S., Campbell, T., Breit, S., and Curmi, P. (2001) Crystal structure of a soluble form of the intracellular chloride ion channel CLIC1 (NCC27) at 1.4-A resolution., *J Biol Chem. 276*, 44993-45000.

[9] Cromer, B., Gorman, M., Hansen, G., Adams, J., Coggan, M., Littler, D., Brown, L., Mazzanti, M., Breit, S., Curmi, P., Dulhunty, A., Board, P., and Parker, M. (2007) Structure of the Janus protein human CLIC2., *J Mol Biol. 374*, 719-731.

[10] Littler, D., Brown, L., Breit, S., Perrakis, A., and Curmi, P. (2010) Structure of human CLIC3 at 2 A resolution., *Proteins 78*, 1594-1600.

[11] Littler, D., Assaad, N., Harrop, S., Brown, L., Pankhurst, G., Luciani, P., Aguilar, M., Mazzanti, M., Berryman, M., Breit, S., and Curmi, P. (2005) Crystal structure of the soluble form of the redox-regulated chloride ion channel protein CLIC4. , *FEBS J. 272*, 4996-5007.

[12] Littler, D., Harrop, S., Brown, L., Pankhurst, G., Mynott, A., Luciani, P., Mandyam, R., Mazzanti, M., Tanda, S., Berryman, M., Breit, S., and Curmi, P. (2008) Comparison of vertebrate and invertebrate CLIC proteins: the crystal structures of Caenorhabditis elegans EXC-4 and Drosophila melanogaster DmCLIC., *Proteins. 71*, 364-378.

[13] Goodchild, S., Howell, M., Cordina, N., Littler, D., Breit, S., Curmi, P., and Brown, L. (2009) Oxidation promotes insertion of the CLIC1 chloride intracellular channel into the membrane., *Eur Biophys J. 39*, 129-138.

[14] Tonini, R., Ferroni, A., Valenzuela, S., Warton, K., Campbell, T., Breit, S., and Mazzanti, M. (2000) Functional characterization of the NCC27 nuclear protein in stable transfected CHO-K1 cells., *FASEB J. 14*, 1171-1178.

[15] Goodchild, S., Howell, M., Littler, D., Mandyam, R., Sale, K., Mazzanti, M., Breit, S., Curmi, P., and Brown, L. (2010) Metamorphic response of the CLIC1 chloride intracellular ion channel protein upon membrane interaction., *Biochemistry. 49*, 5278-5289.

[16] Singh, H., and Ashley, R. (2006) Redox regulation of CLIC1 by cysteine residues associated with the putative channel pore., *Biophys J. 90*, 1628-1638.

[17] Goodchild, S., Angstmann, C., Breit, S., Curmi, P., and Brown, L. (2011) Transmembrane extension and oligomerization of the CLIC1 chloride intracellular channel protein upon membrane interaction., *Biochemistry. 50*, 10887-10897.

[18] Hossain, K., Al Khamici, H., Holt, S., and Valenzuela, S. (2016) Cholesterol Promotes Interaction of the Protein CLIC1 with Phospholipid Monolayers at the Air-Water Interface., *Membranes 6*, 15-28.

[19] Valenzuela, S., Alkhamici, H., Brown, L., Almond, O., Goodchild, S., Carne, S., Curmi, P., Holt, S., and Cornell, B. (2013) Regulation of the Membrane Insertion and Conductance Activity of the Metamorphic Chloride Intracellular Channel Protein CLIC1 by Cholesterol, *PLoS ONE 8*, 56948.

[20] Leiting, B., Marsilio, F., and O'Connell, J. (1998) Predictable deuteration of recombinant proteins expressed in Escherichia coli., *Anal Biochem. 265*, 351-355.

[21] Als-Nielsen, J., Jacquemain, D., Kjaer, K., Leveiller, F., Lahav, M., and Leiserowitz, L. (1994) Principles and applications of grazing incidence X-ray and neutron scattering from ordered molecular monolayers at the air-water interface, *Physics Reports 246*, 251-313.

[22] Eisenberger, P., and Feldman, L. (1981) New approaches to surface structure determinations., *Science 214*, 300-305.

[23] Majewski, J., Kuhl, T., Wong, J., and GS., S. (2000) X-ray and neutron surface scattering for studying lipid/polymer assemblies at the air–liquid and solid–liquid interfaces, *Reviews in Molecular Biotechnology 74*, 207-231.

[24] Majewski, J., Kuhl, T., Wong, J., and Smith, G. (2000) X-ray and neutron surface scattering for studying lipid/polymer assemblies at the air-liquid and solid-liquid interfaces., *J Biotechnol. 74*, 207-231.

[25] Stefaniu, C., and Brezesinski, G. (2014) X-ray investigation of monolayers formed at the soft air/water interface, *Current Opinion in Colloid & Interface Science 19*, 216-227.

[26] James, M., Nelson, A., Holt, S., Saerbeck, T., Hamilton, W., and Klose, F. (2011) The multipurpose time-of-flight neutron reflectometer "Platypus" at Australia's OPAL reactor, *Nuclear Instruments and Methods in Physics Research Section A: Accelerators, Spectrometers, Detectors and Associated Equipment 632*, 112-123.

[27] Clifton, L., Green, R., Hughes, A., and Frazier, R. (2008) Interfacial structure of wild-type and mutant forms of puroindoline-b bound to DPPG monolayers., *J Phys Chem B. 112*, 15907-15913.

[28] Pedersen, J., and Hamley, I. (1994) Analysis of neutron and X-ray reflectivity data by constrained least-squares methods, *Physica B 198*, 16-23.

[29] Yepuri, N., Holt, S., Moraes, G., Holden, P., Hossain, K., Valenzuela, S., James, M., and Darwish, T. (2014) Stereoselective synthesis of perdeuterated phytanic acid, its phospholipid derivatives and their formation into lipid model membranes for neutron reflectivity studies., *Chem Phys Lipids. 183*, 22-33.

[30] Nelson, A. (2006) Co-refinement of multiple-contrast neutron/X-ray reflectivity data using MOTOFIT *Journal of Applied Crystallography 39*, 273-276.

[31] Born, M., and Wolf, E. (1970) *Principles of Optics.*, Oxford, Pergamon Press.

[32] Chiu, S., Jakobsson, E., Subramaniam, S., and Scott, H. (1999) Combined Monte Carlo and molecular dynamics simulation of fully hydrated dioleyl and palmitoyl-oleyl phosphatidylcholine lipid bilayers., *Biophys J. 77*, 2462-2469.

[33] Petrache, H., Tristram-Nagle, S., Gawrisch, K., Harries, D., Parsegian, V., and Nagle, J. (2004) Structure and fluctuations of charged phosphatidylserine bilayers in the absence of salt, *Biophys J. 86*, 1574-1586.

[34] Holt, S., Le Brun, A., Majkrzak, C., McGillivray, D., Heinrich, F., Lösche, M., and Lakey, J. (2009) An ion-channel-containing model membrane: structural determination by magnetic contrast neutron reflectometry., *Soft Matter 5*, 2576-2586.

[35] Foglia, F., Fragneto, G., Clifton, L., Lawrence, M., and Barlow, D. (2014) Interaction of amphotericin B with lipid monolayers., *Langmuir 30*, 9147-9156.

[36] Gramlich, G., Zhang, J., Winterhalter, M., and Nau, W. (2001) A long-lived amphiphilic fluorescent probe studied in POPC air-water monolayer and solution bilayer systems., *Chem Phys Lipids. 113*, 1-9.

[37] Hauser, H., Pascher, I., Pearson, R., and Sundell, S. (1981) Preferred conformation and molecular packing of phosphatidylethanolamine and phosphatidylcholine., *Biochim Biophys Acta. 650*, 21-51.

[38] Smaby, J., Momsen, M., Brockman, H., and Brown, R. (1997) Phosphatidylcholine acyl unsaturation modulates the decrease in interfacial elasticity induced by cholesterol., *Biophys J. 73*, 1492-1505.

[39] Foglia, F., Fragneto, G., Clifton, L., Lawrence, M., and Barlow, D. (2014) Interaction of amphotericin B with lipid monolayers., *Langmuir 30*, 9147-9156.

[40] Clifton, L., Sanders, M., Kinane, C., Arnold, T., Edler, K., Neylon, C., Green, R., and Frazier, R. (2012) The role of protein hydrophobicity in thionin-phospholipid interactions: a comparison of α1 and α2-purothionin adsorbed anionic phospholipid monolayers., *Phys Chem Chem Phys. 14*, 13569-13579.

[41] Helm, C., Tippmann-Krayer, P., Möhwald, H., Als-Nielsen, J., and Kjaer, K. (1991) Phases of phosphatidyl ethanolamine monolayers studied by synchrotron x-ray scattering, *Biophysical Journal 60*, 1457-1476.

[42] Tulk, B., and Edwards, J. (1998) NCC27, a homolog of intracellular Cl-channel p64, is expressed in brush border of renal proximal tubule., *Am J Physiol. 274*, 1140-1149.

[43] Berry, K., Bülow, H., Hall, D., and Hobert, O. (2003) A C. elegans CLIC-like protein required for intracellular tube formation and maintenance., *Science. 302*, 2134-2137.

[44] Alouf, J., Geoffroy, C., Pattus, F., and Verger, R. (1984) Surface properties of bacterial sulfhydryl-activated cytolytic toxins. Interaction with monomolecular films of phosphatidylcholine and various sterols., *Eur J Biochem. 141*, 205-210.

[45] Gilbert, R. (2010) Cholesterol-dependent cytolysins., *Adv Exp Med Biol 677*, 56-66.

[46] Jacobs, T., Darji, A., Frahm, N., Rohde, M., Wehland, J., Chakraborty, T., and Weiss, S. (1998) Listeriolysin O: cholesterol inhibits cytolysis but not binding to cellular membranes., *Mol Microbiol. 28*, 1081-1089.

[47] Tweten, R. (2005) Cholesterol-Dependent Cytolysins, a Family of Versatile Pore-Forming Toxins, Infect Immun. 73, 6199–6209.

Chapter 5

Sterol structural requirements for interaction of CLIC1 with Cholesterol in Phospholipid Monolayers

Chapter 5

Sterol structural requirements for interaction of CLIC1 with Cholesterol in Phospholipid Monolayers

5.1 Introduction

Sterols have been reported to modulate conformation and hence the function of several membrane proteins [1, 2]. Membrane protein interaction with lipids shows distinct specificity in terms of the sterol structure. The structure of the sterol's polar head-group, its sterol rings and its aliphatic side chains have all been shown to influence protein membrane interactions, including the initial binding and subsequent oligomerisation of the protein, once in the membrane in order to form functional channels [3-6]. Previous studies with several different cholesterol-dependent cytolysins (CDCs), for example perfringolysin O (PFO) [7, 8], ostreolysin (Oly) [9], *Vibrio cholerae* cytolysin (VCC) [10], with different natural and synthetic sterols have shown that their binding to membranes and the lytic activity of these proteins were both dependent on the intact sterol 3β-OH group, and were decreased by introducing additional double bonds and methylation of the steroid skeleton [7-10]. In this thesis, we have provided some insights into the regulatory role that cholesterol plays in the spontaneous membrane insertion of the protein CLIC1. However, the manner in which cholesterol interacts with CLIC1 is unknown.

In this chapter, the effect of the structure of membrane sterols and cholesterol derivatives on the spontaneous membrane insertion of CLIC1 protein is presented. In addition to the two cholesterol derivatives: Cholestane and 5-cholesten-3-one, the different natural sterols used in this study were cholesterol, ergosterol, β-sitosterol and 20-hydroxyecdysone. Sterols are complex molecules resulting from millions of years of biochemical evolution and are found in a wide range of membranes across various species [1, 6]. Cholesterol (Chol) is the typical sterol found in the plasma membranes of mammalian cells, whereas ergosterol (Erg) is the major sterol of other eukaryotic organisms such as protozoa, yeast and fungi, while phytosterols (e.g. β-sitosterol and stigmasterol) predominates in the plasma membrane of plants [1, 6]. Invertebrates such as insects and worms, on the other hand, do not produce sterols endogenously and are characterised as sterol

auxotrophs [11-13]. However, all invertebrate organisms demand a nutritional source of sterol to produce ecdysone and its active metabolite, 20-hydroxyecdysone (Hyd), in order to complete development [11-13]. The chemical structure of the different natural sterols and cholesterol derivatives used in this study is depicted in Figure 5.1.

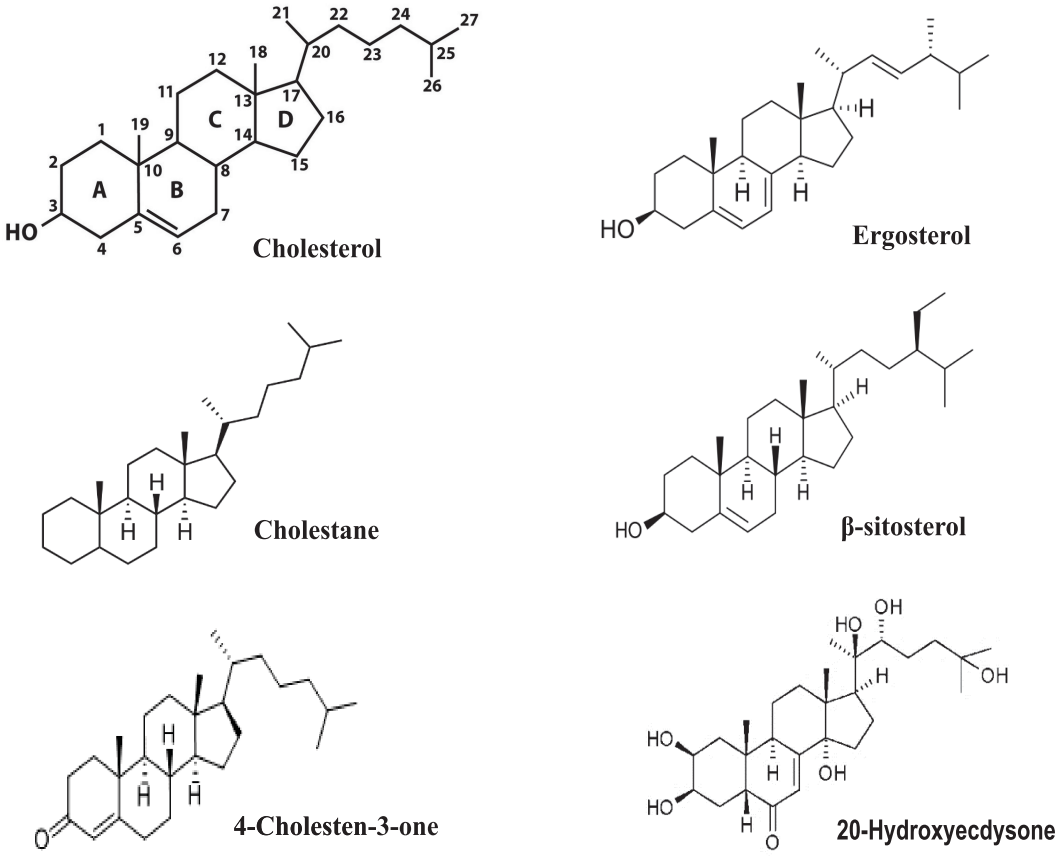

Figure 5.1 Chemical structures of the different natural sterols and cholesterol derivatives used in this study.

We used Langmuir experiments to examine the membrane insertion of CLIC1 into lipid monolayers comprised of 5:1 molar mixtures of POPC with different natural sterols and the cholesterol derivatives mentioned above. Neutron reflectivity (NR) experiments were also carried out in order to elucidate the structural features of the CLIC1-membrane bound form in POPC monolayers containing different natural sterols. The Langmuir data shows that the presence of the free sterol 3β-OH group is an essential requirement for the interaction of CLIC1 with cholesterol. Furthermore, the presence of additional hydroxyl groups, methylation of the sterol skeleton and the structure of the sterol alkyl side chain also modulate the magnitude of CLIC1 interaction with the different sterols.

5.2 Materials and Method

CLIC1 was expressed and purified as described in Chapter 3. Deuterated CLIC1 (d-CLIC1) was expressed and purified by protocols previously described in Chapter 4. 1-palmitoyl-2-oleoyl-*sn*-glycero-3-phosphatidylcholine (POPC) and chain deuterated 1-palmitoyl-(d_{31})-2-oleoyl-sn-glycero-3-phosphatidylcholine (d_{31}-POPC) were purchased from Avanti Polar Lipids (Alabaster, USA) and used as received. Cholesterol (Chol), Ergosterol (Ergo), β-sitosterol (Sito), 20-hydroxyecdysone (Hyd), Cholestane (Ch-ane) and 5-cholesten-3-one (Ch-one) were purchased from Sigma Aldrich (Australia). The chemical structures of the natural sterols and Chol derivatives used in this study are shown in Figure 5.1. All lipids were dissolved in chloroform to a final concentration of 1 mg/ml and stored at -20 ° C. All other reagents used were of analytical grade.

5.2.1 Langmuir Monolayer Experiment

Langmuir monolayer experiments were carried out using 1-Palmitoyl-2-oleoylphosphatidylcholine (POPC) in a 5:1 mole ratio combination with either one of the following sterols: Cholesterol (Chol), β-sitosterol (Sito), Ergosterol (Ergo), 20-hydroxyecdysone (Hyd), Cholestane (Ch-ane) and 5-cholesten-3-one (Ch-one). Recombinant CLIC1-wt (50 μg) was then injected into the aqueous subphase underneath the different POPC:Sterol monolayer and the percentage change in area (ΔA) was recorded as described in Chapter 3, Section 3.3.

5.2.2 Specular Neutron Reflectivity

To elucidate the structural features of CLIC1 in POPC monolayers containing different natural sterols, specular neutron reflectivity (NR) experiments were carried out at the Platypus, time-of-flight reflectometer at the 20MW OPAL Research Reactor at ANSTO (Lucas Heights, Australia) by methods previously described in Chapter 4, Section 4.2.4. Multiple NR profiles were collected for each POPC:Sterol combination with and without CLIC1 using different contrast variation. Both hydrogenated and deuterated POPC and CLIC1 abbreviated as h/d_{31}-POPC and h/d-CLIC1 respectively, were used in D_2O or ACMW KCL/Hepes buffer (pH 6.5) subphase to create contrast variation such that particular components of the monolayer can be highlighted or made invisible to the neutrons. Table 5.1 represents the molecular volumes and the theoretically

calculated SLD_n values of the h/d_{31}-POPC, h/d-CLIC1 and the different sterols used in this study. The NR fits of the different POPC:Sterol monolayers in the absence and presence of CLIC1 were analysed as previously described in Chapter 4, Section 4.2.5. For NR experiments, in order to have a precise measure of parameter uncertainties, a Monte-Carlo (MC) resampling technique was applied to all the reflectivity profiles by methods described by Holt *et.al* (2009) [14].

Table 5.1 Summary of the molecular Volumes (V_m), theoretical neutron scattering length densities (SLD_n) of h/d_{31}-POPC, h/d-CLIC1 and the different sterols in ACMW and D_2O subphase.

Component		V_m Å^3	SLD_n 10^{-6} Å^{-2} (ACMW)	SLD_n 10^{-6} Å^{-2} (D_2O)
h/d-CLIC1		34211	1.85/3.23	2.86/7.48
h/d_{31}-POPC	Whole molecule	1263	0.26/2.82	0.26/2.82
	Head-group	319	1.88	1.88
	Acyl chains	944	-0.283/3.14	-0.28/3.14
Cholesterol		655	0.215	0.361
Ergosterol		658	0.428	0.574
B-sitosterol		710	0.175	0.310
20-hydroxyecdysone		624	0.970	1.892

5.3 Results

5.3.1 Effects of Sterol Structure on CLIC1 Membrane Interactions

To study the chemical moieties in cholesterol that are important for CLIC1 interaction, we compared the spontaneous membrane insertion of the protein in phospholipid monolayers containing the following different sterols: Cholesterol (Chol), Ergosterol (Ergo), β-sitosterol (Sito), 20-hydroxyecdysone (Hyd); and two cholesterol derivatives: Cholestane (Ch-ane) and 5-cholesten-3-one (Ch-one). Monolayers were formed using 1-Palmitoyl-2-oleoylphosphatidylcholine (POPC) alone, or in the 5:1 mole ratio combinations with each one of the different sterols: POPC: Chol or Ergo or Sito or Hyd or Ch-ane or Ch-one. Our previous studies with different phospholipid monolayers have shown that the spontaneous membrane insertion of the CLIC1 protein was dependent on the presence of cholesterol in the membrane. In lipid monolayers where no cholesterol was added, CLIC1 did not insert, however, in the presence of cholesterol, a significant amount of CLIC1 protein showed insertion and/or membrane interactions (details in Chapter 3).

Substitution of cholesterol in the POPC monolayer with different natural sterols and cholesterol derivatives had a significant effect on the spontaneous membrane insertion of CLIC1 as shown in Figure 5.2. It was found that substitution of cholesterol with either Ergo, Sito or Hyd in POPC monolayers significantly increased ($p<0.01$) CLIC1 interaction with the membrane, with CLIC1 showing the greatest amount of insertion into POPC:Hyd monolayer, resulting in a ΔA value of approximately 48.2 ± 2 % (Figure 5.2). In comparison to CLIC1 interaction with POPC:Chol monolayer (ΔA= 19.4 ± 1 %), CLIC1 interaction with POPC:Ergo and POP:Sito monolayers also resulted in significantly greater ΔA values of 24.9 ± 0.6 % and 26.6 ± 0.75 % respectively. However, as seen in Figure 5.2, substitution of ergosterol with β-sitosterol in the POPC monolayer did not result in any significant difference in the spontaneous membrane insertion of the protein.

Conversely, cholesterol substituted with either of the two cholesterol derivatives led to greatly reduced levels of spontaneous membrane insertion of CLIC1 protein

into POPC:Ch-ane and POPS:Ch-one monolayers, producing ΔA values of 1.72 ± 0.2 % and 2.68 ± 0.13 % respectively. Based on the structural analysis of the sterols (Figure 5.1), any change in the 3β-OH group led to an apparent inhibition or decrease in CLIC1 interaction with these sterols. CLIC1 showed significant interaction with all the natural sterols that contain the 3β-OH group but showed very little to almost no interaction with the cholesterol derivatives, cholestane (Ch-ane) and 5-cholesten-3-one (Ch-one), which lacked the 3β-OH group in their structures. From the results in Figure 5.2, it is evident that the spontaneous membrane insertion of CLIC1 is dependent on the presence of an intact 3β-OH group in the sterol structure and the order of preference for CLIC1 interaction with sterols thus established was 20-hydroxyecdysone (Hyd) > β-sitosterol (Sito) and / or ergosterol (Ergo) > cholesterol (Chol). To better understand the ambiguities of CLIC1 interactions with the natural sterols, neutron reflectivity experiments were conducted to structurally characterise CLIC1 insertion into POPC monolayer containing either Ergo/Sito/ Hyd.

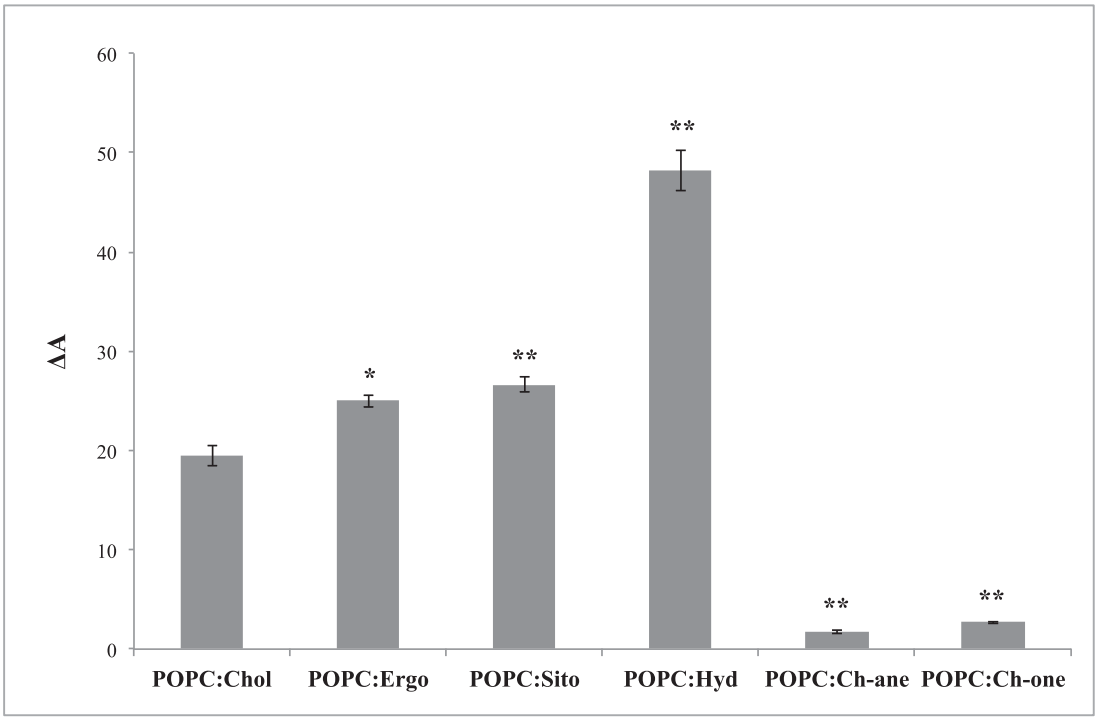

Figure 5.2 CLIC1-wt interaction with different POPC:Sterol monolayers. The figure shows percentage area expansion profiles of different POPC:Sterol monolayers after 3 hours following CLIC1-wt injection into the subphase. Data shown are means ± S.E of at least three independent experiments. The asterisks * and ** correspond to significant ($p < 0.05$ and $p < 0.01$ respectively) difference in the membrane insertion of CLIC1-wt in POPC:Chol monolayer relative to that of CLIC1 insertion into different POPC:Sterol monolayers.

5.3.2 Characterisation of CLIC1 insertion into POPC monolayers containing different natural sterols

We used neutron reflectometry to investigate the molecular structure of CLIC1 during its interaction with POPC monolayers supplemented in a 5:1 mole ratio with each of the different natural sterols: POPC: Ergo/Sito/Hyd. The Platypus, time-of-flight reflectometer at the 20MW OPAL Research Reactor at ANSTO (Lucas Heights, Australia) was used to probe interfacial thickness and density of the lipid-CLIC1 monolayer in the direction normal to the substrate surface as previously described in Chapter 4, Section 4.2.4. Neutron reflectivity profiles were collected for deuterated and hydrogenous POPC and sterol monolayers with and without deuterated CLIC1 protein added beneath the lipid films. Reflectivity data for the monolayers were examined under two solution contrasts (D2O and ACMW). Since, the underlying protein and membrane

structure are invariant under isotopic substitution, hence to characterise the thickness and the composition of the lipid (± sterol) monolayers before and after CLIC1 insertion and to reduce the parameter uncertainties, neutron reflectivity profiles of the same sample were fitted simultaneously using the MOTOFIT analysis package. The analysis was based on modelling the thickness (***t****, Å*), neutron scattering length density ($\boldsymbol{\rho_n}$, $Å^{-2}$), and roughness ($\boldsymbol{\sigma}$, Å) of different layers to achieve the best fitted data with the least χ^2 value. The fitted reflectivity data obtained from the different h-POPC:Sterol and d-POPC:Sterol monolayers at differing solution contrasts were used to determine the relative contribution of the membrane components using a set of linear equation. The individual components of a fitted layer within the monolayer will contribute to the SLD of that respective layer as shown in equation:

$$\rho_{layer} = (SLD_{POPC} \text{ x } \varphi_{POPC}) + (SLD_{Sterol} \text{ x } \varphi_{Sterol}) + (SLD_{Water} \text{ x } \varphi_{Water}) \quad \text{Eq. 5.1}$$

where ρ is the SLD of a given layer, SLD_{POPC} , SLD_{Sterol} and SLD_{Water} are the individual SLDs of the POPC, Sterol and solvent respectively (values are given in Table 5.1) and φ_{POPC} , φ_{Sterol} , and φ_{Water} are the volume fractions of these components within a particular layer. The relative volume fractions of the components were determined for both the lipid head-group and tail group layers. In the presence of d-CLIC1 proteins, the values of SLD_{CLIC1} were added to the previous equation in order to calculate the volume fractions of d-CLIC1 (φ_{CLIC1}) in their respective layers.

5.3.2.1 Characterisation of CLIC1 insertion into POPC:Ergosterol monolayer

Two reflectivity profiles, a d_{31}-POPC:Ergo monolayer on an ACMW KCL/Hepes buffer subphase (pH 6.5) and a d_{31}-POPC:Ergo monolayer on a D_2O KCL/Hepes buffer subphase (pH 6.5), were simultaneously fitted in order to determine the structure of the POPC:Ergo monolayer held at a constant pressure of 20 mN/m. The NR reflectivity and the corresponding scattering length density (ρ_n) profiles for d_{31}-POPC:Ergo monolayer are shown in Figure 5.3A and the structural parameters are illustrated in Table 5.2. A Monte-Carlo (MC) based resampling procedure was applied to the constrained fit from the two different d_{31}-POPC:Ergo monolayers in order to produce a histogram of the frequency

distribution for the thickness of the lipid monolayer, as shown in Figure 5.3A. The addition of ergosterol resulted in structural changes in the POPC monolayer such that it was not possible to fit the d_{31}-POPC:Ergo NR profiles as two distinct layers (head-groups and tails). Instead, the best fitted data with the least χ^2 value was achieve with a one layer model resulting in a total monolayer thickness of 16 ± 1.6 Å. The interfacial area per molecule calculated for the d_{31}-POPC:Ergo monolayer was approximately 66.7 $Å^2$ with a volume fraction of 84% and a surface coverage of 1.65 mg/m^2.

To elucidate the structural features of the CLIC1 membrane-bound form in monolayers containing ergosterol, neutron reflectivity profiles of CLIC1 protein interaction with POPC:Ergo monolayers were collected and analysed as mentioned above. To provide contrasting scattering length density (ρ_n) profiles, NR profiles were generated using deuterated lipid and protein in the following contrasts: d-CLIC1 in d_{31}-POPC:Ergo monolayer on a D_2O buffer subphase and d-CLIC1 in d_{31}-POPC:Ergo monolayer on an ACMW buffer subphase. Simultaneous fitting followed by MC resampling of the constrained fit from the two different samples allowed moderately accurate modeling of the protein-lipid system. The fitted ρ_n (Figure 5.3B) demonstrates that CLIC1 protein interacts with POPC:Ergo monolayer with the expected structure as shown in Table 5.2. The NR data were fitted as a three-layer model where the lower layer of 34.4 ± 6 Å (against the aqueous phase) is composed of ~ 11% CLIC1, the intermediate layer of 13 ± 4 Å is comprised of a portion of lipid tails, lipid head-groups together with CLIC1 protein and the upper layer (12 ± 2.8 Å) consists of CLIC1 proteins surrounded by POPC tails.

These physical changes to the POPC:Ergo monolayer in the presence of the protein suggests deeper penetration of CLIC1 into the acyl chain region giving a total CLIC1 thickness of 59.4 ± 4.3 Å, which is only ~ 3 Å greater than the total CLIC1 thickness of 56.3 ± 6 Å observed in POPC:Chol monolayer (details in Chapter 4). In comparison to CLIC1 interactions with POPC:Chol monolayer, the calculated area per CLIC1 molecule in POPC:Ergo monolayer was found to be slightly less, approximately 567 $Å^2$ vs 607 $Å^2$, with a greater surface coverage of

0.87 mg/m^2 in relation to 0.81 mg/m^2 . As seen in the Langmuir experiments shown in Figure 5.2, CLIC1 interaction with POPC:Ergo monolayer also showed greater insertion in comparison to that observed in POPC:Chol monolayer. These changes in the structural parameters as well as in the spontaneous membrane insertion of CLIC1 in POPC:Ergo monolayer may well be dictated by the substitution of cholesterol by ergosterol in the POPC monolayer and will be discussed later.

Table 5.2 Parameters obtained from simultaneous fits of NR data from POPC:Ergo monolayer with and without CLIC1.

	t Å	ρ_n 10^{-6} Å^2	σ Å	*lipid*	*H2O*	*CLIC1*	A Å^2	A nm^2	Γ mg/m^2
POPC:Ergo									
d_{31}-POPC:Ergo in D2O	16 ± 1.6	2.6	3.7	0.84 ± 0.11	0.16		66.7	0.67	1.65
d_{31}-POPC:Ergo in ACMW		3.3							
POPC:Ergo + CLIC1									
Layer 1									
d_{31}-POPC:Ergo +d-CLIC1 in D2O	12 ± 2.8	4.54	5.32	N/A		0.11	-		
d_{31}-POPC:Ergo +d-CLIC1 in ACMW		2.25							
Layer 2									
d_{31}-POPC:Ergo +d-CLIC1 in D2O	13 ± 4	5.42	5.07	N/A		0.11	-		
d_{31}-POPC:Ergo +d-CLIC1 in ACMW		1.59							
Layer 3									
d_{31}-POPC:Ergo +d-CLIC1 in D2O	34.4 ± 6	6.18	5.40			0.11 ± 0.09	576	5.76	0.87
d_{31}-POPC:Ergo +d-CLIC1 in ACMW		0.3							

Note that each volume fractions are an average of the different contrast

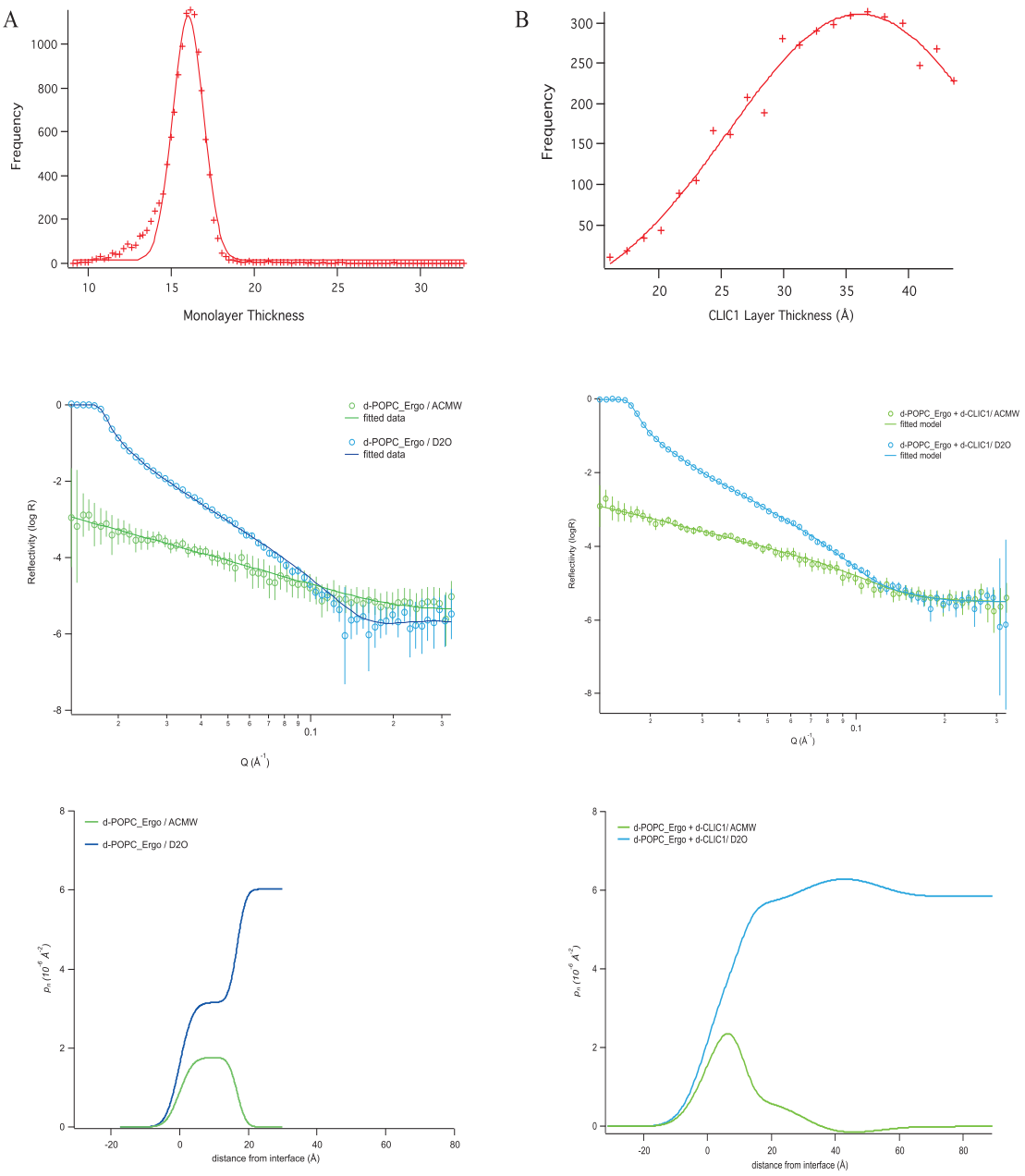

Figure 5.3 Monte-Carlo (MC) resampling, Neutron reflectivity profiles and model data fits, and the scattering length density profiles these fits describe for POPC:Ergo monolayer (A) without CLIC1 and (B) with CLIC1. The two simultaneously fitted isotopic contrasts shown are d_{31}-POPC:Ergo on an ACMW buffer subphase (green line); and d_{31}-POPC:Ergo on a D_2O subphase (blue line) **(A)** in the absence of the protein and **(B)** in the presence of d-CLIC1 protein.

5.3.2.2 Characterisation of CLIC1 insertion into POPC:ß-Sitosterol monolayer

In order to elucidate the structural features of CLIC1 interaction with POPC:ß-sitosterol monolayer, two NR reflectivity profiles of d_{31}-POPC:Sito in the absence and presence of d-CLIC1 were collected as mentioned previously for d_{31}-POPC:Ergo, with the exception, that an additional NR contrast of d-CLIC1 in h-POPC:Sito on ACMW buffer subphase was also collected. The simultaneously fitted NR reflectivity profiles and the corresponding ρ_n profiles of d_{31}-POPC:Sito monolayer (5:1 mole ratio) held at 20 mN/m, in the absence and presence of CLIC1 protein are illustrated in Figure 5.4A and B respectively. In the presence of ß-Sitosterol, the POPC monolayer was condensed to an area per lipid molecule of 83 $Å^2$ with a surface coverage of 1.08 mg/m^2 and a total thickness of 14.2 Å. The simultaneous fits to the NR data for the d_{31}-POPC:Sito monolayers was divided into two discrete layers: a hydrophobic acyl chain region of 7.9 ± 1.3 Å, and a lipid head-group region of 6.24 ± 1.5 Å with volume fractions of 88% and 67% respectively (Table 5.3).

The MC resampling data and the simultaneously fitted NR profiles with the corresponding scattering length density profiles for CLIC1 interaction with POPC:Sito monolayer is illustrated in Figure 5.4B. The structural parameters obtained from the best three layer fit is provided in Table 5.3. The best model-to-data fit (as shown in Figure 5.4) used a three slab structure with layers one and two representing the lipid acyl chains and the head-group regions of the POPC:Sito monolayer respectively and a third layer representing CLIC1 protein in the aqueous subphase below the lipid layer. The layers were found to be 12.5, 11.9 and 18.7 Å in thickness respectively. Deuterated CLIC1 (d-CLIC1) protein was found to be incorporated within the head-group region and protein-only layer corresponding to 25 % volume of these layers (2 and 3) being occupied by the protein. Calculation of the surface coverage showed a total of 0.9 mg/m^2 CLIC1 in the POPC:Sito monolayer occupying 1118 $Å^2$ area per protein molecule.

The scattering length density profiles of Layer 2, corresponding to the head-group region of the POPC:Sito monolayer, increased following CLIC1 interaction resulting in a decrease in the lipid head-group volume fraction from 67% to 54%. On the other hand, the scattering length density profiles obtained from the three

different samples of Layer 1 (comprising of lipid acyl chain) resulted in an average lipid acyl chain volume fraction of 86 %, thereby suggesting the absence or the presence of very little protein within that layer (see Table 5.3). However, the increase in thickness of the acyl chains from 7.91 Å to 12.5 Å in the presence of CLIC1 may be due to the incorporation of a part of the head-group region within Layer 1.

Table 5.3 Parameters obtained from simultaneous fits of NR data from POPC:Sito monolayer with and without CLIC1.

	t Å	ρ_n 10^{-6} Å^2	σ Å	$lipid$	$CLIC1$	A Å^2	A nm^2	Γ mg/m^2
d_{31}-POPC:Sito								
Acyl chain Layer								
d_{31} -POPC:Sito in D2O	7.91 ± 1.3	3.08	2.78	0.88 ± 0.08				
d_{31} -POPC:Sito in ACMW		3.42						
Head-group Layer						82.7	0.83	1.08
d_{31} -POPC:Sito in D2O	6.24 ± 1.5	3.14	4.55	0.67 ± 0.15				
d_{31} -POPC:Sito in ACMW		1.32						
POPC:Sito + CLIC1								
Layer 1								
d_{31} -POPC:Sito +d-CLIC1 in D2O	12.5 ± 3	3.23	5.04	0.86 ± 0.1	0.0	-		
d_{31} -POPC:Sito +d-CLIC1 in ACMW		2.3						
h -POPC:Sito + d-CLIC1 in ACMW		1.08						
Layer 2								
d_{31} -POPC:Sito +d-CLIC1 in D2O	11.9 ± 3.3	4.89	3.72	0.54 ± 0.19	0.25 ± 0.13	-		
d_{31} -POPC:Sito +d-CLIC1 in ACMW		1.43						
h -POPC:Sito + d-CLIC1 in ACMW		1.43						
Layer 3								
d_{31} -POPC:Sito +d-CLIC1 in D2O	18.7 ± 0.69	6.81	5.13		0.25 ± 0.13	1118	11.2	0.9
d_{31} -POPC:Sito +d-CLIC1 in ACMW		0.24						
h -POPC:Sito + d-CLIC1 in ACMW		0.24						

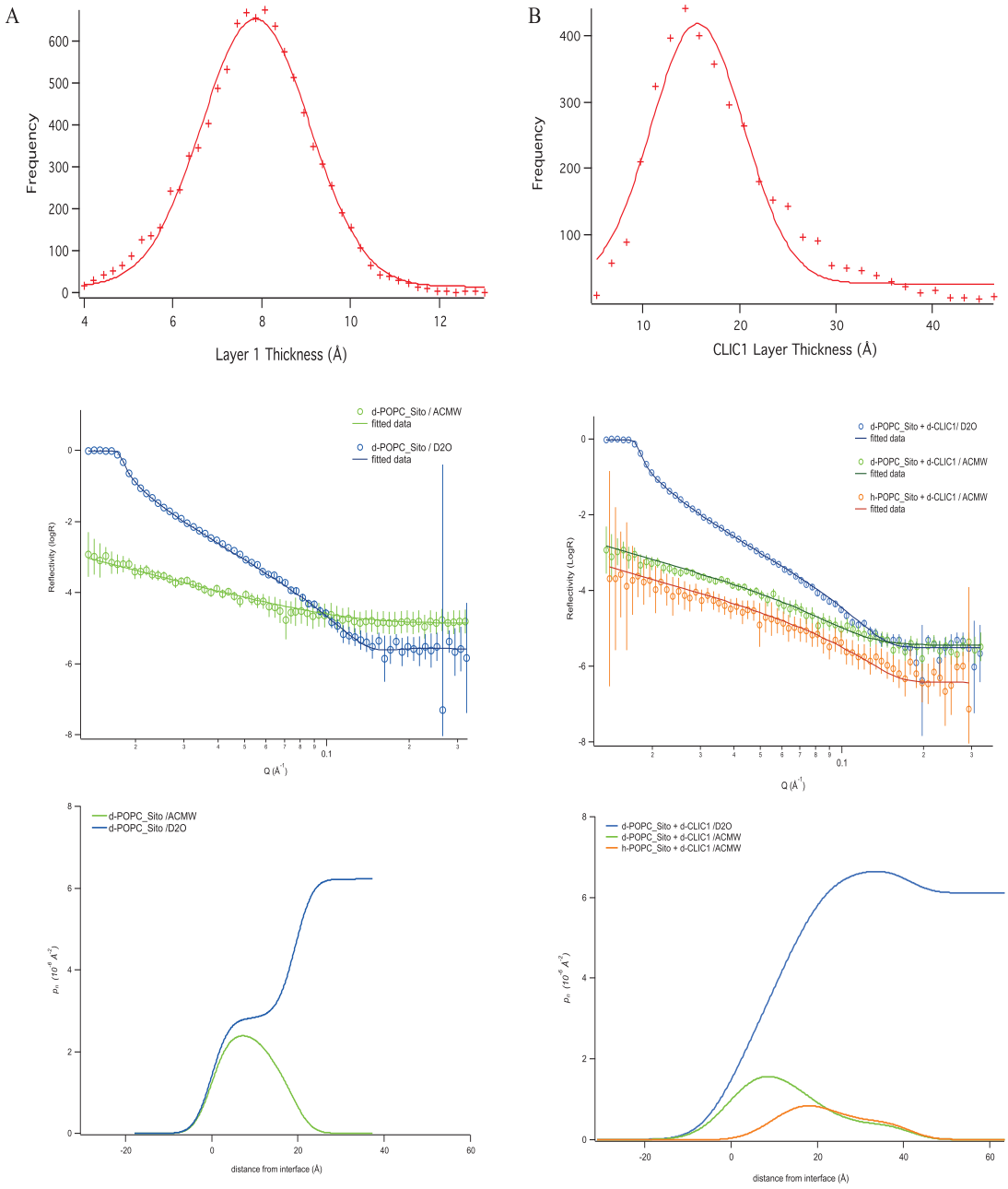

Figure 5.4 Monte-Carlo (MC) resampling, Neutron reflectivity profiles and model data fits, and the scattering length density profiles these fits describe for POPC:Sito monolayer (A) without CLIC1 and (B) with CLIC1. The simultaneously fitted isotopic contrasts shown are d_{31}-POPC:Sito on an ACMW buffer subphase (green line); and d_{31}-POPC:Sito on a D_2O subphase (blue line) **(A)** in the absence of the protein and **(B)** in the presence of d-CLIC1 protein with an additional contrast of h-POPC:Sito + d-CLIC1 (orange line).

5.3.2.3 Characterisation of CLIC1 insertion into POPC:Hydroxyecdysone monolayer

Two NR reflectivity profiles for d_{31}-POPC:Hyd monolayer on either D_2O or ACMW KCl/Hepes buffer subphase and three reflectivity profiles for CLIC1 insertion into d_{31} /h-POPC:Hyd monolayer (similar contrast to those mentioned above for POPC:Sito monolayer) were collected in order to determine the structural features of the lipid monolayer in the absence and presence of d-CLIC1 protein. The model fits for the NR reflectivity profiles and the scattering length density profile for d_{31}-POPC:Hyd monolayer (in the absence of protein) was determined by fitting the monolayer to a simple two-layer model, starting from air to buffer subphase with one layer corresponding to the phospholipid acyl chains and the second to the phospholipid head-group regions (see Figure 5.5A). The structural parameters obtained from the fit are shown in Table 5.4. A volume fraction of ($\varphi_{lipid\ acyl}$) of ~ 90 % was calculated for the d_{31}-POPC:Hyd acyl chain region having a thickness of 11.2 ± 2.8 Å. The head-group region was less densely packed, giving a volume fraction of $\varphi_{lipid\ head}$ of ~ 57 % with a thickness of 6.1 ± 1.8 Å. d_{31}-POPC:Hyd has a surface coverage of 1.8 mg/m^2 occupying an area per lipid molecule of approximately 66.7 Å^2 (Table 5.4).

Langmuir experiments showed that CLIC1 had the greatest amount of insertion (Figure 5.2) in POPC monolayers supplemented with hydroxyecdysone in a mole ratio of 5:1. Comparison of the fitted NR and ρ_n profiles of the d_{31} /h-POPC:Hyd monolayer with and without d-CLIC1 protein, as shown in Figure 5.5B & A respectively, suggests that d-CLIC1 is uniformly distributed across the three interfacial layers with a volume fraction of ~ 21 % throughout the monolayer. The Monte-Carlo resampling, applied to the constrained fit from the three different samples, resulted in a CLIC1 best-fit thickness of 28.3 ± 7 Å followed by a Layer 2 and Layer 1 thickness of 10.5 ± 3 Å and 12.3 ± 3.5 Å respectively. This produced a calculated surface excess of 1.07 mg/m^2 CLIC1 within the lipid monolayer. The increase in the scattering length density of the lipid head-groups from 1.21 x 10^{-6} Å^{-2} to 2.38 x 10^{-6} Å^{-2} in the presence of d-CLIC1 in d_{31}-POPC:Hyd (5:1 mole ratio) in ACMW suggests the presence of CLIC1 protein within the head-group region of the monolayer. On the other hand, the scattering

length density of the lipid acyl chains decreased from 3 x 10^{-6} Å^{-2} to 1.8 x 10^{-6} Å^{-2} in the presence of d-CLIC. The non-deuterated head-group region of d_{31}-POPC, which have significantly lower scattering length density in comparison to that of the deuterated tail, most likely caused the decrease in the ρ_n density of this upper layer as more of the head-group region became incorporated into this layer. This suggests that the upper layer is comprised of the lipid tails, a portion of the lipid head-groups, and protein all of which, together with increased hydration, contribute to the overall ρ_n fitted for this layer. As a result of the lack of sufficient contrast between the acyl chain and head-group layer of d_{31}-POPC:Hyd monolayer in the presence of deuterated protein, it was not possible to precisely distinguish between the first two layers and hence, their volume fractions could not be determined.

Table 5.4 Parameters obtained from simultaneous fits of NR data from POPC:Hyd monolayer with and without CLIC1.

	t Å	ρ_n 10^{-6} Å^2	σ Å	$lipid$	$CLIC1$	A Å^2	A nm^2	Γ mg/m^2
d_{31}-POPC:Hyd								
Acyl chain Layer								
d_{31} -POPC:Hyd in D2O	11.2 ± 2.8	3.68	3.4	0.90 ± 0.1				
d_{31} -POPC:Hyd in ACMW		3.07						
Head-group Layer						66.7	0.67	1.8
d_{31} -POPC:Hyd in D2O	6.1 ± 1.8	4.3	3.9	0.57 ± 0.19				
d_{31} –POPC:Hyd in ACMW		1.21						
POPC:Hyd + CLIC1								
Layer 1								
d_{31} -POPC:Hyd +d-CLIC1 in D2O	12.3 ± 3.5	3.76	6.62	N/A	0.21± 0.16	-		
d_{31} -POPC:Hyd +d-CLIC1 in ACMW		1.8						
h -POPC:Hyd + d-CLIC1 in ACMW		1.05						
Layer 2								
d_{31} -POPC:Hyd +d-CLIC1 in D2O	10.5 ± 3	4.85	4.06	N/A	0.21 ± 0.16	-		
d_{31} -POPC:Hyd +d-CLIC1 in ACMW		2.38						
h -POPC:Hyd + d-CLIC1 in ACMW		2.38						
Layer 3								
d_{31} -POPC:Hyd +d-CLIC1 in D2O	28.3 ± 7	6.44	4.64		0.21 ± 0.16	669.5	6.69	1.07
d_{31} -POPC:Hyd +d-CLIC1 in ACMW		0.41						
h -POPC:Hyd + d-CLIC1 in ACMW		0.41						

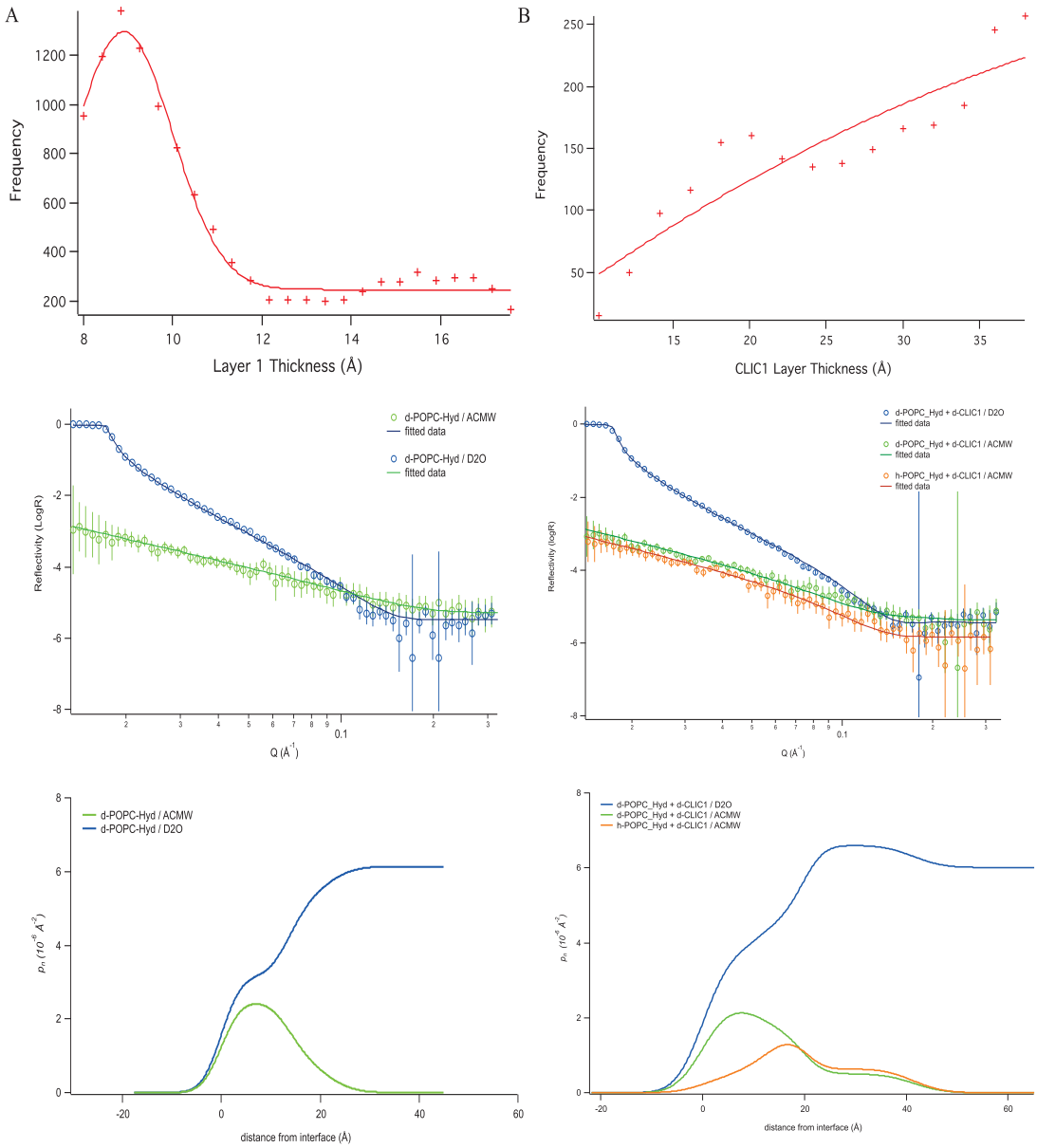

Figure 5.5 Monte-Carlo (MC) resampling, Neutron reflectivity profiles and model data fits, and the scattering length density profiles these fits describe for POPC:Hyd monolayer (A) without CLIC1 and (B) with CLIC1. The simultaneously fitted isotopic contrasts shown are d_{31}-POPC:Hyd on an ACMW buffer subphase (green line); and d_{31}-POPC:Hyd on a D_2O subphase (blue line) **(A)** in the absence of the protein and **(B)** in the presence of d-CLIC1 protein with an additional contrast of h-POPC:Hyd + d-CLIC1 (orange line).

5.4 Discussion

A particularly effective method of investigating the effect of sterols on plasma membrane properties and thus on the spontaneous membrane insertion of CLIC1 protein is to make a comparative study of different lipid-sterol interactions in an artificial model membrane. By selecting the well-defined lipid monolayer system with the sterol component being changed in a systematic way, we were able to gain insights into the structural and functional roles of sterols and, at a more detailed level, into the importance of each of the sterol structural components, on the spontaneous membrane insertion of CLIC1 into lipid monolayers. In this study, the following different natural sterols: Cholesterol (Chol), Ergosterol (Ergo), β-sitosterol (Sito), 20-hydroxyecdysone (Hyd); and cholesterol derivatives: Cholestane (Ch-ane) and 5-cholesten-3-one (Ch-one) were used to investigate the structural features of cholesterol necessary for interaction with CLIC1.

Cholesterol is an essential constituent of the plasma membrane of most eukaryotic cells, where it has been shown to play a crucial role in membrane organisation, dynamics, function and sorting [15-17] and has been reported to be necessary for the insertion and functional activity of several membrane proteins [3-5, 18]. Structurally it consists of a fused tetracyclic sterol ring attached to a hydrocarbon side chain on carbon 17 (C-17) and a hydrophilic 3β-OH group on C-3 (see Figure 5.1). In comparison to Chol, the structure of ergosterol differs in three places: Ergo has two additional double bonds, one at C-7 on the fused sterol ring and at C-22 on its alkyl chain, and a methyl group at C-24. β-sitosterol shares the same backbone structure with cholesterol, but they are different in the alkyl tail part due to the presence of an extra ethyl group at C-24 (Figure 5.1). On the other hand, Hyd, which is predominantly found in insects, has five additional –OH groups in its fused ring and alkyl chain structure and a ketone group at C-6. In comparison, the cholesterol derivative, Ch-ane lacks the 3β-OH group and the double bond at C-5 on its ring structure, while Ch-one the 3β-OH group is replaced by a ketone group as shown in Figure 5.1.

To investigate the effect of sterol structural features on the membrane insertion ability of CLIC1, the following different natural sterols and cholesterol derivatives

(mentioned above) were studied using a Langmuir monolayer system. Monolayers were formed using POPC in the 5:1 mole ratio combination with each of the different sterols. From the Langmuir experiments shown in Figure 5.2, the preference of CLIC1 insertion into POPC monolayers, supplemented with different natural sterols, was found to be in the following order: hydroxyecdysone > ergosterol and / or β-sitosterol > cholesterol. On the other hand, CLIC1 showed very little to almost no interaction with the cholesterol derivatives, Ch-ane and Ch-one, both of which lacked the polar hydroxyl group in their structure (unlike the nature sterols). Therefore, based on the structural features of the different sterols used in this study, CLIC1 interaction with cholesterol appears to be dependent on the presence of the intact 3β-OH group located at the C-3 position within the sterol ring. In addition, CLIC1 interaction with lipid monolayers containing different sterols was shown to increase by the introduction of additional hydroxyl groups and methylation of the steroid skeleton (as seen for Hyd and Sito/Ergo respectively in Figure 5.2).

Several studies have shown that structural modification of the sterols can affect the lipid acyl chain conformation (see review articles [19, 20]). In the early 1970's, Demel *et al.* (1972) [21] studied the force vs. area characteristics of monolayers of 3β and 3α-hydroxysterols containing Chol, Ergo or Sito as well as other sterols which are not considered here. From that study, they concluded that the interaction of the phospholipid and sterol in monolayers is governed by factors such as the van der Waals interaction between the lipid acyl chain and the sterol ring structure and its branched alkyl side chain, as well as the hydrogen bonding between the 3β-OH group and the aqueous medium [21]. The rigid ring structure of the sterol has been shown to limit the conformational *cis-trans* freedom of the lipid acyl chains, thereby, producing the ordering (condensing) effect of the sterol on the lipid molecules [22, 23]. However, modifications of this van der Waals interactions can consequently affect the lipid-sterols' packing ability and cause different sterols to have different solubility limits in the lipid membrane as well as different ordering abilities on the lipid acyl chains [20, 22-24]. In order to determine if the difference in CLIC1 interaction with the natural sterols was attributed to the difference in their packing behaviour within the POPC monolayer, neutron

reflectivity experiments were performed to elucidate the structural features of the different POPC:Sterol monolayers in the absence and presence of CLIC1 protein.

Previously, in Chapter 4, neutron reflectivity experiments performed on POPC:Chol monolayers have shown that addition of cholesterol resulted in the ordering of the phospholipids to an area per molecule of 47.06 $Å^2$ with a calculated surface coverage of 1.99 mg/m^2. In this Chapter, Monte-Carlo analysis of the fitted NR and ρ_n profiles of the different POPC:Sterol monolayers showed that addition of Ergo (Figure 5.3A) and Hyd (Figure 5.5A) to POPC monolayers resulted in a similar but greater area per lipid molecule of 66.7 $Å^2$ (Table 5.2 and 5.4 respectively) suggesting reduced lipid ordering ability of these sterols in relation to cholesterol. A similar effect was also evident from the Surface pressure-Area isotherms shown in Appendix Figure A2. The variation between the different sterols was in good agreement with previously published data, which have shown that the presence of the additional two double bonds and the methyl group in the alkyl chain of ergosterol, cause the sterol to become rigid and bulky in such a way that it limits the ability of the sterol to intercalate between POPC acyl chains, thereby, showing reduced capacity to order the lipid molecule [6, 21, 22, 24-26]. Furthermore, in a review article by Wenz (2012) [27], who conducted a systematic study of the relationship between the sterol molecular structure and the effects of sterols on membrane physical properties, showed that addition of polar hydroxyl (-OH) groups to the sterol structure (as seen in HYD) caused 'sterols membrane disrupting' properties with reduced membrane ordering ability [27].

In addition, previous studies that investigated the effects of plant sterols and cholesterol on the phase properties of different lipids using differential scanning calorimetry (DSC) [28, 29], X-ray diffraction [28] and ^{2}H-NM [30-32] studies stated that the bulky alkyl chains of plant sterols (β-sitosterol) make them less soluble in phospholipids compared to cholesterol. In short, they concluded that plant sterols are not as effective as cholesterol in reducing lipid bilayer permeability due to their lower solubility in the membrane [28-32]. Such an observation was consistent with our results shown in Figure 5.4A and Table 5.3. Substitution of Chol by Sito resulted in a reduced condensing effect on the POPC monolayer to a successive

area per lipid molecule of 83 Å^2 with a surface coverage of 1.08 mg/m^2, which was comparatively lower than that observed for cholesterol (1.99 mg/m^2).

Via the use of Langmuir experiments, we have demonstrated that CLIC1 interactions with POPC monolayers is dependant upon the type of natural sterol present in the monolayer. As seen in Figure 5.2, CLIC1 showed the greatest amount of insertion into POPC:Hyd monolayers (ΔA = 48.2 ± 2 %). One possibility for such an interaction may be due to the presence of additional –OH groups in Hyd that can facilitate greater hydrogen bonding interactions between the sterol molecule and the polar residues in CLIC1, thereby, increasing the spontaneous membrane insertion of the protein. It can also be speculated that the difference in CLIC1 interaction with POPC monolayers containing either Chol, Ergo, Sito or Hyd is attributed to the difference in the packing behaviour of the phospholipid monolayer in the presence of the different natural sterols. Structural analysis of the CLIC1 membrane-bound form using neutron reflectivity experiments has shown that there is a vast structural similarity between CLIC1 interaction with POPC monolayer in the presence of Chol, Ergo and Hyd, with the exception of the structural features of the protein in POPC:Sito monolayer.

Monte-Carlo analysis of the fitted NR and the corresponding ρ_n profiles for CLIC1 interaction with POPC:Chol monolayer is shown in Figure 4.6 and 4.7 and the structural parameters obtained from the fit is provided in Table 4.3 in Chapter 4. The conformational changes of CLIC1 in the POPC:Chol monolayer resulted in a total CLIC1 thickness of 56.3 ± 6 Å and the monolayer was covered with approximately 0.81 mg/m^2 of protein, which occupied an area per protein molecule of 607 Å^2 (6.07 nm^2). Similar results, where CLIC1 showed deeper membrane penetration into the hydrophobic acyl chains of the lipid film, were also obtained when POPC was supplemented with Ergo (as shown in Figure 5.3B) and Hyd (as shown in Figure 5.5B). The values of the total CLIC1 thickness and the area per protein molecule obtained from MC analysis of the fitted NR and ρ_n profiles were 59.4 ± 1.6 Å and 576 Å^2 (5.76 nm^2) for POPC:Ergo (Table 5.2) and 51.1 ± 4 Å and 669 Å^2 (6.69 nm^2) for POPC:Hyd (Table 5.4) respectively. In comparison to that observed in POPC:Chol monolayer, CLIC1's interaction with different sterol monolayers leads to an increase in thickness (of ~ 3 Å) and a

decrease in the protein interfacial molecular area (by ~ 30 Å^2) in the case of POPC:Ergo and vice versa in the case of POPC:Hyd with a decrease in thickness (of ~5 Å) and an increase in area per molecule by ~ 60 Å^2. A possible explanation for such discrepancies may arise either from a difference in the orientation of the different sterols, Chol, Ergo and Hyd, within the POPC monolayer in the presence of the protein or from a difference in the folding conformation of the N-terminal domain of CLIC1 upon interaction with the different POPC:Sterol monolayers or a combination of both these factors. Unfortunately, due to the lack of sufficient contrast variations between the POPC, sterol and CLIC1 proteins, it was neither possible to elucidated the structural conformation of the N-terminal domain of CLIC1 protein within the monolayer nor the position of the sterol molecule within the lipid-protein monolayer structure.

In contrast to the other natural sterols used in this study, MC analysis of the fitted NR and ρ_n profiles for CLIC1 interaction with POPC:Sito monolayer (as shown in Figure 5.4B) reveals a very different structural conformation of the protein, where CLIC1 inserted across the core of the lipid head-group region but showed very little interaction with the hydrophobic acyl chain region. CLIC1 interaction with POPC:Sito monolayer resulted in a CLIC1 thickness of 30 ± 6 Å (Table 5.3) which is consistent with the thickness of the short axis of the CLIC1 protein of 23 Å from X-ray crystallography data. This suggests that the protein lies flat with an interfacial molecular area of 1118 Å^2 (11.2 nm^2) which was only a ~ 0.4 Å^2 increase in area than that observed for CLIC1 interaction with phospholipid monolayers in the absence of sterols (1085 Å^2) (details mentioned in Chapter 4). As a result, it can be speculated that the structural conformation of CLIC1 in POPC:Sito monolayer is similar to the model structure (as shown in Figure 4.11, Chapter 4) proposed for CLIC1 insertion into phospholipid monolayer in the absence of cholesterol; while the structural conformation of CLIC1 in POPC:Ergo and POPC:Hyd is similar to that proposed for CLIC1 interaction with phospholipid:cholesterol monolayers (see Figure 4.11, Chapter 4).

Previously, we have confirmed that cholesterol is required for the penetration of the N-terminal domain of CLIC1 into the hydrophobic acyl chains of the lipid monolayer, which is considered necessary for the formation of functional ion

channels. Therefore, from the neutron reflectivity results, it can be speculated that CLIC1 may form functional ion channels in plasma membranes containing either ergosterol or hydroxyecdysone. However, the fact that CLIC1 does not insert across the lipid acyl chain region in POPC:Sito monolayer does not completely rule out the possibility of CLIC1 forming functional pores within plant membranes. Unlike mammalian and fungal cell membranes which contain only one major sterol (cholesterol or ergosterol respectively) plasma membranes of plant cells have a characteristically complex sterol mixture[1] which can, therefore, further affect the membrane insertion ability of the protein. Like the naturally existing sterol molecules, CLIC proteins are evolutionarily conserved across species; with almost all vertebrates expressing six CLIC proteins (CLIC1-6) and CLIC-like proteins have also been identified in invertebrates such as nematodes and insects and even in plants [33-36]. The ability of CLIC1 to interact with all the naturally existing sterols used in this study strongly suggests the possibility of a species specificity among the CLIC and CLIC-like proteins and their corresponding membrane sterols and hence, demands further investigation.

5.5 Conclusion

Our results provide insights into the structural features of sterols that are deemed necessary for CLIC1 interaction with cholesterol within mammalian membranes. From the Langmuir monolayer results of CLIC1 insertion into POPC monolayers containing naturally occurring sterols and cholesterol derivatives, it was conclusive that CLIC1 interaction with cholesterol is structurally dependent on the presence of the intact 3β-OH group in the sterol ring. Modification of the sterol structure by the introduction of additional hydroxyl groups (as seen in the case for Hyd) and methylation of the alkyl chain (as seen in Ergo and Sito) was shown to facilitate greater spontaneous membrane insertion of the protein within the phospholipid monolayer. The preference of CLIC1 insertion into POPC monolayers, supplemented with different natural sterols, was found to be in the following order: hydroxyecdysone (Hyd) > ergosterol (Ergo) and / or β-sitosterol (Sito) > cholesterol (Chol). This order of preference was further confirmed by NR experiments where the surface coverage of CLIC1 within the different POPC:Sterol monolayers were 1.07 mg/m^2 for Hyd > 0.9 mg/m^2 for Sito > 0.87 mg/m^2 for Ergo > 0.81 mg/m^2 for Chol.

Furthermore, neutron reflectivity experiments have shown that CLIC1 inserts in a similar structural orientation within POPC monolayers containing either cholesterol, ergosterol or 20-hyroxyecdysone, resulting in a total CLIC1 thickness that ranges from ~ 51 Å to 59 Å and ranging in an area per molecule of 576 $Å^2$ to 669 $Å^2$ depending on the type of sterol present. In addition, we have also shown that CLIC1 was unable to penetrate into the acyl chain regions of the POPC:Sito monolayer, unlike that seen for the other natural sterols, resulting in a different conformation which was rather similar to that observed for CLIC1 insertion into phospholipid only monolayers (ie., containing no sterols).

5.6 References

[1] Henriksen, J., Rowat, A., Brief, E., Hsueh, Y., Thewalt, J., Zuckermann, M., and Ipsen, J. (2006) Universal behavior of membranes with sterols., *Biophys J. 90*, 1639-1649.

[2] Mannock, D., Lewis, R., McMullen, T., and McElhaney, R. (2010) The effect of variations in phospholipid and sterol structure on the nature of lipid-sterol interactions in lipid bilayer model membranes., *Chem Phys Lipids. 163*, 403-448.

[3] Epand, R. (2006) Cholesterol and the interaction of proteins with membrane domains., *Prog Lipid Res. 45*, 279-294.

[4] Epand, R. (2008) Proteins and cholesterol-rich domains., *Biochim Biophys Acta. 1778*, 1576-1582.

[5] Epand, R., Thomas, A., Brasseur, R., and Epand, R. (2010) Cholesterol interaction with proteins that partition into membrane domains: an overview., *Subcell Biochem. 51*, 253-278.

[6] Róg, T., Pasenkiewicz-Gierula, M., Vattulainen, I., and Karttunen, M. (2009) Ordering effects of cholesterol and its analogues., *Biochim Biophys Acta. 1788*, 97-121.

[7] Nelson, L., Chiantia, S., and London, E. (2010) Perfringolysin O association with ordered lipid domains: implications for transmembrane protein raft affinity., *Biophys J. 99*, 3255-3263.

[8] Nelson, L., Johnson, A., and London, E. (2008) How interaction of perfringolysin O with membranes is controlled by sterol structure, lipid structure, and physiological low pH: insights into the origin of perfringolysin O-lipid raft interaction., *J Biol Chem. 283*, 4632-4642.

[9] Rebolj, K., Ulrih, N., Macek, P., and Sepcić, K. (2006) Steroid structural requirements for interaction of ostreolysin, a lipid-raft binding cytolysin, with lipid monolayers and bilayers., *Biochim Biophys Acta. 1758*, 1662-1670.

[10] Harris, J., Bhakdi, S., Meissner, U., Scheffler, D., Bittman, R., Li, G., Zitzer, A., and Palmer, M. (2002) Interaction of the Vibrio cholerae cytolysin (VCC) with cholesterol, some cholesterol esters, and cholesterol derivatives: a TEM study., *J Struct Biol. 139*, 122-135.

[11] Bellés, X., Martín, D., and Piulachs, M. (2005) The mevalonate pathway and the synthesis of juvenile hormone in insects., *Annu Rev Entomol. 50*, 181-199.

[12] Clayton, R. (1964) The Utilization of Sterols by Insects. , *J Lipid Res. 5*, 3-19.

[13] Gilbert, L., Rybczynski, R., and Warren, J. (2002) Control and biochemical nature of the ecdysteroidogenic pathway., *Annu Rev Entomol.*, 883-916.

[14] Holt, S., Le Brun, A., Majkrzak, C., McGillivray, D., Heinrich, F., Lösche, M., and Lakey, J. (2009) An ion-channel-containing model membrane: structural determination by magnetic contrast neutron reflectometry., *Soft Matter. 5*, 2576-2586.

[15] Liscum, L., and Underwood, K. (1995) Intracellular cholesterol transport and compartmentation., *J Biol Chem. 270*, 15443-15446.

[16] Mouritsen, O., and Zuckermann, M. (2004) What's so special about cholesterol?, *Lipids 39*, 1101-1113.

[17] Simons, K., and Ikonen, E. (2000) How cells handle cholesterol., *Science 290*, 1721-1726.

[18] Gilbert, R. (2010) Cholesterol-dependent cytolysins., *Adv Exp Med Biol 677*, 56-66.

[19] Miao, L., Nielsen, M., Thewalt, J., Ipsen, J., Bloom, M., Zuckermann, M., and Mouritsen, O. (2002) From lanosterol to cholesterol: structural evolution and differential effects on lipid bilayers., *Biophys J. 82*, 1429-1444.

[20] Bloom, M., Evans, E., and Mouritsen, O. (1991) Physical properties of the fluid lipid-bilayer component of cell membranes: a perspective., *Q Rev Biophys. 24*, 293-397.

[21] Demel, R., Bruckdorfer, K., and van Deenen, L. (1972) Structural requirements of sterols for the interaction with lecithin at the air water interface., *Biochim Biophys Acta. 255*, 311-320.

[22] Shaghaghi, M., Chen, M., Hsueh, Y., Zuckermann, M., and Thewalt, J. (2016) Effect of sterol structure on the physical properties of 1-palmitoyl-2-oleoyl-sn-glycero-3-phosphocholine membranes determined using 2H nuclear magnetic resonance., *Langmuir.*

[23] Thewalt, J., and Bloom, M. (1992) Phosphatidylcholine: cholesterol phase diagrams., *Biophys J. 63*, 1176-1181.

[24] Urbina, J., Pekerar, S., Le, H., Patterson. J., Montez, B., and Oldfield, E. (1995) Molecular order and dynamics of phosphatidylcholine bilayer membranes in the presence of cholesterol, ergosterol and lanosterol: a comparative study using 2H-, 13C- and 31P-NMR spectroscopy., *Biochim Biophys Acta. 1238*, 163-176.

[25] Hsueh, Y., Chen, M., Patty, P., Code, C., Cheng, J., Frisken, B., Zuckermann, M., and Thewalt, J. (2007) Ergosterol in POPC membranes: physical properties and comparison with structurally similar sterols., *Biophys J. 92*, 1606-1615.

[26] Bernsdorff, C., and Winter, R. (2003) Differential properties of the sterols cholesterol, ergosterol, beta-sitosterol, trans-7-dehydrocholesterol, stigmasterol and lanosterol on DPPC bilayer order. , *J Physical Chemistry B 107*, 10658-10664.

[27] Wenz, J. (2011) Predicting the effect of steroids on membrane biophysical properties based on the molecular structure., *Biochim Biophys Acta. 1818*, 896-906.

[28] McKersie, B., and Thompson, J. (1979) Influence of plant sterols on the phase properties of phospholipid bilayers., *Plant Physiol. 63*, 802-805.

[29] Halling, K., and Slotte, J. (2004) Membrane properties of plant sterols in phospholipid bilayers as determined by differential scanning calorimetry, resonance energy transfer and detergent-induced solubilization., *Biochim Biophys Acta. 1664*, 161-171.

[30] Dufourc, E., Parish, E., Chitrakorn, S., and Smith, I. (1984) Structural and dynamical details of cholesterol-lipid interaction as revealed by deuterium NMR, *Biochemistry. 23*, 6062–6071.

[31] Schuler, I., Milon, A., Nakatani, Y., Ourisson, G., Albrecht, A., Benveniste, P., and Hartman, M. (1991) Differential effects of plant sterols on water permeability and on acyl chain ordering of soybean phosphatidylcholine bilayers., *Proc Natl Acad Sci U S A. 88*, 6926-6930.

[32] Krajewski-Bertrand, M., Milon, A., and Hartmann MA. (1992) Deuterium-NMR investigation of plant sterol effects on soybean phosphatidylcholine acyl chain ordering., *Chemistry and Physics of Lipids 63*, 235-241.

[33] Berry, K., Bülow, H., Hall, D., and Hobert, O. (2003) A C. elegans CLIC-like protein required for intracellular tube formation and maintenance., *Science. 302*, 2134-2137.

[34] Elter, A., Hartel, A., Sieben, C., Hertel, B., Fischer-Schliebs, E., Lüttge, U., Moroni, A., and Thiel, G. (2007) A plant homolog of animal chloride intracellular channels (CLICs) generates an ion conductance in heterologous systems., *J Biol Chem. 282*, 8786-8792.

[35] Littler, D., Harrop, S., Brown, L., Pankhurst, G., Mynott, A., Luciani, P., Mandyam, R., Mazzanti, M., Tanda, S., Berryman, M., Breit, S., and Curmi, P. (2008) Comparison of vertebrate and invertebrate CLIC proteins: the crystal structures of Caenorhabditis elegans EXC-4 and Drosophila melanogaster DmCLIC., *Proteins. 71*, 364-378.

[36] Littler, D., Harrop, S., Goodchild, S., Phang, J., Mynott, A., Jiang, L., Valenzuela, S., Mazzanti, M., Brown, L., Breit, S., and Curmi, P. (2010) The enigma of the CLIC proteins: Ion channels, redox proteins, enzymes, scaffolding proteins?, *FEBS Lett. 584*, 2093-2101.

Chapter 6

A conserved GXXXG motif in the transmembrane domain may serve as the Cholesterol-Binding motif for the CLIC1 proteins

Chapter 6

A conserved GXXXG motif in the transmembrane domain may serve as the Cholesterol-Binding motif for the CLIC1 proteins

6.1 Introduction

The crucial role of cholesterol in facilitating the structural rearrangements of proteins upon association with the lipid bilayer has been well documented and has been a subject of intense investigation [1-6]. The detailed mechanism underlying the effect of membrane cholesterol on the structure and function of integral membrane proteins is still not clear and appears to be complex [7-9]. Cholesterol has been reported to modulate conformation and hence the function of integral membrane proteins either through a specific and localised (direct) interaction [10, 11] or indirectly, by altering the membrane physical properties in which the protein is embedded [12-14]. Yet another possibility could be a combination of both. One particular proposed model is based on the concept that there exist specific amino acid segments or motifs that facilitate direct interactions of proteins with membrane cholesterol [15, 16]. A variety of such cholesterol-binding motifs have now been identified that facilitate specific and localised interactions between the protein and cholesterol molecules [3, 11].

For example, the CRAC motif (Cholesterol Recognition/interaction Amino acid Consensus) found in several proteins, including the scaffolding proteins, flotillin and caveolins [17, 18], ATP-binding cassette (ABC) transporters [19], the G-protein coupled receptor (GPCRs) family [20] etc., has been shown to facilitate direct binding of these proteins with cholesterol. Moreover, several viral proteins like the HIV gp41 [21] and more importantly influenza M2 protein [22] were reported to bind cholesterol via the CRAC motif. This motif is usually located near the transmembrane helix and is represented by the amino acid sequence L/VXXXXXR/K or YXXXXXR/K, where the X represents any amino acid [3, 23]. As the basic amino acid needs to be located at the lipid-water interface, proteins exhibiting the CRAC motif usually interact with the inner leaflet of the membrane. Another cholesterol-binding domain, the CARC motif, which is the opposite orientation of the CRAC motif, so far only described for the human nicotinic acetylcholine receptor (nAChR), is located in proteins binding

cholesterol at the outer leaflet of the membrane [24]. A different kind of cholesterol-binding motif was reported for the amyloid precursor protein (APP) [11]. Studies by the group of Charles Sanders revealed a GXXXG motif to be involved in cholesterol binding [1, 9]. NMR studies of the 99 residues comprising the C-terminal domain (C99) of the APP protein have demonstrated cholesterol binding. To further investigate the amino acids being involved in cholesterol binding, they performed NMR studies with mutants of C99 [11]. Although they did not publish a high-resolution structure, they have shown that the GXXXG motif in APP protein acts as the cholesterol-binding site that enables interaction with cholesterol [11] and such an interaction then facilitates conformational changes in the N-loop of the protein [25].

Apart from being a cholesterol-binding motif, this GXXXG motif (or GXXXG-like motif where the glycine (Gly) residues are substituted by alanine or serine) has also been shown to mediate interactions of transmembrane helices within the membrane [26-28]. Hence the GXXXG motif was also considered important for the homo and hetero-oligomerisation of numerous membrane proteins such as the Glycophorin A [28], ErbB family [29], members of growth factor receptor tyrosine kinases; the multispan membrane protein APH-1 [30] and several others. So far, Langmuir film experiments and reflectivity data, reported in this thesis, have clearly shown that cholesterol acts as the binding molecule used by CLIC1 for its initial docking onto the membrane and upon interaction, facilitates conformational changes in the N-terminal domain of CLIC1 that allows for the insertion of the protein into the hydrophobic core of the membrane. Investigations of amino acid sequence alignments have shown CLIC1 also contains the GXXXG motif (amino acid sequence $G^{18}AKIG^{22}$) near the putative transmembrane domain that is also highly conserved amongst all the human CLIC proteins as well as in the invertebrate CLIC1-like protein (*Dm*CLIC) as shown in Figure 6.1. Whether the GXXXG motif in CLIC proteins acts as the cholesterol-binding motif or facilitates the homo or hetero-oligomerisation of the protein within the membrane in order to form functional ion channels was unclear.

In this thesis, we hypothesise that this GXXXG motif may act as the cholesterol-binding site in the CLIC proteins. In order to determine the importance of the

GXXXG motif for the interaction of CLIC1 with cholesterol, we have performed site-directed mutagenesis to individually substitute the glycine residues at positions 18 and 22 of CLIC1 to alanine in order to produce the following CLIC1 mutants: G18A and G22A. This chapter reports the Langmuir film experiments that were performed to study the spontaneous membrane insertion of these CLIC1 mutants into phospholipid monolayers containing cholesterol. The Langmuir data of the G18A and G22A CLIC1 mutants show that the GXXXG motif in CLIC1 acts as the cholesterol-binding site for the initial recognition and interaction of the protein with cholesterol.

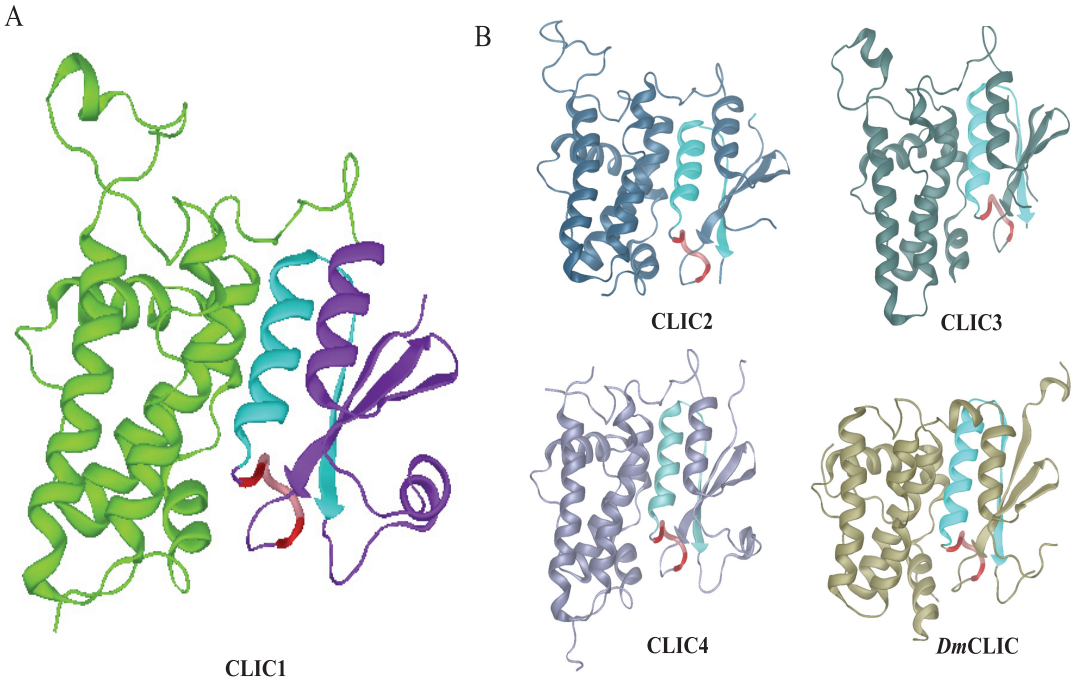

Figure 6.1 Schematic diagrams of reduced CLIC proteins in ribbon showing the putative transmembrane region and the GXXXG motif. (A) The N-and C-domains of CLIC1 are shown in purple and green respectively. The putative transmembrane region (TMR) comprising the α1 helix and the β2 strand, located in the N-terminal domain is shown in blue. The GXXXG motif is shown in red. The PDB code was 1k0m. **(B)** Schematic diagrams of reduced CLIC2, CLIC3, CLIC4 and *Dm*CLIC proteins with the TMR shown in blue and the GXXXG motif shown in red. The PDB codes were CLIC2 (PDB: 2R4V), CLIC3 (PDB: 3FY7), CLIC4 (PDB: 2AHE) and *Dm*CLIC (PDB: 2YV7).

6.2 Materials and Method

The cDNA encoding the wild-type His-CLIC1fusion protein, cloned into the pET-28a vector was used to generate point mutations in CLIC1 using the QuikChange™ site-directed mutagenesis kit purchased from Stratagen (La Jolla, USA). The oligonucleotide primers were synthesised by Sigma Aldrich (Australia). All sequencing reactions were done by Macrogen Inc. (Seoul, Korea). The *Escherichia coli* XL1-Blue super-competent cells came with the QuikChange™ site-directed mutagenesis kit purchased from Stratagen (La Jolla, USA) and the *Escherichia coli* BL21 (DE3) pLysS super-competent cells were purchased from New England Biolabs® Inc. (Ipswich, MA). The plasmid DNA QIAprep® Spin Miniprep Kit was purchased from QIAGEN (Australia). 1-palmitoyl-2-oleoyl-*sn*-glycero-3-phosphatidylcholine (POPC), used in Langmuir experiments was purchased from Avanti Polar Lipids (Alabaster, USA) and used as received. Cholesterol, Isopropyl-thio-β-D-galactopyranoside (IPTG), Dithiothreitol (DTT), *tris*-2-carboxyethyl-phosphine (TCEP) and thrombin from bovine plasma were purchased from Sigma Aldrich. All other reagents used were of analytical grade.

6.2.1 Site-directed mutagenesis using polymerase chain reaction (PCR)

In vitro site-directed mutagenesis is a widely use technique which was first introduced in the 1970s to study protein structure-function relationships and gene expression, and for carrying out vector modifications [31]. The QuikChange™ site-directed mutagenesis kit (Stratagen) is used to make point mutations, switch amino acids, and delete or insert single or multiple amino acids in the target vector of choice. In this thesis, site-directed mutagenesis was used to generate eleven different CLIC1 mutants: G18A, G22A, K13A, N23A, F26A, R29A, K37A, D76A, N78A, F111A and Y233A, in which a single amino acid at different positions of the CLIC1 protein was substituted to alanine as shown in Figure 6.2. Most of the amino acids mutated are conserved in all vertebrate CLICs and mutation of some of these amino acids have shown to produce inactive CLIC4 [32]. In addition, the amino acids were also mutated based on their importance in different functional activities of the protein. The glycine residues at position 18 and 22 (G18 and G22) forms part of the GXXXG motif and hence was

substituted to alanine to determine the role of this motif. The amino acids lysine (K13), phenylalanine (F26) and aspartic acid (D76) have been shown to bind GSH and are considered important for the enzymatic activity of CLIC1. R29A and K37A have been shown to be important for the ion channel activity of the protein [33] while the others were considered structurally important. Before the site directed mutagenesis reaction could be carried out, it was necessary to design the appropriate mutagenic oligonucleotide primers for each of the CLIC1 mutants. This designed primer then determined the efficiency of the reaction because a 100 % base pairing at either end of the target sequence was necessary to successfully generate the CLIC1 mutants [31].

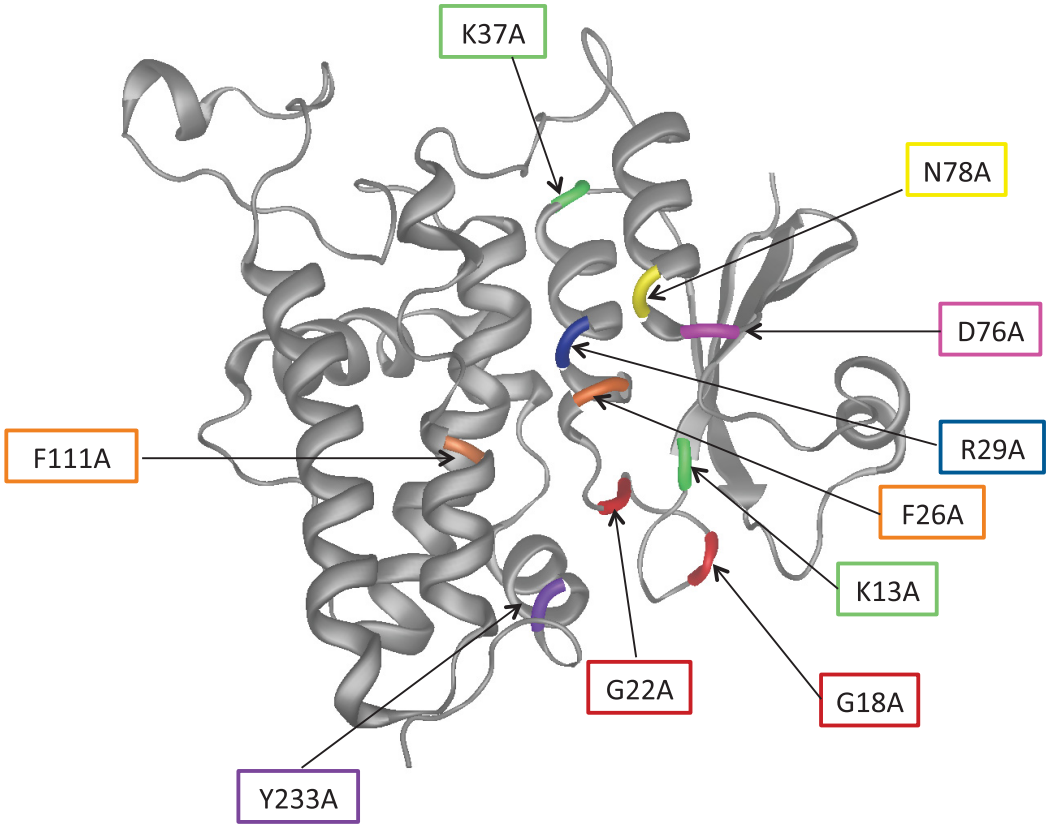

Figure 6.2 Schematic diagram of reduced CLIC1 showing the positions of the different amino acids that were mutated to alanine. The glycine (G) residues are shown in red, lysine (K) in green, phenylalanine (F) in orange, arginine (R) in blue, aspartic acid (D) in pink, asparagine (N) in yellow and tyrosine (Y) in purple.

Table 6.1 Sequences of the Oligonucleotides

CLIC1_Mutant	Primers	Oligonucleotides
G18A	Forward (FW)	5′-GCTGGCAGTGATGCGGCCAAGATTGGG-3′
	Reverse (RV)	5′-CCCAATCTTGGCCGCATCACTGCCAGC-3′
G22A	Forward (FW)	5′-GGGGCCAAGATTGCGAACTGCCCATTC-3′
	Reverse (RV)	5′-GAATGGGCAGTTCGCAATCTTGGCCCC-3′
K13A	Forward (FW)	5′-GGTCGAATTGTTCGTGGCGGCTGGCAGTGATGG-3′
	Reverse (RV)	5′-CCATCACTGCCAGCCGCCACGAACAATTCGACC-3′
N23A	Forward (FW)	5′-GGCCAAGATTGGGGCCTGCCCATTCTCCCAG-3′
	Reverse (RV)	5′-CTGGGAGAATGGGCAGGCCCCAATCTTGGCC-3′
F26A	Forward (FW)	5′-GGGAACTGCCCAGCCTCCCAGAGACTGTTC-3′
	Reverse (RV)	5′-GAACAGTCTCTGGGAGGCTGGGCAGTTCCC-3′
R29A	Forward (FW)	5′-CCCATTCTCCCAGGCACTGTTCATGGTACTGTGG-3′
	Reverse (RV)	5′-CCACAGTACCATGAACAGTGCCTGGGAGAATGGG-3′
K37A	Forward (FW)	5′-GGTACTGTGGCTCGCGGGAGTCACCTTCAATG-3′
	Reverse (RV)	5′-CATTGAAGGTGACTCCCGCGAGCCACAGTACC-3′
D76A	Forward (FW)	5′-GCACTGAAGTGCACACAGCCACCAACAAGATTG-3′
	Reverse (RV)	5′-CAATCTTGTTGGTGGCTGTGTGCACTTCAGTGC-3′
N78A	Forward (FW)	5′-GTGCACACAGACACCGCCAAGATTGAGGAATTTCTGG-3′
	Reverse (RV)	5′-CCAGAAATTCCTCAATCTTGGCGGTGTCTGTGTGCAC-3′
F111A	Forward (FW)	5′-CACAGCTGGGCTGGACATAGCGGCCAAATTTTCTGCC-3′
	Reverse (RV)	5′-GGCAGAAAATTTGGCCGCTATGTCCAGCCCAGCTGTG-3′
Y233A	Forward (FW)	5′-GAGATCGAGCTCGCCGCGGAGCAAGTGGCAAAGG-3′
	Reverse (RV)	5′-CCTTTGCCACTTGCTCCGCGGCGAGCTCGATCTC-3′

The underline nucleotides represent the mutation that generates the subsequent amino acid to Alanine substitution. The abbreviated letters representing the amino acids are as follows: G-Glycine, K-Lysine, N-Asparagine, F-Phenylalanine, R-Arginine, D-Aspartic Acid and Y-Tyrosine.

6.2.1.1 Oligonucleotide primer design

The oligonucleotide primers used to generate point mutations in CLIC1-wt were designed using PrimerX online software tool (http://www.bioinformatics.orf/primerx) and analysed using the computer software package Gene Runner v3.04. After designing and analysing the targeted mutagenic oligonucleotides, using both the CLIC1 sequence part to be mutated (NCBI Reference Sequence: NM_001288.4) and the matching sequence on the plasmid vector, the oligonucleotides were obtained from Sigma Aldrich (Australia). The sequences of the oligonucleotides are presented in Table 6.1.

6.2.1.2 Purification of CLIC1-pET-28a plasmid

The pET-28a vector containing the gene for human CLIC1 (NP_001279) at the *Nde I* and *Not I* cloning sites was ideal for introducing point mutations because not only the resulting expression construct consisted of an N-terminal 6x His-tag and thrombin cleavage site, followed by the complete CLIC1 coding sequence, but also consisted of a lac operon coding sequence which helped enhance the concentration of the protein during expression of both CLIC1 wild-type and mutant proteins [33, 34]. Glycerol stocks of *Escherichia coli* BL21 (DE3) transformed with the CLIC1-pET-28a plasmid were spread onto sterile LB-Kanamycin agar plates and incubated overnight at 37 °C. A single colony was collected from the transformants and added to 100 ml of sterile 2 x YT media containing kanamycin (30 μg/ml) and incubated overnight (~16 hours) at 37 °C with shaking at 200 rpm. This overnight culture was then used for small-scale plasmid DNA purification following the instructions of a commercially available QIAprep® Spin Miniprep Kit from QIAGEN. Briefly, the procedure used alkali and detergent (NaOH-SDS) treatment in the presence of RNase A to lyse the bacterial cells and denature chromosomal DNA and proteins. Subsequently, the lysate was neutralised using potassium acetate to precipitate the denatured proteins, chromosomal DNA, cellular debris and SDS for successful removal by centrifugation. The CLIC1-pET-28a plasmid DNA, which was not denatured, bound to a silica matrix and was washed and eluted with autoclaved, deionised water. The purified plasmid was then quantified using a NanoDrop ND-1000 spectrophotometer. Point mutations were individually introduced by thermal

cycling quick change PCR base site-directed mutagenesis technique using the CLIC1-pET-28a vector as the target plasmid.

6.2.1.3 Polymerase chain reaction (PCR)

The QuikChange™ site-directed mutagenesis method allowed for DNA amplification using thermostable polymerases for nucleotide incorporation. The thermal cycles caused denaturation of the CLIC1-pET-28a plasmid DNA to form single-stranded regions [35]. The two synthesised mutagenic oligonucleotide primers (forward and reverse), each complementary to opposite strands of the vector, were then annealed to their respective target strand. At this point, pfu Turbo DNA polymerase replicated both plasmid strands with high fidelity, without displacing the mutagenic oligonucleotide primers [35]. In other words, both oligonucleotide primer strands, during the thermal cycles, were extended by pfu Turbo DNA polymerase in a circular manner, therefore; generating a mutant-CLIC1-pET-28a plasmid containing staggered nicks [35]. The PCR reaction used to generate the mutant plasmid was carried out according to the kit instructions in a Mastercycler Gradient PCR Machine (Eppendorf, USA) using the following program as shown in Table 6.2. The lyophilised forward and reverse primers were dissolved in autoclaved deionised water to a concentration of 100 μM and diluted to working concentrations of 100 ng/μl each. Following PCR, the product was treated with *Dpn I* at 37°C for an hour. The *Dpn I* endonuclease is specific for methylated DNA. The parental DNA template (CLIC1-pET-28a) being isolated from E. coli cells is methylated and therefore was susceptible to *Dpn I* digestion. On the other hand, the mutated vector DNA being non-methylated was not digested by *Dpn I* and was available for transformation into *E.coli* XL1-Blue super-competent cells.

Table 6.2 PCR reaction mixture and PCR program for site-directed mutagenesis of CLIC1-pET28a plasmid DNA.

PCR Reaction Mixture		PCR Program		
Component	**Amount**	**Cycles**	**Temp (°C)**	**Time**
10x Reaction Buffer (kit)	5 µL	1	95	30 sec
dsDNA template plasmid	115 ng	18	95	30 sec
dNTP mix (kit)	1.2 µL		55	1 min
Fwd primer (100 ng/uL)	140 ng		68	10.5 min
Rev primer (100 ng/uL)	140 ng			
Autoclaved dH_2O:	to 50 µL			
Pfu Turbo enzyme (kit)	1 µL			

6.2.1.4 Transformation into E.coli XL1-Blue super-competent cells

The resulting mutant-CLIC1 plasmid vectors were propagated by transformation into *E.coli* XL1-Blue super-competent cells. The XL1-blue strain of *E.coli* is resistant to tetracycline and contains mutations that render the bacteria endonuclease and recombinant deficient (Stratagen.com). These features allow the mutant-CLIC1-pET-28a plasmids to be methylated without being incorporated into the *E.coli* genome resulting in more stable and higher quality plasmids. With the aim to introduce the mutated pET-28a plasmid DNA into *E.coli* cells, heat shock transformation was applied as previously described by Froger *et al.* (2007) [36]. Although the exact mechanism of heat shock is unclear, it is believed that the increased temperature puts the cells under stress, resulting in the creation of micro-pores in the plasma membrane through which the cells can take up the plasmids [37]. Approximately, 2 µl of the PCR product of mutant plasmid DNA was added to a 50 µl freshly thawed aliquot of *E.coli* XL1-Blue super-competent cells and placed on ice for 30 min, heat-shocked at 42 °C for 45 seconds and returned to the ice for a further 2 minutes. Thereafter, 1 ml of NZY^+ media (10 g NZ amine, 5 g yeast extract, 5 g NaCl in 1 litre of H_2O, before use add supplements: 12.5 ml of 1M $MgCl_2$, 12.5 ml of 1M $MgSO_4$ and 20 ml of 2M glucose) was added and the cells were incubated at 37 °C for 60 minutes to allow cellular growth and stabilisation. Cells were then spread onto LB-Kanamycin agar plates

and incubated at 37 °C overnight. A single colony was selected and cultured overnight at 37 °C in 100 ml 2x YT media. The CLIC1 mutant plasmids were then isolated using the QIAprep® Spin Miniprep kit (QIAGEN) by methods described in section 6.2.1.2 and sent for DNA sequencing.

6.2.1.5 DNA sequencing

CLIC1 cDNA, which encoded the following eleven different CLIC1 mutants: G18A, G22A, K13A, N23A, F26A, R29A, K37A, D76A, N78A, F111A and Y233A, were sequenced to confirm the incorporation of the correct mutations into the CLIC1-pET-28a plasmid. DNA sequencing was also done in order to confirm the absence of other non-specific mutations that may have generated during the PCR reactions. The mutant-CLIC1-pET-28a plasmids were sent to Macrogen Inc. (Seoul, Korea) for sequencing. The alignments of sequences between the wild type and mutant CLIC1 proteins were performed using the program Clustalw 1.8. Following the conformation of the correct point mutation, each plasmid encoding a particular mutant-CLIC1 was used to transform *Escherichia coli* BL21 (DE3) pLysS super-competent cells.

6.2.1.6 Transformation into E.coli BL21 (DE3) pLysS super-competent cells

Transformation of *E.coli* BL21 (DE3) pLysS cells (New England Biolabs® Inc, MA) with the mutant-CLIC1-pET-28a vector was performed using the heat shock method described above. A control pUC19 DNA was used to check for contamination. 50 µl competent BL21 (DE3) pLysS cells were thawed on ice for 10 minutes. One hundred ng of double–stranded DNA was added to the cells and the reaction mixture stored on ice for 30 minutes. The cells were heat-shocked for 45 seconds at 42 °C and then immediately placed on ice for 2 minutes. 950 µl of 37 °C SOC medium (2% (w/v) tryptone, 0.5% (w/v) yeast extract, 10mM NaCl, 2.5mM KCl, 10mM $MgCl_2$, 10mM $MgSO_4$ and 20mM glucose) was added to the reaction mixture, and the cells were incubated on a shaking incubator at 37 °C for 90 minutes. Stock and concentrated samples were then spread onto LB-Kanamycin agar plates. For the stock sample, 100 µl of the reaction mixture was plated. For the concentrated sample, the remaining 900 µl cells were centrifuged at 12 000 rpm in an Eppendorf MiniSpin for one minute, 800 µl of the supernatant was discarded and the cells resuspended in the remaining 100 µl SOC medium.

The resuspended cells were then plated onto LB-Kanamycin agar plates, and incubated overnight (~ 16 hours) at 37 °C. The mutant-CLIC1 agar plates were then subsequently used to prepare glycerol stocks for each of the respective mutants.

6.2.1.7 Preparation of CLIC1-mutant Glycerol Stocks

Glycerol stock of *E.coli* BL21 (DE3) pLysS transformed with the His-tagged mutant-CLIC1-pET-28a vector was prepared by inoculating 50 mL of 2x YT medium (containing 30 μg/mL Kan) with a single colony of the transformed bacteria from its respective LB-Kanamycin agar plate. The bacterial cells were incubated at 37 ºC with 200 rpm shaking until a mid-exponential growth phase (OD_{600} = 0.6) was achieved. 60% (v/v) final concentration of sterile glycerol was added, and the cells were aliquoted into sterile 2 ml cryo-tubes, and stored at -80 ºC.

6.2.2 Over-expression and Purification of CLIC1 mutants: G18A and G22A

Since the main focus of this study was to determine the importance of the GXXXG motif for the interaction of CLIC1 with cholesterol, only the G18A and G22A CLIC1 mutants were over-expressed and purified, while due to time constraint it was not possible to purify the other mutants for functional characterisation. Over-expression and purification of G18A and G22A CLIC1 mutants were performed using the protocol previously described for CLIC1-wt in Chapter 3, Section 3.2; with the exception that CLIC1 mutants were over-expressed in 4 litres of 2x YT media instead of the 2 litres used for CLIC1-wt over-expression. Briefly, glycerol stock of cells containing the cDNA of the respective G18A or G22A-CLIC1 were used to inoculate 400 ml of 2x YT media containing 30 μg/mL Kan and the cells incubated overnight at 37 ºC with 200 rpm shaking. This overnight culture was added to fresh 2x YT media containing Kan (30 μg/mL), incubated at 37 ºC to reach an OD_{600nm} of 0.6 - 0.8 followed by subsequent IPTG (1 mM) induction. The cells were left overnight for further growth at 20 °C with shaking at 180 rpm to achieve optimum CLIC1 mutant over-expression.

The cells were then harvested by centrifugation in a CR22GIII High Speed Refrigerated Centrifuge (Hitachi) (at 6200 rpm, 30 minutes at 6°C). The resulting pellet was resuspended in Lysis buffer and the cells were mechanically lysed on ice by sonication for 3 x 30 seconds pulsed (intensity 3, pulse 0.5 sec) using a Vibra^{M} Cell sonicator (Sonics and Materials Inc.). The crude lysate was centrifuged to collect the supernatant at 12,000 rpm for 45 minutes at 6°C, which was then filtered to eliminate any remaining cell debris, and loaded onto a Ni-NTA column pre-equilibrated with Binding buffer at pH 8. The soluble His-tagged G18A or G22A CLIC1 in the supernatant was isolated as the protein bound via the His-tag to the Ni-NTA resin while the rest of the unwanted protein solution passes through the column. The column was then subsequently washed to remove any impurities and the desired mutant-CLIC1 eluted as previously described in Chapter 3, Section 3.2.2.1.

Thereafter, bovine plasma thrombin (50 units per litre of cell culture) was added to the eluted His-G18A or G22A CLIC1 and digestion was allowed to occur on a rotor for 16 hours at 4°C resulting in the cleavage of mutant-CLIC1 from 6x Histidine tag. The G18A and G22A CLIC1 was further purified by SEC, using a Hiprep 16/60 Sephacryl S-100 column (VWR International) connected to the ÄKTA prime plus system. The protocol used for the purification of mutant-CLIC1 proteins by SEC is outlined in details in Chapter 3, Section 3.2.2.2. 1 mM DTT or 0.5 mM TCEP was added to the purified G18A and G22A CLIC1 fractions to prevent oxidative dimerization of the protein [38]. G18A and G22A CLIC1 proteins were aliquoted and stored in the storage buffer (20mM HEPES, 0.1M KCl, 1mM DTT and 1mM NaN_3, pH 6.5) at -80 °C. Bradford protein quantification assay and SDS-PAGE analysis (described in Chapter 3) were then conducted to determine mutant-CLIC1 protein concentration and purity respectively.

6.2.3 Circular Dichroism Spectroscopy

Circular Dichroism (CD) is an excellent method for rapidly evaluating the secondary structure, folding and binding properties of protein [39, 40]. CD spectroscopy is a technique that is based on the fact that when molecules are exposed to left and right-handed circularly polarized light, they interact with the

light in different ways. Circularly polarized light exists in two non-superimposable forms that are mirror images of one another, therefore making the light chiral in nature [39, 40]. Since most biological molecules display chirality, they are able to differentiate between the two chiral forms of light. CD spectroscopy takes advantage of this unique property and measures the differential absorption of the left and right-handed circularly polarized light by optically active chromophores [39]. The relevant optically active chromophores in proteins are the peptide backbone, disulphide groups and aromatic residues [41, 42]. In this study, far-UV-CD was employed for the characterisation of the secondary structure of the wild-type, G18A and G22A CLIC1 proteins. The secondary structural conformations of proteins, such as α-helices and β-sheets, present distinct spectral features in the far-UV CD spectrum (250-170) [41, 42]. Proteins with a high α-helical content display characteristic double minima, with broad ellipticities at 208 and 222 nm, as well as an intense positive ellipticity near 190 nm. Because the spectra of proteins are so dependent on their conformations, CD can be used to estimate the structure of the protein under examination and monitor conformational changes due to temperature, mutations, heat, denaturants or binding interactions [41, 42].

CD measurements of 2 μM wild-type, G18A and G22A CLIC1 proteins were undertaken on a Jasco J-810 spectropolarimeter at 20 °C. The spectropolarimeter was constantly flushed with nitrogen and data was acquired using the Spectra Manager software v. 2.00. All spectra were the result of 10 accumulations recorded at a speed of 50 nm/min. A 1 nm bandwidth and a 0.2-0.5 nm data pitch were used, with a response time of 1 second. All spectra were buffer-corrected, averaged and converted to mean residue ellipticity [θ] (deg.cm^2.dmol^{-1}.residue^{-1}), using the following equation:

$$[\theta] = \frac{100\,\theta}{Cnl} \qquad \text{Eq. 6.1}$$

where θ is the buffer-collected raw ellipticity data (mdeg); *C* is the concentration of proteins (mM), *n* is the number of residues in the protein and *l* is the path length of the cuvette (mm). The number of residues (*n*) in wild-type and mutant-

CLIC1 proteins was 243 and a 2 mm path length (*l*) quartz cuvette was used for all far-UV CD measurements. The presence of the reducing agent, DTT, in the protein samples increased the signal-to-noise ratio during CD measurements. DTT, being optically active, can undergo unequal absorption of the left and right-handed circularly polarized light and as a result interfered with the protein spectra. To mitigate the problem, the protein samples were dialysed and filtered through 0.2 μm filters before the protein spectrums were obtained.

6.2.4 Dialysing DTT from CLIC1-wt and mutant proteins in solution

DTT was removed from the storage buffer containing wild-type, G18A and G22A CLIC1 proteins by dialysing with large volumes of dialysis KCl/Hepes buffer (5 mM HEPES, 0.5M KCl, and 0.2 mM NaN_3, pH 6.5). Dialysis was carried out using a cellulose dialysis tube (Sigma Aldrich) with a molecular weight cut-off of 7 kDa. Prior to sample dialysis, the dialysis tube was cut to a size dependent on the respective sample volume of 1 ml. Afterwards the membrane was incubated in the dialysis buffer for 1-2 hours prior to sample addition. The tubing was closed at the end by a locking clamp and loaded with 1 ml of the protein solution and closed with a second locking clamp. The sample-filled tubing was first dialysed in 500 ml dialysis buffer, with the buffer changed at least two times. The tube was then placed into a flask containing 1 liter of dialysis buffer and incubated at 4°C overnight with gentle stirring of the buffer. Following dialysis, protein concentration was determined using the Bradford protein quantification assay to ensure no loss of the protein occurred during the dialysis process.

6.2.5 Functional analysis of G18A and G22A CLIC1 mutants

In order to determine the structural and functional effects of mutating the glycine residues in position 18 and 22 in CLIC1 protein, enzymatic function of these mutants was measured in the HEDS enzyme assay by methods previously described in Chapter 3, Section 3.2.6. Briefly, 5 μM final concentration of reduced monomeric CLIC1-wt or CLIC1 mutants: G18A and G22A were added into a mixture of 5 mM potassium phosphate buffer (pH 7), 1 mM EDTA, 250 μM NADPH, 50 nM GR and 1 mM HEDS. 5 μM of HcTrx-5 (IS5) protein was used as the positive control. The mixtures containing the protein samples were

incubated for 5 minutes at 37 ºC. The reaction was then initiated by the addition of 1mM GSH and the consumption of NADPH was monitored at A_{340nm}.

6.2.6 Spontaneous membrane insertion of G18A and G22A CLIC1 mutants

To assess the spontaneous membrane insertion ability of the G18A and G22A CLIC1 mutants, Langmuir monolayer film experiments were conducted and their results compared to that of the wild-type, C24A and C59A CLIC1 mutant proteins. Langmuir experiments were performed as previously described in Chapter 3, Section 3.3. A POPC:Chol monolayer (5:1 mole ratio) was spread onto a 25ml KCl/Hepes buffer (pH 6.5) subphase in a Nima Technologies 601 Langmuir trough. The barrier then symmetrically compressed the monolayer at 20 cm^2/min to a target pressure (π) of 20 mN/m. Recombinant wild-type, G18A, G22A, C24A or C59A CLIC1 proteins were then injected into the subphase underneath the lipid monolayer to achieve a final protein concentration of 2 µg/ml. The data is represented as percentage surface area expansion $\Delta A = [(A-Ai)/Ai]*100$, where A is the surface area at time t and Ai is the initial surface area of the monolayer when it reached 20 mN/m. Since the monolayer was kept at a constant π, the barrier expanded as a result of protein insertion and the percentage area expansion was taken as a measure of favourable protein-lipid interactions.

To determine the cholesterol-binding ability of the GXXXG motif, 50 µg of G18A, G22A, C24A and C59A CLIC1 mutants were pre-incubated with 50 µl of the cholesterol stock solution (1 mg/ml in chloroform) in a 200 µl KCl/Hepes buffer (pH 6.5). The chloroform was removed using N_2 gas for duration of 1 hour before the CLIC1 mutant proteins were added. The protein-cholesterol mixture was then incubated for an hour on ice prior to the addition of these pre-incubated protein samples to the corresponding POPC:Chol monolayer held at a constant π of 20 mN/m in the Langmuir trough.

6.3 Results

6.3.1 DNA Sequencing results

DNA sequencing performed by Macrogen Inc. (Seoul, Korea) confirmed the point mutation of the codons for eleven different CLIC1 mutants: G18A, G22A, K13A, N23A, F26A, R29A, K37A, D76A, N78A, F111A and Y233A. The results are described in Table 6.3. The DNA sequence of the mutated CLIC1 proteins were aligned with the original full-length CLIC1 DNA sequence for comparison and confirmation reasons. The table shows the part of the DNA sequences of the CLIC1 mutants aligned with the complementary DNA sequence of CLIC1-wt, with the targeted mutated codons highlighted in red. The codons highlighted in red represent the point mutations that generate the subsequent amino acid substitution to Alanine. The abbreviated letters representing the amino acids are as follows: G-Glycine, K-Lysine, N-Asparagine, F-Phenylalanine, R-Arginine, D-Aspartic Acid and Y-Tyrosine. The site-directed mutagenesis of the CLIC1-pET-28a vector to generate the different CLIC1 mutants was successful as can be seen in Table 6.3, except for the N23A-CLIC1 mutant. Comparison of the DNA sequence of the N23A CLIC1-pET-28a vector with the full length DNA sequence of CLIC1-wt shows that the mutation was unsuccessful, resulting in additional nucleotide mutations in one of the DNA strands (reverse) of the N23A-CLIC1 plasmid. The successfully mutated plasmid vectors were then transformed into *E.coli* BL21 (DE3) pLysS cells for protein over-expression and purification.

Table 6.3: CLUSTAL.W alignment of the DNA Sequences of the eleven different CLIC1-mutants with CLIC1-wt.

Mutant	CLUSTAL.W alignment of nucleotides
CLIC1 G18A_FW	GTTCGTGAAGGCTGGCAGTGAT**GGG**GCCAAGATTGGGAACTGCCCATTCT 79 GTTCGTGAAGGCTGGCAGTGAT**GCG**GCCAAGATTGGGAACTGCCCATTCT 200 **********.**********
CLIC1 G18A_RV	**CCC**ATCACTGCCAGCCTTCACGAACAATTCGACCTGCGGTTGTTCTTCAG 722 **CGC**ATCACTGCCAGCCTTCACGAACAATTCGACCTGCGGTTGTTCTTCAG 800 *.**********
CLIC1 G22A_FW	TTCGTGAAGGCTGGCAGTGATGGGGCCAAGATT**GGG**AACTGCCCATTCTC 80 TTCGTGAAGGCTGGCAGTGATGGGGCCAAGATT**GCG**AACTGCCCATTCTC 200 **********.**********
CLIC1 G22A_RV	CCACAGTACCATGAACAGTCTCTGGGAGAATGGGCAGTT**CCC**AATCTTGG 671 CCACAGTACCATGAACAGTCTCTGGGAGAATGGGCAGTT**CGC**AATCTTGG 750 **********.**********
CLIC1 K13A_FW	TTCGTG**AAG**GCTGGCAGTGATGGGGCCAAGATTGGGAACTGCCCATTCTC 80 TTCGTG**GCG**GCTGGCAGTGATGGGGCCAAGATTGGGAACTGCCCATTCTC 200 ******..**********
CLIC1 K13A_RV	CCCATCACTGCCAGC**CTT**CACGAACAATTCGACCTGCGGTTGTTCTTCAG 722 CCCATCACTGCCAGC**CGC**CACGAACAATTCGACCTGCGGTTGTTCTTCAG 800 **********..**********
CLIC1 N23A_FW	TTCGTGAAGGCTGGCAGTGATGGGGCCAAGATTGGG**AAC**TGCCCATTCTC 80 TTCGTGAAGGCTGGCAGTGATGGGGCCAAGATTGGG**GCC**TGCCCATTCTC 200 **********..**********
CLIC1 N23A_RV	G--GCCCCATCACTGCCAGCCTT-CACGAA-CAATTCGACCT-GCGGTTG 714 GGTGCCCATCCACTGCCAGCCATTCACGAATCAACTCGACCATGAGGATG 800 * ****.: **********:* ****** *** ******: *.**:**
CLIC1 F26A_FW	TTCGTGAAGGCTGGCAGTGATGGGGCCAAGATTGGGAACTGCCCA**TTC**TC 80 TTCGTGAAGGCTGGCAGTGATGGGGCCAAGATTGGGAACTGCCCA**GCC**TC 200 **********..***
CLIC1 F26A_RV	CCACAGTACCATGAACAGTCTCTGGGA**GAA**TGGGCAGTTCCCAATCTTGG 671 CCACAGTACCATGAACAGTCTCTGGGA**GGC**TGGGCAGTTCCCAATCTTGG 750 **********..**********
CLIC1 R29A_FW	CCA**GAG**ACTGTTCATGGTACTGTGGCTCAAGGGAGTCACCTTCAATGTTA 130 CCA**GGC**ACTGTTCATGGTACTGTGGCTCAAGGGAGTCACCTTCAATGTTA 250 ****..**********

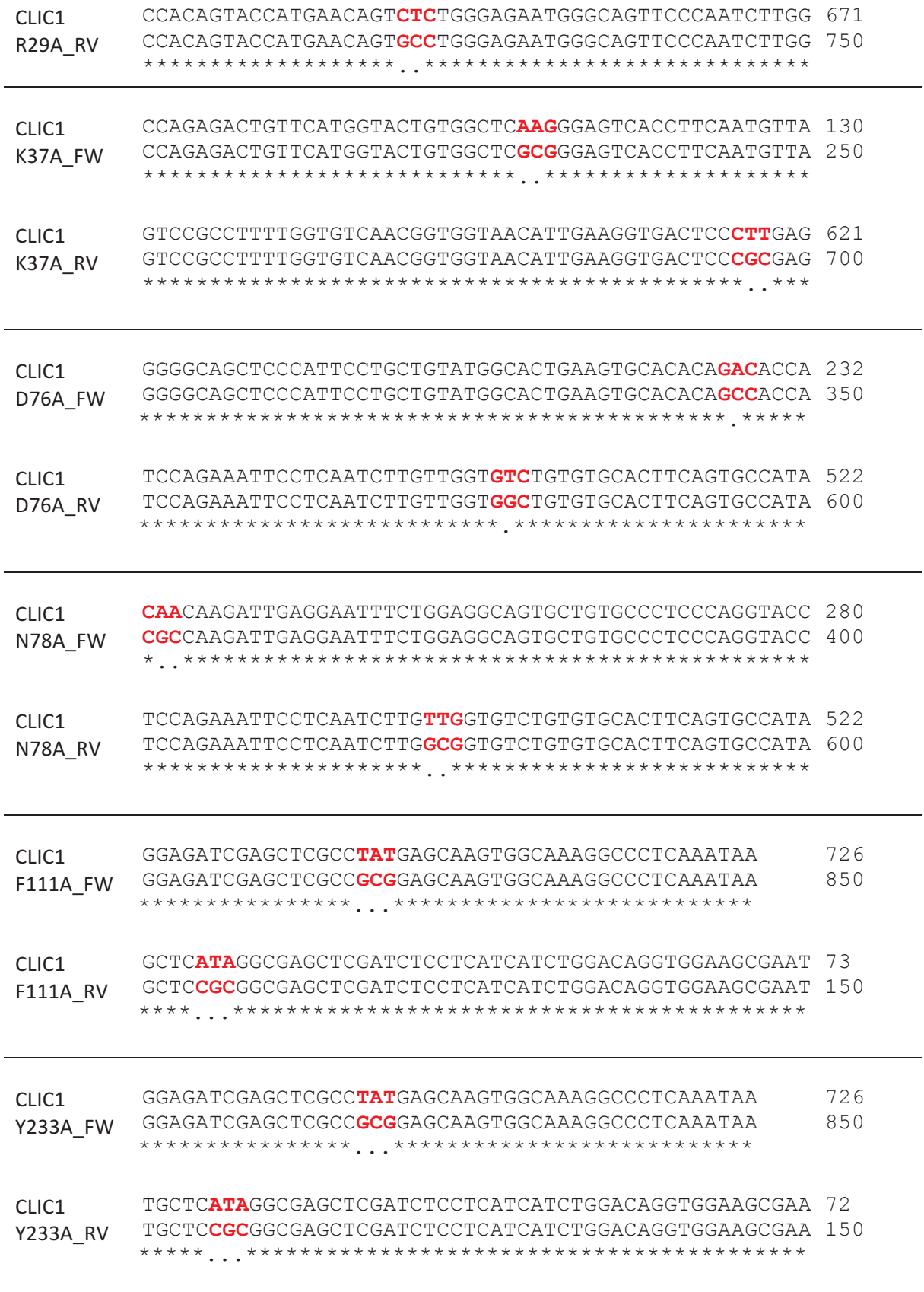

The targeted mutated codons are highlighted in red.

6.3.2 Over-expression and purification of G18A and G22A CLIC1 mutants

Recombinant G18A and G22A CLIC1 mutant proteins were readily purified from *E.coli* cell lysates following expression and two chromatography steps. The over-expression conditions for mutated CLIC1 proteins had been previously determined [33, 34] and the recombinant proteins were over-expressed and purified as described in Section 6.2.2. The initial purification step was performed manually by gravity flow nickel-affinity chromatograph, yielding a protein recovery of approximately 6-8 mg per liter bacterial culture for both the mutant proteins, G18A and G22A, which was comparatively lower than that obtained from CLIC1-wt purification. The purity of the G18A and G22A CLIC1 mutants were assessed by SDS-PAGE (Figure 6.3). As seen in Figure 6.3, the protein bands for all the CLIC1-wt and mutant proteins were found to have a molecular mass of approximately 27 kDa, corresponding to that previously reported [43]. Therefore, it can be concluded that the mutant proteins had been successfully purified. Protein concentration was then determined by Bradford assay for each of the G18A and G22A CLIC1 SEC fractions collected, using the standard BSA concentration graph. The purified protein fractions were aliquoted and stored at -80°C and were subjected to structural and functional analysis.

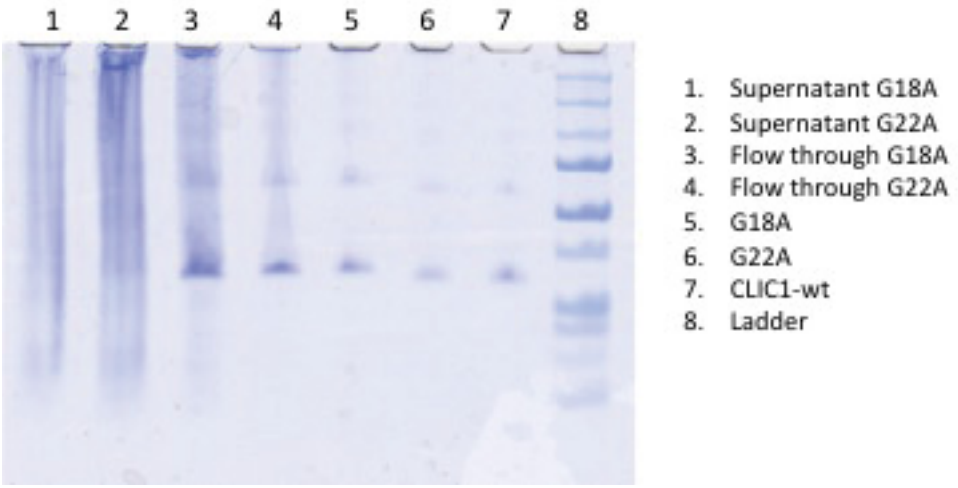

Figure 6.3 SDS-PAGE gel showing a representative G18A and G22A CLIC1 purification. The supernatant of the lysate of G18A and G22A CLIC1 proteins are shown in Lanes 1 and 2 respectively. The flow through off the Ni-NTA column for G18A and G22A CLIC1 are shown in Lane 3 and 4 respectively. Lanes 5 and 6 indicate the SEC fractions of G18A and G22A CLIC1 respectively. The recombinant CLIC1-wt protein band in Lane 7 indicates that the protein bands in Lanes 5-6 correlate to the molecular weight of approximately 27 kDa which is similar to that observed for CLIC1-wt.

6.3.3 Structural analysis of G18A and G22A CLIC1 mutants using Circular Dichroism Spectroscopy

A qualitative estimation of the second structural content of the G18A and G22A CLIC1 mutants were made using the far-UV circular dichroism (CD) at 20 °C and compared to the CD spectra obtained for CLIC1-wt. The far-UV CD spectra of the wild-type and the CLIC1 mutants were recorded over the wavelength range of 190-250 nm and plotted as mean residue ellipticity versus wavelength (Figure 6.4). The CD spectra of the wild-type, G18A and G22A CLIC1 proteins show clear negative troughs at 208 nm and 222 nm, as well as a strong positive peak at around 190 nm, which are characteristic markers of predominantly α-helical proteins [41, 42]. In addition, the deeper 208 nm trough, as seen in Figure 6.3, indicates proteins with α-helical and β-sheet content in different domains, whereas for complete α-helical proteins the peak at 208 nm is less negative than that at 222 nm [41, 42]. The crystal structure of CLIC1 has 10 α-helices and 4 β-strands, in different domains, so the spectra was as expected and matches very closely with the published literature [44, 45]. Since, the three spectra overlay showed no major shift in distribution between alpha and beta sheet content (Figure 6.4), it was concluded that replacing Gly^{18} and Gly^{22} with Alanine did not result in major significant changes to the secondary structure of CLIC1.

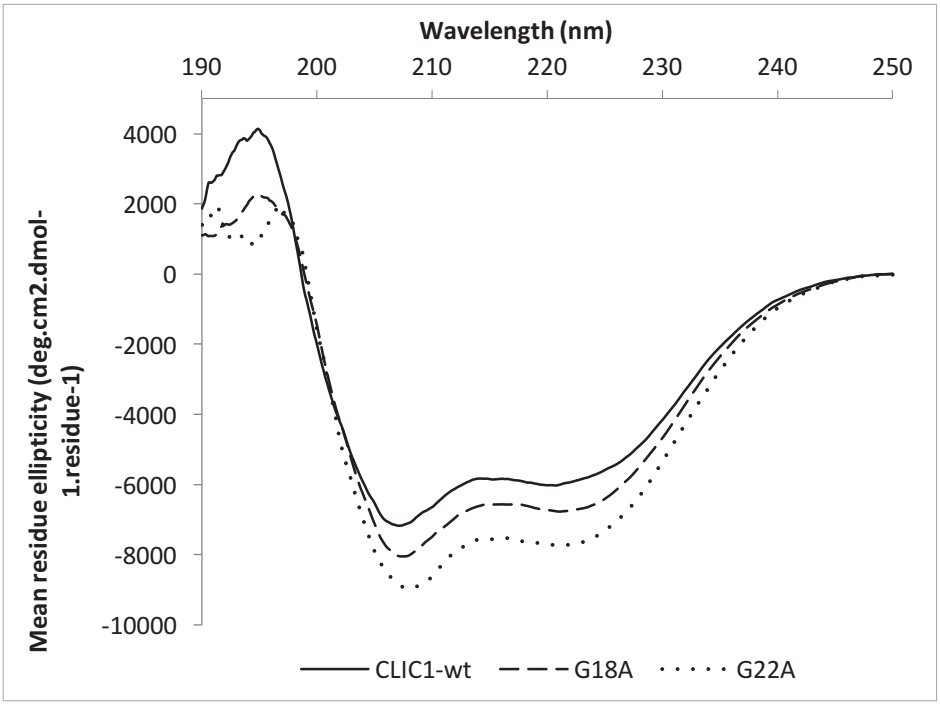

Figure 6.4 Far-UV CD spectra of CLIC1-wt, G18A and G22A CLIC1 proteins. The CLIC1-wt, G18A and G22A spectra show characteristics of a predominantly α-helical protein displaying two troughs; one at 208 nm and one at 222 nm.

6.3.4 Functional activity of G18A and G22A CLIC1 mutants

In order to assess the effect of the point mutations on the protein's enzymatic activity, HEDS enzyme assay was performed using G18A and G22A CLIC1 mutants and their results compared to that of the CLIC1-wt protein. The CLIC1-wt and mutant proteins displayed similar far-UV CD spectra that indicated that the mutations did not cause significant global changes to the CLIC1 protein (Figures 6.4) and hence, was expected to show similar functional activity. The enzymatic activities of the wild-type, G18A and G22A CLIC1 proteins are illustrated in Figure 6.5, with the protein IS5 used as the positive control. The results were an average of at least three individual measurements. Both G18A and G22A CLIC1 mutants were capable of reducing the HEDS substrate in the presence of glutathione reductase (GR), indicating significant enzymatic activity. However, G18A and G22A CLIC1 mutants showed reduced enzymatic activity in comparison to that of CLIC1-wt (Figure 6.5), that warrants further investigation.

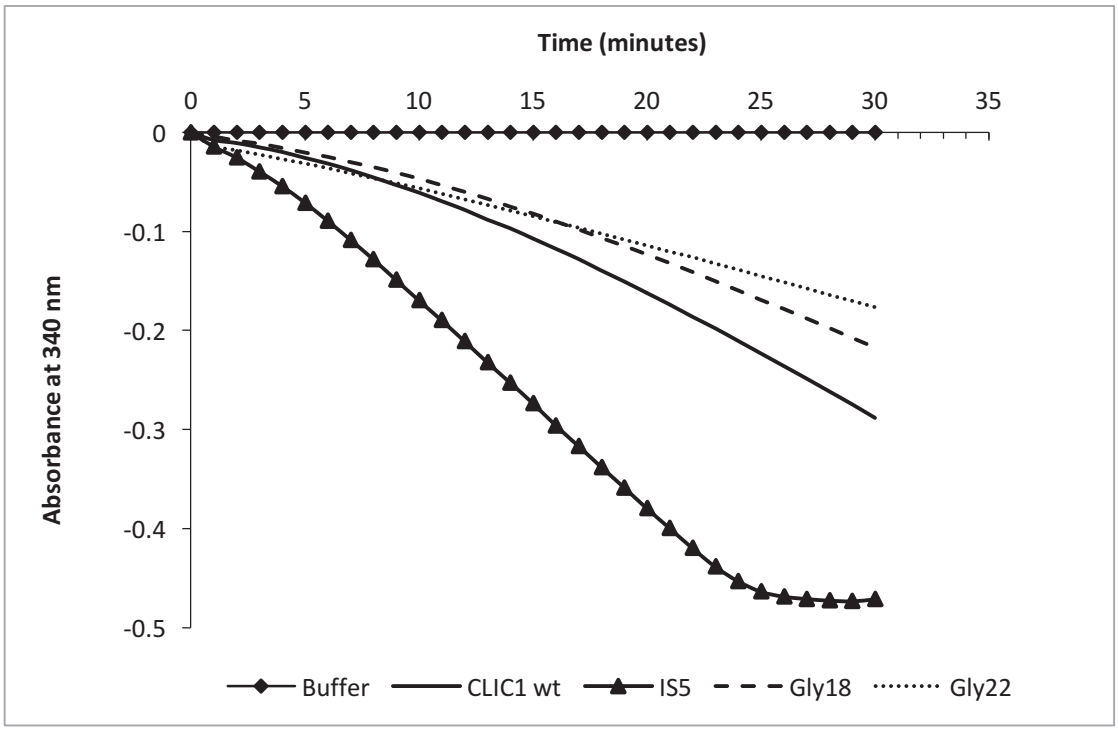

Figure 6.5 Oxidoreductase activity of the G18A and G22A CLIC1 proteins. The CLIC1 mutants G18A and G22A showed similar enzymatic activity as CLIC1 wild-type protein.

6.3.5 Spontaneous membrane insertion of G18A and G22A CLIC1 mutants

To evaluate the spontaneous membrane insertion ability of the G18A and G22A CLIC1 mutants, Langmuir film experiments were performed using POPC:Chol monolayers in a mole ratio of 5:1. The POPC:Chol monolayer was held at a constant pressure of 20 mN/m and the percentage surface area expansion, ΔA, after 3 hours of G18A or G22A CLIC1 injection into the subphase was recorded and compared to the CLIC1-wt interaction with POPC:Chol monolayer. The interaction of the G18A and G22A CLIC1 mutants with the POPC:Chol monolayer is shown in Figure 6.6. Two other CLIC1 mutants: C24A and C59A were used as controls to allow relative comparisons to be made between mutant forms of the protein and wild-type. As such, the aim was to ensure interpretation of the results obtained were assessed based on protein-lipid interactions rather than effects due to the site-directed mutagenesis of the CLIC1 protein itself. Previous studies of C24A and C59A CLIC1 mutants demonstrated that although they maintain the ability to significantly insert into planar bilayer membranes (albeit less so than CLIC1-wt) they failed to form conductive ion channels [46].

Thereby, suggesting that the cysteine residues at positions 24 and 59 are critical pore forming residues but their presence is not an absolute requirement for the membrane binding ability of the protein [46]. Similar results were obtained in our Langmuir experiments (Figure 6.6), where C24A and C59A CLIC1 mutants showed less, but significant membrane insertion into POPC:Chol monolayers (compared to CLIC1-wt) resulting in ΔA values of 9.9 ± 0.34 % and 10.5 ± 0.27 % respectively.

On the other hand, the G18A and G22A CLIC1 mutants resulted in a percentage change in area, ΔA, of only 2.9 ± 0.42 % and 1.94 ± 0.31 % respectively, which was significantly less ($p < 0.01$) than the ΔA value of 18.01 ± 0.73 % observed for CLIC1-wt (Figure 6.6). Our previous results have shown that cholesterol regulates the spontaneous membrane insertion of CLIC1 protein and likely acts as the binding molecule used by CLIC1 for its initial docking onto the membrane [6, 47]. However, the G18A and G22A CLIC1 mutants, even in the presence of cholesterol in the phospholipid monolayer, showed greatly reduced interaction with the monolayer. These findings thereby suggest that substituting the glycine residues at positions 18 or 22 to alanine in CLIC1 significantly reduces the ability of the protein to recognise cholesterol in the membrane, which in turn decreases the initial docking and hence the insertion of the G18A and G22A CLIC1 proteins.

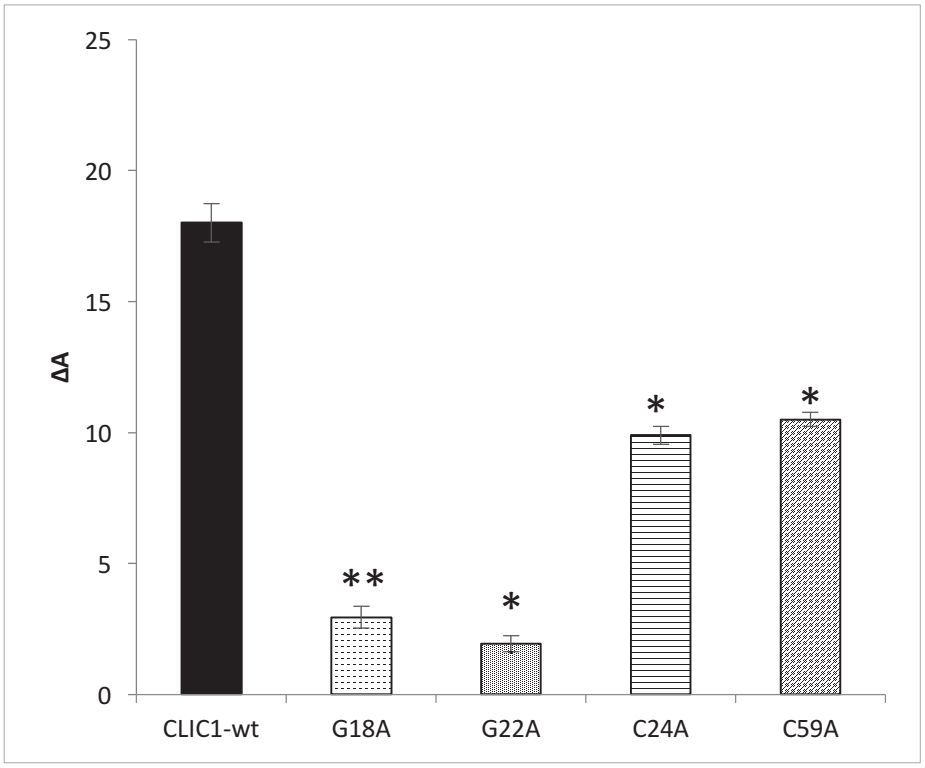

Figure 6.6 CLIC1 wild-type and mutant proteins interaction with POPC:Chol monolayer. The figure shows percentage area expansion profiles of POPC:Chol monolayer after 3 hours following CLIC1-wt, G18A, G22A, C24A and C59A injection into the subphase. Data shown are means ± S.E of at least three independent experiments. The asterisks * and ** correspond to significant ($p < 0.05$ and $p < 0.01$ respectively) difference in the membrane insertion of CLIC1 mutants relative to that of CLIC1-wt. (N=3)

6.3.5 Pre-incubation of G18A and G22A CLIC1 mutants with Cholesterol

To further evaluate the role of the GXXXG motif as the cholesterol-binding site in CLIC1, 50 μg of the following CLIC1 mutants: G18A, G22A, C24A and C59A were pre-incubated with 50 μg of cholesterol for an hour on ice, prior to the addition of these pre-incubated samples to the corresponding POPC:Chol monolayer, held at a constant pressure of 20 mN/m in the Langmuir trough. Figure 6.7 shows the percentage area expansion (ΔA) of the POPC:Chol monolayer after 3 hours following injection of the non-preincubated and pre-incubated CLIC1 mutants: G18A, G22A, C24A and C59A into the subphase.

Previously from the Langmuir data of the pre-incubation of CLIC1-wt with cholesterol presented in Chapter 3, Figure 3.12, we have speculated that pre-

incubation of CLIC1-wt with cholesterol results in the formation of a relatively stable interaction (pre-complex) between the protein and cholesterol in the aqueous subphase, which in turn prevented CLIC1 from inserting into the POPC:Chol monolayer. As seen in Figure 6.7, there were no significant change in the ΔA values of the non-preincubated and pre-incubated G18A and G22A CLIC1 mutants. Pre-incubating G18A with cholesterol resulted in a slightly higher ΔA value of 3.5 ± 0.12 % in comparison to that of the non-incubated G18A CLIC1 protein (ΔA= 2.9 ± 0.42 %). Similarly, G22A pre-incubated with cholesterol also resulted in a greater ΔA value of 3.7 ± 0.09 %. These results strongly suggest that unlike CLIC1-wt, the G18A and G22A CLIC1 mutants do not preferentially interact with the cholesterol molecule in the aqueous subphase, and as a result, the free cholesterol molecules in the subphase, being hydrophobic in nature, likely insert into the monolayer causing the additional increase in area in comparison to that observed for the non-preincubated G18A and G22A CLIC1 mutants.

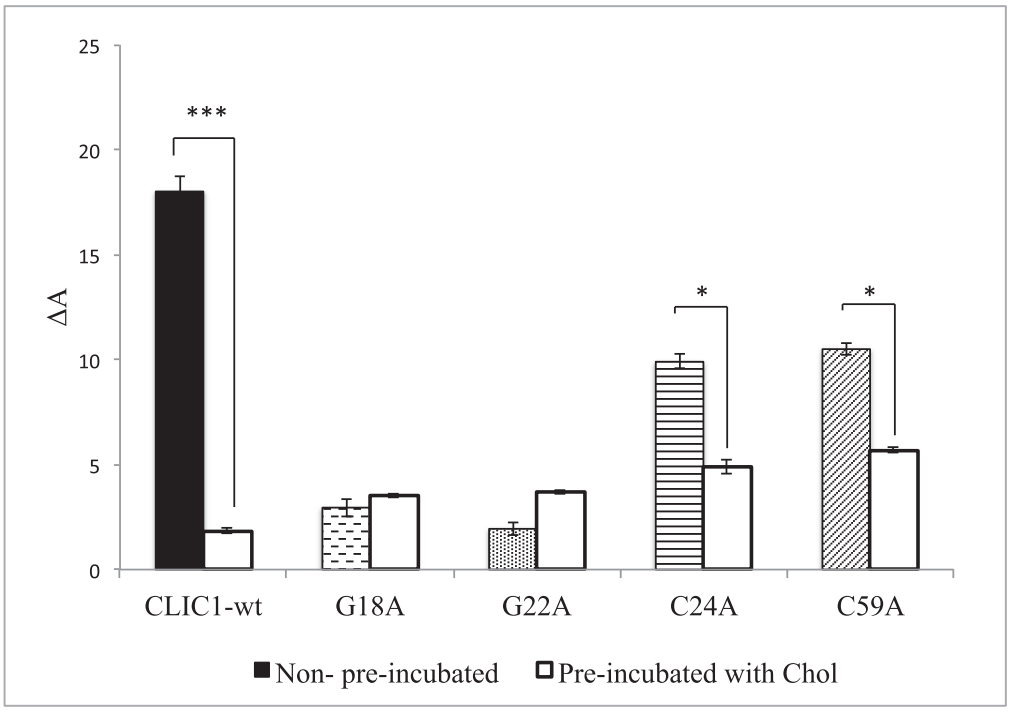

Figure 6.7 Percentage area expansion profiles of POPC:Chol monolayer after 3 hours following injection of non-incubated and pre-incubated CLIC1 wild-type and mutant proteins. Data shown are means ± S.E of at least three independent experiments. The asterisks * and *** correspond to significant ($p < 0.05$ and $p < 0.001$ respectively) difference in the membrane insertion of CLIC1 mutants relative to that of CLIC1-wt. (N= 3)

The critical role of the GXXXG motif was further confirmed by the pre-incubation of the C24A and C59A mutants with cholesterol, which resulted in significantly ($p < 0.05$) reduced ΔA values of 4.9 ± 0.33 % and 5.7 ± 0.16 % respectively. From this result one can propose that the C24A and C59A mutants when pre-incubated with cholesterol interact with the free cholesterol molecules, decreasing the ratio of free to cholesterol bound protein, and thereby reducing its membrane insertion. However, there were clear differences in the ΔA values of these mutants upon pre-incubation with cholesterol in comparison to that observed for pre-incubated CLIC-wt (ΔA= 1.84 ± 0.12 %). A possible reason behind such a difference may be due to the presence of a reduced binding affinity between these cysteine mutants and cholesterol in comparison to CLIC1-wt, which may result in a stronger interaction with cholesterol. Another possibility may be due to the inability of the C24A and C59A mutants to response to redox environment. Redox environment has also been shown to facilitate the spontaneous membrane insertion of CLIC1 into artificial lipid membranes [38, 46, 48, 49]. Studies have shown that upon oxidation, the N-terminal domain of CLIC1 undergoes a reversible structural transition to a stable dimeric form due to the formation of an intramolecular disulphide bond between the Cys^{24} (C24) and Cys^{59} (C59) residues (details mentioned in Chapter 1) and substitution of these cysteine residues in CLIC1 with alanine results in loss of redox sensitivity [38, 46, 48, 49]. Given the fact that in this study CLIC1 interacts with lipid monolayers at the air-water interface, the environment is not completely reducing and some oxidation of the protein may be occurring, which will be absent in the case of C24A and C59A mutants. Whether this accounts for the differences seen between the CLIC1-wt and the C24A or C59A mutants or whether a difference in the binding affinity for cholesterol exists between the CLIC1-wt and mutant proteins demands further investigation that was beyond the scope of this study.

Although there were differences between the cysteine mutants and CLIC1-wt, the C24A and C59A CLIC1 mutants, which also have an intact GXXXG motif within their protein structure, showed reduced but similar protein-cholesterol interaction to that observed for CLIC1-wt. Therefore, it can be speculated that the Gly^{18} and Gly^{22} residues in CLIC1, which form a typical GXXXG motif, seem particularly important for direct binding of CLIC1 to cholesterol.

6.4 Discussion

Impedance spectroscopy studies using tBLMs have shown that the ion channel activity of CLIC1 is cholesterol-dependent and pre-incubation of CLIC1 with cholesterol completely diminished the ion channel activity [6]. The Langmuir results shown in Chapter 3 of this thesis also support this finding, showing that cholesterol regulates the autonomous insertion of CLIC1 into model membranes and pre-incubating CLIC1 with cholesterol likely results in the formation of a CLIC1-cholesterol pre-complex that then prevents the membrane insertion of the pre-incubated protein. The mechanism by which CLIC1 interacts with cholesterol is currently unknown, however we have shown (in Chapter 5) that the 3β-OH group of cholesterol is essential for its interaction with the protein. The focus of this chapter was to investigate the role of the specific amino acid sequence, GXXXG motif within CLIC1, for interaction with cholesterol. In this study, we have mutated the two glycine residues at positions 18 and 22 that form part of the GXXXG motif in CLIC1, and subsequently observed their ability to interact with cholesterol using Langmuir film experiments.

Studies with mutant peptides or proteins are ideally suited for the identification of key residues involved in physiochemical properties of many integral membrane proteins. For example, studies with mutant peptides of the amyloid precursor protein allowed for the identification of the GXXXG motif involved in cholesterol binding and channel formation [11]. However, mutagenesis of specific residues often results in structural alterations or denaturation of the protein and hence poses a considerable challenge. To investigate the effect of point mutants on the structure and function of CLIC1, we have performed CD analysis and HEDS enzyme assay on G18A and G22A CLIC1 mutants and compared their results to that of CLIC1-wt. Expression and purification of recombinant CLIC1 mutants by the method described by Goodchild *et al.* (2011) [34] resulted in effective purification of reduced monomeric G18A and G22A CLIC1 proteins (Figure 6.3). As seen in Figure 6.4, the CD spectra of wild-type, G18A and G22A CLIC1 proteins show characteristics of a predominantly α-helical protein displaying two troughs; one at 208 nm and one at 222 nm. Since, the three spectra overlay with each other, strongly suggest that replacing Gly^{18} and Gly^{22} with alanine did not result in any significant changes to the secondary structure of CLIC1. In addition, the results

from the HEDS enzyme assay as seen in Figure 6.5 confirmed that the purified G18A and G22A CLIC1 mutants are functionally active and provide further reassurance that they have the correct structural conformation.

Previous NMR studies of the C99 residues of the amyloid precursor protein (APP) and C99 mutant peptides incorporated in model membranes containing the cholesterol derivate CHOBIMALT, showed that the APP protein binds to cholesterol via a GXXXG motif [11]. They have shown that the transmembrane domain of the C99, form the structure involved in cholesterol binding, whereby the helix has a bend after the double GXXXG motif. This structure forms a pocket in which cholesterol can be integrated [1, 9, 11]. Herein, we report that substitution of the glycine residues at positions 18 and 22 with alanine significantly impaired the spontaneous membrane binding ability of the protein as seen in Figure 6.6. On the hand, CLIC1-wt and C24A and C59A CLIC1 mutants demonstrated significantly higher membrane interaction with POPC monolayers containing cholesterol. These results strongly suggest that the Gly^{18} and Gly^{22} residues, which form part of the GXXXG motif are essential for the spontaneous membrane insertion of CLIC1 and may likely act as the cholesterol-binding motif for the initial recognition and binding to membrane cholesterol.

Furthermore, pre-incubation of the G18A and G22A CLIC1 with free cholesterol prior to their addition to POPC:Chol monolayer (Figure 6.7) showed no significant change in the interaction between the pre-incubated G18A and G22A CLIC1 with the monolayer in comparison to that of the non-incubated samples. The percentage change in area (ΔA) of the pre-incubated G18A and G22A CLIC1 mutants were found to be slightly greater than that observed for the corresponding non-incubated samples. For G18A there was an increase in the ΔA value from 2.9 ± 0.42 % to 3.5 ± 0.12 % upon pre-incubation with cholesterol, while pre-incubating G22A protein resulted in a ΔA value of 3.7 ± 0.09 % which was greater than the 1.94 ± 0.31 % change in area observed for the non-incubated G22A protein. A possible explanation may be that during pre-incubation, the free cholesterol molecules were unable to bind to the mutant proteins due to the substitution of the glycine residues and hence cholesterol was available to cause perturbation in the POPC:Chol monolayer resulting in the additional increase in the ΔA values. The importance of

the GXXXG motif in binding cholesterol was also highlighted from the fact that like CLIC1-wt, pre-incubation of C24A and C59A CLIC1 mutants showed reduced membrane insertion following the formation of a CLIC1-cholesterol pre-complex. These findings strongly suggest that the G18A and G22A proteins were unable to form a CLIC1-cholesterol pre-complex unlike CLIC1-wt, C24A and C59A proteins which contain an intact GXXXG motif, and hence, this GXXXG motif plays a crucial role in CLIC1 interaction with cholesterol.

Studies with the APP protein have shown that the GXXXG motif creates a flat surface that enables interaction with the flat surface of cholesterol, which is made by Van der Waals forces [11, 25]. In addition, they claim that after interaction of the cholesterol to the GXXXG motif the N-loop undergoes a conformational change that allows for interaction by the formation of a hydrogen bond of the hydroxyl group of cholesterol with an asparagine (N) and a glutamic acid (E) within the loop [11, 25]. Finally, a phenylalanine (F) could form CH-π stacking interactions with the sterol ring, as also shown for the other cholesterol binding motifs like the CRAC/CARC motifs. The CRAC motif is also believed to drive cholesterol binding by specifically reorganizing its –OH moiety [3]. While CLICs do not contain the canonical CRAC sequence, amino acid sequence analysis of all the CLIC proteins, as shown in Figure 6.8, illustrates that its GXXXG motif bears some resemblance, suggesting that CLICs may bind cholesterol through interactions akin to those previously documented for other cholesterol binding proteins.

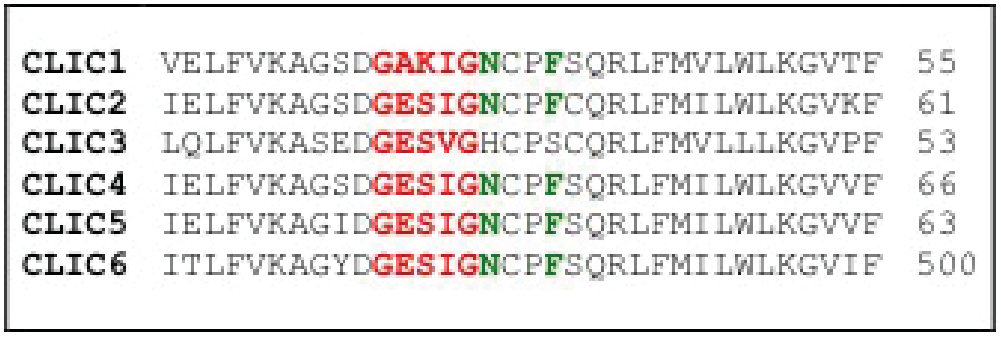

Figure 6.8 Amino Acid Sequence Alignment of Human CLIC proteins showing the GXXXG motif. The GXXXG motif is shown in red and the conserved asparagine (N) and phenylalanine residues shown in green. CLIC1 (accession number: CAG46868.1), CLIC2 (accession number: CAA03948.1), CLIC3 (accession number: NP_004660.2), CLIC4 (accession number: CAG38532.1), CLIC5 (accession number: AAF66928.1), CLIC6 (accession number: NP_444507.1). The alignment was produced using Clustalw.

Apart from the two conserved glycine residues (Gly^{18} and Gly^{22}), all vertebrate CLICs contain a polar serine (Ser), a charged glutamic acid and a hydrophobic residue in the GXXXG motif, with the exception of CLIC1, which has two hydrophobic residues and a charged lysine (Lys) residue instead. There is also a conserved asparagine residue just beside the GXXXG motif in all CLIC proteins at position 23 and a conserved phenylalanine at position 26 except in CLIC3 (Figure 6.8). While the structural details of the CLIC-cholesterol complex await full elucidation, it can be speculated that the GXXXG motif in CLIC1 may bind cholesterol with similar interactions like those observed in APP-cholesterol interaction, with lysine/glutamic acid and asparagine forming a hydrogen bond with the 3β-OH group of cholesterol and the phenylalanine forming CH-π stacking interactions with the sterol ring. However, the question whether cholesterol binds with the same affinity to both CLIC1 monomers and dimers or whether a single cholesterol molecule makes contact with 2 or more CLIC proteins is unclear and warrants further investigation.

6.5 Conclusion

The spontaneous membrane-binding/ insertion ability and hence the ion-channel activity of CLIC1 is critically controlled by membrane cholesterol. Although, Langmuir and impedance spectroscopy studies on CLIC1 interaction with model membranes have confirmed the formation of a relatively stable CLIC1-cholesterol complex [6, 47], the mechanism behind such an interaction is largely unclear. We have identified for the first time a cholesterol-binding motif in CLIC1 and have shown that this GXXXG motif is important for the spontaneous membrane insertion of CLIC1 into model membranes. This study supports the model that the GXXXG motif in CLIC1 acts as the cholesterol-binding site used by the protein for its initial recognition and binding to membrane cholesterol. The GXXXG motif most probably forms a pocket into which cholesterol is integrated and upon interactions stimulates conformational changes in the N-terminal domain of the protein for insertion into the phospholipid bilayer. This is then followed by subsequent oligomerisation/assembly of CLIC1 monomers within the membrane in order to form functional ion channels. Although we speculate that cholesterol may facilitate the quaternary assembly of CLIC1 ion channels within the membrane. Further investigations are required using complimentary techniques such as small angle X-ray scattering (SAXS analysis) in order to determine how cholesterol may affect the oligomerisation/assembly of CLIC1 within model membranes and whether the GXXXG motif is also involved in the homo or hetero-oligomerisation of the protein within the membrane.

6.6 References

[1] Barrett, P., Song, Y., Van Horn, W., Hustedt, E., Schafer, J., Hadziselimovic, A., Beel, A., and Sanders, C. (2012) The amyloid precursor protein has a flexible transmembrane domain and binds cholesterol., *Science 336*, 1168-1171.

[2] Burger, K., Gimpl, G., and Fahrenholz, F. (2000) Regulation of receptor function by cholesterol., *Cell Mol Life Sci. 57*, 1577-1592.

[3] Epand, R. (2006) Cholesterol and the interaction of proteins with membrane domains., *Prog Lipid Res. 45*, 279-294.

[4] Gilbert, R. (2010) Cholesterol-dependent cytolysins., *Adv Exp Med Biol 677*, 56-66.

[5] Pucadyil, T., and Chattopadhyay, A. (2006) Role of cholesterol in the function and organization of G-protein coupled receptors., *Prog Lipid Res. 45*, 295-333.

[6] Valenzuela, S., Alkhamici, H., Brown, L., Almond, O., Goodchild, S., Carne, S., Curmi, P., Holt, S., and Cornell, B. (2013) Regulation of the Membrane Insertion and Conductance Activity of the Metamorphic Chloride Intracellular Channel Protein CLIC1 by Cholesterol, *PLoS ONE 8*, 56948.

[7] Jafurulla, M., Rao, B., Sreedevi, S., Ruysschaert, J., Covey, D., and Chattopadhyay, A. (2014) Stereospecific requirement of cholesterol in the function of the serotonin1A receptor., *Biochim Biophys Acta. 1838*, 158-163.

[8] Paila, Y., and Chattopadhyay, A. (2010) Membrane cholesterol in the function and organization of G-protein coupled receptors., *Subcell Biochem. 51*.

[9] Beel, A., Sakakura, M., Barrett, P., and Sanders, C. (2010) Direct binding of cholesterol to the amyloid precursor protein: An important interaction in lipid-Alzheimer's disease relationships?, *Biochim Biophys Acta. 1801*, 975-982.

[10] Gimpl, G., Burger, K., and Fahrenholz, F. (2002) A closer look at the cholesterol sensor., *Trends Biochem Sci. 27*, 596-599.

[11] Di Scala, C., Chahinian, H., Yahi, N., Garmy, N., and Fantini, J. (2014) Interaction of Alzheimer's β-amyloid peptides with cholesterol: mechanistic insights into amyloid pore formation., *Biochemistry 53*, 4489-4502.

[12] Lee, A. (2004) How lipids affect the activities of integral membrane proteins., *Biochim Biophys Acta. 1666*, 62-87.

[13] Yeagle, P. (1985) Cholesterol and the cell membrane., *Biochim Biophys Acta. 822*, 267-287.

[14] Ohvo-Rekilä, H., Ramstedt, B., Leppimäki, P., and Slotte, J. (2002) Cholesterol interactions with phospholipids in membranes., *Prog Lipid Res. 41*, 66-97.

[15] Epand, R. (2008) Proteins and cholesterol-rich domains., *Biochim Biophys Acta. 1778*, 1576-1582.

[16] Poveda, J., Fernández, A., Encinar, J., and González-Ros, J. (2008) Protein-promoted membrane domains., *Biochim Biophys Acta. 1778*, 1583-1590.

[17] Palmer, M. (2004) Cholesterol and the activity of bacterial toxins., *FEMS Microbiol Lett. 238*, 281-289.

[18] Luetterforst, R., Stang, E., Zorzi, N., Carozzi, A., Way, M., and Parton, R. (1999) Molecular characterization of caveolin association with the Golgi complex: identification of a cis-Golgi targeting domain in the caveolin molecule., *J Cell Biol. 45*, 1443-1459.

[19] Sharpe, L., Rao, G., Jones, P., Glancey, E., Aleidi, S., George, A., Brown, A., and Gelissen, I. (2015) Cholesterol sensing by the ABCG1 lipid transporter: Requirement of a CRAC motif in the final transmembrane domain., *Biochim Biophys Acta. 1851*, 956-964.

[20] Chini, B., and Parenti, M. (2004) G-protein coupled receptors in lipid rafts and caveolae: how, when and why do they go there?, *J Mol Endocrinol. 32*, 325-338.

[21] Vincent, N., Genin, C., and Malvoisin, E. (2002) Identification of a conserved domain of the HIV-1 transmembrane protein gp41 which interacts with cholesteryl groups., *Biochim Biophys Acta. 1567*, 157-164.

[22] Schroeder, C. (2010) Cholesterol-binding viral proteins in virus entry and morphogenesis., *Subcell Biochem. 51*, 77-108.

[23] Li, H., and Papadopoulos, V. (1998) Peripheral-type benzodiazepine receptor function in cholesterol transport. Identification of a putative cholesterol recognition/interaction amino acid sequence and consensus pattern., *Endocrinology 139*, 4991-4997.

[24] Baier, C., Fantini, J., and Barrantes, F. (2011) Disclosure of cholesterol recognition motifs in transmembrane domains of the human nicotinic acetylcholine receptor., *Sci Rep. 1*, 69.

[25] Di Scala, C., Troadec, J., Lelièvre, C., Garmy, N., Fantini, J., and Chahinian, H. (2014) Mechanism of cholesterol-assisted oligomeric channel formation by a short Alzheimer β-amyloid peptide., *J Neurochem. 128*, 186-195.

[26] Senes, A., Engel, D., and DeGrado, W. (2004) Folding of helical membrane proteins: the role of polar, GxxxG-like and proline motifs., *Curr Opin Struct Biol. 14*, 465-479.

[27] Kleiger, G., Grothe, R., Mallick, P., and Eisenberg, D. (2002) GXXXG and AXXXA: common alpha-helical interaction motifs in proteins, particularly in extremophiles., *Biochemistry 41*, 5990-5997.

[28] Russ, W., and Engelman, D. (2000) The GxxxG motif: a framework for transmembrane helix-helix association., *J Mol Biol. 296*, 911-919.

[29] Prakash, A., Janosi, L., and Doxastakis, M. (2011) GxxxG motifs, phenylalanine, and cholesterol guide the self-association of transmembrane domains of ErbB2 receptors., *Biophys J. 101*, 1949-1958.

[30] Lee, S., Shah, S., Yu, C., Wigley, W., Li, H., Lim, M., Pedersen, K., Han, W., Thomas, P., Lundkvist, J., Hao, Y., and Yu, G. (2004) A conserved GXXXG motif in APH-1 is critical for assembly and activity of the gamma-secretase complex., *J Biol Chem. 279*, 4144-4152.

[31] Smith., M. (1993) *Synthetic DNA and Biology*, World Scientific Publishing Co., Singapore.

[32] Ponsioen, B., van Zeijl, L., Langeslag, M., Berryman, M., Littler, D., Jalink, K., and Moolenaar, W. (2009) Spatiotemporal regulation of chloride intracellular channel protein CLIC4 by RhoA., *Mol Biol Cell. 20*, 4664-4672.

[33] Averaimo, S., Abeti, R., Savalli, N., Brown, L., Curmi, P., Breit, S., and Mazzanti, M. (2013) Point mutations in the transmembrane region of the clic1 ion channel selectively modify its biophysical properties., *PLoS One. 8*, e74523.

[34] Goodchild, S., Angstmann, C., Breit, S., Curmi, P., and Brown, L. (2011) Transmembrane extension and oligomerization of the CLIC1 chloride intracellular channel protein upon membrane interaction., *Biochemistry. 50*, 10887-10897.

[35] Xia, Y., Chu, W., Qi, Q., and Xun, L. (2015) New insights into the QuikChange™ process guide the use of Phusion DNA polymerase for site-directed mutagenesis., *Nucleic Acids Res. 43*, e12.

[36] Froger, A., and Hall, J. (2007) Transformation of plasmid DNA into E. coli using the heat shock method., *J Vis Exp. 6*, 253.

[37] Panja, S., Aich, P., Jana, B., and Basu, T. (2008) How does plasmid DNA penetrate cell membranes in artificial transformation process of Escherichia coli?, *Mol Membr Biol. 25*, 411-422.

[38] Littler, D., Harrop, S., Fairlie, W., Brown, L., Pankhurst, G., Pankhurst, S., DeMaere, M., Campbell, T., Bauskin, A., Tonini, R., Mazzanti, M., Breit, S., and Curmi, P. (2004) The intracellular chloride ion channel protein CLIC1 undergoes a redox-controlled structural transition., *J Biol Chem. 279*, 9298-9305.

[39] Greenfield, N. (2006) Using circular dichroism spectra to estimate protein secondary structure, *Nat Protoc. 1*, 2876-2890.

[40] Woody, R. (1995) Circular dichroism., *Methods Enzymol. 246*, 34-71.

[41] Kelly, S., and Price, N. (1997) The application of circular dichroism to studies of protein folding and unfolding., *Biochim Biophys Acta. 1338*, 161-185.

[42] Kelly, S., and Price, N. (2000) The use of circular dichroism in the investigation of protein structure and function., *Curr Protein Pept Sci. 1*, 349-384.

[43] Valenzuela, S., Martin, D., Por, S., Robbins, J., Warton, K., Bootcov, M., Schofield, P., Campbell, T., and Breit, S. (1997) Molecular cloning and expression of a chloride ion channel of cell nuclei., *J Biol Chem. 272*, 12575-12582.

[44] Fanucchi, S., Adamson, R., and Dirr, H. (2008) Formation of an unfolding intermediate state of soluble chloride intracellular channel protein CLIC1 at acidic pH., *Biochemistry. 47*, 11674-11681.

[45] Harrop, S., DeMaere, M., Fairlie, W., Reztsova, T., Valenzuela, S., Mazzanti, M., Tonini, R., Qiu, M., Jankova, L., Warton, K., Bauskin, A., Wu, W., Pankhurst, S., Campbell, T., Breit, S., and Curmi, P. (2001) Crystal structure of a soluble form of the intracellular chloride ion channel CLIC1 (NCC27) at 1.4-A resolution., *J Biol Chem. 276*, 44993-45000.

[46] Singh, H., and Ashley, R. (2006) Redox regulation of CLIC1 by cysteine residues associated with the putative channel pore., *Biophys J. 90*, 1628-1638.

[47] Hossain, K., Al Khamici, H., Holt, S., and Valenzuela, S. (2016) Cholesterol Promotes Interaction of the Protein CLIC1 with Phospholipid Monolayers at the Air-Water Interface., *Membranes 6*, 15-28.

[48] Goodchild, S., Howell, M., Cordina, N., Littler, D., Breit, S., Curmi, P., and Brown, L. (2009) Oxidation promotes insertion of the CLIC1 chloride intracellular channel into the membrane., *Eur Biophys J. 39*, 129-138.

[49] Goodchild, S., Howell, M., Littler, D., Mandyam, R., Sale, K., Mazzanti, M., Breit, S., Curmi, P., and Brown, L. (2010) Metamorphic response of the CLIC1 chloride intracellular ion channel protein upon membrane interaction., *Biochemistry. 49*, 5278-5289.

Chapter 7

Conclusion and Future Directions

Chapter 7

Conclusion and Future Directions

The Chloride Intracellular Ion Channel Proteins, CLICs, are metamorphic proteins, adopting more than one stable conformation and they also exist in two forms, namely, a cytosolic soluble form with a thioredoxin-fold and an insoluble membrane-bound form with an undefined topology [1-16]. The mechanism by which CLIC proteins change from their soluble to membrane-bound form is also still largely unknown. Previous studies have shown that in order for CLIC proteins to bind to and transverse membranes and form functional ion channels, it is necessary for the N-terminal domain (consisting of the TMR (helix 1 and β-sheet 2)) to undergo structural rearrangements in order to expose hydrophobic surfaces that are presumed to bind and insert into membranes [4, 8, 9, 16-18]. Factors such as redox environment [5, 7, 8, 10, 13, 18, 19], pH [9, 16, 20-22] and lipid composition [10, 23] have been shown to play a crucial role in regulating the spontaneous membrane insertion of CLIC proteins. Several different studies, based on the ion channel activity of the protein CLIC1, have shown that maximal binding and insertion of CLIC1 occurs at low pH (5.5) [4, 16, 20, 21], under oxidising conditions [7, 10, 18, 19] and in a lipid membrane comprised of POPE:POPS:Cholesterol in a mole ratio of 4:1:1 [10]. However, conflicting data were also published showing that the structural integrity of CLIC1 was unchanged under varying pH environments [14, 24] and that CLIC1 was able to form equally effective functional channels under reducing conditions [8-10]. This therefore suggests the involvement of other factors that may be deemed necessary for the spontaneous membrane insertion of the CLIC proteins.

The focus of this thesis was to investigate the various lipid environments encountered by CLIC1 *in vivo* and to determine their effects on the membrane insertion, structure and unfolding kinetics of the protein so as to propose a mechanism by which CLIC1 can autonomously insert into membranes to form functional ion channels. Membrane insertion of CLIC1 was examined *in vitro* using a Langmuir monolayer model membrane at the air-water interface. Pure and mixed lipid monolayers were formed using different phospholipids and sterol molecules at varying mole ratio combinations. X-ray and neutron reflectivity

techniques were employed to elucidate the structural features of the CLIC1 membrane-bound form within different phospholipid and sterol monolayers. In parallel with these studies, we also investigated the role of a conserved GXXXG motif in CLIC1's spontaneous membrane insertion.

The Langmuir results described in Chapter 3 of this thesis have demonstrated that CLIC1 showed little to no interaction with POPC and POPS monolayers respectively, while protein insertion into these phospholipid monolayers was significantly and vastly increased following the addition of cholesterol. In stark contrast, CLIC1 showed greater interaction with POPE monolayer only and a decrease in CLIC1 insertion was observed following the addition of cholesterol into POPE monolayers. The crystal structure of CLIC1 protein resolved at 1.4 Å by X-ray crystallography showed a highly negatively charged loop between helices h5 and h6 in CLIC1 giving the molecule a net charge of -7 [4]. It is speculated here that it is the presence of this net negative charge that inhibited CLIC1 from inserting into the anionic POPS monolayer by generating possible repulsive forces while conversely contributing favourably to its interaction with the neutral POPC and POPE phospholipids. XR and NR reflectivity data shown in Chapter 4 confirmed that the variations in CLIC1 interaction with different phospholipid monolayers arise due to a difference of orientation of the protein within the phospholipid monolayers in the absence and presence of cholesterol.

The XR and NR fitted parameters of CLIC1 interactions with phospholipid monolayers without cholesterol are shown in Chapter 4. The reflectivity data resulted in an average CLIC1 layer thickness of 25.1 Å within the phospholipid head-group region of the monolayer, with no significant penetration of CLIC1 into the acyl chain region of the monolayers. This layer thickness is consistent with the thickness of the short axis of the CLIC1 protein of 23 Å obtained from published X-ray crystallography data [4]. This suggests that the protein lies flat with an interfacial area of 1080 ± 0.6 $Å^2$ (10.8 nm^2) and a surface coverage of approximately 0.49 ± 0.3 mg/m^2 in phospholipid monolayers in the absence of cholesterol. However, in order to form functional ion channels, it is necessary for CLIC1 to completely transverse the lipid membrane.

Our results in Chapter 3 provide insight into the regulatory role that lipids, particularly cholesterol, play in the spontaneous membrane insertion of CLIC1. We have shown through Langmuir experiments, CLIC1 has a relatively strong preference for associating with or intercalating into pure or mixed phospholipid monolayers that also contain cholesterol, with the protein showing maximum binding and insertion into monolayers comprised of POPE:POPS:Chol, in a mole ratio of 4:1:1. The Langmuir results in this study complement and support our previously published study of CLIC1 ion channel activity within tBLMs monitored using impedance spectroscopy, that revealed CLIC1 only forms functional ion channels in membranes containing cholesterol [23]. Hence, from our Langmuir results together with the previously published tBLMs results [23], we propose here a mechanism for the insertion of CLIC1 protein into lipid membranes.

XR and NR studies of CLIC1 interaction with different phospholipid monolayers containing cholesterol confirmed that cholesterol is required for the penetration of the N-terminal domain of CLIC1 into the hydrophobic acyl chains of the lipid monolayer, which is considered necessary for the formation of functional ion channels. Since, in this study a lipid monolayer is used instead of a bilayer, based on previous studies we assume that the C-domain of CLIC1 remains in the buffer subphase, while the N-terminal domain, comprised of two α-helices, are folded rather than extending out completely A relatively stable orientation of CLIC1 was observed upon interaction with phospholipid monolayers containing cholesterol, resulting in an average total CLIC1 thickness of approximately 50.3 ± 7 Å throughout the entire monolayer. This is in excellent agreement with the X-ray crystallography results that suggested CLIC1 be a flat molecule with dimensions of 55 x 52 x 23 Å [4]. The average area per CLIC1 molecule within the different phospholipid-cholesterol monolayers was calculated to be approximately 706 ± 1 $Å^2$ (7 nm^2) with a surface coverage of 0.8 mg/m^2.

Analogously, neutron reflectivity experiments of CLIC1 interactions with phospholipid monolayers in the presence of different natural sterols have shown that CLIC1 inserts in a similar structural orientation within POPC monolayers containing either cholesterol, ergosterol or 20-hyroxyecdysone, resulting in a total

CLIC1 thickness that ranges from ~ 51 Å to 59 Å and ranging in an area per CLIC1 molecule of 576 $Å^2$ to 669 $Å^2$ depending on the type of sterol present. It is, therefore, evident from the reflectivity results that CLIC1 in the absence of sterol is unable to penetrate into the hydrophobic acyl core of the lipid membrane. In addition, the Langmuir monolayer results of CLIC1 insertion into POPC monolayers containing naturally occurring sterols and cholesterol derivatives as shown in Chapter 5, concluded that CLIC1 interaction with cholesterol is structurally dependent on the presence of the intact 3β-OH group in the sterol ring. Modification of the sterol structure by the introduction of additional hydroxyl groups (as seen in the case for 20-hydroxyecdysone) and methylation of the alkyl chain (as seen in ergosterol and β-sitosterol) was shown to facilitate greater spontaneous membrane insertion of the protein within the phospholipid monolayer.

In addition to the Langmuir results shown in this thesis that demonstrate the spontaneous membrane-binding/ insertion ability of CLIC1 is critically controlled by membrane cholesterol, we have also confirmed the formation of a relatively stable CLIC1-cholesterol pre-complex. We have identified for the first time a cholesterol-binding motif in CLIC1 and have shown that this GXXXG motif is important for the formation of a CLIC1-cholesterol pre-complex and hence for the spontaneous membrane insertion of CLIC1 into model membranes. Therefore, from all the Langmuir, XR and NR results shown in different Chapters in this study we postulate a structural model for the spontaneous membrane insertion of CLIC1 protein into lipid membranes as shown in Figure 7.1.

A proposed mechanism of insertion of CLIC1 proteins into lipid membranes containing cholesterol

This thesis supports the model that the GXXXG motif in CLIC1 acts as the cholesterol-binding site used by the protein for its initial recognition and binding to membrane cholesterol. We have shown that CLIC1 is able to interact with the phospholipid head-groups in the absence of cholesterol. Thus, it seems that the GXXXG motif most likely goes into the membrane and binds to membrane cholesterol via the 3β-OH group in the sterol ring in order to form a CLIC1-cholesterol pre-complex. This binding interaction, then stimulates

conformational changes in the N-terminal domain (consisting of the TMR (helix 1 and β-sheet 2)) of CLIC1. This in turn, may facilitate structural changes to expose the hydrophobic transmembrane region in the N-terminal domain for greater interaction and insertion of CLIC1 within the hydrophobic tails of lipid membranes such that the protein occupies an area per CLIC1 molecule between 5 ~ 7 nm^2. In a phospholipid-sterol monolayer, the total CLIC1 thickness throughout the entire monolayer ranges from ~ 51 Å to 59 Å (see Figure 7.1). Unfortunately, due to lack of sufficient contrast variation, it was not possible to fully elucidate the structural conformation of the N-terminal domain within the lipid acyl chain regions and hence was speculated to be in a folded state within the lipid monolayer. However, it should be taken into account that although the experiments were done in a reducing environment in the presence of DTT, due to the open nature of the Langmuir trough we could not completely rule out the effects of possible oxidation on the protein and lipids at the air-water interface. As a result, it can also be speculated that at the air-water interface, oxidation can promote major structural rearrangements of the N-terminal domain such that all the β-strands present in the reduced monomeric form may become disordered and the N-terminal domain is entirely α-helical, exposing the large TRM hydrophobic surface for interaction with the membrane. It is likely that in the presence of the bilayer the N-terminal domain may be extended out completely such that the N- and C-domains are located on opposite sides of the membrane with cysteine residue 24 located on the trans face of the membrane (see Figure 7.1).

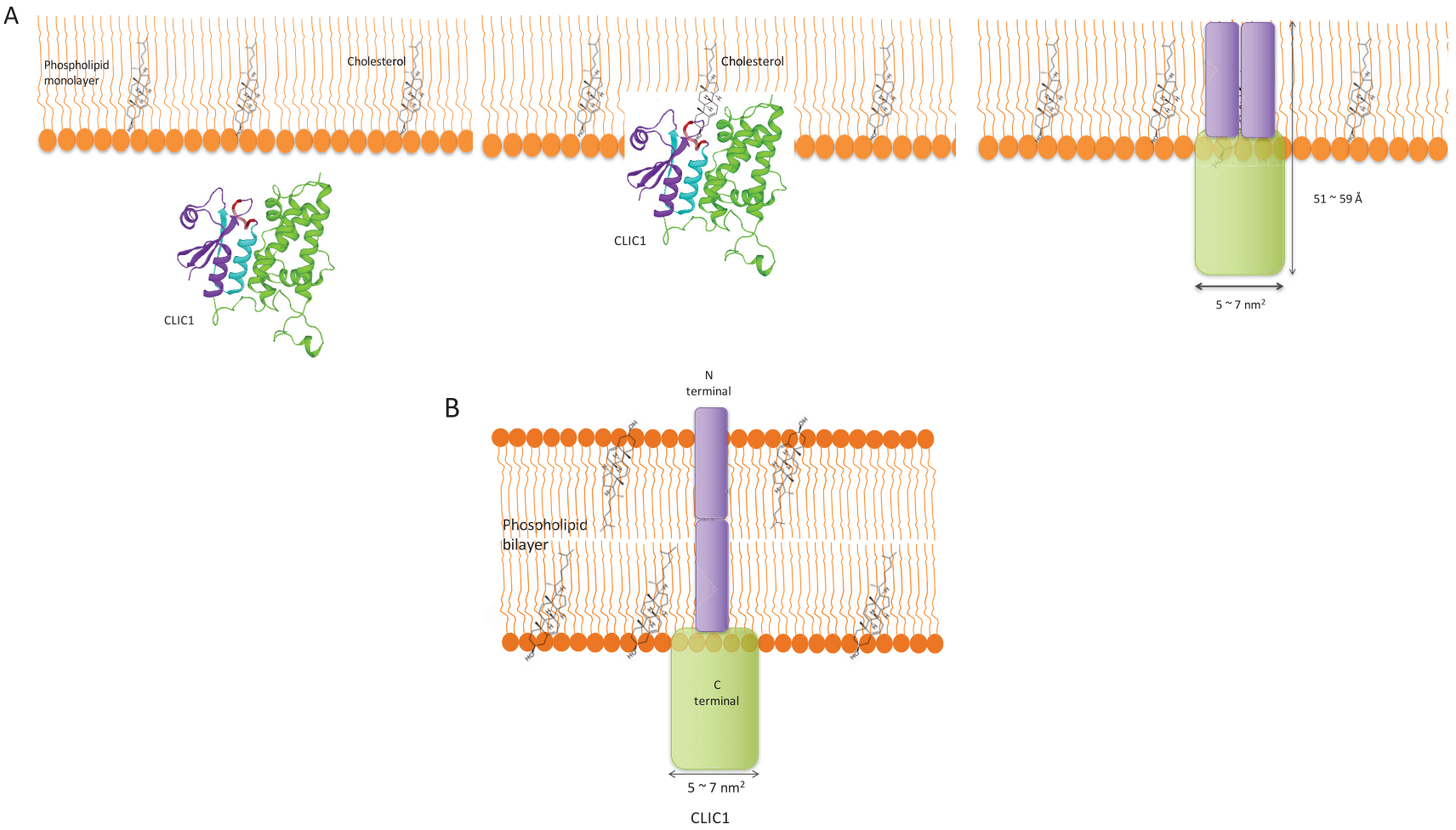

Figure 7.1 A schematic representation of a postulated structural model for CLIC1 interacting with A) a lipid monolayer and B) a lipid bilayer. **A)** This schematic diagram shows that as CLIC1 migrates to the vicinity of the lipid monolayer, the GXXXG motif, shown in red, interacts with the cholesterol molecules via its 3β-OH group in the sterol ring shown in black. This interaction promotes conformational changes in the N-terminal domain for deeper penetration into the monolayer with the expected structure shown above. B) Based on the lipid monolayer data, this is a model of the presumed structural features of the CLIC1membrane-bound form within a phospholipid bilayer.

Future Directions

There is a large amount of evidence from this work that supports the idea that cholesterol regulates the spontaneous membrane insertion of the CLIC1 proteins. Our group has demonstrated that CLIC1 interactions within a phospholipid monolayer bear strong similarities to those observed within the tBLMs [23]. Earlier studies have shown that CLIC1 (and other CLIC proteins) can spontaneously form electro-physiologically active anion channels in artificial bilayers where the electro-physiological properties resemble those of the CLIC currents observed in cells [4, 13, 16]. Hence to demonstrate that the regulatory role of cholesterol in CLIC's membrane insertion in not only limited to *in vitro* assays, it is important to study the effects of cholesterol on the spontaneous membrane insertion of CLIC proteins *in vivo* and *in situ,* by using cellular models. In order to demonstrate the spontaneous membrane insertion of CLIC1 *in situ,* CLIC1 association with cholesterol-depleted cellular membranes can be employed. In addition, studies to detect direct association of CLIC1 with cholesterol by microscopy can also be made possible by the use of fluorescently tagged cholesterol and protein molecules. *In situ* analysis of CLIC1 interaction with cholesterol thus opens up a multitude of opportunities for further study.

Our group has demonstrated using both Langmuir and tBLM studies [23] that pre-incubation of CLIC1 with cholesterol caused reduced membrane insertion of the protein thereby resulting in the complete abrogation of ion channel activity. From these results, we have speculated that CLIC1 has the ability to form a relatively stable CLIC1-cholesterol complex. However, to fully understand the interaction of CLIC1 with cholesterol in membranes and the structural features of the CLIC1-cholesterol complex will most likely require further complementary techniques such as small-angle X-ray scattering (SAXS), small-angle neutron (SANS) scattering techniques and molecular dynamic simulations. These techniques should provide detailed structural data on which to model the interaction of CLIC proteins with cholesterol within lipid membranes. In humans, members of the CLIC family have been linked to nasopharyngeal carcinoma, gastric cancer, hepatocarcinoma, colorectal cancer, gallbladder carcinoma, ovarian and breast cancer [25-30]. CLIC1 has the potential to be used as an effective biomarker or as a potent therapeutic target in cancer therapy. Structurally understanding the

mechanism by which CLIC proteins interact with the membrane is, therefore, crucial if these applications are to be realised.

In Chapter 5, we have shown that CLIC1 can also interact with other naturally occurring sterols such as ergosterol, ß-sitosterol and 20-hydroxyecdyson. Cholesterol (Chol) is the typical sterol found in the plasma membranes of mammalian cells, whereas ergosterol (Erg) is the major sterol of other eukaryotic organisms such as protozoa, yeast and fungi, while β-sitosterol and 20-hydroxyecdyson predominate in the plasma membrane of plants and insects respectively. The preference of CLIC1 insertion into POPC monolayers, supplemented with different natural sterols, was found to be in the following order: 20-hydroxyecdysone > ergosterol and / or β-sitosterol > cholesterol. The chemical structure of 20-hydroxyecdysone is vastly similar to several mammalian oxysterols and steroid hormones, as a result, one may speculate additional functional role of CLIC1 protein in tissues containing high levels of cholesterol or its involvement in the transportation of cholesterol or in the functional activity of steroid hormones. An adjunct study would be to investigate the possible interaction between the CLIC1 protein and the different classes of sterol molecules present in mammalian cells.

This discovery of CLIC1 interaction with other natural sterols also opens up an array of future studies to explore the feasibility of exploiting these properties of CLIC proteins for therapeutic and prophylactic purposes such as in their use as fungicidal agents, or as pesticides. Like the sterol molecules, CLIC proteins are also evolutionarily conserved across species [4, 8, 9]. Almost all vertebrates express six CLIC proteins (CLIC1-6) that exist predominantly as soluble proteins in the cytoplasm or found bound to membrane where they function as ion channels [4, 8, 9]. CLIC-like proteins are also present in invertebrates including nearly all arthropods and nematodes [31]. The nematode *Caenorhabditis elegans* is known to contain two CLIC homologues, EXC-4 and EXL-1 (EXC-4 like protein 1) which are exclusively membrane–bound proteins [31, 32]. The arthropod *Drosophila melanogaster* contains a single CLIC1-like protein referred to as *Dm*CLIC [31]. It was found that only the first 55 residues of EXC-4, which corresponds to the putative TMD and contains the GXXXG motif, are needed to maintain membrane localisation [31, 32]. Hence, it is also important to explore whether there is a species

specificity amongst the different natural sterols and CLIC and CLIC-like proteins. Future experiments will be needed to investigate the possibility of other vertebrate CLIC proteins and invertebrate CLIC-like proteins binding specific sterol molecules, particularly given the conserved conformational geometry of the GXXXG motif (see Figure 6.1) amongst all the vertebrate CLICs and CLIC-like proteins.

References

[1] Berryman, M., Bruno, J., Price, J., and Edwards, J. (2004) CLIC-5A functions as a chloride channel in vitro and associates with the cortical actin cytoskeleton in vitro and in vivo. , *J. Biol. Chem. 279*, 34794-34801.

[2] Cromer, B., Gorman, M., Hansen, G., Adams, J., Coggan, M., Littler, D., Brown, L., Mazzanti, M., Breit, S., Curmi, P., Dulhunty, A., Board, P., and Parker, M. (2007) Structure of the Janus protein human CLIC2., *J Mol Biol. 374*, 719-731.

[3] Friedli, M., Guipponi, M., Bertrand, S., Bertrand, D., Neerman-Arbez, M., Scott, H., Antonarakis, S., and Reymond, A. (2003) Identification of a novel member of the CLIC family, CLIC6, mapping to 21q22.12., *Gene. 320*, 31-40.

[4] Harrop, S., DeMaere, M., Fairlie, W., Reztsova, T., Valenzuela, S., Mazzanti, M., Tonini, R., Qiu, M., Jankova, L., Warton, K., Bauskin, A., Wu, W., Pankhurst, S., Campbell, T., Breit, S., and Curmi, P. (2001) Crystal structure of a soluble form of the intracellular chloride ion channel CLIC1 (NCC27) at 1.4-A resolution., *J Biol Chem. 276*, 44993-45000.

[5] Littler, D., Assaad, N., Harrop, S., Brown, L., Pankhurst, G., Luciani, P., Aguilar, M., Mazzanti, M., Berryman, M., Breit, S., and Curmi, P. (2005) Crystal structure of the soluble form of the redox-regulated chloride ion channel protein CLIC4. , *FEBS J. 272*, 4996-5007.

[6] Littler, D., Brown, L., Breit, S., Perrakis, A., and Curmi, P. (2010) Structure of human CLIC3 at 2 A resolution. , *Proteins 78*, 1594-1600.

[7] Littler, D., Harrop, S., Fairlie, W., Brown, L., Pankhurst, G., Pankhurst, S., DeMaere, M., Campbell, T., Bauskin, A., Tonini, R., Mazzanti, M., Breit, S., and Curmi, P. (2004) The intracellular chloride ion channel protein CLIC1 undergoes a redox-controlled structural transition., *J Biol Chem. 279*, 9298-9305.

[8] Littler, D., Harrop, S., Goodchild, S., Phang, J., Mynott, A., Jiang, L., Valenzuela, S., Mazzanti, M., Brown, L., Breit, S., and Curmi, P. (2010) The enigma of the CLIC proteins: Ion channels, redox proteins, enzymes, scaffolding proteins?, *FEBS Lett. 584*, 2093-2101.

[9] Singh, H. (2010) Two decades with dimorphic Chloride Intracellular Channels (CLICs). *FEBS Lett. 584*, 2112-2121.

[10] Singh, H., and Ashley, R. (2006) Redox regulation of CLIC1 by cysteine residues associated with the putative channel pore., *Biophys J. 90*, 1628-1638.

[11] Singh, H., and Ashley, R. (2007) CLIC4 (p64H1) and its putative transmembrane domain form poorly selective, redox-regulated ion channels., *Mol Membr Biol. 24*, 41-52.

[12] Singh, H., Cousin, M., and Ashley, R. (2007) Functional reconstitution of mammalian 'chloride intracellular channels' CLIC1, CLIC4 and CLIC5 reveals differential regulation by cytoskeletal actin., *FEBS J. 274*, 6306-6316.

[13] Tulk, B., Kapadia, S., and Edwards, J. (2002) CLIC1 inserts from the aqueous phase into phospholipid membranes, where it functions as an anion channel., *Am J Physiol Cell Physiol. 282*, 1103-1112.

[14] Valenzuela, S., Berkahn, M., Porkovich, A., Huynh, T., Goyette, J., Martin, D., and Geczy, C. (2011) Soluble structure of CLIC and S100 proteins investigated by atomic force microscopy, *Biomaterials and Nanobiotechnology 2*, 8-17.

[15] Valenzuela, S., Martin, D., Por, S., Robbins, J., Bootcov, M., Schofield, P., Campbell, T., and Breit, S. (1996) NCC27- A novel nuclear chloride ion channel associated with macrophage activation., *Journal of leukocyte biology* 106-106.

[16] Warton, K., Tonini, R., Fairlie, W., Matthews, J., Valenzuela, S., Qiu, M., Wu, W., Pankhurst, S., Bauskin, A., Harrop, S., Campbell, T., Curmi, P., Breit, S., and Mazzanti, M. (2002) Recombinant CLIC1 (NCC27) assembles in lipid bilayers via a pH-dependent two-state process to form chloride ion channels with identical characteristics to those observed in Chinese hamster ovary cells expressing CLIC1., *J Biol Chem. 277*, 26003-26011.

[17] Goodchild, S., Angstmann, C., Breit, S., Curmi, P., and Brown, L. (2011) Transmembrane extension and oligomerization of the CLIC1 chloride intracellular channel protein upon membrane interaction., *Biochemistry. 50*, 10887-10897.

[18] Goodchild, S., Howell, M., Littler, D., Mandyam, R., Sale, K., Mazzanti, M., Breit, S., Curmi, P., and Brown, L. (2010) Metamorphic response of the CLIC1 chloride intracellular ion channel protein upon membrane interaction., *Biochemistry. 49*, 5278-5289.

[19] Goodchild, S., Howell, M., Cordina, N., Littler, D., Breit, S., Curmi, P., and Brown, L. (2009) Oxidation promotes insertion of the CLIC1 chloride intracellular channel into the membrane., *Eur Biophys J. 39*, 129-138.

[20] Achilonu, I., Fanucchi, S., Cross, M., Fernandes, M., and Dirr, H. (2012) Role of individual histidines in the pH-dependent global stability of human chloride intracellular channel 1., *Biochemistry. 51*, 995-1004. .

[21] Fanucchi, S., Adamson, R., and Dirr, H. (2008) Formation of an unfolding intermediate state of soluble chloride intracellular channel protein CLIC1 at acidic pH., *Biochemistry. 47*, 11674-11681.

[22] Legg-E'silva, D., Achilonu, I., Fanucchi, S., Stoychev, S., Fernandes, M., and Dirr, H. (2012) Role of arginine 29 and glutamic acid 81 interactions in the conformational stability of human chloride intracellular channel 1., *Biochemistry. 51*, 7854-7862.

[23] Valenzuela, S., Alkhamici, H., Brown, L., Almond, O., Goodchild, S., Carne, S., Curmi, P., Holt, S., and Cornell, B. (2013) Regulation of the Membrane Insertion and Conductance Activity of the Metamorphic Chloride Intracellular Channel Protein CLIC1 by Cholesterol, *PLoS ONE 8*, 56948.

[24] Stoychev, S., Nathaniel, C., Fanucchi, S., Brock, M., Li, S., Asmus, K., Woods, V. J., and Dirr, H. (2009) Structural dynamics of soluble chloride intracellular channel protein CLIC1 examined by amide hydrogen-deuterium exchange mass spectrometry., *Biochemistry. 48*, 8413-8421.

[25] Chen, C., Wang, C., Huang, Y., Chien, K., Liang, Y., Chen, W., and Lin, K. (2007) Overexpression of CLIC1 in human gastric carcinoma and its clinicopathological significance., *Proteomics. 1*, 155-167.

[26] Huang, J., Chao, C., Su, T., Yeh, S., Chen, D., Chen, C., Chen, P., and Jou, Y. (2004) Diverse cellular transformation capability of overexpressed genes in human hepatocellular carcinoma., *Biochem Biophys Res Commun. 315*, 950-958.

[27] Kim, W., Oe Lim, S., Kim, J., Ryu, Y., Byeon, J., Kim, H., Kim, Y., Heo, J., Park, Y., and Jung, G. (2003) Comparison of proteome between hepatitis B virus- and hepatitis C virus-associated hepatocellular carcinoma., *Clin Cancer Res. 9*, 5493-5500.

[28] Petrova, D., Asif, A., Armstrong, V., Dimova, I., Toshev, S., Yaramov, N., Oellerich, M., and Toncheva, D. (2008) Expression of chloride intracellular channel protein 1 (CLIC1) and tumor protein D52 (TPD52) as potential biomarkers for colorectal cancer., *Clin Biochem. 41*, 1224-1236.

[29] Wang, J., Peng, S., Li, J., Wang, Y., Zhang, Z., Cheng, Y., Cheng, D., Weng, W., Wu, X., Fei, X., Quan, Z., Li, J., Li, S., and Liu, Y. (2009) Identification of metastasis-associated proteins involved in gallbladder carcinoma metastasis by proteomic analysis and functional exploration of chloride intracellular channel 1., *Cancer Lett. 281*, 71-81.

[30] Wang, J., Xu, X., Wang, W., Shao, W., Li, L., Yin, W., Xiu, L., Mo, M., Zhao, J., He, Q., and He, J. (2011) The expression and clinical significance of CLIC1 and HSP27 in lung adenocarcinoma., *Tumour Biol. 32*, 1199-1208.

[31] Littler, D., Harrop, S., Brown, L., Pankhurst, G., Mynott, A., Luciani, P., Mandyam, R., Mazzanti, M., Tanda, S., Berryman, M., Breit, S., and Curmi, P. (2008) Comparison of vertebrate and invertebrate CLIC proteins: the crystal structures of Caenorhabditis elegans EXC-4 and Drosophila melanogaster DmCLIC., *Proteins. 71*, 364-378.

[32] Berry, K., Bülow, H., Hall, D., and Hobert, O. (2003) A C. elegans CLIC-like protein required for intracellular tube formation and maintenance., *Science. 302*, 2134-2137.

Appendix

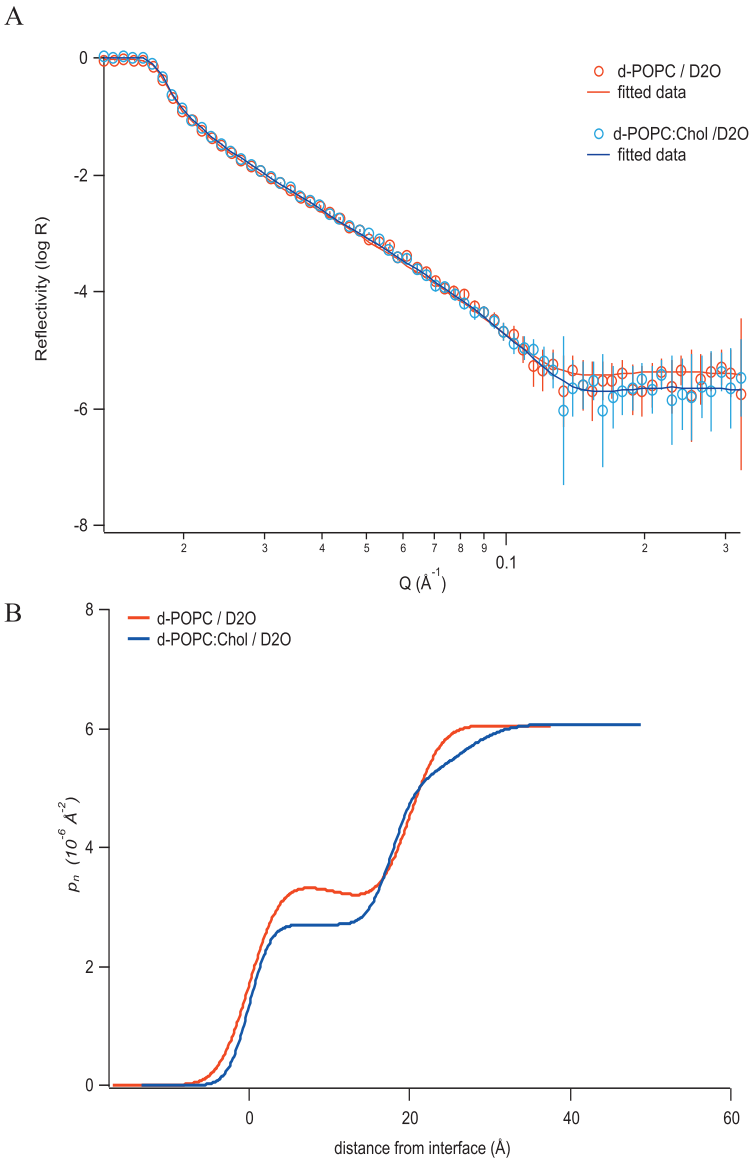

Figure A1 (A) Neutron reflectivity profile and model data fit and (B) the scattering length density profile the fit describes for air-water interface containing POPC (orange line) and POPC:Chol (blue line) monolayers held at a constant pressure of 20 mN/m. The air-water interface was set to be between the acyl chains and head-group region of the POPC and POPC:Chol monolayers.

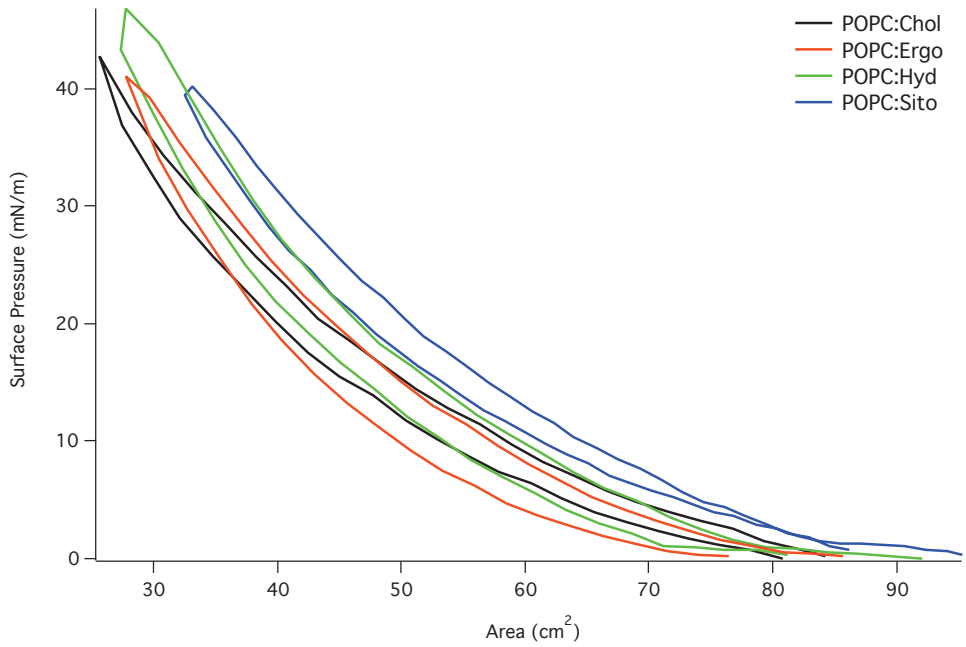

Figure A2 Surface pressure-Area isotherms of POPC monolayers supplemented with different natural sterols in a mole ratio of 5:1. The isotherms shown are for POPC:Chol (black line), POPC:Ergo (red line), POPC:Hyd (green line) and POPC:Sito (blue line). All the isotherms exhibit that the monolayers are in the liquid-expanded phase and do not exhibit any clear phase transitions. POPC:Chol monolayer was When compressed, POPC:Chol monolayer occupied the least area, whereas, POPC:Sito monolayer occupied the largest at 40 mN/m.